SUBSTRATE STIFFNESS REGULATES CAPILLARY NETWORK ASSEMBLY

A Dissertation

Presented to the Faculty of the Graduate School

of Cornell University

In Partial Fulfillment of the Requirements for the Degree of

Doctor of Philosophy

by

Joseph Peter Califano

May 2012

SUBSTRATE STIFFNESS REGULATES CAPILLARY NETWORK ASSEMBLY

Joseph Peter Califano, Ph.D.

Cornell University 2012

Tissue assembly is a fundamental biological process that arises from complex cell-cell and cell-extracellular matrix interactions. Angiogenesis is the process of capillary formation that enables normal physiological responses like wound healing and mediates disease states like tumorigenesis. During angiogenesis, capillary endothelial cells degrade the basement membrane, proliferate, migrate, and assemble a new vascular network. While there is much focus on growth factor signaling cascades that enable angiogenesis, less attention has been paid to the role of mechanics in capillary formation. Notably, capillary network assembly has been demonstrated on compliant, but not stiff, substrates suggesting that the mechanical microenvironment also mediates angiogenesis. However, it is unknown whether, or how, substrate stiffness regulates capillary network assembly.

Herein, we demonstrate that substrate stiffness regulates capillary network assembly and mediates endothelial cell behaviors that enable assembly. Compliant (E<1 kPa), but not stiff (E>1 kPa), substrates promote the self-assembly of endothelial cell networks that result from a balance of cell-cell and cell-matrix adhesion. Substrate stiffness alters the localization of VE-cadherin and focal adhesions, mediators of endothelial cell-cell and cell-matrix adhesion, respectively. Endothelial network assembly also requires polymerization of the matrix protein fibronectin that stabilizes cell-cell interactions. Analogously, we demonstrate that mammary cell network

assembly is also sensitive to substrate stiffness and requires the deposition of laminin. Our findings indicate that compliant substrates foster network assembly by promoting cell-cell adhesion, cell-matrix interactions, and reducing cell-matrix adhesion.

We further investigate the role of substrate stiffness in mediating changes in cell shape and contractility. We determine that substrate stiffness and ligand density alter cell area, and that both stiffness and cell area are significant predictors of traction force generation in endothelial cells during cell-cell contact. In addition, we demonstrate that substrate stiffness alters the synthesis and deposition of fibronectin and extra domain B-fibronectin, an isoform preferentially localized to neovasculature, by modulating cell shape and the directionality of traction forces in endothelial cells.

Taken together, these data demonstrate that substrate stiffness regulates capillary network assembly by altering endothelial cell behaviors that facilitate assembly. These findings contribute to the understanding of how the mechanical microenvironment regulates capillary network assembly and enable approaches to control angiogenesis for therapeutic use.

BIOGRAPHICAL SKETCH

Joseph Peter Califano was born in Albany, New York to Antonio and Donna in the spring of 1984, and grew up with his older brother Anthony in Colonie, New York. He attended Colonie Central High School with keen interests in music, biology, and chemistry, and graduated in 2002. Joe attended Rensselaer Polytechnic Institute as a Math and Science Medal scholarship recipient, and majored in Biomedical Engineering with a minor in Social Psychology. He graduated *summa cum laude* with a B.S. in Biomedical Engineering in May 2006. In August 2006, Joe entered the Ph.D. program in Biomedical Engineering at Cornell University and joined the lab of Cynthia A. Reinhart-King. At Cornell, Joe's thesis work was focused on understanding the role of the mechanical and chemical microenvironment in blood vessel development. He received an M.S. in Biomedical Engineering in 2009, was awarded a National Science Foundation GK-12 Fellowship in 2010, and completed his Ph.D. in the spring of 2012. In addition to practicing science, Joe enjoys running, reading, cooking, and eating.

For my Family and Friends

ACKNOWLEDGMENTS

My name appears at the top of this dissertation, but there are many people who made this work possible.

I would first like to acknowledge and thank my advisor Dr. Cynthia A. Reinhart-King. I am sincerely grateful to Cindy for her advice, encouragement, support, and for giving me the independence and guidance to direct the course of my research. I am grateful for her mentorship in communicating science effectively, and for trusting me to help set up her lab, an incredible and unique learning experience. I am indebted to Cindy for teaching me how to be a successful scientist, and it was my pleasure to work with her.

I would like to recognize and thank my committee members, Dr. Lawrence Bonassar and Dr. Thomas Sato for their support and supervision of this work.

I am sincerely grateful for the opportunity to work with collaborators within and outside of the Reinhart-King lab. I want to acknowledge John Huynh, Brooke Mason, Casey Kraning-Rush, Jon Charest, and Shawn Carey for terrific collaborations in original research and book chapters. I would like to thank Dr. Nozomi Nishimura, Dr. Chris Schaffer, Dr. Kuldeep Rana, and Dr. Michael King, Emily Brooks and Dr. Claudia Fischbach, Abdurrahman Gumus and Dr. George Malliaras, Dr. Paraskevi Giannakakou, and Dr. Brian DeRubertis and Dr. Angela Vouyouka for their collaboration on challenging and exciting research projects. I would like to also thank Dr. Micah Dembo, Dr. Jane Sottile, Dr. Harold Erickson, and Dr. Tomoo Ohashi for graciously providing tools and advice necessary for the completion of this work.

I gratefully thank the funding sources that have supported this work, including a Sigma Xi Grant-In-Aid of Research, and a National Science Foundation GK-12 Fellowship.

I would like to thank Dr. Michael Shuler who graciously provided me with a home in his laboratory and a place to present my early work at his group meetings. His questions challenged me to think about my work in a variety of contexts. I am indebted to Paula Miller who taught me cell culture and tips on lab management and organization. I am thankful for discussions and advice about research from the students in the Shuler lab during my time there.

Thanks to Dr. Chris Schaffer, Dr. Shivaun Archer, Kevin Dilley, and Nev Singhota for their advice and mentorship about teaching, GK-12 education, and outreach. I want to acknowledge and thank Mrs. Jackie Henkel, Mr. Mike McNall, and the students in 7th grade science at Eagle Hill Middle School for a fantastic teaching experience and for helping and allowing me to implement my curriculum. Thanks also to Dr. Angela Vouyouka for her mentorship and allowing me to follow her through the ORs of Weill Cornell Medical College—it was an amazing experience I'll never forget.

I am indebted to my fellow graduate students in the Reinhart-King (CRK) lab. John Huynh, Brooke Mason, and Casey Kraning-Rush (not to mention their counterparts Joanna, Blake, and Jason) served as my lab family, and I am forever grateful for their friendship, encouragement, and insights about science. They could all be counted on for good company, good advice, and good meals, and it was my privilege to work with them. I would also like to thank Jon Charest, Shawn Carey, Courtney Faber, Na Young Kim, Abdurrahman Gumus, and Josie Bodle for their collaborations, scientific

expertise, and friendship. Thanks to all other members of the CRK lab including the undergrads that I was fortunate to mentor. Tracy Cheung, Alina Starchenko, and Kelly McBride served as devoted worker-bees and friends, and I am certain they will all find success in their future endeavors.

Special thanks to Dr. Christine Montague and Dr. Libin Yuan. This work could not have been completed without their collaboration, and insights and expertise in molecular biology. Their patience and helpful discussions about science and life outside of science were truly appreciated.

Thanks to John Nguyen who served as a colleague, roommate, and West Coast liaison. I am grateful for his friendship, advice, and insights about science and life. I'm also grateful to John Huynh for his excellent roommate-ship—fun times were had on Miller St.

I am grateful for the friendship of my fellow graduate classmates, Emily Brooks, Janet Shen, Gilda Shayan, and Phil Buskohl. We started this journey together and I am thankful for their continued friendship and encouragement. Thanks also to Michelle Martinez for her friendship and accompaniment as we explored the eateries of Ithaca together.

I would be remiss to not acknowledge the excellent teachers who inspired my interest in science and engineering. From RPI, I want to thank Dr. Deepak Vashishth and Dr. Rena Bizios for their instruction, their enthusiasm about BME and research, and their continued encouragement and support. I would not have ended up in graduate school without their mentorship. At CCHS, my interest in science was awakened by Mrs.

Villa and Mr. Diana. I am undoubtedly on this path because of their pedagogical excellence.

Thanks to my RPI “brother” Barret LaGrave (Gravester) for his friendship both in and out of the Poly. I’m also grateful for the continued friendship and encouragement of Dara Farber. Her wisdom and uncanny ability to teach me things about myself helps keep everything in perspective.

Lastly, but most importantly, I must acknowledge and thank my family including my parents, Antonio and Donna, and my brother, Anthony. Their unconditional love, support, and encouragement serves as a beacon in the night throughout this journey called life. *Ti saluto*!

TABLE OF CONTENTS

LIST OF FIGURES

CHAPTER 2

CHAPTER 3

LIST OF TABLES

CHAPTER 4

LIST OF ABBREVIATIONS

ANOVA	Analysis of variance
BAEC	Bovine aortic endothelial cell
BSA	Bovine serum albumin
DAPI	4’,6-diamidino-2-phenylindole
DOC	Deoxycholate
EC	Endothelial cell
EGTA	Ethylene glycol tetraacetic acid
FITC	Fluorescein isothiocyanate
FN	Fibronectin
GFP	Green fluorescent protein
HEPES	4-(2-hydroxyethyl)-1-piperazineethanesulfonic acid
HUVEC	Human umbilical vein endothelial cell
MEC	Mammary epithelial cell
N6	N-6-((acryloyl)amino) hexanoic acid, succinimidyl ester
PA	Poly(acrylamide)
PBS	Phosphate-buffered saline
RGD	Arginine-glycine-aspartic acid
RT	Room temperature
SMC	Smooth muscle cell
TBS	Tris-buffered saline
TFM	Traction force microscopy
Triton	Octyl phenol ethoxylate
Tween	Polyoxyethylene 20 sorbitan monolaurate
YFP	Yellow fluorescent protein

LIST OF SYMBOLS

Symbol	Description	Units
°C	Degree Celsius	Degree
E	Young's Modulus	$Pa=N/m^2$
F	Traction Force	N
ν	Poisson's Ratio	---

PREFACE

Well, here it is. The work presented herein is the result of a six-year journey that included two lab relocations, thousands of synthesized polymer substrates, and countless hours spent analyzing and interpreting data. More importantly, it is the result of fantastic collaborations and friendships with esteemed colleagues whose influence extends well beyond the scope of this document.

In the final analysis, my hope is that we have made a significant contribution to the understanding of capillary network assembly. Perhaps one day our findings will be used to help treat disease. As a student of BME, this would be the most rewarding outcome possible. While this dissertation is the culmination of my work at Cornell, it is just the beginning of things to come. Enjoy!

JPC

Ithaca, NY

March 2012

CHAPTER 1

INTRODUCTION

Tissue assembly is a fundamental biological process that results from complex interactions between cells and the extracellular matrix (ECM) [1,2]. In the vasculature, angiogenesis is the process of new blood vessel formation from existing vessels. During angiogenesis, normally quiescent endothelial cells (EC) degrade the basement membrane, proliferate, migrate, and assemble into new capillary networks [3]. While angiogenesis is critical during development and in normal physiological responses like wound healing, it is exploited in disease states like cancer.

Research in angiogenesis grew out of early observations of vascularization in tumors [4,5] suggesting that tumors stimulate capillary formation [6] enabling their growth [7]. By the early 1970s, based on observation in the 1960s that solid tumors were incapable of growth beyond a critical size (3-4 mm) without new blood vessel ingrowth [8,9], Dr. Judah Folkman postulated his pioneering hypothesis that angiogenesis could be targeted to inhibit solid tumor growth [10]. Continued work in this field lead Folkman to publish *Angiogenesis In Vitro* in December 1980 [11] . This seminal work was the first demonstration of angiogenesis *in vitro* and indicated that ECs possess the blueprints required to assemble capillary networks [11].

Since then, research in angiogenesis has focused primarily on understanding the molecular pathways that govern the angiogenic response in disease. For example, vascular endothelial growth factor (VEGF) has emerged as a critical stimulus of EC proliferation, migration [12], and angiogenesis in the tumor microenvironment [13].

In several disease states, an increase in tissue stiffness is associated with altered angiogenesis, *i.e.* new vessel formation that exhibits differences in function and structure compared to vessels in healthy tissue. In diabetic wounds, where collagen glycation increases tissue stiffness [14], wound healing is impaired by deficient angiogenesis [15]. Moreover, in tumor growth, where tumors are associated with an increase in ECM stiffness [16], angiogenic vessels are tortuous and leaky [17]. These findings suggest that, in addition to the biochemical microenvironment, the biomechanical microenvironment plays a role in mediating capillary network assembly in disease.

A hallmark of *angiogenesis in vitro* is the assembly of EC networks, a response where ECs self-organize into ring-like networks with a morphology reminiscent of capillary beds found *in vivo* [11,18]. Several studies suggest that EC network formation is sensitive to the stiffness of the microenvironment. For example, while ECs assemble networks on compliant 2D fibrin and matrigel substrates, ECs decrease network formation on stiff fibrin gels [19] and on matrigel rigidified by polymerization with collagen I [20] or glycation [21]. Similarly, ECs exhibit a decrease in network formation on collagen gels made stiffer by increased collagen concentration [22] or by glycation [23]. In 3D, ECs seeded within fibrin or collagen gels decrease network assembly with increasing gel stiffness [24,25]. While these findings suggest that network assembly is associated with compliant, but not stiff, substrates, the role of matrix mechanics as a mediator of angiogenesis has not been fully described; it is unclear whether, or how, substrate stiffness regulates EC network assembly.

Previous work indicating that EC network assembly is associated with compliant, but not stiff, matrices have been performed with protein substrates where the mechanical

properties are varied by changing protein concentration [19,22,26]. However, this approach may change the number or availability of cell-matrix binding sites that fundamentally alter EC behaviors [27], and makes it difficult to decouple the relative contributions of mechanics and chemistry in these systems. To overcome these challenges, we have utilized polyacrylamide (PA) substrates, a system that allows independent variation of matrix stiffness and chemistry [26,28-31]. While PA substrates are typically inert to EC adhesion, they can be functionalized to display a protein at the substrate surface [32] that enables cell adhesion and allows for the independent variation of mechanical properties and surface chemistry [33].

Understanding how substrate stiffness regulates EC network assembly is crucial for the control of angiogenesis. This is an important consideration for the clinical prevention of angiogenesis in disease states that are associated with an increase in tissue stiffness, like tumorigenesis [16] and diabetes [34], or to promote angiogenesis to vascularize engineering constructs for replacement tissues.

Mechanisms of Stiffness Sensing

The control of capillary network assembly by the mechanical microenvironment requires that cells are aware of, and can respond to, matrix stiffness. Adherent cells are capable of probing the stiffness of the local microenvironment [35], and "stiffness sensing" has been demonstrated in a variety of cell types including endothelial [20,30,36], smooth muscle [29,37], and transformed cells [38,39]. Substrate stiffness engages the mediators of cellular contractility that ultimately effect changes in cell behaviors that enable EC network assembly such as adhesion, spreading, and cell-cell interactions.

Substrate adhesion is enabled by integrins, heterodimeric transmembrane glycoproteins that mechanically link the cell to the ECM [40,41]. Integrins cluster into focal adhesions that anchor actin stress fibers, through a variety of adaptor proteins [42], to the plasma membrane. Integrins thus serve as force transducers that can sense substrate stiffness, mediate cellular contractility, and enable mechanotransduction [43-48].

Within cells, contractility is regulated in part by the Rho family of GTPases. In general, Rho-Kinase (ROCK) is activated by Rho-GTP and alters the activity of myosin light chain kinase, an activator of myosin motor proteins [49]. Myosin motors interact with and tense actin stress fibers [50-52] that create cellular contraction that may be transmitted by integrins [53] to the ECM as traction forces [54]. In ECs, Rho-mediated signaling is thought to facilitate stiffness sensing that enables angiogenic network assembly [55].

The Measurement of Cellular Traction Forces

Cellular traction forces were first observed in seminal experiments as wrinkles or strains in flexible silicone rubber substrates [56]. Since then, several methods have been developed to quantify traction forces generated by adherent cells, including microfabricated post array detectors [57,58] or cantilevers [59], and micropatterned silicone elastomeric substrates [60].

In our own work, we have utilized a technique developed by Dembo and colleagues known as traction force microscopy (TFM) [61,62]. TFM is a tool that maps the magnitude, direction, and spatial orientation of traction stresses exerted by an adherent cell on a deformable substrate (PA gels). This is done by tracking the displacement of

fiduciary markers (fluorescent beads) embedded within the deformable substrate with optical flow algorithms [62]. The displacements are translated into a strain field and traction stresses are computed using Bayesian statistics that determine the most likely traction fields that explain a given strain field [63]. In isolated ECs, the magnitude of traction stresses approaches 10 kPa [30].

The measurement of traction forces has elucidated the complex relationship between cell size, cell adhesion, and force generation. In a variety of cell types, including ECs, there is a positive correlation between the magnitude of traction force and cell size [30,64]. As ECs spread, there is an increase in focal adhesion assembly [27], a response that requires cytoskeletal tension [65]. While focal adhesion size is dependent on the actin cytoskeleton [60], small nascent adhesions are capable of exerting large traction forces [31] that enable cell migration [66].

Traction forces have been implicated in mediating cell-cell interactions and EC network assembly. EC attachment to flexible ECM networks enables the development of traction forces and network assembly [67] that can be disrupted by inhibiting traction forces [22]. These traction force-mediated cell-matrix interactions are thought to create tension-based "guidance pathways" that allow ECs to sense each other at a distance and organize into multicellular structures [68]. It has been demonstrated that ECs sense and respond to the traction stresses exerted by adjacent cells causing alterations in cell migration and cell clustering [36]. These findings suggest that EC network assembly results in part from cellular contractility and traction forces that mediate cell adhesion, spreading, migration, and cell-ECM interactions; however these relationships are not well characterized.

Substrate Stiffness Mediates Cellular Responses that Enable Tissue Assembly

Substrate stiffness has emerged as an important mediator of cellular responses like adhesion, spreading, and migration that are requisite for tissue assembly. Stiff substrates promote an increase in focal adhesion organization [29,69-72] and support increases in cell spreading and actin stress fiber formation [26,71]. In addition, EC shape alters cell-cycle dynamics [73-77] that are critical determinants of growth [78,79].

Substrate stiffness and cell shape alter the polarization and alignment of actin stress fibers in cells [80,81]. The actin cytoskeleton is a critical determinant of cell shape, where the removal of a single actin stress fiber results in rearrangements in shape and cytoskeletal organization throughout the cell [51]. Importantly, EC shape alters the availability of Rho GTPase activating proteins [82] implicated in capillary formation *in vitro* and retinal angiogenesis *in vivo* [83]. These findings demonstrate crosstalk between substrate stiffness, actin cytoskeletal organization, and cell shape that facilitate cellular force balance [45], and suggest that substrate stiffness alters and enables capillary formation.

Substrate stiffness has been shown to alter cellular traction forces and cell migration [37,84,85]. In fibroblasts, traction force generation increases with increasing substrate stiffness [70,86], and cells exhibit durotaxis, migration toward substrates of increasing stiffness [86]. In ECs, it is established that force increases linearly with cell area in response to changes in ligand density [30,31]. However, the relationship between substrate stiffness, cell area, and traction force generation is not well understood. Moreover, much of the work investigating EC traction forces has been performed on isolated cells, and traction force profiles, as well as the role of substrate stiffness in

mediating force profiles, of cells in contact are undefined.

Substrate Stiffness Alters Preferences for Cell-Cell vs. Cell-Substrate Adhesion

In addition to behaviors like adhesion, spreading, growth, and migration, preferences for cell-cell and cell-substrate interactions also enable tissue assembly. Seminal work by Guo *et al*. hypothesized that substrate stiffness mediates a balance between cell-cell and cell-matrix adhesion that governs tissue assembly [87]. When tissue explants were plated on stiff substrates, cells from the explant migrated out of the tissue to cover the substrate. In contrast, explants plated on compliant substrates did not exhibit the migration of cells out of the tissue. It was proposed that these differences were due to preferences for cell-matrix vs. cell-cell adhesion that responded to substrate stiffness in order to optimize mechanical input. For example, when cells sense a stiff substrate (where the substrate resistance to deformation is increased) cells prefer cell-matrix interactions that provide a more optimal mechanical signal than cell-cell interactions. In contrast, when cells sense a compliant substrate (where the substrate resistance to deformation is decreased), cells seek out cell-cell contacts that bolster mechanical input and thus prefer cell-cell rather than cell-matrix interactions.

These findings suggest that, like integrins, the mediators of cell-cell interactions are capable of transmitting force. Cell-cell adhesion is mediated in part by cadherins, transmembrane, calcium-dependent, intercellular adhesion proteins [88]. It has been demonstrated that cadherins are capable of transmitting traction forces [89,90], and that these forces require actomyosin activity [91]. Importantly, significant crosstalk exists between cadherins and integrins [92] that serve as mechanosensors during tissue morphogenesis [93]. In ECs, cell-cell adhesion is mediated in part by vascular endothelial (VE)-cadherin [94]. VE-cadherin-mediated cell-cell interactions alter

cytoskeletal tension [95], cell spreading, focal adhesion formation [96], and require actin cytoskeletal assembly and myosin activity [91]. In turn, changes in Rho-mediated contractility influence cell-cell contacts [97]. These data suggest that cellular contractility is involved in feedback mechanisms that relate cell-cell and cell-substrate adhesions.

Taken together, these findings suggest that EC network assembly results from alterations in substrate stiffness-mediated preferences for cell-cell vs. cell-matrix interactions; however, it is not clear how substrate stiffness contributes to these interactions in capillary network assembly.

Fibronectin Assembly is Requisite for Capillary Network Assembly

EC network assembly is thought to be guided in part by the ECM [67]. During network assembly in 3D fibrin matrices, ECs require fibronectin (FN) matrix fibrillogenesis to promote cytoskeletal organization and actomyosin-dependent tension [98]. These findings implicate ECM FN as an important mediator of capillary network assembly.

FN is a dimeric glycoprotein found in the ECM and basement membranes that is required for embryonic development [99] and cardiovascular tissue morphogenesis [100]. During FN matrix assembly, or polymerization, FN dimers are converted into an insoluble fibrillar matrix [101]. FN is assembled into fibrils by cells [102] through cell-generated forces that stretch and unfold dimer arms [103]. It is thought that Rho-mediated contractility enables FN assembly by exposing cryptic self-assembly sites [104] in FN type III repeats, homology domains containing a β-sandwich structure that can be unfolded to a mechanically stable state [105].

In tissues, FN may contain extra domain B (EDB), a type-III homology domain resulting from differential exon splicing [106]. While essentially undetectable in normal adult tissues [107], EDB-FN is a specific marker for angiogenic blood vessels [108] and may be an important clinical target for localizing tumor vasculature [109]. This has ramifications in cancer, where solid tumors are associated with an increase in tissue stiffness [16], alterations in local vasculature [110], and growth requiring neovascularization [111].

These data implicate EC traction forces in mediating FN assembly; however the relationship between ECs and FN deposition is unknown. Furthermore, these data indicate that FN matrix assembly mediates capillary network assembly, and suggest that substrate stiffness alters EC-FN interactions that enable EC network assembly; however, the role of substrate stiffness in mediating EC-FN interactions unknown.

Dissertation Organization

The goal of this work is to investigate the role of substrate stiffness in regulating capillary network assembly. We demonstrate that substrate stiffness regulates capillary network assembly and alters EC behaviors that enable network formation. In Chapter 2, we determine that network assembly is controlled by plating cells on substrates that minimize cell-substrate adhesion. Compliant (E<1 kPa), but not stiff (E>1 kPa), substrates promote the self-assembly of EC networks. This work demonstrates that EC network assembly requires the polymerization of ECM FN that stabilizes cell-cell interactions. This work is the first demonstration that substrate stiffness regulates capillary network assembly.

In Chapter 3, we investigate the role of substrate stiffness in mediating cell-cell and

cell-matrix adhesion in ECs. We determine that substrate stiffness alters the localization of VE-cadherin-mediated cell-cell adhesions and focal adhesion organization. In addition, we determine that the response to stiffness during network assembly is not unique to ECs. Analogous to ECs, mammary cells assemble into networks on compliant substrates and require laminin deposition. Moreover, laminin-deficient mammary cells are induced to assemble networks in the presence of exogenous laminin indicating that the ECM is a crucial regulator of tissue assembly. We determine that vascular, mammary, and mesenchymal cell network assembly on compliant substrates is associated with ECM colocalization and a reduction in cell-matrix adhesion. This work is the first demonstration that compliant substrates promote network assembly in a variety of cell types by altering cell-cell and cell-matrix adhesion, and cell-matrix colocalization.

In Chapter 4, we investigate the relationship between substrate stiffness, cell area, and traction force generation in ECs. We determine that substrate stiffness and cell area are both significant predictors of traction force generation during cell-cell contact. This work is the first demonstration that substrate stiffness contributes to force generation during endothelial cell-cell interaction.

In Chapter 5, we investigate the role of substrate stiffness in mediating FN deposition. We determine that substrate stiffness alters the deposition of FN through changes in cell shape and ROCK-mediated traction forces. Furthermore, we determine that substrate stiffness alters the synthesis and deposition of EDB-FN, an FN isoform specific to neovasculature. This work is the first demonstration that the mechanical microenvironment plays a role in mediating EC-FN interactions.

In Chapter 6, conclusions and future directions are presented. Chapter 7 overviews my experience as an NSF STEM Fellow in GK-12 Education, where we developed laboratory activities and taught a science curriculum to local middle school students that focused on polymer science.

CHAPTER 2

A BALANCE OF SUBSTRATE MECHANICS AND MATRIX CHEMISTRY REGULATES ENDOTHELIAL CELL NETWORK ASSEMBLY

Published in *Cellular and Molecular Bioengineering* [112][1].
Selected as an *Outstanding Paper* from the 2008 Biomedical Engineering Society (BMES) Annual Meeting [113].

2.1 Abstract

Driven by specific extracellular matrix cues, endothelial cells can spontaneously assemble into networks. Cell assembly is, in part, dictated by both substrate stiffness and extracellular matrix chemistry; however, the balance between substrate mechanics and matrix chemistry in promoting cell assembly is not well understood. Because both mechanics and chemistry can alter cell-substrate and cell-cell adhesion, we hypothesized that cell assembly can be promoted on substrates that minimize cell-substrate adhesivity while promoting cell-cell connections. To investigate these hypotheses, bovine aortic endothelial cells (EC) were seeded on variably compliant polyacrylamide (PA) substrates derivatized with type I collagen and observed over time. Our results indicate that cell assembly can be induced on substrates that are sufficiently compliant (E=200 Pa) and present significant amounts of substrate-bound ligand, and on substrates that are stiffer (E=10000 Pa) but which present less adhesive ligand. In both of these cases, cell-substrate adhesivity is decreased, which may enhance cell-cell adhesivity. Moreover, our data indicate that fibronectin polymerization stabilizes cell-cell contacts and is necessary for network formation to

[1] Figure 2.9 contributed by Tracy Cheung.

occur regardless of substrate compliance or the density of substrate-bound ligand. These data demonstrate the balance between substrate mechanics and chemistry in directing cell assembly.

2.2 Introduction

Angiogenesis is the process of new blood vessel formation. Regulated by factors including shear stress, growth factors, and cytokines, endothelial cells (EC) migrate from pre-existing vessels, proliferate, and differentiate to form new blood vessels [3]. The extracellular matrix (ECM), which includes collagen and fibronectin (FN) [114,115], provides ECs with chemical and mechanical cues that drive migration and invasion [116], events integral to new vessel formation. While these events occur *in vivo*, ECs can be induced to assemble into capillary-like networks that mimic angiogenesis *in vitro* [117] under the appropriate conditions. Because vascularization is critical to most successful tissue engineering, understanding and controlling these conditions may be critical to the *in vitro* development of transplantable organs.

Cell assembly has been shown to be influenced by ECM protein type [118,119], ECM concentration [120,121] and substrate stiffness [122,123] through their effects on cell shape [124], motility, and differentiation [125]. Tissue formation may arise from the optimization of mechanical and chemical input from both cell-cell cohesivity and cell-substrate adhesivity [126,127]. Recent evidence suggests that cellular organization may be directed in part by substrate mechanics; in contrast to compliant substrates, rigid gel substrates promote cytoskeletal and focal adhesion organization and cell spreading [128]. On compliant substrates, cells tend to aggregate rather than migrate away from each other. Substrate mechanics may have a direct effect on EC sorting and subsequent *in vitro* organization. Recent data from our lab suggests that ECs on

compliant substrates prefer cell-cell connections and cluster while those on stiff substrates prefer cell-substrate connections and migrate away from each other [36]. ECs exhibit an increase in projected area and the appearance of actin stress fibers with increasing substrate stiffness [129], and others have suggested that EC capillary morphogenesis may be modulated by a balance between substrate stiffness and traction force generation [123]. Taken together, these data indicate that substrate compliance can directly affect cell organization.

Endothelial cell assembly is further influenced by ECM concentration. EC attachment increases with increasing collagen concentration and promotes the formation of capillary networks at intermediate adhesivity [120]. It has been suggested that FN may control EC assembly by supporting tension-dependent cell shape changes [130]. While it is well accepted that both matrix chemistry and mechanics affect endothelial network formation, the balance between substrate mechanics and matrix chemistry in promoting EC assembly is not well understood.

In this study, the effects of substrate mechanics and matrix chemistry on EC adhesion were investigated to understand the integration of mechanical and chemical signals that mediate cell assembly and network formation. Bovine aortic ECs were seeded on variably compliant polyacrylamide (PA) substrates derivatized with type I collagen. Our results indicate that cell assembly occurs on compliant substrates and not on stiff substrates at a high concentration of matrix collagen, that cell assembly is induced on stiff substrates by lowering the concentration of collagen, and that overall cell assembly is dependent on the ability of ECs to polymerize FN. These results indicate that ECs may integrate mechanical and chemical cues to achieve a balance in cell-cell vs. cell-substrate adhesion; when cell-substrate adhesivity is low, cell-cell connectivity

is increased, and conversely, when cells are firmly adherent to a substrate, they are less likely to assemble.

2.3 Materials and Methods

Coverslip Activation

Coverslips were prepared as previously described [131,132]. Square glass coverslips (No. 2, 22 x 22mm, VWR, West Chester, PA) were passed through the flame of a Bunsen burner, coated with 0.1 N NaOH (Sigma-Aldrich, St. Louis, MO), and allowed to dry. The coverslips were coated with 3-aminopropyl-trimethoxysilane (Sigma-Aldrich, St. Louis, MO), washed in 18.2 MΩcm purified deionized water, and incubated with a coating of a 0.5% solution of glutaraldehyde (70% aqueous stock solution, Sigma-Aldrich, St. Louis, MO) in phosphate-buffered saline ((PBS), Invitrogen, Carlsbad, CA) at room temperature for 30 minutes. The coverslips were washed with 18.2 MΩcm purified deionized water and allowed to dry overnight.

Poly(acrylamide) Gel Synthesis

Gels of various Young's Moduli (E=200, 1000, 2500, 5000, and 10000 Pascals) were synthesized by varying the ratio of acrylamide to bis-acrylamide in the gel solution mixture [129]. Gel mixtures were prepared with 3-7.5% acrylamide (40% w/v solution), 0.04-0.35% N,N'-methylene-bis-acrylamide (2% w/v solution), 0.05% N,N,N,N-tetramethylethylenediamine (Bio-Rad, Hercules, CA), and 30 mM 4-(2-hydroxyethyl)-1-piperazineethanesulfonic acid ((HEPES), pH 6.0, Sigma-Aldrich, St. Louis, MO). The solutions were adjusted to pH 6.0 with 2N HCl (Sigma-Aldrich, St. Louis, MO) and degassed for 30 minutes. Additional solution components were 20 µmol/ml N-6-((acryloyl)amido)hexanoic acid ((N-6), synthesized in our lab according to the method of Pless *et al*. [133]) dissolved in ethanol (Sigma-Aldrich, St. Louis,

MO), and 2% 0.5 μm diameter fluorescent beads (Molecular Probes, Carlsbad, CA). Polymerization was initiated by the addition of a 0.1% ammonium persulfate (Bio-Rad, Hercules, CA) solution in water to the acrylamide mixture. 20 μl of the mixture was pipetted onto an activated coverslip and a circular coverslip (No. 2, 18 mm diameter, VWR, West Chester PA) was used to flatten the drop. Polymerization was allowed to occur for 30 minutes at room temperature. The circular coverslip was removed, and the gel was incubated with 1, 5, 10, 50, or 100 μg/ml of type I rat-tail collagen (Becton Dickinson, Franklin Lakes, NJ) in HEPES (pH 8.0, Sigma-Aldrich, St. Louis, MO) for two hours at 4°C. The un-reacted N-6 linker was capped with 0.1% ethanolamine (Sigma-Aldrich, St. Louis, MO) in HEPES (pH 8.0, Sigma-Aldrich, St. Louis, MO). Gels were washed with sterile PBS and stored in six-well plates.

Cell Culture

Bovine aortic ECs were maintained at 37°C and 5% CO_2 in Medium 199 (Invitrogen, Carlsbad, CA) supplemented with 10% FetalClone III (HyClone, Logan, UT), and 1% each of penicillin-streptomycin, MEM amino acids (Invitrogen, Carlsbad, CA), and MEM vitamins (Mediatech, Manassas, VA). ECs were used from passages 8-12.

Fibronectin Inhibitor and Control

Fibronectin polymerization was inhibited by adding 500 nM pUR4B (a kind gift from Dr. Jane Sottile) to the EC suspension just prior to gel plating. 500 nM III-11C was added to the EC suspension to serve as a control to pUR4B [134,135] (also a kind gift from Dr. Sottile).

EC Network Assembly, Area, and Perimeter Studies

ECs were plated on gels of various Young's Moduli (200-10000 Pa) at a density of 100,000 or 200,000 cells per well of a six-well plate for cell-assembly studies and 50,000 cells per well for area and perimeter studies. 10X magnification images of cells were captured with an Olympus IMT-2 inverted phase contrast microscope with a QImaging Retiga 1300 camera or a Zeiss Axio Observer D1m inverted phase contrast microscope with an AxioCam camera for the duration of the experiment. Media were replenished every other day.

For cell-assembly studies, aspect ratios of ECs within a network morphology were measured with ImageJ (version 1.37, available from the National Institutes of Health, Bethesda, MD, at http://rsb.info.nih.gov/ij/). The aspect ratio was defined as the ratio of straight line-segment lengths drawn onto images of ECs corresponding to the long and short axis of the cells. Aspect ratio measurements were constrained to ECs that were in contact with at least two additional cells. Data were measured and pooled into two groups (n = 150 for each condition) representing the presence or absence of cell assembly across multiple experiments and time points. For area and perimeter studies, ImageJ was used to outline and quantify cells. Area and perimeter measurements were constrained to ECs that were not in contact with any other cells in pre-network, sub-confluent cultures. Data were measured (n = 50 for each gel compliance) across multiple experiments at 24 hours after plating.

Statistical Analysis of Assembly, Area, and Perimeter Measurements

The natural log of aspect ratios, cell area, and cell perimeter measurements were taken to ensure normality of the data. Data were compared with analysis of variance and Tukey's Honestly Significantly Different test or Student's *t* test (Figure 2.8D only) in

JMP software (v.7, SAS, Cary, NC).

Immuno- and Fluorescent Staining for Fibronectin Localization

ECs on PA gels were fixed in 3.7% formaldehyde (Mallinckrodt Baker, Phillipsburg, NJ) at 4°C overnight and washed with PBS as described elsewhere [136]. Samples were incubated with 1% Triton in PBS and 0.02% Tween (Mallinckrodt Baker, Phillipsburg, NJ)/1% bovine serum albumin ((BSA), Sigma-Aldrich, St. Louis, MO) in PBS for one hour. Gels were incubated 1:50 with a mouse monoclonal fibronectin primary antibody (Santa Cruz Biotechnology, Santa Cruz, CA) in PBS/3% BSA in a humidified chamber at 4°C overnight. A 1:200 fluorescein isothiocyanate (FITC)-conjugated goat anti-mouse secondary antibody (Santa Cruz Biotechnology, Santa Cruz, CA) in PBS/3% BSA was applied to the samples for one hour at room temperature. EC filamentous actin was stained with Alexa Fluor 546 phalloidin (Molecular Probes, Carlsbad, CA) 1:25 in PBS and nuclei were stained with 4',6-diamidino-2-phenylindole ((DAPI), Sigma-Aldrich, St. Louis, MO) 1:10 in 18.2 MΩcm purified deionized water. Fluorescent localization was visualized with a Zeiss Axio Observer Z1m with a Hamamatsu ORCA-ER camera. Images were pseudo-colored with Axiovision software v. 4.6.

2.4 Results

Compliant Substrates Promote EC Network Assembly

Previous data suggest that compliant substrates promote cell assembly of a variety of cell types [118,126], including ECs [122,123]. However, in EC network formation, the relative contributions of matrix mechanics and chemistry are unclear. PA gels permit the independent manipulation of the substrate stiffness and matrix chemistry to study the effects of mechanics and chemistry on cell assembly [126,128]. Here, PA

gels were synthesized with Young's Moduli of 200, 1000, 2500, 5000, and 10000 Pa, derivatized with 100 μg/ml of type I collagen, and seeded with ECs. On 200 and 1000 Pa gels, ECs organized into two-dimensional (2D) network structures characterized by cords and looping-cell morphologies (Figures 2.1A and 2.1B, respectively), often seen in tube formation assays. Cords and loops of ECs presented as early as 24 hours after plating and endured for the duration of the experiment. On stiffer gels (2500, 5000, and 10000 Pa), ECs failed to assemble into cords or loops and appeared uniformly distributed throughout the course of observation (Figures 2.1C-2.1E, respectively).

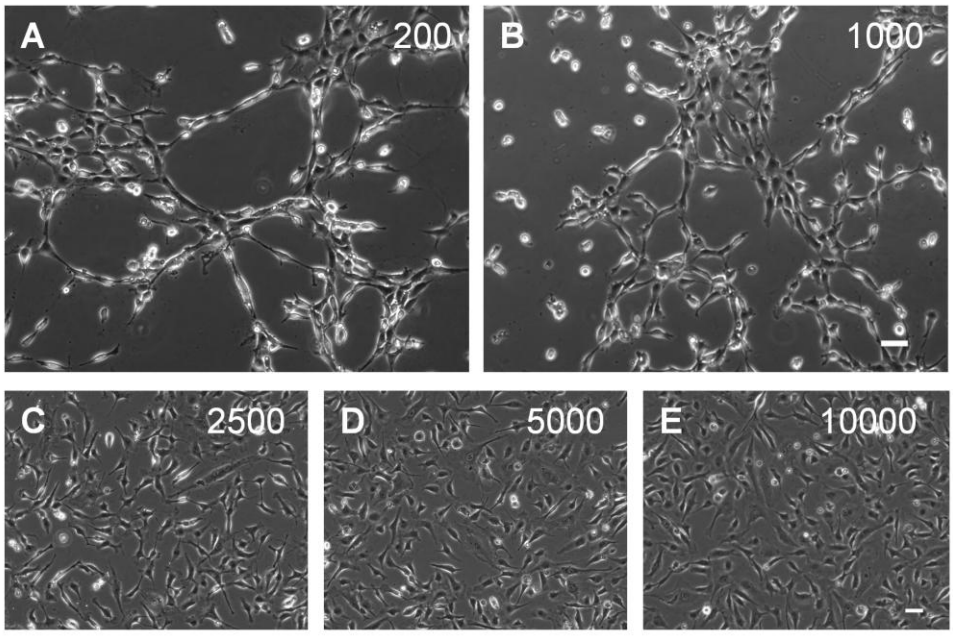

Figure 2.1. Compliant substrates derivatized with collagen promote EC network assembly.
(**A and B**) Phase contrast images of ECs on PA gels derivatized with 100 μg/mL of collagen I assemble into networks on 200 and 1000 Pa substrates, respectively. This phenotype was characterized by cords of cells and ring-like morphologies. (**C–E**) This organization was not present when substrate stiffness was increased to 2500, 5000, and 10,000 Pa, respectively. Scale bars are 50 μm.

In addition to collagen, we investigated the role of substrate stiffness in mediating network assembly on substrates derivatized with FN (Figure 2.2) and an RGD sequence-containing peptide (Figure 2.3). These data indicate that compliant substrates promote network assembly independent of ligand type.

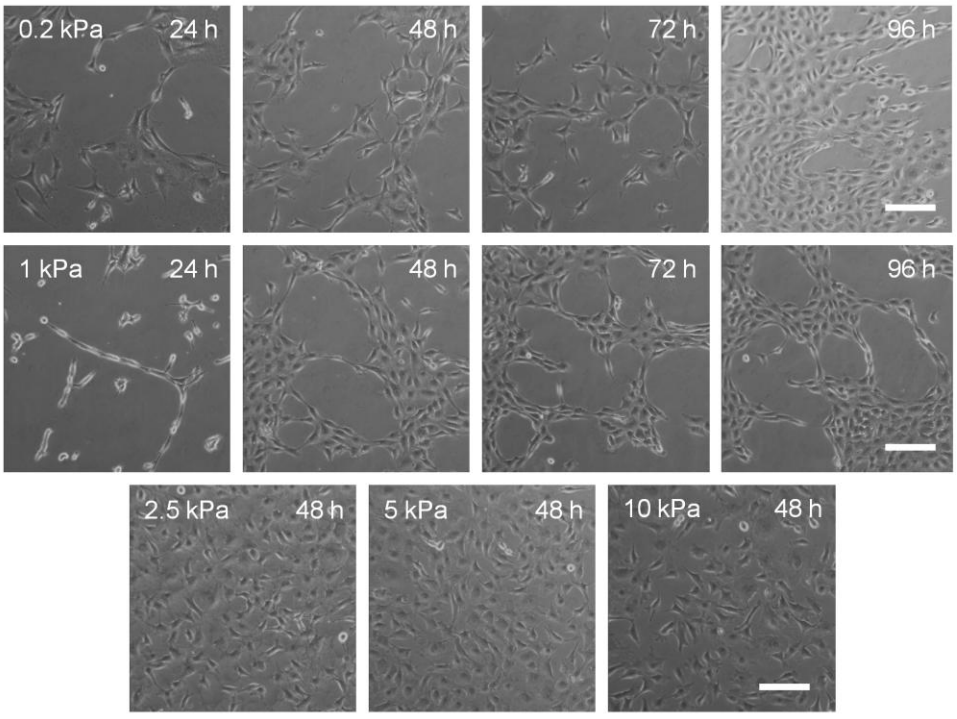

Figure 2.2. Compliant substrates derivatized with FN promote EC network assembly.
ECs were plated on variably compliant (E=0.2-10 kPa) substrates derivatized with 100 μg/mL fibronectin (FN). After 24 hours, ECs on 0.2-1 kPa substrates began to form cords and lacunae, hallmarks of developing networks. Networks continued to develop over 48-96 hours after plating. In contrast, cells on 2.5-10 kPa substrates did not assemble networks but were instead uniformly distributed. Scale bars are 100 μm.

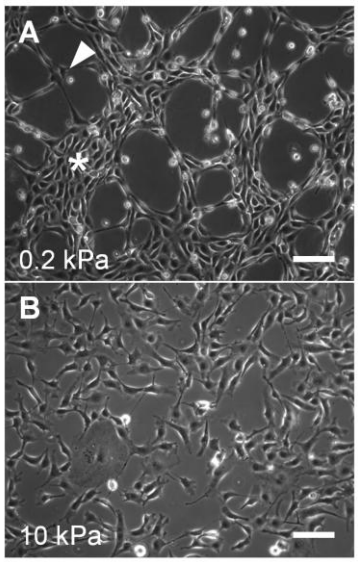

Figure 2.3. Compliant substrates derivatized with RGD promote EC network assembly.
ECs were plated on compliant (*E*=0.2 kPa) and stiff (*E*=10 kPa) substrates derivatized with 100 μg/mL of an RGD sequence-containing peptide (NH_2-YAVTGRGDS-OH, ChemPep, Wellington, FL). The RGD sequence is found in FN and mediates integrin-FN attachment [137]. (**A**) Similar to collagen-derivatized substrates, ECs self-assembled into networks characterized by clusters (*) and cords (arrow head) of cells on compliant substrates. (**B**) On stiff substrates, networks did not form and cells were uniformly distributed across the substrate. Scale bars are 100 μm.

Time lapse microscopy of cell assembly on compliant gels indicated that early cords or line segments of processional ECs branched between nodes of cells and matured into closed-loop ring patterns of cells over time. Cells were observed to sprout from cords to create additional connections (Figure 2.4).

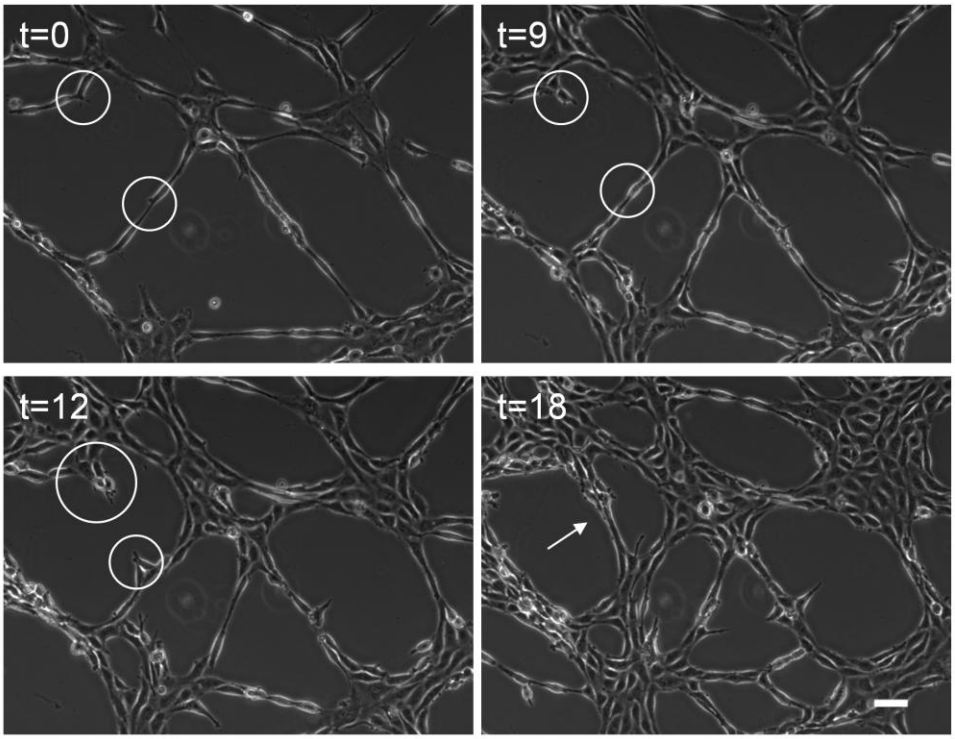

Figure 2.4. Network development over time.
Time-lapse images of EC network development over an 18 hour period. T = 0 corresponded to 96 hours after PA gel seeding. Networks developed as cords of cells that joined together to form 2D ring-like morphologies over time. Circled regions highlight ECs that formed an additional connection (arrow) by sprouting from existing cords. Time in hours. Scale bar is 50 μm.

Cell Network Assembly is Induced on Stiff Substrates by Decreasing Collagen I Concentration

Because ECs tended to form networks on compliant gels where cells are also less spread and adherent, we hypothesized that a decrease in cell-substrate adhesivity enhances cell assembly. To test this hypothesis, PA gels of varying stiffness were synthesized and conjugated with decreased collagen (1 μg/ml) to decrease cell-substrate adhesivity relative to substrates conjugated with 100 μg/ml of collagen. Notably, lowering the concentration of collagen I shifted cell assembly to gels of 2500, 5000, and 10000 Pa (Figures 2.5B-2.5D, respectively), where it was not seen

previously on gels with increased collagen (see Figures 2.1C-2.1E). Cord development occurred on 2500 and 5000 Pa gels as well (Figures 2.5B and 2.5C, respectively) but qualitatively did not develop into looping morphologies as complete as those on 10000 Pa gels (Figure 2.5D). On 200 and 1000 Pa gels, ECs were adherent to the gel but retained a rounded morphology (Figure 2.5A), and thus were unable to form loops. It should be noted that while decreasing the substrate adhesivity on a stiff gel increased network assembly, cell assembly on stiffer gels derivatized with 1 μg/ml of collagen I were less extensive than assemblies formed at 100 μg/ml on compliant gels.

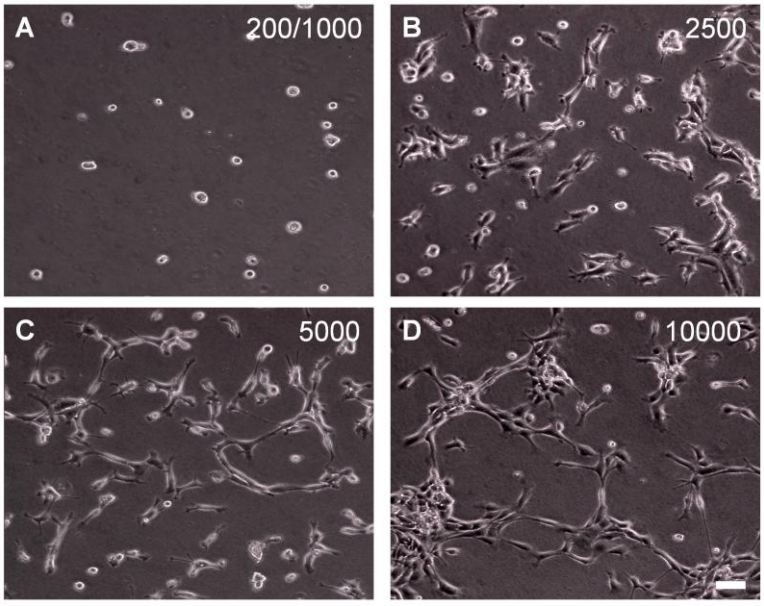

Figure 2.5. Cell network assembly is induced on stiff substrates by decreasing collagen concentration.
(**A**) ECs on PA gels derivatized with 1 μg/mL of collagen I showed limited spreading and an inability to organize into networks but remained adherent to the gel. (**B–D**) Cell network assembly was shifted to 2500, 5000, and 10,000 Pa gels, respectively, in comparison to cells on gels derivatized with 100 μg/mL collagen. Scale bar is 50 μm.

Similar to decreased collagen concentration, network assembly was induced on stiff substrates by decreasing concentrations of FN (Figure 2.6) and an RGD-containing peptide (Figure 2.7).

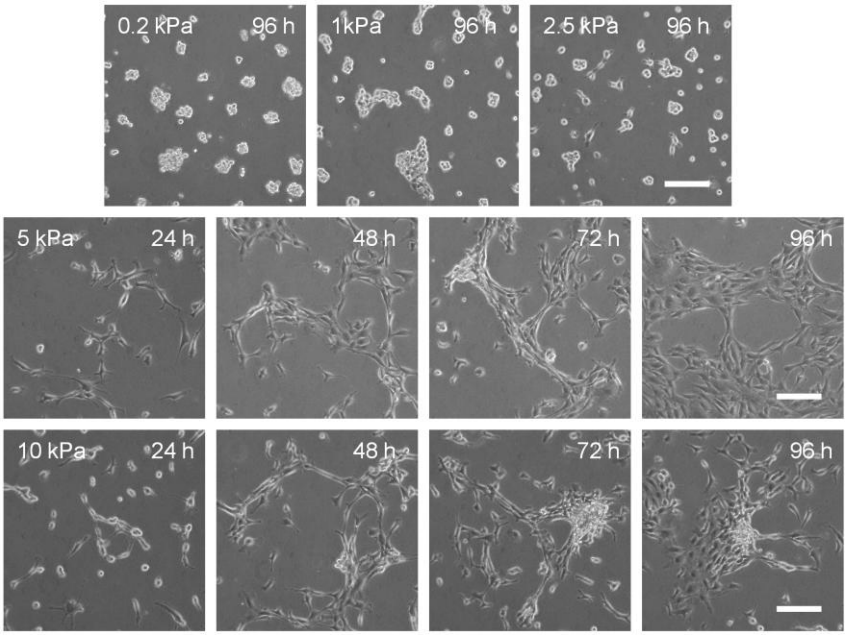

Figure 2.6. Network assembly is induced on stiff substrates by decreasing FN concentration.
ECs were plated on variably compliant (E=0.2-10 kPa) substrates derivatized with 1 μg/mL FN. On 0.2-2.5 kPa substrates, network assembly did not occur but cells instead formed aggregates over 96 hours. Similar to results found with collagen, network assembly was induced on stiffer 5-10 kPa substrates. Scale bars are 100 μm.

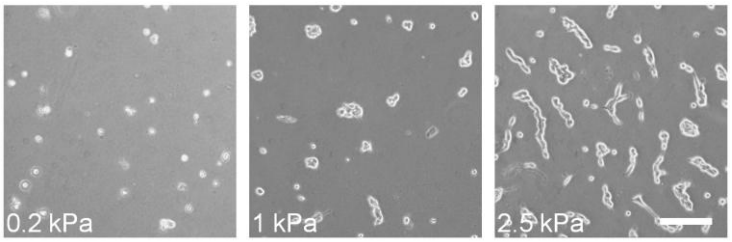

Figure 2.7. Cell-cell adhesion is induced on stiff substrates by decreasing RGD concentration.
ECs were plated on variably compliant (E=0.2-2.5 kPa) substrates derivatized with 1 mg/mL of an RGD-sequence containing peptide (NH_2-YAVTGRGDS-OH). After 96 hours, cells on 0.2 kPa substrates were not well spread. On 1 kPa substrates, cells began to form clusters and formed network-like cords on 2.5 kPa substrates. Scale bar is 100 μm.

Taken together, these data indicate that compliant substrates foster network assembly regardless of matrix ligand type, and that network assembly results from a balance of substrate stiffness and matrix chemistry.

Ratio of Area to Perimeter Correlates with EC Assembly

To explore the mechanism of cell assembly, we measured changes in cell morphology as a function of gel modulus and ligand density. Area and perimeter measurements were limited to ECs that were not in contact with any other cells in pre-network, sub-confluent cultures. Cell area (Figure 2.8A, white bars) and perimeter (Figure 2.8B, white bars) increased with increasing substrate stiffness. When the collagen concentration was decreased to 1 μg/ml, the cell area (Figure 2.8A, black bars) and perimeter (Figure 2.8B, black bars) decreased. Cell adhesion and spreading were insufficient to measure on 200 and 1000 Pa gels derivatized with only 1 μg/ml collagen. Notably, area and perimeter alone were not necessarily predictors of cell assembly as cell areas of statistical similarity were observed in cases of both the presence and absence of cell assembly (*e.g.* Figure 2.8B, compare the statistically similar 2500 Pa gel white bar, where networks did not form, to the 5000 Pa gel black bar, where networks did form). However, it was determined that the ratio of EC area to perimeter did correlate with cell assembly. Sub-confluent ECs with a significantly lower ratio of area to perimeter developed into network structures (Figure 2.8C, below the dashed line), whereas those with a higher ratio typically did not form network structures (Figure 2.8C, above the dashed line). Therefore, the ratio of area to perimeter appeared to be a predictor of future EC assembly, where rounder cells were less likely to form spontaneous networks.

Assembled ECs have an Increased Aspect Ratio

To quantify cell assembly, observed in Figures 2.1 and 2.4, the aspect ratio of ECs in cell assemblies was measured (Figure 2.8D). The aspect ratio was defined as the ratio of the long axis to the short axis of ECs making at least two cell-cell contacts. The aspect ratio of ECs assembled in cords or loops (Figure 2.8D, starred (+) bar) was significantly different than the aspect ratios of ECs not arranged in networks (Figure 2.8D, (-) bar). Cell assembly was not quantified by more traditional methods including skeletonizing the micrographs [123] or measuring lengths of cords [138], because in our samples cell assembly was most extensive approximately four days after plating when cells on stiffer substrates were 100% confluent, and these measurements could not be done.

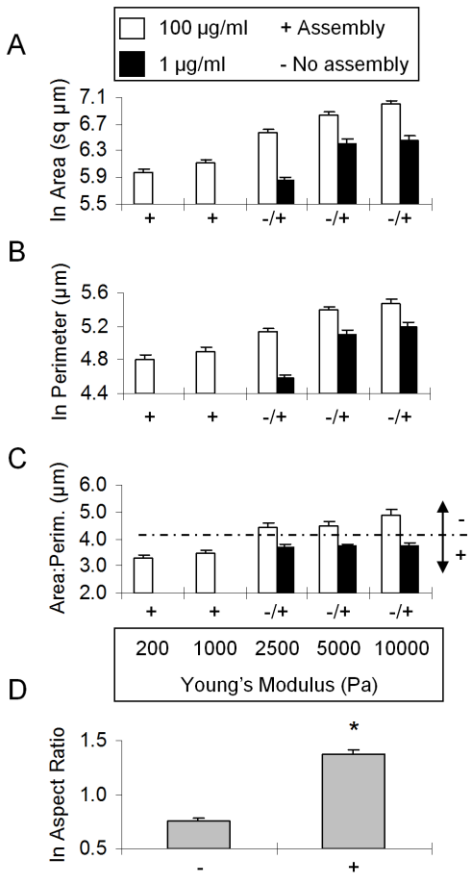

Figure 2.8. Ratio of area to perimeter predicts EC network assembly.
(**A** and **B**) Cell area and perimeter increase on PA gels derivatized with 100 µg/mL of type I collagen with an increase in substrate stiffness (white bars). Cell area and perimeter was reduced by lowering the collagen I concentration to 1 µg/mL but still increased with substrate stiffness (black bars; insufficient spreading to measure on 200 and 1000 Pa gels). (**C**) Measurements of ratios of EC area to perimeter showed statistical significance between the occurrence (bars below dashed line) and absence (bars above dashed line) of cell network assembly. Note that the occurrence and absence of cell network assembly show statistical similarity within each group. (**D**) Aspect ratios showed statistical significance between the occurrence (+) and absence (-) of cell network assembly. ‘‘*’’ Indicates $p<0.001$, +/- indicates the presence or absence of cell network assembly, respectively. Mean + SEM.

With the help of Tracy Cheung, we also characterized the role of substrate stiffness in mediating EC proliferation (Figure 2.9). Our data indicate that proliferation increases with increasing substrate stiffness over time, and that proliferation rate is dependent on ligand concentration.

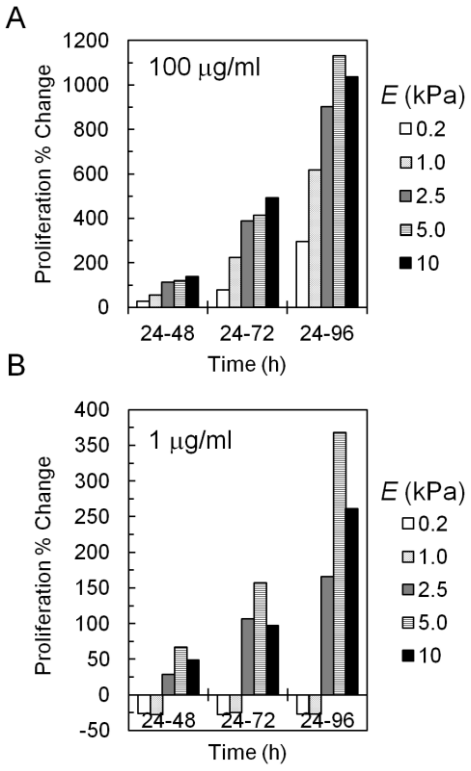

Figure 2.9. Substrate stiffness and ligand concentration alter EC proliferation. ECs were plated on variably compliant (E=0.2-10 kPa) substrates derivatized with 100 or 1 μg/mL collagen I. To measure proliferation, Tracy Cheung painstakingly imaged the entire substrate and counted cells at each time point. (**A**) On substrates derivatized with 100 mg/mL collagen, cell proliferation increased with time and with substrate stiffness. (**B**) On substrates derivatized with 1 μg/mL collagen, cells failed to proliferate on 0.2-10 kPa substrate. On 2.5-10 kPa substrates, proliferation increased over time and was greatest on 5 kPa substrates, but was less than proliferation observed on substrates derivatized with 100 μg/mL collagen.

FN Fibers Colocalize with EC Network Assembly

Recent data suggest that FN is required for EC assembly in 3D [139]. While it is known that cell spreading and FN polymerization are linked [140], and spreading

increases with matrix stiffness [129], it is unclear how matrix stiffness affects FN polymerization during cell assembly. To assay for the presence of FN in networks formed on 2D compliant gels, ECs on PA gels of varying compliance were stained with a FITC-conjugated anti-fibronectin antibody. FN fibrils colocalized with ECs organized into networks (Figure 2.10A) whereas FN was uniformly distributed in samples where networks did not form (Figure 2.10B). Interestingly, FN also colocalized with networks formed on gels conjugated with decreased collagen, however the FN appeared more web-like (Figure 2.10C) in comparison to the FN fibrils formed by cells in networks on compliant gels.

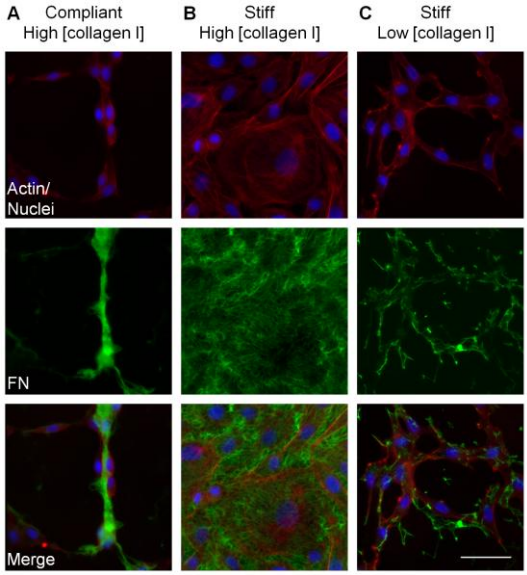

Figure 2.10. FN colocalizes with EC network assembly.
PA gels of 200, 1000, 2500, 5000, and 10,000 Pa were derivatized with 100 μg/mL of type I collagen and plated with ECs. Samples were fixed and stained with a FITC-conjugated anti-fibronectin antibody. (**A**) ECs assembled into cords and loops that were colocalized with FN. (**B**) FN was uniformly distributed in samples where networks did not form. (**C**) FN signal appeared web-like on 10,000 Pa gels when the collagen I concentration was lowered to 5 or 10 μg/mL. Scale bar is 50 μm.

ECs Do Not Require Exogenous FN to Assemble into Network-like Structures

Because EC assembly was associated with FN (see Figure 2.10A), and others' data suggest that cell assembly proceeds independently of exogenous layers of ECM [118],

we sought to determine whether serum-derived FN was *necessary* for 2D cell assembly on compliant substrates. ECs were seeded on variably compliant PA gels derivatized with collagen, either in the presence of media with fibronectin-free serum (experimental condition) or in the presence of media with complete serum (control). FN-free media appeared to have no effect on cell assembly at a high collagen I concentration (100 μg/ml, as depicted in Figure 2.1), however cell assembly on stiff 10000 Pa gels derivatized with low amounts of collagen was shifted to gels derivatized with 5 and 10 μg/ml of collagen I where it was previously seen at 1 μg/ml. Despite the lack of exogenous FN in the media, FN staining still colocalized with networks of cells, indicating cells were secreting and polymerizing their own FN (Figure 2.11).

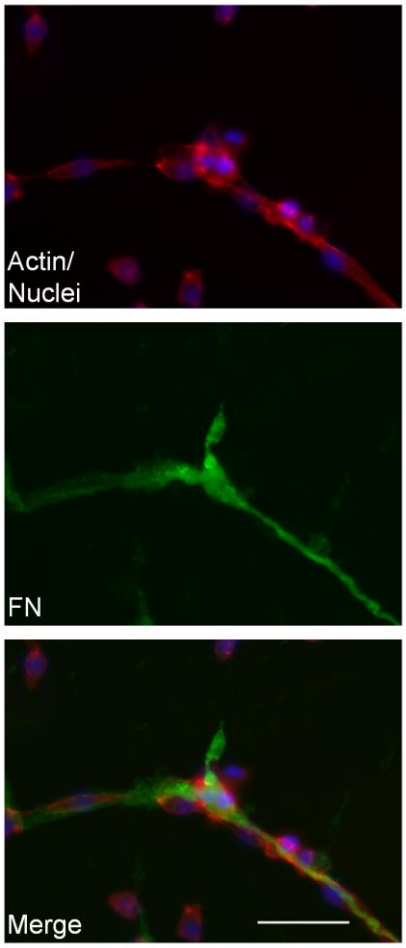

Figure 2.11. ECs do not require exogenous FN to assemble into network-like structures.
ECs were seeded on PA gels and derivatized with collagen I in media with FN-free serum (a gift from Dr. Jane Sottile; experimental condition) or in media with complete serum (control). Samples were seeded with ECs and stained with a FITC-conjugated anti-FN antibody. In the presence of media containing FN-free serum, cell network assembly occurred on 200 and 1000 Pa gels and was associated with FN staining. Scale bar is 50 μm.

EC Assembly on Compliant Substrates Requires FN Polymerization

Our data indicate that EC assembly is associated with FN deposition (Figure 2.10) and yet is independent of exogenous FN from serum (Figure 2.11). To determine whether FN polymerization is requisite for cell assembly, 500 nM pUR4B, a fibronectin polymerization inhibitor, or a control peptide, III-11C [134,135], was added to cultures on variably compliant PA gels.

In the presence of the FN polymerization inhibitor, no networks formed on any type of gel, whereas in the presence of the control peptide, networks formed under the same conditions where they formed previously. On 200 Pa gels, where EC networks typically form, EC assembly was very transient in the presence of pUR4B (Figure 2.12A). Cells were adherent and appeared to form small cords, but ECs in this configuration were not seamlessly well connected and were generally rounded in shape, unlike those observed on 200 Pa gels without the inhibitor. Time lapse images revealed that ECs on 200 Pa gels treated with pUR4B appeared more motile than control cells in networks (data not shown) and failed to develop stable assemblies of cords or loops; instead, transient cell-cell connections formed that disassembled over time (Figure 2.12A).

Immunostaining of cells treated with FN inhibitor revealed a punctuate distribution of FN surrounding the cells (Figure 2.12B). This was in stark contrast to the fibrils formed between cells when the inhibitor was not added (see Figure 2.10).

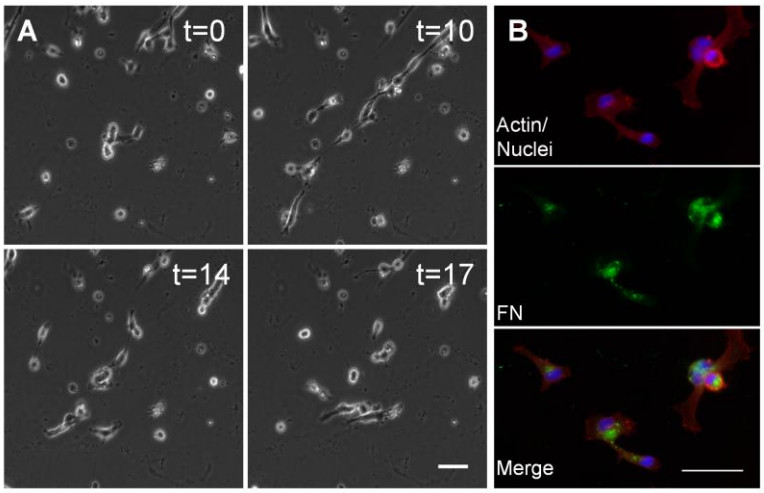

Figure 2.12. EC network assembly on compliant substrates requires FN polymerization.
(**A**) ECs were seeded on PA gels with media containing 500 nM pUR4B FN polymerization inhibitor or 500 nM III-11C control peptide (gifts from Dr. Jane Sottile). On 200 Pa gels in the presence of pUR4B, EC network assembly was disrupted with regions of transient assembly. Time-lapse images over a 17 hour period revealed that ECs treated with pUR4B failed to develop complete network structures; instead, cell clusters made transient cell–cell connections that disassembled over time. T = 0 corresponded to 48 hours after plating. Time in hours. (**B**) On 1000 and 10,000 (1 μg/mL of collagen I) Pa gels, cell network assembly was ablated in the presence of pUR4B. FN surrounding cells treated with pUR4B appeared punctate. Scale bars are 50 μm.

Interestingly, individual, subconfluent cells on stiffer, 2500 and 10000 Pa gels conjugated with 100 μg/ml of collagen, that normally would not form networks, when treated with FN polymerization inhibitor, displayed a morphology that was typically indicative of future cell assembly (Figure 2.13). Cells were more elongated and spindle-shaped. However, despite this pre-network-like morphology, these cells did not form networks. Time-lapse microscopy of cells on these substrates in the presence of FN inhibitor indicated that cells formed connections and elongated, but upon elongation, the connection between cell tethers either broke or one of the cells released from the substrate and rounded up (Figure 2.13). In the presence of FN inhibitor, these cells displayed impaired cell-cell and cell-substrate adhesion, perhaps attributed

to their cell shape change and inability to form stable cell-cell connections.

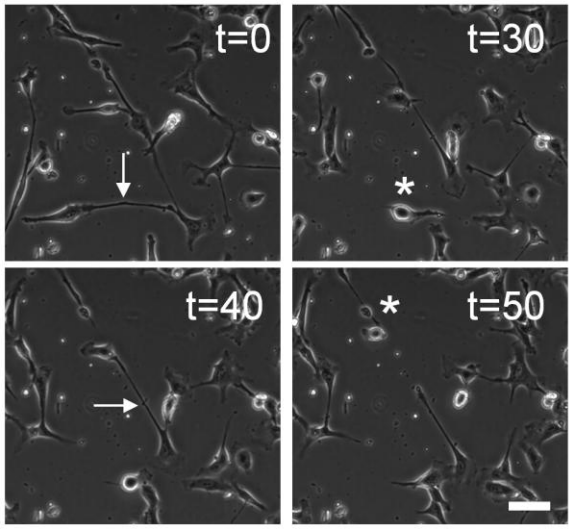

Figure 2.13. Inhibiting FN polymerization disrupts the balance between cell–cell and cell–substrate adhesivity.
ECs were seeded on 10,000 Pa gels conjugated with 100 μg/mL of collagen I in the presence of FN polymerization inhibitor and recorded using time-lapse microscopy. When FN polymerization is inhibited, cells appear more elongated and spindle-shaped with long cell–cell connections (arrows) which are typical of cells prior to network formation. However networks do not form; cell–cell connections are transient and tend to break and/or result in cells rounding and releasing from the substrate (asterisk). Time in minutes. Scale bar is 50 μm.

2.5 Discussion

To investigate the balance of substrate mechanics and matrix chemistry in mediating EC assembly, variably compliant PA gels were synthesized and derivatized with two (high and low) concentrations of type I collagen. Cell assembly occurred on 200 and 1000 Pa gels, and not on 2500, 5000, or 10000 Pa gels when the collagen concentration was 100 μg/ml. Cell assembly was shifted to stiffer gels (2500, 5000, and 10000 Pa) when the concentration of collagen was lowered to 1 μg/ml. We hypothesize that EC assembly results from a balance between cell-cell and cell-matrix interactions as modulated by substrate stiffness and ECM matrix chemistry, and that

cell assembly results from an optimization of mechanical input [126].

The formation of cell assemblies due to substrate stiffness may be due to an alteration of associated focal adhesion and cytoskeletal proteins that mediate cell-substrate interactions through a tactile-sensing feedback mechanism linked to adhesion and net contractile forces [35]. It is well established that focal adhesion size and number and stress fibers are reduced on compliant substrates [129] and substrates with less ligand available to bind [128]. Cell assembly is disrupted when traction forces are inhibited [119], and it has been shown that a decrease in substrate rigidity, through a decrease in collagen content, induces EC cord-like morphologies with associated decreased concentrations of actin, talin, and vinculin [122]. Additionally, type I collagen mediates capillary cell assembly via β1 integrin-activated Src and Rho activation that disrupts VE-cadherin interactions at the cell-cell junctions and induces actin stress fibers [141]. Changes in these cell-cell-, cell-substrate-, and cytoskeletal-associated proteins may affect cell-generated tensile forces based on ECM density; high ECM density promotes cell spreading while lower concentrations permit EC shape changes that promote capillary tube formation [124]. Changing the density of ECM attachment sites causes cell shape changes that can affect differentiation of capillary cells [73,130] resulting in enhanced tube formation [142]. These results suggest that on a high collagen concentration-derivatized compliant substrate, and on a low collagen concentration-derivatized stiff substrate (conditions that promoted EC assembly), inadequate mechanical input, as mediated by substrate stiffness and matrix ligand concentration, drove ECs to prefer cell-cell contacts that increased mechanical input and fostered cell assembly.

FN polymerization colocalizes with EC networks. It was shown previously that tube

formation was associated with FN [143,144] and that ECs form networks of cords independent of exogenous layers of ECM [118]. Cell assembly on PA gels was associated with FN deposition and independent of exogenous soluble FN. On stiff 10000 Pa gels, a low collagen concentration resulted in cell assembly with or without FN-containing serum used in the media. This result suggests that a decreased adhesivity (due to a decreased collagen concentration), and not soluble ECM, induced cell assembly. The inhibitor pUR4B is a 49-mer peptide that binds to, and inhibits, FN matrix polymerization [134] by interfering with the interaction of FN and molecules at cell-surface assembly sites [145]. It has been suggested that FN polymerization is integral to maintaining ECM FN [146], and it has been shown to regulate neovessel formation by supporting cytoskeletal organization and the development of actomyosin-dependent tension [139]. Our data further show that EC 2D cell assembly requires FN polymerization. Figure 2.12A indicates that EC plated on 200 Pa gels, where networks normally form, when treated with pUR4B form transient assemblies characterized by rounded cells. Time lapse images revealed that these ECs appeared more motile, and made transient cell-cell connections compared with control cells in networks. These results suggest that ECs require FN polymerization to stabilize cell-cell interactions that promote cell assembly. While pericellular FN polymerization plays a role in 3D neovascularization [139] that may occur during angiogenesis, both the combination of a compliant substrate that drives EC proximity, and FN polymerization which stabilizes cell-cell contacts, facilitate EC 2D assembly.

Our data also indicate that FN polymerization plays a key role in the balance between cell-cell and cell-substrate adhesion that drives network assembly. When ECs are unable to polymerize FN, their ability to spread is impaired [140], therefore the cells

are generally smaller, appear more spindle-shaped and appear to be less adherent to the substrate. When cell-substrate adhesion is decreased, cells typically shift the balance to cell-cell adhesion [127], and increased cell assembly and aggregation. So we might expect that by inhibiting FN polymerization, cell assembly might increase due to a decrease in cell spreading and cell-substrate adhesion. However, FN polymerization also appears to reinforce cell-cell connections (Figure 2.12). Therefore, when FN fibril formation is inhibited, cell-cell adhesions are unstable and transient. Clearly, there exists a balance where FN polymerization supports and strengthens the formation of stable cell-cell contacts without enhancing cell spreading to the extent that cell-cell contact is no longer preferred over cell-substrate adhesion.

Together, these data indicate that substrate mechanics or decreased cell-substrate adhesivity through changes in matrix density can drive cells into a network-like assembly, and FN polymerization is required to form stable cell-cell contacts. These results should help further guide the design of biomaterials intended to foster angiogenesis.

CHAPTER 3

SUBSTRATE STIFFNESS ALTERS CELL-CELL AND CELL-MATRIX INTERACTIONS THAT REGULATE NETWORK ASSEMBLY

Portions of this chapter are in preparation for submission.[1,2]

3.1 Abstract

Tissue formation arises from a complex interaction between cells and their extracellular matrix, and is thought to result from a balance of cell-cell and cell-matrix adhesivity. In our previous work, we demonstrate that substrate stiffness mediates capillary network formation, the self-assembly of endothelial cell networks on compliant, but not stiff, substrates. While it is known that substrate stiffness alters cell aggregation, the role of substrate stiffness in mediating cell-cell and cell-matrix interactions that give rise to capillary network assembly are not well described. Herein, we demonstrate that substrate stiffness alters the expression and spatial localization of vascular-endothelial (VE) cadherin, a prominent mediator of endothelial cell-cell adhesion. Our data indicate that compliant substrates promote cell-cell interactions characterized by tight and mature VE-cadherin-mediated cell-cell junctions. Endothelial cells on compliant substrates exhibit a reduction in cell-substrate adhesion suggesting a preference for cell-cell vs. cell-substrate adhesion. In addition, we demonstrate the sensitivity of network assembly to substrate stiffness in mammary and mesenchymal tissue-derived cells and show that network assembly on compliant substrates is associated with i) extracellular matrix colocalization and/or ii)

[1] Figure 3.1E-F contributed by Dr. Christine Montague.
[2] Figure 3.5C contributed by Alina Starchenko.

a reduction in cell-substrate adhesion. These findings demonstrate that network assembly results from a balance between cell-cell and cell-matrix adhesion, and suggest that substrate stiffness is a critical regulator of network assembly.

3.2 Introduction

Tissue formation is a fundamental biological process that involves a complex interaction between cells and the extracellular matrix (ECM), and is thought to arise from a balance of cell-cell and cell-matrix adhesive forces [147]. When cell-matrix adhesion is reduced, cells are prone to cluster (prefer cell-cell interactions). In contrast, when cell-cell adhesion is reduced, cells tend to disperse (prefer cell-substrate interactions). This response is also recapitulated by altering the mechanical environment of cells. On compliant substrates, cells prefer cell-cell interactions and cluster, while those on stiff substrates tend to disperse [87]. These findings suggest that substrate stiffness plays a role in mediating cell-cell and cell-matrix adhesion events that enable tissue assembly; however these relationships are poorly understood.

In our previous work, we have demonstrated that compliant, but not stiff, substrates promote capillary network assembly [112]. This response is characterized by the self-assembly of endothelial cells (EC) into clusters and cords of cells that form interconnected ring-like networks reminiscent of capillary beds [11]. While we have established that ECs prefer cell-cell contacts on compliant substrates [36,112], the mechanisms mediating these preferences are unknown.

Endothelial cell-cell adhesion is largely mediated by vascular endothelial (VE)-cadherin, a major transmembrane receptor governing intercellular adhesion [148]. Cell-matrix adhesion is mediated by focal adhesions, clusters of integrins that act as

mechanosensors and link the ECM to the cytoskeleton [43]. In addition, ECM proteins play a prominent role in mediating cell-cell adhesion. We have shown previously that the assembly of ECM fibronectin (FN) stabilizes cell-cell interactions and is requisite for capillary network assembly [112]. These findings suggest that substrate stiffness promotes capillary network assembly by altering VE-cadherin and focal adhesion-mediated cell-cell and cell-substrate interactions in ECs; however these interactions are not well described.

In this study, we examined the role of substrate stiffness in altering the mediators of cell-cell and cell-matrix interactions that regulate capillary network assembly. Our data indicate that substrate stiffness alters the localization of VE-cadherin in ECs. Compliant substrates reduce cell-substrate adhesivity and promote network assembly characterized by tight and mature VE-cadherin-mediated cell-cell junctions. We extend these findings to other cell types and demonstrate that network assembly on compliant substrates is not unique to ECs. Cells derived from mammary and mesenchymal tissue are induced to assemble networks on compliant substrates and exhibit ECM colocalization and a reduction in cell-substrate adhesion. In contrast, cells lacking strong cell-ECM associations and exhibiting insensitivity to alterations in cell-substrate adhesion did not assemble networks. Together, these data suggest that substrate stiffness alters cell-cell and cell-substrate interactions that regulate network assembly.

3.3 Materials & Methods

Cell Culture

Bovine aortic endothelial cells (VEC Technologies, Rensselaer, NY) were maintained as described previously [112,149]. MCF-10A mammary epithelial cells (American

Type Culture Collection, Rockville, MD, CRL-10317) were maintained in DMEM supplemented with 5% (v/v) horse serum, 20 ng/mL EGF (Invitrogen), 10 μg/mL insulin, 0.5 μg/mL hydrocortisone, 100 ng/mL cholera toxin (Sigma-Aldrich, St. Louis, MO), and 1% (v/v) penicillin-streptomycin (Invitrogen) [150]. MDA-MB-231 highly metastatic breast adenocarcinoma cells (ATCC, HTB-26) were maintained in Minimum Essential Medium supplemented with 10% (v/v) FBS, and 1% (v/v) penicillin-streptomycin (Invitrogen). C3H/10T1/2 mouse mesenchymal progenitor cells (ATCC) were maintained in BME media supplemented with 10% (v/v) heat-inactivated FBS and 1% (v/v) L-glutamine (Invitrogen). After passage 5, cells were maintained in DMEM supplemented with 10% (v/v) FBS, 1% (v/v) L-glutamine, and 1% (v/v) penicillin-streptomycin (Invitrogen) according to ATCC protocol. A7r5 rat smooth muscle cells were maintained in DMEM supplemented with 10% (v/v) FBS and 1% (v/v) penicillin-streptomycin (Invitrogen). BEAS-2B bronchial epithelial cells (ATCC, CRL-9609) were maintained in BECB Medium supplemented with SingleQuots (Lonza) according to ATCC protocols, and 1% (v/v) penicillin-streptomycin (Invitrogen). A549 metastatic lung carcinoma cells (ATCC, CCL-185) were a kind gift from Dr. Paraskevi Giannakakou (Weill Cornell Medical College) and were maintained in RPMI 1640 supplemented with 10% (v/v) FBS and 1% (v/v) penicillin-streptomycin (Invitrogen). All cells were cultured at 37^{o}C and 5% CO_2. Live cell imaging was performed in a custom temperature, humidity, and CO_2-controlled stage of a Zeiss Axio Observer Z1m inverted phase contrast microscope with a Hamamatsu ORCA-ER camera.

Polyacrylamide Substrates and Stiffness Characterization

Variably compliant poly(acrylamide) (PA) gels were prepared as described previously [28,112,149] and derivatized with an applied type I collagen (BD, Franklin Lakes, NJ)

concentration of 100 μg/ml, or a mixture of 10%:90% collagen to laminin (Sigma) for Figures 3.16-3.17. Matrigel substrates (Figure 3.16A-B) were prepared in well-plates according to the manufacturer's instructions. PA substrates were synthesized with Young's Moduli (*E*) of 0.2-10 kPa to mimic physiologically relevant tissue stiffness [151]. Substrate stiffness was confirmed by measuring *E* at the gel surface using Hertz theory as described previously [30,149].

Western Blot for VE-Cadherin

Subconfluent ECs on PA (*E*=0.2-10 kPa) substrates or polystyrene were lysed with buffers to separate Triton-soluble and Triton-insoluble proteins [152]. Triton-soluble fractions were extracted with 1% (w/v) NP-40 and 1% (v/v) Triton in Tris-buffered saline (TBS; 10 mM Tris-HCl, 150 mM NaCl) with 2 mM $CaCl_2$ (JT Baker, Phillipsburg, NJ) pH 7.5, and protease inhibitor cocktail (1:500, Sigma-Aldrich, St. Louis, MO). The Triton-insoluble fractions were extracted with 0.5% (w/v) sodium dodecyl sulfate and 1% (w/v) NP-40 (JT Baker) in TBS. The supernatants were analyzed with a protein assay (Bio-Rad, Hercules, CA) and subjected to gel electrophoresis (15 μg per sample; 8% acrylamide gel) and Western blot. Antibodies to VE-cadherin (C-19, Santa Cruz Biotechnology, Santa Cruz, CA), and to β-actin (AC-15, Sigma) were detected by chemiluminescence on a Bio-Rad ChemiDoc imaging system. Densitometry of VE-cadherin was performed with Quantity One (v. 4.6.5; Bio-Rad) and expressed as a ratio to β-actin. Total cell VE-Cadherin was calculated by adding the VE-Cadherin/β-Actin ratios for Triton-soluble and Triton-insoluble fractions and the VE-Cadherin in each fraction was determined as a percent of the total VE-Cadherin. Results are the average of three independent experiments.

Centrifugation Assay

A centrifugation assay was performed as described previously by Guo *et al*. [87]. Cells were plated on variably compliant (E=0.5-10 kPa) PA gels and allowed to adhere for 25 minutes. A chamber was assembled by the addition of a silicone o-ring and top coverslip, inverted, and centrifuged at 500 xg for 10 minutes. Substrates were imaged and cells were counted with ImageJ [153]. The percentage of adherent cells was determined as the ratio of adherent cells after centrifugation to the number of cells from static controls. For ECs, (Figure 3.5C), ratios were normalized to the 10 kPa substrate and fit with a logistic equation (modified from [154]) of the form $f=1/(1+\exp(-b[E-p])$, where f is the adherent cell fraction, b and p are the fitted slope and inflection point, respectively, and E is the substrate Young's Modulus in kPa. Data were the average of three independent experiments.

Fluorescent Localization

Cells on PA gels were processed for fluorescence imaging as described previously [112]. Briefly, samples were fixed in 3.7% (w/v) formaldehyde for 30 minutes, permeabilized with 1% (w/v) Triton, washed with 0.2% (v/v) Tween in PBS, blocked with 3% (w/v) BSA in 0.2% (v/v) Tween in PBS for one hour, and incubated overnight at 4°C 1:50 in 1% BSA (w/v) in PBS with either an anti-VE-cadherin (C19), E-cadherin (H-108), fibronectin (A17), laminin (GB3) (SCBT), or collagen (755P; Millipore) primary antibody. For paxillin staining, samples were blocked with 40% (v/v) heat-denatured FBS in PBS for one hour, and incubated with an anti-paxillin primary antibody (177; BD) overnight. Samples were incubated with Alexa Fluor secondary antibodies, or Alexa Fluor-labeled phalloidin for one hour, stained with DAPI to localize cell nuclei, and imaged with a Zeiss Axio Observer Z1m or Zeiss 700 LSM confocal microscope with a Hamamatsu ORCA-ER camera.

EGTA and VE-Cadherin Blocking

To disrupt cell-cell interactions, ECs were plated in the presence of 5 mM ethylene glycol tetraacetic acid (EGTA) in complete media or vehicle control. To specifically block VE-cadherin engagement, ECs were plated in the presence of 5 μg/mL VE-cadherin blocking antibody [155] (BV9; SCBT) in complete media or vehicle control. VE-cadherin was stained and imaged as described above.

Laminin Knockdown

To knockdown laminin expression, MCF-10A cells were transfected with siRNA against laminin-5 chains α3, β3, or γ2, or a control siRNA (SCBT) by incubation in Lipofectamine 2000 (Invitrogen). Cells were plated on compliant (E=0.2 kPa) substrates 24 hours after transfection for two days. Separate preliminary experiments determined laminin expression with Western blotting over the same time course using anti-laminin α3 (N20), β3 (A6), or γ2 (B2) antibodies (SCBT).

Statistics

Data for figures Figures 3.1F, 3.5C were analyzed with analysis of variance (ANOVA) and Tukey's HSD test. Data for centrifugation tests were analyzed with Student's *t* test. Plots were reported as mean +/- SE. Analyses were performed with JMP (SAS, Cary, NC).

3.4 Results

Substrate Stiffness Alters VE-Cadherin Localization

We have shown previously that substrate stiffness is a critical mediator of capillary network assembly, the self-assembly of endothelial cell (EC) networks [112]. On compliant (E=0.2 kPa) substrates, ECs assembled into networks characterized by

clusters of ECs connected by cords of aligned cells (Figure 3.1A). When substrate stiffness was increased (E=10 kPa), network assembly did not occur and cells were instead uniformly distributed across the substrate (Figure 3.1B).

Endothelial cell-cell connections are largely mediated by VE-cadherin, an EC-specific adherens junction protein [156]. To investigate the role of VE-cadherin in mediating cell-cell interactions with respect to substrate stiffness, ECs were plated on compliant (E=0.2 kPa) and stiff (E=10 kPa) substrates and stained to localize VE-cadherin. On compliant substrates where networks spontaneously assembled, cells formed tight cell-cell junctions that were colocalized with a continuous signal of VE-cadherin at the membrane of adjoining cells (Figure 3.1C arrow heads; inset is a magnification of the boxed region). When substrate stiffness was increased, ECs did not form tight cell-cell junctions, and VE-cadherin localization at the membrane of adjoining cells appeared punctate (Figure 3.1D).

To quantify the localization of VE-cadherin with respect to stiffness, ECs plated on variably compliant substrates (E=0.2-10 kPa, and tissue culture plastic [TCP; polystyrene; E=3 GPa [157]]) were analyzed by Western blot (Figure 3.1E). VE-cadherin was fractionated into soluble and insoluble fractions with Triton, where insoluble VE-cadherin corresponds to association with the cytoskeleton (Ctsk) and mature inter-endothelial junctions [152]. A plot of the average percent of total VE-cadherin indicated that on compliant (E=0.2 kPa) substrates, a greater fraction of total VE-cadherin was associated with the cytoskeleton (Figure 3.1F). The proportion VE-cadherin associated with the cytoskeleton (Ctsk[+]) decreased with substrate stiffness (black bars) while the soluble fraction ((Ctsk[-]); non-cytoskeleton associated) of VE-cadherin increased proportionately with stiffness (white bars). These data indicate that

compliant substrates foster the development of EC network assemblies characterized by tight and mature VE-cadherin-associated cell-cell interactions.

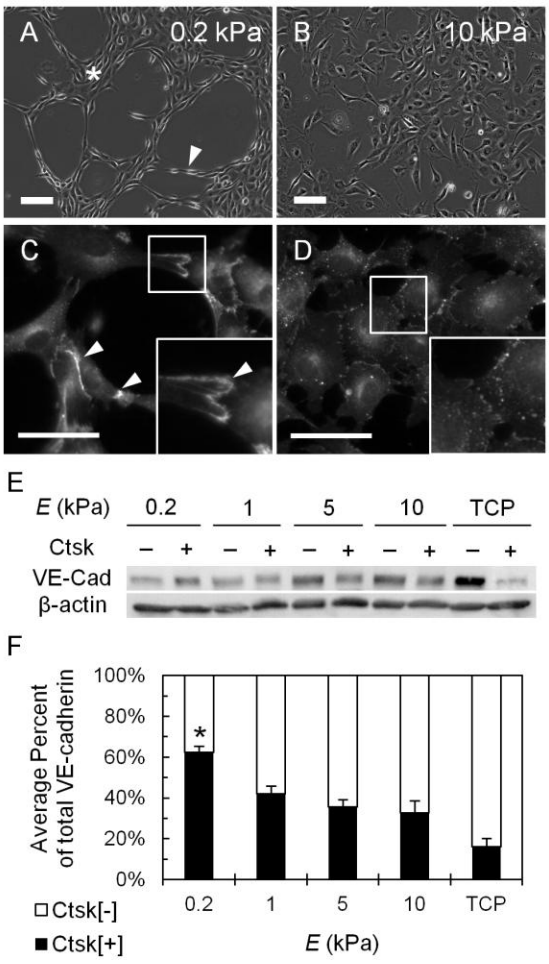

Figure 3.1. Substrate stiffness alters the localization of VE-cadherin in ECs. (**A**) On compliant (*E*=0.2 kPa) substrates, ECs self-assembled into networks characterized by clusters of cells (*) connected by cords of cells (arrow head). (**B**) On stiff (*E*=10 kPa) substrates, cells were uniformly distributed. Scale bars are 100 μm. (**C**) On compliant substrates, VE-cadherin localization was continuous at cell-cell junctions (arrow heads, inset is a magnification of the boxed region). (**D**) On stiff substrates, VE-cadherin localization was punctate at cell-cell junctions. Scale bars are 50 μm. (**E**) Western blot of VE-cadherin fractionated to localize association with the cytoskeleton (Ctsk +/-; *E*, Young's Modulus; TCP, tissue culture plastic). (**F**) A plot of the average percent of total VE-cadherin fractionated for localization with the cytoskeleton indicated a significant decrease in cytoskeleton-associated VE-cadherin with increasing substrate stiffness (mean + SE, *$p<0.001$). Dr. Christine Montague performed the Western blot in (**E**)-(**F**).

Capillary Network Assembly on Compliant Substrates Requires VE-Cadherin Engagement

Our data indicate that substrate stiffness alters the localization of VE-cadherin in ECs. To determine whether VE-cadherin is requisite for mediating network assembly, ECs were plated in the presence of ethylene glycol tetraacetic acid (EGTA). Treatment with EGTA sequesters extracellular calcium and prevents cadherin-cadherin interactions [152,158]. ECs on compliant (E=0.2-0.5 kPa) substrates plated with EGTA were adherent to the substrate but poorly spread, and networks did not assemble, however cell spreading was not disrupted on stiffer glass or TCP substrates (Figure 3.2A). In control samples, networks assembled on compliant substrates but not on stiff glass or TCP (Figure 3.2B). To determine whether this response was reversible, ECs were plated in the presence of EGTA for 24 hours and replenished with fresh media. As before, treatment with EGTA prevented cell spreading and network assembly on compliant (E=0.2 kPa) substrates (Figure 3.2C), but did not disrupt spreading on stiff (E=10 kPa) substrates (Figure 3.2). After the addition of complete media, samples on compliant substrates (initially treated with EGTA) assembled into networks (Figure 3.2C, arrow) that appeared similar to controls (double arrow). On stiff substrates, cells did not assemble networks and grew to confluence similar to controls after complete media was replenished (Figure 3.2D, double arrow).

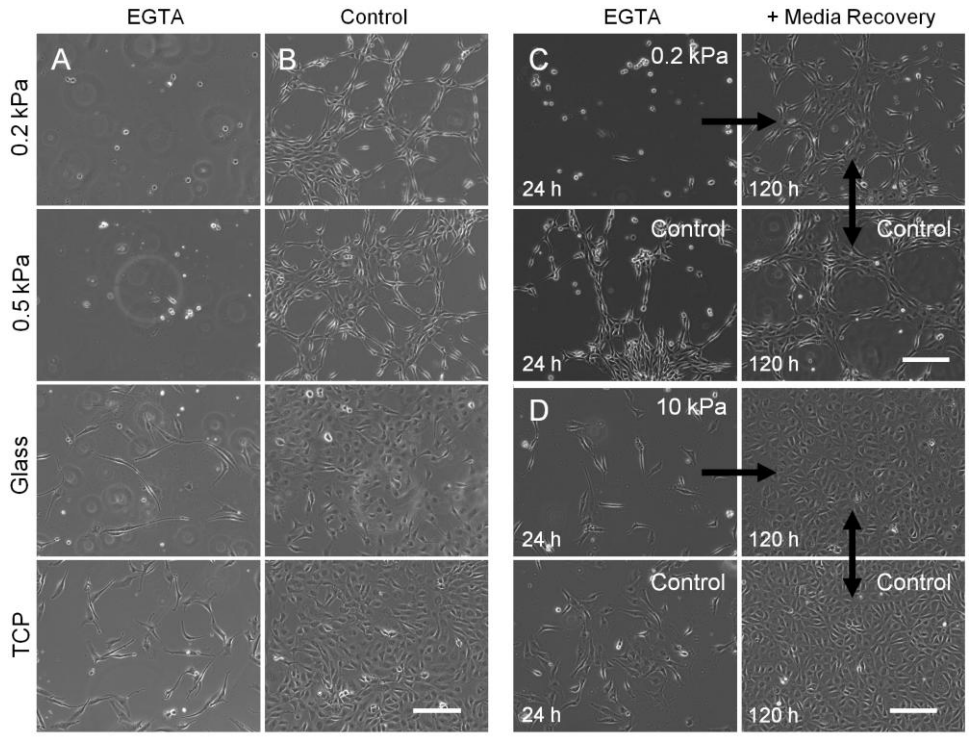

Figure 3.2. EGTA treatment prevents EC network assembly.
ECs were plated on compliant (*E*=0.2-5) and stiff (glass, TCP) substrates in the presence of 5 mM EGTA. (**A**) On compliant substrates, ECs were poorly spread and did not assemble networks. On stiffer substrates, spreading was not disrupted and cells did not assemble networks. (**B**) Control samples exhibit network assembly on compliant but not stiff substrates. (**C**) ECs on compliant (*E*=0.2 kPa) substrates were plated in the presence of 5 mM EGTA for 24 hours then replenished with fresh media (arrow). Network assembly was recovered by 120 hours after plating and appeared similar to controls (double arrow). (**D**) On stiff substrates, cells did not form network assemblies after EGTA-treated cells were replenished with fresh media. Scale bars are 200 μm.

To confirm that EGTA disrupted VE-cadherin, EC in assembled networks on compliant substrates were treated with EGTA and fixed and stained for VE-cadherin. Staining indicated that EGTA disrupted VE-cadherin at the cell-cell junction 30 minutes and 2 hours after treatment compared to controls (Figure 3.3). Notably, assembled networks did not disassemble in this time frame. These data indicate that EGTA disrupts network assembly on compliant substrates by altering the localization of VE-cadherin in ECs, and suggests that VE-cadherin engagement may not be

requisite for maintaining established network morphologies.

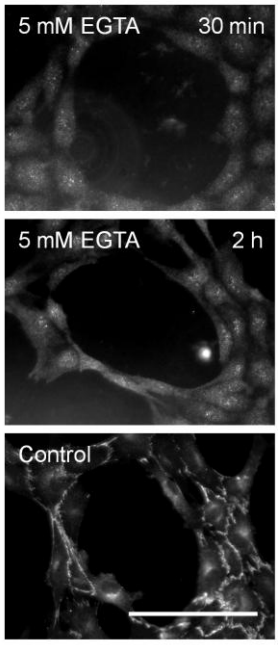

Figure 3.3. EGTA disrupts VE-cadherin localization at cell-cell junctions.
ECs on compliant (*E*=0.2 kPa) substrates in assembled networks were treated with 5 mM EGTA and stained for VE-cadherin. VE-cadherin localization was disrupted 30 minutes and 2 hours after treatment compared to controls. Scale bar is 100 μm.

While treatment with EGTA disrupts VE-cadherin-mediated cell-cell interactions, there may be additional and unintended side effects of extracellular calcium depletion. To determine whether VE-cadherin was requisite for network assembly, ECs were plated on compliant (*E*=0.2 kPa) substrates in the presence of a VE-cadherin function-blocking antibody. Blocking VE-cadherin prevented network assembly compared to control samples (Figure 3.4A). These results were reminiscent of our previous findings indicating that network assembly requires FN polymerization [112]. To determine whether blocking VE-cadherin engagement altered FN deposition, ECs were plated on compliant (*E*=0.2 kPa) substrates in the presence of a VE-cadherin function-blocking antibody and fixed and stained for FN. ECs plated with the

blocking antibody failed to assemble networks or deposit FN fibrils (Figure 3.4B, inset is a magnification of the boxed region). Instead, FN appeared punctate within the cell, similar to results found when samples were treated with an FN polymerization inhibitor [112]. These data indicate that VE-cadherin engagement is requisite for network assembly and that cell-cell interactions mediate FN deposition that regulates network assembly.

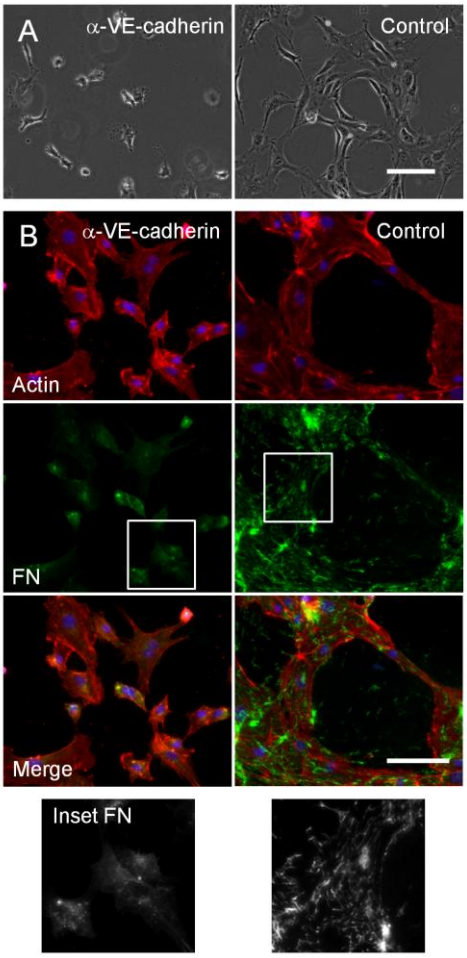

Figure 3.4. Treatment with a VE-cadherin blocking antibody prevents EC network assembly.
(**A**) ECs plated on compliant (E=0.2 kPa) substrates in the presence of 5 μg/mL VE-cadherin function-blocking antibody failed to assemble networks compared to controls. (**B**) Treatment with a VE-cadherin blocking antibody disrupted FN deposition. Inset is a magnification of the boxed region. Scale bars are 100 μm.

Substrate Stiffness Alters Focal Adhesion Assembly and Cell-Substrate Adhesion

Tissue formation is thought to result from a balance of cell-cell and cell-matrix adhesion [147]. Our data indicate that substrate stiffness alters VE-cadherin-mediated cell-cell adhesion. Cell-substrate adhesion is mediated by focal adhesions that link the ECM to the cytoskeleton and participate in mechanosensing [43]. To determine the role of substrate stiffness in mediating focal adhesion organization, ECs were plated on compliant (E=0.2 kPa) and stiff (E=10 kPa) PA substrates and stained for paxillin, a focal adhesion adaptor protein. On compliant substrates, paxillin signal was localized to a few small adhesion sites with significant diffuse staining (Figure 3.5A, inset is a magnification of the boxed region). In contrast, paxillin signal appeared to localize in numerous elongated adhesions suggesting an increase in focal adhesion size and density with increasing substrate stiffness (Figure 3.5B). Focal adhesion organization on stiff substrates also appeared colocalized with the ends of actin filaments (Figure 3.5B, merge). These data indicate that substrate stiffness alters focal adhesion organization, and suggest that there are differences in cell-substrate adhesion with stiffness.

To determine adhesive strength, we performed a centrifugation assay on ECs plated on variably compliant (E=0.5-10 kPa) substrates. A plot of the ratio of adherent cells (cells present after centrifugation compared to static controls) indicated that cell adhesivity to the substrate increased significantly with increasing substrate stiffness (Figure 3.5C). These data were fit with a logistic model [adapted from [154]] that accurately described the experimental data (sum of squares error = 0.001) indicating that the adherent cell fraction increased in a sigmoidal fashion with increasing substrate stiffness. These data indicate that substrate stiffness alters focal adhesion organization and cell-substrate adhesion.

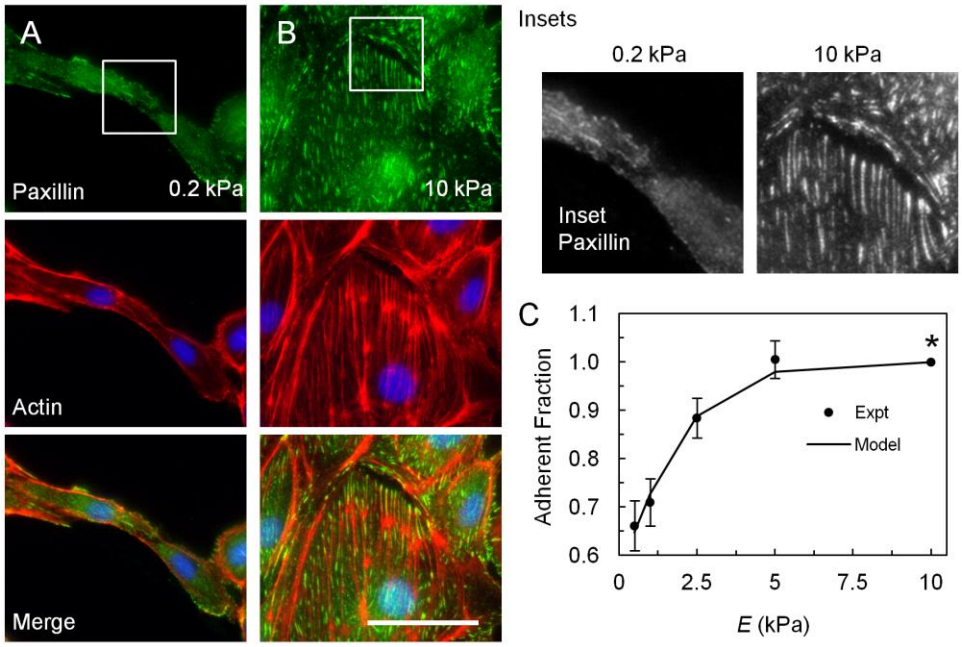

Figure 3.5. Substrate stiffness alters focal adhesion localization and cell-substrate adhesion.
ECs were plated on compliant (E=0.2 kPa) and stiff (E=10 kPa) substrates and stained for paxillin. (**A**) On compliant substrates, paxillin was localized to a few small adhesions with significant diffuse staining. (**B**) On stiff substrates, paxillin was localized in numerous elongated adhesions. Insets are magnifications of the boxed regions. Scale bar is 50 μm. (**C**) ECs were plated on variably compliant substrates (E=0.5-10 kPa) substrates and subjected to a centrifugation assay. Quantification of the adherent cell fraction indicated that cell-substrate adhesion increased with increasing substrate stiffness (mean ± SE, *$p<0.05$). Alina Starchenko performed the centrifugation assay in (**C**).

Taken together, these data indicate that compliant substrates promote capillary network assembly by altering VE-cadherin and focal adhesion localization, mediators of cell-cell and cell-substrate adhesion.

Mammary Cell Network Assembly on Compliant Substrates Requires Laminin and is Associated with a Reduction in Cell-Substrate Adhesion

Our data indicate that substrate stiffness alters the cell-cell and cell-matrix interactions

that mediated capillary network assembly. To determine whether the sensitivity of network assembly to substrate stiffness was specific to ECs, we investigated network assembly in cell types derived from mammary, mesenchymal, and lung tissues that exhibited tissue morphogenesis, *i.e.* network assembly. Cells derived from mammary tissue exhibit morphogenesis that is regulated primarily by the ECM protein laminin [159]. To determine the role of substrate stiffness in mediating mammary cell network assembly, MCF-10A human mammary epithelial cells (10A) were plated on compliant (E=0.2 kPa) and stiff (E=10 kPa) substrates and stained for laminin. Analogous to ECs with FN [98,112], 10As on compliant substrates assembled networks associated with laminin (Figure 3.6A). On stiff substrates, cells did not assemble networks, and cells and laminin were uniformly distributed across the substrates (Figure 3.6B). Note that laminin staining displayed the characteristic leopard-spot pattern [160]. Like FN, laminin was colocalized with 10As in network assemblies. We observed laminin fibrils that spanned a network cord despite an individual retracted cell suggesting that laminin fibril deposition supports network assembly (Figure 3.6C).

To determine the role of substrate stiffness in mediating cell-substrate adhesion, 10As were subjected to a centrifugation assay. Similar to ECs, 10As exhibited an increase in adherent fraction with increasing substrate stiffness (Figure 3.6D). These results indicate that compliant substrates promote a reduction in cell-substrate adhesion and network assembly associated with laminin in 10As.

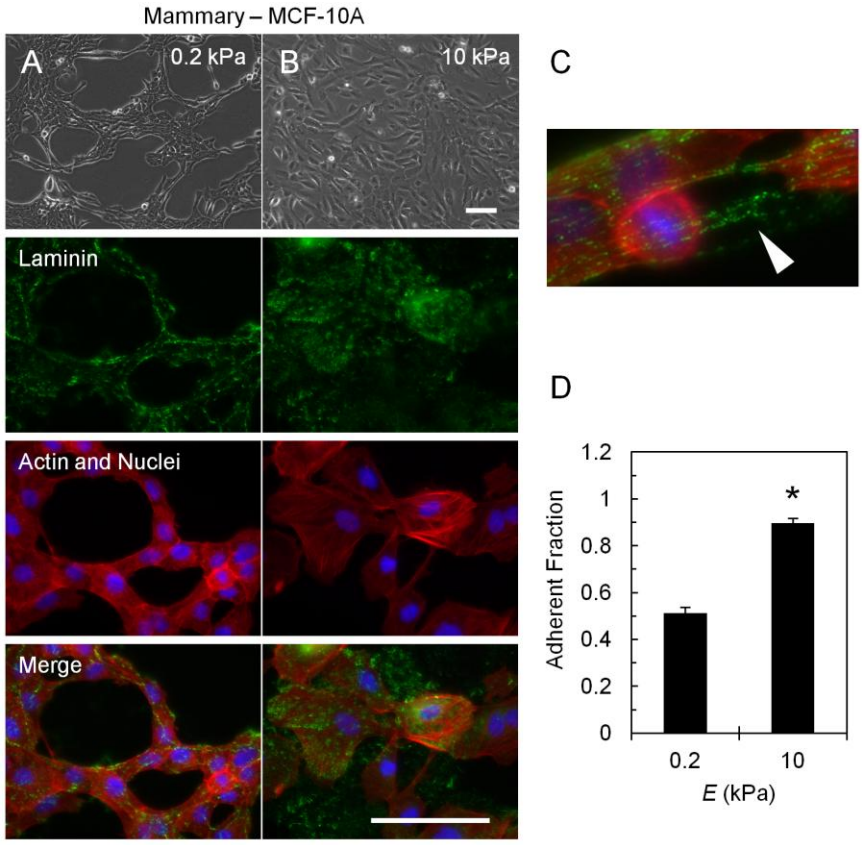

Figure 3.6. Compliant substrates promote mammary cell network assembly colocalized with laminin and reduced cell-substrate adhesion.
(**A**) MCF-10A mammary epithelial cells plated on compliant (*E*=0.2 kPa) substrates assembled into networks associated with laminin. (**B**) On stiff (*E*=10 kPa) substrates, cells and laminin were uniformly distributed. Scale bars are 100 μm. (**C**) Laminin ECM was stretched across a retracted cell in a network cord. (**D**) Quantification of a centrifugation assay indicated a significant increase in cell-substrate adhesion with increasing substrate stiffness (mean + SE, *$p<0.05$).

To determine if laminin was requisite for network assembly, 10As were treated with siRNA against the laminin-5 subunits (α3, β3, γ2), and plated on compliant (*E*=0.2 kPa) substrates. A Western blot of laminin expression indicated that there was a decrease in laminin expression over 24-48 hours (Figure 3.7A-C). Treatment with siRNA against laminin α3 prevented network assembly in 10As (Figure 3.7A). However, treatment with siRNA against laminin β3 or γ2 did not prevent network

assembly (Figure 3.7B-C). These data indicate that laminin is requisite for 10A network assembly on compliant substrates, and suggest that the α3 chain of laminin-5 mediates cell-cell interactions that enable network formation.

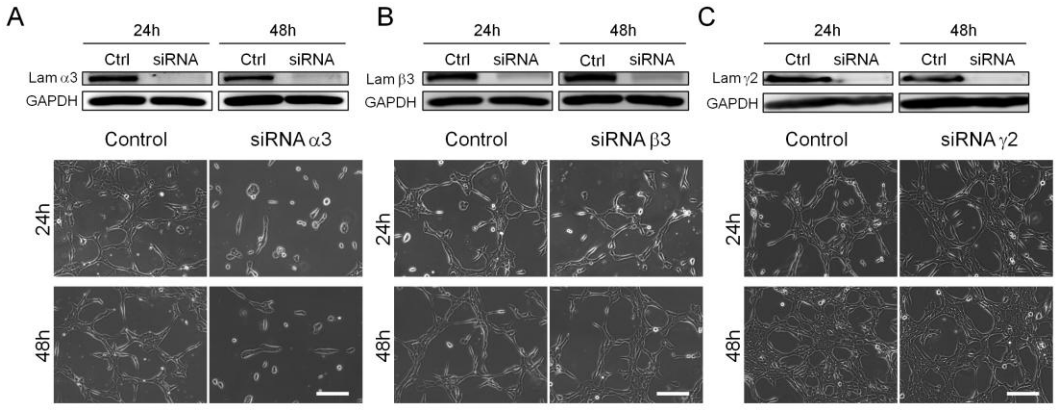

Figure 3.7. Laminin α3 is requisite for mammary cell network assembly. MCF-10A mammary epithelial cells were treated with siRNA against laminin-5 subunits α3, β3, or γ2 and plated on compliant (*E*=0.2 kPa) substrates. (**A-C**) Western blot for laminin indicated a decrease in laminin expression over two days. (**A**) 10As treated with siRNA against laminin α3 did not assemble networks compared to control siRNA. (**B-C**) 10As treated with siRNA against β3 or γ2, respectively, did assemble networks. Scale bars are 200 μm.

FN is requisite for network assembly in ECs [112]. To determine whether FN mediates mammary cell network assembly, 10As were plated on compliant (*E*=0.2 kPa) and stiff (*E*=10 kPa) substrates and stained for FN. On compliant substrates, 10As assembled networks that were colocalized with FN (Figure 3.8A). On stiff substrates, cells were uniformly distributed across the substrate and FN signal was not closely associated with cells (Figure 3.8B). These data suggest that multiple ECM proteins contribute to network assembly.

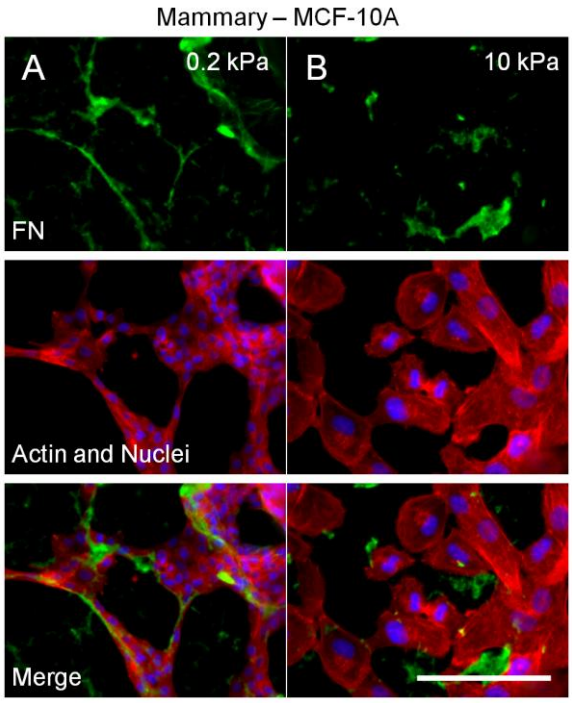

Figure 3.8. Networks of mammary epithelial cells are associated with fibronectin.
MCF-10A mammary epithelial cells were plated on compliant (*E*=0.2 kPa) and stiff (*E*=10 kPa) substrates and stained for FN. (**A**) On compliant substrates, 10As formed networks associated with FN. (**B**) On stiff substrates, cells were uniformly distributed and not closely associated with FN. Scale bar is 200 μm.

In addition to capillary and mammary tissue-derived cells, mesenchymal tissue-derived cells support tissue morphogenesis [161]. To determine the role of substrate stiffness in mediating mesenchymal cell network assembly, C3H/10T1/2 murine mesenchymal stem cells (C3H) were plated on compliant (*E*=0.2 kPa) and stiff (*E*=10 kPa) substrates. C3Hs plated on compliant substrates formed network assemblies associated with FN (Figure 3.9A). On stiff substrates, networks did not assemble, and cells and FN were instead uniformly distributed across the substrate (Figure 3.9B). To determine whether substrate stiffness mediated cell-substrate adhesion, CH3s were subjected to a centrifugation assay. Similar to ECs and 10As, C3Hs exhibited an

increase in adherent fraction with increasing substrate stiffness. These results suggest that mesenchymal cell network assembly is sensitive to substrate stiffness.

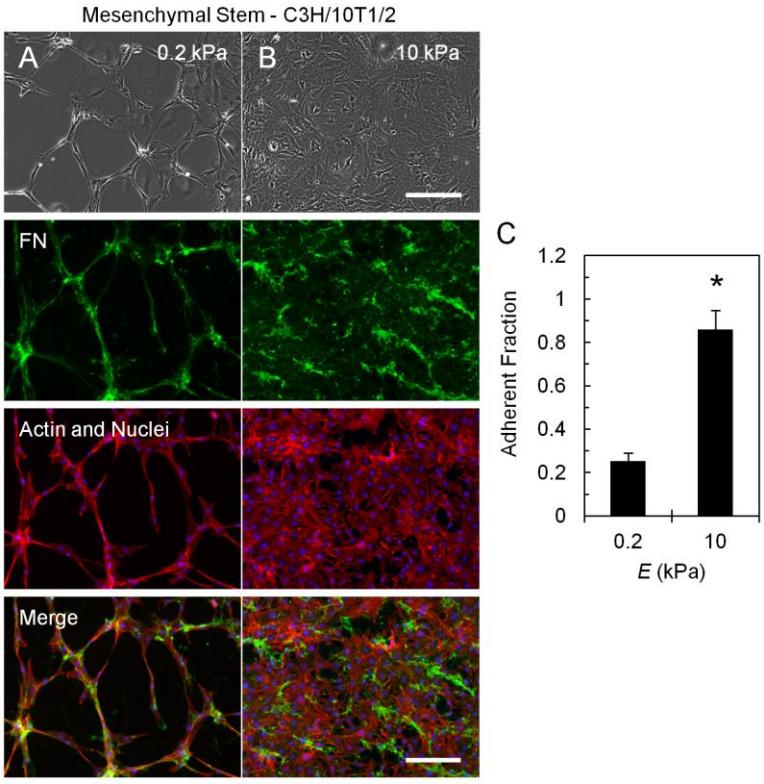

Figure 3.9. Compliant substrates support mesenchymal cell network assembly colocalized with FN.
C3H/10T1/2 murine mesenchymal stem cells were plated on compliant (E=0.2 kPa) and stiff (E=10 kPa) substrates. (**A**) On compliant substrates, C3H cells assembled into networks associated with FN. (**B**) On stiff substrates, cells did not assemble networks, and cells and FN were uniformly distributed across the substrate. Scale bars are 200 μm. (**C**) Quantification of a centrifugation assay indicated a significant increase in cell-substrate adhesion with increasing substrate stiffness (mean + SE, *$p<0.05$).

In the vasculature, smooth muscle cells (SMC) support EC network assembly [162]. To determine the role of substrate stiffness in mediating network assembly, A7r5 rat SMCs were plated on compliant (E=0.2-1 kPa) and stiff (E=10 kPa) substrates and stained for collagen or FN. On compliant, but not stiff, substrates, SMCs formed

network assemblies (Figure 3.10A). Network assemblies on compliant substrates were colocalized with collagen, but cells were uniformly distributed and not colocalized with collagen on stiff substrates (Figure 3.10B). On compliant (*E*=1 kPa) substrates, SMCs did not assemble networks despite colocalization with some fibrillar FN (Figure 3.10C). On stiff substrates, SMCs did not assemble networks and FN appeared aggregated with some fibrils (Figure 3.10C). Notably, SMC network assemblies on compliant substrates were less robust and persistent than those observed in ECs, 10As, and C3Hs. This was likely due to a reduction in migration and proliferation observed in these cells on compliant substrates.

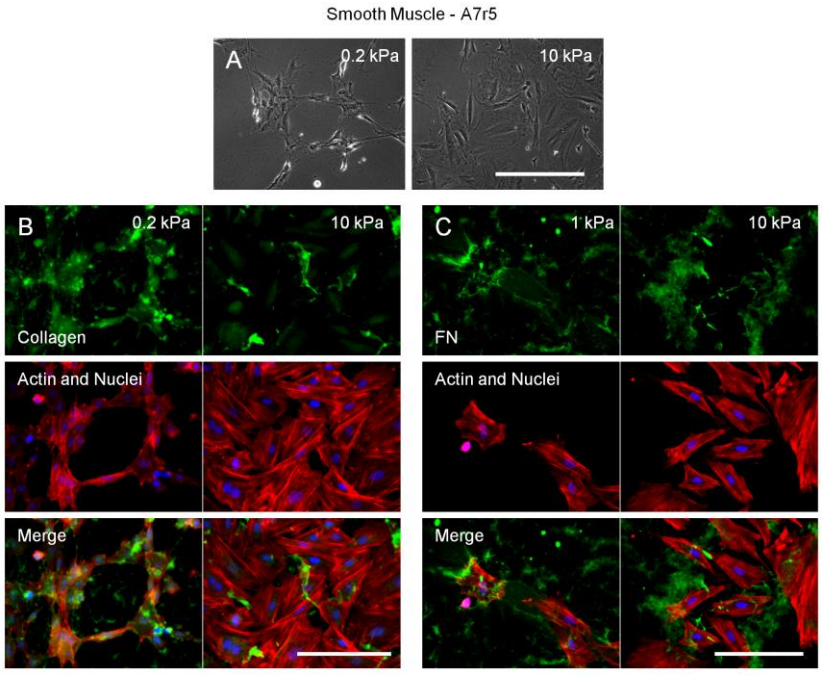

Figure 3.10. Compliant substrates support SMC network assembly associated with collagen.
(**A**) A7r5 rat SMCs assembled networks on compliant (*E*=0.2 kPa) but not stiff (*E*=10 kPa) substrates. (**B**) Network assemblies were colocalized with collagen on compliant substrates. On stiff substrates cells did not assemble networks and were uniformly distributed. (**C**) On compliant (*E*=1 kPa) substrates networks did not assemble despite interaction with FN. On stiff substrates, SMCs did not assemble and FN was aggregated with some fibrils. Scale bar is 200 μm.

Laminin-Deficient Mammary Cells Fail to Assemble Networks and Do Not Exhibit a Reduction in Cell-Substrate Adhesion on Compliant Substrates

Our data indicate that compliant substrates facilitate network assembly in vascular, mammary, and mesenchymal tissue-derived cell types. In these cases, cells on compliant substrates are associated with a reduction in cell-substrate adhesion and are colocalized with ECM proteins. In MCF-10A mammary epithelial cells, laminin was colocalized with network assemblies. MDA-MB-231 (231) cells are derived from a highly metastatic mammary tumor and are deficient in laminin production compared to normal mammary cells [163]. To determine whether laminin-deficient mammary cells assembled networks, 231s were plated on compliant (E=0.2 kPa) and stiff (E=10 kPa) substrates. In contrast to 10As, 231s did not assemble into networks on compliant substrates (Figure 3.11A). Instead, cells were uniformly distributed across the substrate on compliant and stiff substrates (Figure 3.11A). As expected, immunostaining for laminin was undetectable in 231s on compliant and stiff substrates (Figure 3.11B). To determine cell-substrate adhesivity, 231s were plated on compliant and stiff substrates and subjected to a centrifugation assay. In contrast to ECs, 10As, and C3Hs, 231s did not exhibit a significant difference in cell-substrate adhesion with substrate stiffness (Figure 3.11C). These findings indicate that 231s do not assemble networks, do not colocalize with laminin, and do not exhibit a reduction in cell-substrate adhesion on compliant substrates.

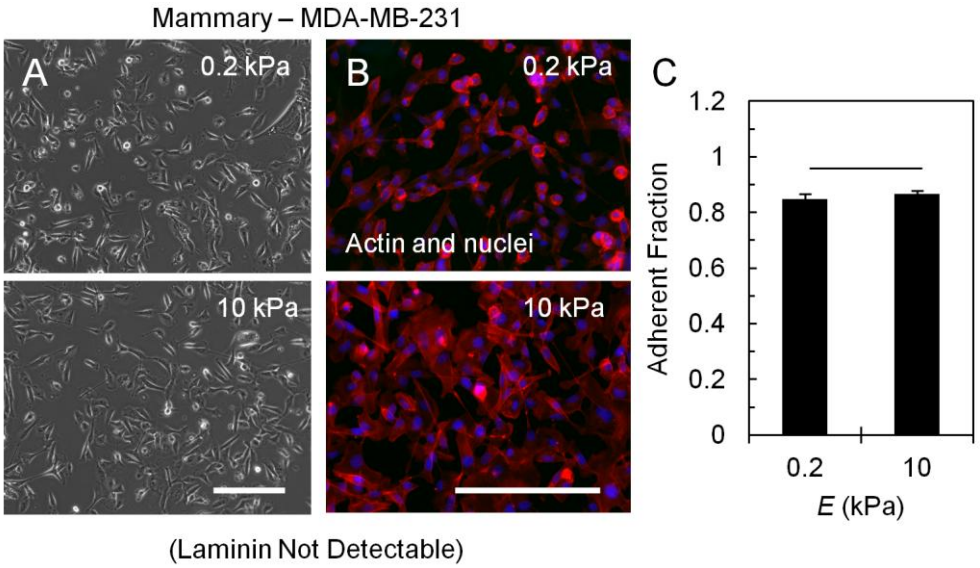

Figure 3.11. Laminin-deficient mammary cells fail to assemble networks on compliant substrates.
(**A**) MDA-MB-231 metastatic mammary epithelial cells did not assemble networks on compliant (E=0.2 kPa) or stiff (E=10 kPa) substrates. Cells were uniformly distributed across the substrate. (**B**) Immunostaining indicated that laminin was undetectable on compliant and stiff substrates. Scale bars are 200 μm. (**C**) Quantification of a centrifugation assay indicated that cell-substrate adhesion did not change with substrate stiffness (mean + SE).

In addition to vascular, mammary, and mesenchymal cell network assembly, we asked whether lung cell network assembly was sensitive to substrate stiffness. Lung tissue-derived cells have been shown to be capable of network assembly *in vitro* [164,165]. To determine the role of substrate stiffness in mediating lung cell network assembly, BEAS-2B human bronchial epithelial cells (2B) were plated on compliant (E=0.2 kPa) and stiff (E=10 kPa) substrates and stained for laminin. Analogous to 231s, 2Bs did not assemble into networks on compliant or stiff substrates (Figure 3.12A), were not associated with detectible laminin (Figure 3.12B), and did not exhibit a significant difference in cell-substrate adhesion with substrate stiffness (Figure 3.12C).

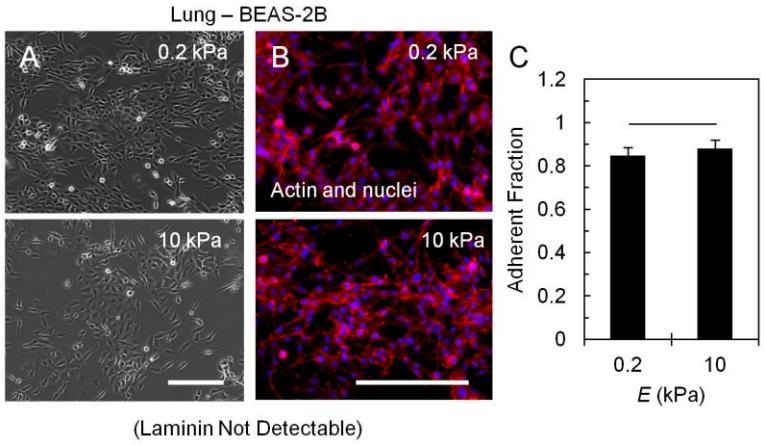

Figure 3.12. Lung cells fail to assemble networks and do not exhibit a reduction in cell-substrate adhesion on compliant substrates.
(**A**) BEAS-2B bronchial epithelial cells did not assemble networks on compliant (*E*=0.2 kPa) or stiff (*E*=10 kPa) substrates. Cells were instead uniformly distributed across the substrate. (**B**) Immunostaining indicated that laminin was undetectable on compliant and stiff substrates. Scale bars are 200 μm. (**C**) Quantification of a centrifugation assay indicated that cell-substrate adhesion did not change with substrate stiffness (mean + SE).

Like 2Bs, A549 human alveolar adenocarcinoma epithelial cells also did not assemble into networks on compliant or stiff substrates (Figure 3.13A), and were not associated with laminin (Figure 3.13B). These findings further suggest that like 231s, 2Bs and A549s are insensitive to substrate stiffness-mediated alterations in cell-cell and cell-matrix interactions that regulate network assembly.

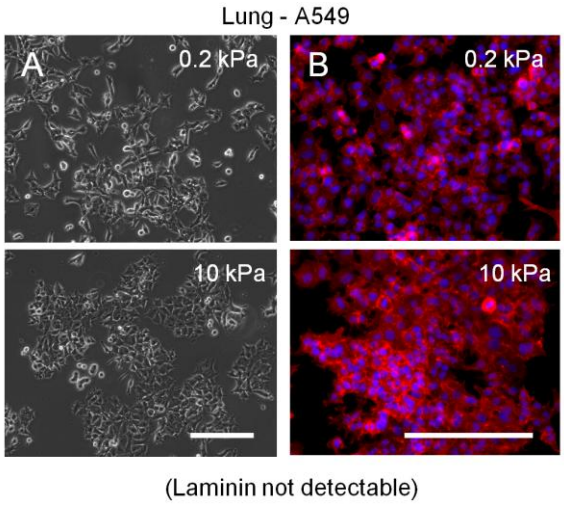

Figure 3.13. Metastatic lung carcinoma cells fail to assemble networks on compliant substrates.
(**A**) A549 metastatic lung carcinoma cells did not assemble networks on compliant (*E*=0.2 kPa) or stiff (*E*=10 kPa) substrates. Cells were instead uniformly distributed across the substrate. (**B**) Immunostaining indicated that laminin was undetectable on compliant and stiff substrates. Scale bars are 200 μm.

MCF-10A mammary epithelial cells assembled into networks that were associated with both laminin and FN. To determine if 231s, 2Bs, and A549s (cells with undetectable laminin staining) were associated with FN, cells were plated on compliant (*E*=0.2 kPa) and stiff (*E*=10 kPa) substrates and stained for FN. In all cases, FN appeared uniformly distributed across the substrate (Figure 3.14A-C). Network assembly did not occur on compliant substrates, and cells were also uniformly distributed. These findings suggest that cell-ECM colocalization is an important mediator of network assembly.

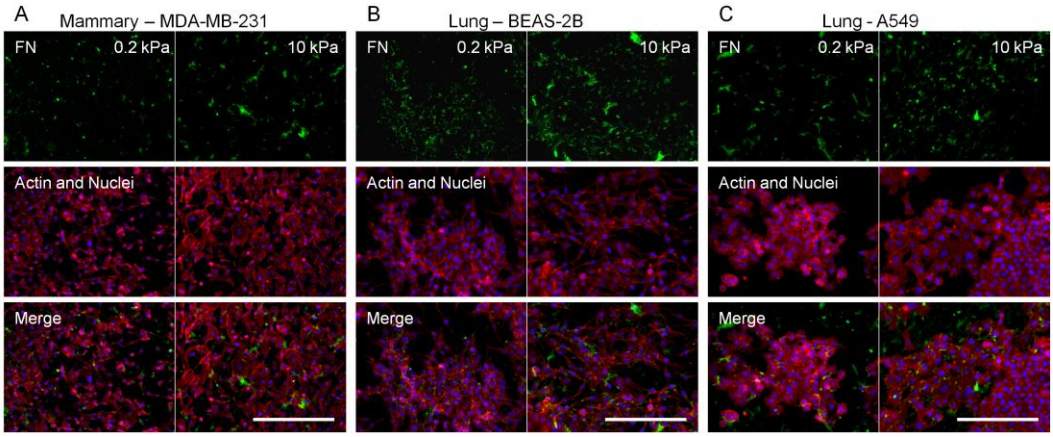

Figure 3.14. Mammary and lung tissue-derived cells that do not assemble networks are not associated with FN.
(**A**) MDA-MB-231 cells on compliant (*E*=0.2 kPa) and stiff (*E*=10 kPa) substrate failed to assemble networks. Cells and FN were uniformly distributed across the substrate. (**B-C**) Similarly, BEAS-2B and A549 cells failed to assemble networks on compliant substrates. Instead, cells and FN were uniformly distributes across the substrates. Scale bars are 200 μm.

Our findings indicate that 10As assemble networks on compliant substrates but 231s do not. Similar to VE-cadherin in ECs, E-cadherin mediates cell-cell interactions in epithelial cells [166]. To determine whether substrate stiffness alters the localization of E-cadherin in mammary epithelial cells, 10As and 231s were plated on compliant (*E*=0.2) and stiff (*E*=10 kPa) PA substrate and stained for E-cadherin. On compliant substrates, 10As assembled networks characterized by a continuous signal of E-cadherin localized to cell-cell junctions (Figure 3.15A). In contrast, E-cadherin signal was punctate or not detectable at cell-cell junctions of 10As on stiff substrates (Figure 3.15B). In contrast, 231s did not exhibit detectable E-cadherin signal at cell-cell junctions on compliant (Figure 3.15C) or stiff (Figure 3.15D) substrates. These data indicate that E-cadherin mediates cell-cell interactions between 10As on compliant substrates, that E-cadherin localization in 10As changes with substrate stiffness, and that 231s do not express E-cadherin.

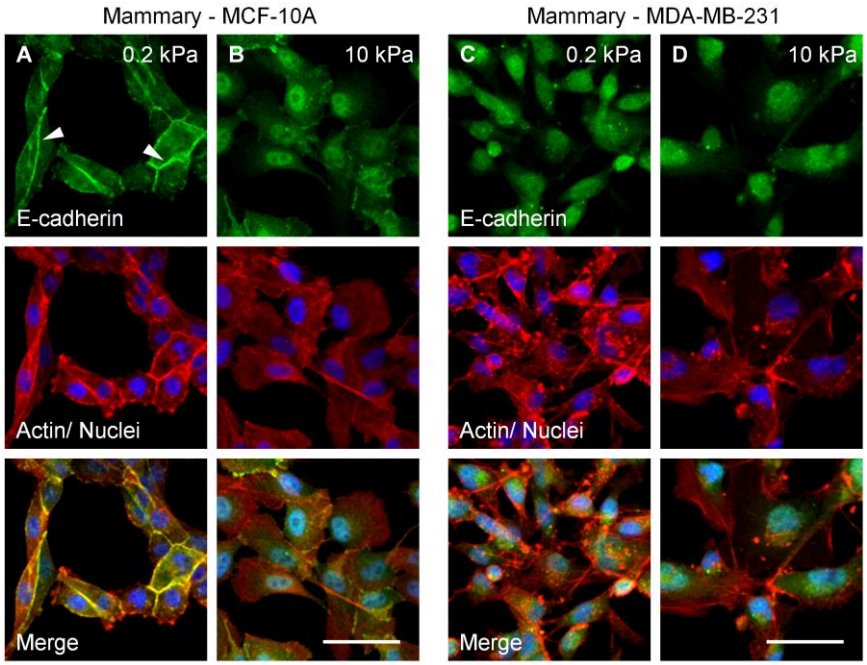

Figure 3.15. Substrate stiffness alters the localization of E-cadherin in mammary cells that assemble networks.
MCF-10A and MDA-MB-231 mammary epithelial cells were plated on compliant (*E*=0.2 kPa) and stiff (*E*=10 kPa) substrates and stained for E-cadherin. (**A**) 10As assembled networks with E-cadherin localized as a continuous signal at cell-cell junctions. (**B**) On stiff substrates, E-cadherin at cell-cell junctions was punctate or not detectable. In 231 cells, networks did not assemble, and E-cadherin was not detectable at cell-cell junctions on compliant (**C**) or stiff (**D**) substrates. Scale bars are 100 μm.

Exogenous Laminin Induces Network Assembly in Laminin-Deficient Mammary Cells

MDA-MB-231 metastatic mammary epithelial cells are laminin-deficient and fail to assemble into networks (Figure 3.11). To determine whether network assembly could be recovered with exogenous laminin, 231s were plated on matrigel, a compliant substrate rich in laminin [167,168]. At 24 hours after plating, 231s formed transient network assemblies compared to cells on tissue culture plastic (TCP) that were uniformly distributed (Figure 3.16A). Network assemblies did not persist, but

disassembled into clusters of cells on matrigel by 72 hours while control samples remained uniformly distributed across the substrate (Figure 3.16B).

In addition to laminin, matrigel is composed of multiple ECM proteins and growth factors [167,168]. To determine whether laminin, and not other proteins, were responsible for contributing to network assembly, 231s were plated on compliant (E=0.2 kPa) PA substrates derivatized with laminin (90% laminin:10% collagen). On laminin-coated substrates, 231s assembled into network-like structures by 72 hours after plating (Figure 3.16C). In contrast, 231s on collagen-coated substrates did not assemble networks and were uniformly distributed across the substrate (Figure 3.16D). These data indicate that laminin (and not additional proteins/growth factors) induced 231 network assembly on compliant substrates, and suggest that substrate stiffness and ECM chemistry are critical regulators of mammary cell network assembly.

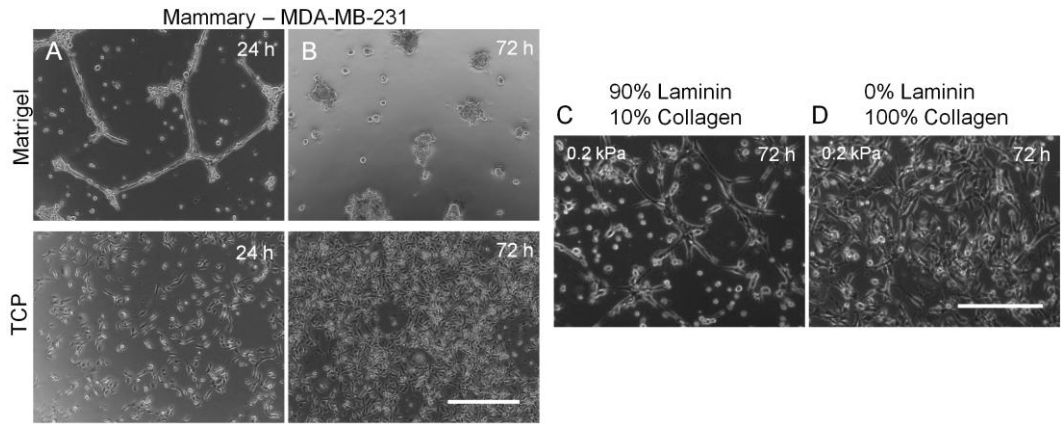

Figure 3.16. Exogenous laminin induces network assembly in laminin-deficient mammary cells.
MDA-MB-231 cells were plated on matrigel, TCP, or PA substrates derivatized with laminin/collagen. (**A**) After 24 hours, 231s formed network assemblies compared to controls that were uniformly distributed across the plate. (**B**) Networks disassembled into clusters of cells by 72 hours. Scale bar is 500 μm. (**C**) 231s plated on compliant (E=0.2 kPa) PA substrates derivatized with laminin (90% laminin:10% collagen) assembled into networks. (**D**) 231s plated on PA substrates derivatized only with collagen did not assemble networks and were uniformly distributed across the substrate. Scale bar is 200 μm.

Our findings indicate that 231 mammary cell network assembly was induced on substrates derivatized with laminin, but not collagen. Interestingly, exogenous laminin has been shown to induce E-cadherin expression in 231s in 3D cultures [169]. To determine if 231 network assembly was associated with changes in E-cadherin localization, cells on laminin or collagen-derivatized substrates were fixed and stained for E-cadherin. On compliant (E=0.2 kPa) substrates, 231s assembled networks with cell-cell junctions mediated by E-cadherin (Figure 3.17A; inset is a magnification of the region identified by the yellow arrow). In contrast, E-cadherin was not detectable at the cell-cell junction of cells on stiff (E=10 kPa) substrates derivatized with laminin (Figure 3.17B), or on compliant or stiff substrates derivatized with collagen (Figures 3.17C-D). Instead, laminin staining was diffuse throughout the cell. These findings suggest that E-cadherin expression enables 231 network assembly on compliant

substrates, and that substrate stiffness and matrix ligand type alter preferences for cell-cell vs. cell-substrate adhesion in mammary epithelial cells.

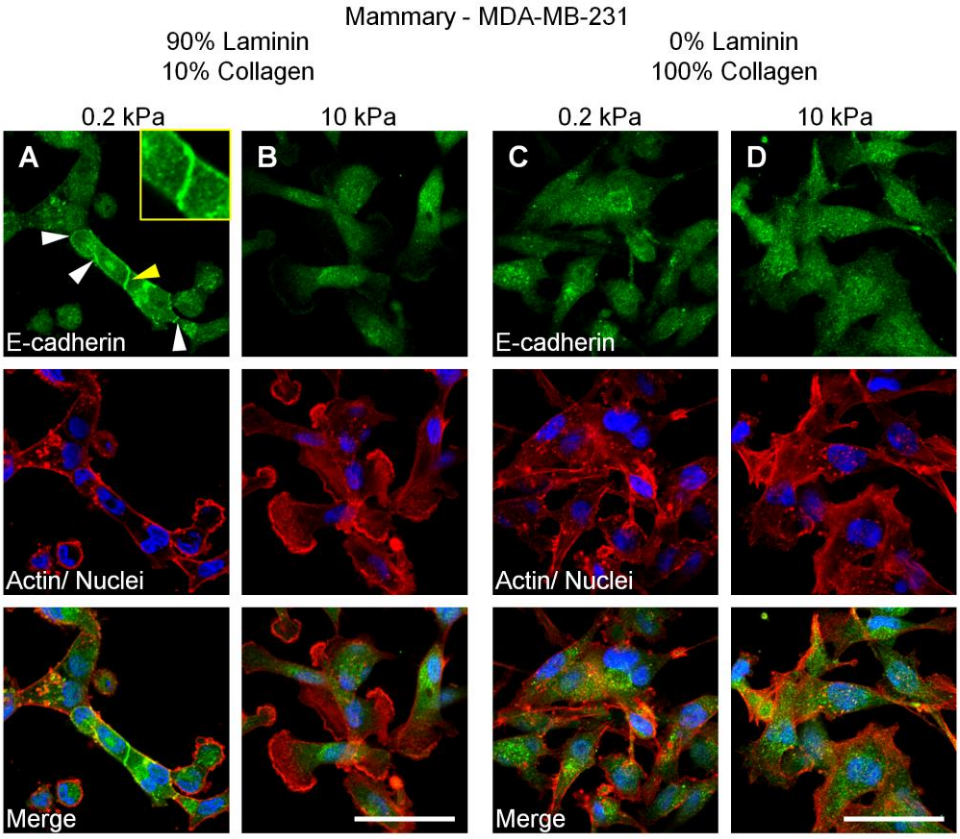

Figure 3.17. Compliant substrates derivatized with laminin induce E-cadherin mediated cell-cell interactions in mammary cells.
MDA-MB-231 mammary epithelial cells were plated on compliant (*E*=0.2 kPa) and stiff (*E*=10 kPa) PA substrates derivatized with laminin (90% laminin:10% collagen) or collagen alone and stained for E-cadherin. (**A**) On compliant substrates derivatized with laminin, 231s assembled networks with cell-cell junctions mediated by E-cadherin. (**B**) On stiff substrates 231s did not assemble networks and E-cadherin was undetectable at cell-cell junctions. (**C**-**D**) 231s plated on PA substrates derivatized collagen did not exhibit E-cadherin mediated cell-cell junctions on compliant or stiff substrates. Instead, E-cadherin localization was diffuse throughout the cell. Scale bars are 50 μm.

3.5 Discussion

In this study, we investigated the role of substrate stiffness in mediating cell-cell and cell-matrix interactions and determined that compliant substrates promote the self-assembly of tissue-like structures in cell types derived from vascular, mammary, and mesenchymal tissues.

Tissue formation is thought to result from differences in intercellular adhesions [147] that are sensitive to substrate stiffness. Guo *et al*. hypothesized that cell clustering is dependent on substrate rigidity and results from attempts to optimize mechanical input [87]. For example, cells on mechanically rigid substrates receive adequate mechanical input from the substrate and prefer cell-substrate to cell-cell interactions. When substrate stiffness is reduced, insufficient mechanical input from the substrate causes cells to seek out additional input from neighboring cell-cell interactions.

Our results support these hypotheses. On compliant substrates, ECs assembled into networks and formed tight cell-cell junctions mediated by VE-cadherin. Substrate stiffness altered the cellular localization of VE-cadherin indicating that cell-cell junctions were mature. At the same time, ECs on compliant substrates exhibited a reduction in focal adhesion organization and a measurable decrease in cell-substrate adhesion. On stiff substrates, ECs did not form tight cell-cell junctions and exhibited an increase in cell-substrate adhesion. These data demonstrate a clear role for substrate mechanics in modulating cell-cell adhesion and tissue formation. This response may be relevant in cancer, where the tumor microenvironment is associated with ECM stiffening [16,39] and vasculature that is poorly organized and leaky [17]. Our data indicate that stiff substrates promote loose cell-cell junctions (here and [170]), suggesting that the increased ECM stiffness of the tumor microenvironment

promotes pathologic vessel formation, and that controlling ECM stiffening may be a target for cancer treatment.

Network assembly is not unique to ECs. Previous reports indicate that mammary, lung, and mesenchymal tissue-derived cells are capable of tissue morphogenesis—*i.e.* tissue/network assembly. Our data indicate that compliant substrates promote network assembly in mammary, mesenchymal, and vascular tissue-derived cell types. In each of these cases (ECs, 10As, C3Hs, A7r5s), cells exhibit i) networks tightly colocalized with ECM on compliant substrates and/or ii) a measurable reduction in cell-matrix adhesion on compliant substrates. Cells that did not assemble networks (231s, 2Bs, A549s) exhibit i) no obvious association with ECM and/or ii) no measurable reduction in cell-matrix adhesion on compliant substrates. These findings indicate that there is a correlation between compliant substrates and preferences for cell-cell vs. cell-substrate adhesion, and support the hypothesis that network assembly arises from a balance of cell-cell and cell-matrix adhesion, *i.e.* reduced mechanical input on compliant substrate drives network assembly. While these findings are in no way exhaustive, they provide evidence that substrate stiffness alters the cell-cell and cell-matrix interactions that regulate network assembly.

Interestingly, our data indicate that in addition to cell-cell and cell-matrix adhesion, ECM colocalization is requisite for network assembly. We previously determined that ECs require FN polymerization to assemble networks [112]. Specifically, FN polymerization stabilized cell-cell interactions. Herein, we demonstrated that laminin is required for the assembly of mammary cells. A requirement for ECM in mediating cell-cell interactions likely results from crosstalk between ECM proteins (FN, laminin) and cadherins. For example, integrin engagement by FN alters VE-cadherin-mediated

cell-cell interactions and actin cytoskeletal organization [171] necessary for the polymerization of FN into fibrils [172,173]. We demonstrated that blocking VE-cadherin engagement prevented network assembly, but also altered FN deposition, suggesting feedback mechanisms governing cell-cell and cell-matrix interactions. More work is needed to fully understand the role of these interactions in mediating vascular cell network assembly.

Our findings with MDA-MB-231 mammary epithelial cells provide additional insight about the complexity of these interactions. 231s are deficient in the production of laminin (Figure 3.11B, [163]), a protein that is crucial for mammary cell network assembly on compliant substrates (Figure 3.7, [160]), and also did not exhibit alterations in cell-substrate adhesion with changes in substrate stiffness (Figure 3.11C). Moreover, E-cadherin was undetectable in these cells (Figure 3.15). However, 231s were induced to form network-like assemblies when plated on laminin-rich matrigel substrates or compliant substrates derivatized with laminin (Figure 3.16). These results suggest that the presence of exogenous laminin on compliant substrates directs 231s to prefer cell-cell vs. cell-substrate adhesion. Indeed, similar to another report [169], laminin induced changes in E-cadherin localization in 231s (Figure 3.17) suggesting that E-cadherin expression enabled network assembly. (In addition, 2Bs have been shown to assemble into networks on matrigel, but not collagen- or FN-coated TCP [164] suggesting the induction of cell-cell adhesion molecules in this cell type as well). These findings indicate that both substrate stiffness and ECM type alters the expression of cell-cell adhesion proteins and preferences for cell-cell vs. cell-matrix interactions that govern network assembly in mammary (and lung) epithelial cells. This has important ramifications for cancer, where preferences for cell-cell interactions are involved with epithelial to

mesenchymal transition and metastasis [174].

In conclusion, these data indicate that substrate stiffness regulates network assembly by altering cell-cell and cell-matrix adhesion, and cell-ECM colocalization, and suggest that the sensitivity of network assembly to stiffness is universal across tissue type.

CHAPTER 4

SUBSTRATE STIFFNESS AND CELL AREA PREDICT CELLULAR TRACTION STRESSES IN SINGLE CELLS AND CELLS IN CONTACT

Published in *Cellular and Molecular Bioengineering* [149].

Portions of this chapter were recognized with a *Graduate Research Award* by the Biomedical Engineering Society (BMES) in 2009.

4.1 Abstract

Abstract—Cells generate traction stresses against their substrate during adhesion and migration, and traction stresses are used in part by the cell to sense the substrate. While it is clear that traction stresses, substrate stiffness, and cell area are related, it is unclear whether or how area and substrate stiffness affect force generation in cells. Moreover, multiple studies have investigated traction stresses of single cells, but few have focused on forces exerted by cells in contact, which more closely mimics the *in vivo* environment. Here, cellular traction forces were measured where cell area was modulated by ligand density or substrate stiffness. We coupled these measurements with a multilinear regression model to show that both projected cell area and underlying substrate stiffness are significant predictors of traction forces in endothelial cells, and interestingly, substrate ligand density is not. We further explored the effect of cell–cell contact on the interplay between cell area, substrate stiffness, and force generation and found that again both area and stiffness play a significant role in cell force generation. These data indicate that cellular traction force cannot be determined by cell area alone and that underlying substrate stiffness is a significant contributor to traction force generation.

4.2 Introduction

Cellular traction forces are involved in cell adhesion and migration, [87,175] extracellular matrix (ECM) assembly and reorganization, [173] and cellular mechanotransduction [176,177]. The advent of multiple methods to measure cellular traction stresses has lead to numerous studies of the origin of force generation and its relationship to normal and pathologic conditions [16,178-180]. Recent work suggests that cellular force generation is dictated in part by the elasticity of the surrounding matrix [81], where cell traction force increases with substrate stiffness [86]. These studies imply that increased tissue stiffness increases the intrinsic force state of the cell. The ramifications of these studies have been far-reaching, as there are a number of pathological states where tissues stiffen, including cancer progression [16], wound healing [26], and atherosclerosis [176]. However, in addition to increasing force generation, ECM stiffness also increases cell area [31,112]. Together, these results suggest a potential relationship between substrate stiffness, cell area, and traction force generation; however, the specific interplay of these parameters is unknown. It is not clear whether increased ECM stiffness drives increases in cell area that increase cell force, or if ECM stiffness and cell area can drive increased force independently (Figure 4.1).

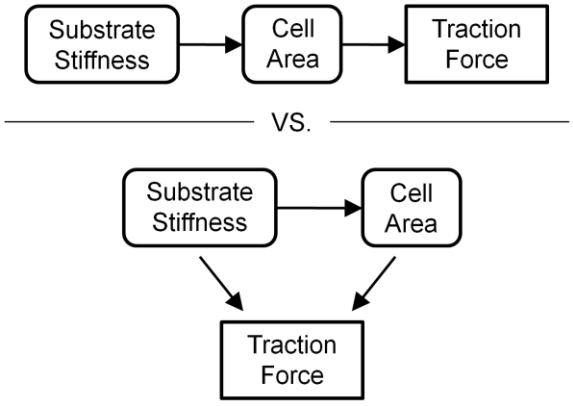

Figure 4.1. Proposed interplay between substrate stiffness, cell area, and traction force in ECs.

Much of what is known about cellular traction stress generation is based on studies of single cells in isolation. However, this does not accurately depict the physiological state in many cases. Many cells whose traction stresses have been studied extensively, such as epithelial and endothelial cells, are in contact with adjacent cells, however, much less is known about traction forces of cells in contact. Interestingly, there is mounting evidence to show that increased matrix stiffness disrupts cell–cell contacts [16,112], yet little is known about the changes in traction generation of cells in contact that accompany such changes in matrix stiffness. It is unclear if substrate mechanics plays a role in dictating cell forces once cells are in contact. There is evidence to suggest that substrate mechanics has a more pronounced effect on cell area and stress fiber formation when cells are in isolation. On compliant substrates, isolated cells exhibit fewer well-formed stress fibers and are typically less well spread. Upon cell–cell contact, stress fiber formation increases [71]. Recent work investigating cells in contact indicate that monolayer geometry may influence the magnitude and orientation of traction forces across cell aggregates [181,182]. However, it is not known whether or how cell area and substrate stiffness contribute to traction force generation of cells

in contact, and whether these effects parallel the results found for single cells.

Using measures of cellular traction forces coupled with a multilinear regression model, we show that both cell area and substrate stiffness are significant predictors of traction force generation in single and two endothelial cells (EC) in contact. These data show for the first time that cell area is not the sole predictor of traction generation and that substrate stiffness plays a significant role in dictating force generation in cells even when they are in contact with other cells. Our study indicates that both substrate stiffness and cell area play an important role in contributing to the mechanical response of cells.

4.3 Materials and Methods

Cell Culture

Bovine aortic endothelial cells (VEC Technologies) were maintained at 37 °C and 5% CO2 in Medium 199 (Invitrogen) supplemented with 10% FetalClone III (Fisher), and 1% each of penicillin–streptomycin, MEM amino acids (Invitrogen), and MEM vitamins (Mediatech). ECs were used up to passage 12.

Polyacrylamide Gel Synthesis

Variably compliant poly(acrylamide) (PA) gels were prepared by altering the ratio of acrylamide to bis-acrylamide (BioRad) in the polymerization solution as described previously [28,112]. Gels were functionalized with N-6-((acryloyl)amino)hexanoic acid, succinimidyl ester (synthesized in our lab [32]) to allow covalent attachment of type I collagen (Sigma) to the gel surface. Gels were polymerized and covalently bound to activated glass coverslips as described previously [112], and were derivatized with an applied collagen concentration of 100 μg/mL for variable stiffness

studies, and 0.01–100 μg/mL for variable concentration studies. Gels were synthesized with Young's Moduli (E) of 1, 2.5, 5, and 10 kPa to mimic physiologically relevant tissue stiffness [151].

PA Gel Stiffness Characterization

The stiffness of PA gels was confirmed by measuring Young's Modulus (E) at the gel surface using Hertz theory [86]. $E = 3(1-\nu^2)f/4d^{3/2}r^{1/2}$, where d is the indentation depth of a steel ball with radius r exerting a buoyancy-corrected force f on the surface of a gel with Poisson's ratio $\nu = 0.3$ [183]. A steel ball (r = 0.32 mm, Abbott Ball Co.) was placed on gels embedded with fluorescent beads (Invitrogen, 500 nm diameter) and indentation depth was measured by focusing the microscope on beads that returned to their original position in the gel after removal of the ball as we have done previously to confirm E [30].

Traction Force Microscopy

Traction force microscopy (TFM) was used to quantify cellular traction forces. TFM maps the magnitude and spatial orientation of traction stresses exerted by a cell on its substrate by tracking displacements created in the substrate domain by the cell [61]. Cells were seeded on PA gels embedded with fluorescent beads, allowed to attach and spread overnight, and were imaged in a custom temperature, humidity, and CO_2-controlled stage of a Zeiss Axio Observer Z1m microscope with a Hamamatsu ORCA-ER camera. Bead fields were imaged before (stressed configuration) and after removal (relaxed configuration) of the cell with trypsin (Invitrogen). These images allowed substrate displacements to be tracked with correlation-based optical flow [184]. Substrate displacements were translated into a strain field that was used to compute traction stresses using Bayesian statistics that maximized the most likely traction field

that describes the given strain field [185]. The substrate strains were converted to traction stresses using the LIBTRC analysis library developed by Professor Micah Dembo of Boston University, who also invented the basic theory that underlies TFM. Images were processed with LIBTRC to determine the cellular traction vectors, T (stress vectors), the total magnitude of the force, $|F|$, and the projected cell area. $|F|$ is an integral of the traction field magnitudes over the cell area,

$|F| = \iint \left(T_x^2(x,y) + T_y^2(x,y)\right)^{1/2} dxdy$, where $T(x,y) = [T_x(x,y),\ T_y(x,y)]$ is the continuous field of local cellular traction vectors defined at local spatial positions (x, y) in the projected cell area [31]. Note that the mean traction vector over the entire cell area is assumed to be zero to satisfy a constraint of global force balance.

Statistics and Regression Modeling

Data for Figures 4.3, 4.5-4.6 were analyzed with analysis of variance (ANOVA) and Tukey's Honestly Significant Difference test, or Student's *t* for Figure 4.8, after natural log transformation to ensure assumptions of normality and equal variance. For regression modeling, force and area data were transformed by natural log to ensure model assumptions of residual normality and equal variance. All regression model parameter residuals had a Cook's distance less than one indicating that no data point influentially distorted the regression outcome, and all parameter estimate variance inflation factors were less than three indicating the regression model did not suffer from multicollinearity [186]. ANOVA, Student's *t*, and regression modeling were performed in JMP software (SAS Institute). Sample sizes (n) for single cells (Figures 4.3, 4.5, and 4.8) were n = 24, 14, 25, and 38 for E = 1, 2.5, 5, and 10 kPa substrates, respectively, and n = 17, 23, 6, 15, and 12 for collagen concentrations of 0.01, 0.1, 1, 10, and 100 μg/mL, respectively (Figure 4.5). Sample sizes for two-cells in contact (Figure 4.8) were n = 16 and 20 (pairs of cells) for E = 1 and 10 kPa substrates,

respectively. All analyses satisfied a statistical power of 0.8 or higher and a level of significance of 0.05 was assumed for all statistics.

4.4 Results

Endothelial Cell Traction Force and Area Increase with Increasing Substrate Stiffness

To investigate the role of substrate stiffness in mediating EC traction force generation, cells were seeded on PA substrates where the applied collagen concentration was fixed (100 μg/mL) across stiffness. Figure 4.2 shows representative traction maps of ECs on compliant to stiff (E = 1–10 kPa) PA substrates. The magnitude and orientation of the traction stresses, T, are shown by the color-coded vector plot over the projected cell area. Traction vectors are oriented toward the center of the cell (contractile) and are largest at the cell edge of lamellipodia. Note that cell morphology changes from spindle shaped on compliant gels toward more isotropic spreading with increasing substrate stiffness. Further analysis showed that the magnitude of the traction force, $|F|$, increased significantly (*) over the range of increasing substrate stiffness E = 1–10 kPa (Figure 4.3A) with a concomitant significant increase in projected cell area with substrate stiffness at fixed applied collagen concentration (100 μg/mL) (Figure 4.3B). A plot of the traction force of each cell normalized by its projected area and averaged for each substrate stiffness demonstrated the same statistically significant positive correlation suggesting substrate stiffness influenced traction force generation (Figure 4.3C).

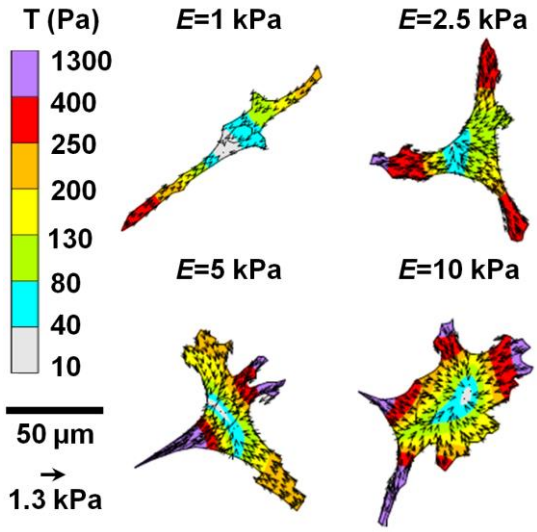

Figure 4.2. Representative images of EC morphology and traction stresses on variably compliant substrates.
Representative images of EC morphology and traction stresses, T, on poly(acrylamide) gel substrates of increasing substrate stiffness (E = 1-10 kPa). Inner circles depict localization of cell nuclei.

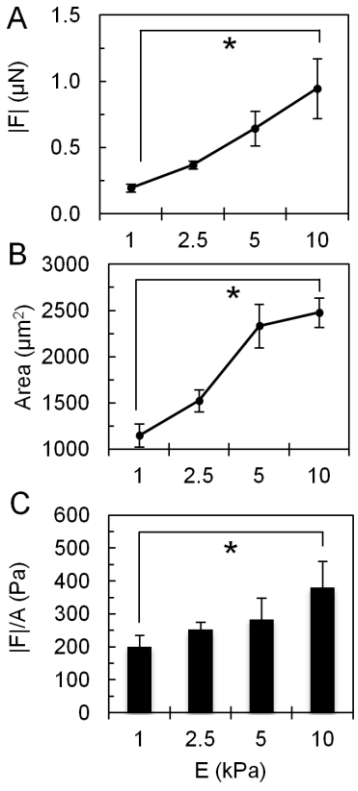

Figure 4.3. Traction force magnitude and cell area increase with increasing substrate stiffness.
Traction force $|F|$ (**A**) and cell area (**B**) versus substrate stiffness over the range E = 1-10 kPa at constant collagen concentration (100 μg/mL). Mean ± SEM. (**C**) $|F|$ of each cell normalized by its projected area ($|F|$/A) and averaged for each substrate stiffness. Mean + SEM. * indicates $p<0.0001$.

A Linear Regression Model Indicates Substrate Stiffness and Cell Area Are Predictors of Cellular Traction Force

We established experimentally that cells of greater spread area exerted greater traction force, but it was not clear whether cells of a similar area exerted the same traction force across substrate stiffness levels. To determine if the ratio of traction force to spread cell area was independent of substrate stiffness, we plotted force vs. area for each stiffness level (E = 1–10 kPa), and fit the data with linear regression lines (Figure 4.4; inset represents magnification of the boxed region to emphasize regression trends between stiffness levels). The data plot indicated that cell area alone could not always predict traction force. Small cell areas usually correlated with less traction forces on compliant 1 kPa gels (Figure 4.4 inset—open circles); however, as cell area increased, the traction force magnitude output varied with substrate stiffness (Figure 4.4 inset—*e.g.*, see shaded region centered at 1750 μm^2). Moreover, the slopes of the linear regression lines were non-parallel and increased with substrate stiffness suggesting that stiffness was a crucial parameter that contributed to the interaction between cell area and traction force. Re-plotting this data set as traction force normalized by cell area against substrate stiffness indicated a statistically significant positive association with increasing stiffness (Figure 4.3C). To formally test whether substrate stiffness and cell area were significant predictors of traction force, we used a least-squares multiple linear regression model that related force to area and stiffness. We used an additive linear model of the form

$$Y = \beta_0 + \beta_1 x_1 + \beta_i x_i + \varepsilon, \quad (1)$$

where Y represents the response traction force, β_0 is the intercept, β_1 is the partial slope of quantitative variable x_1 representing area, β_i is the partial slope of qualitative

variable x_i representing the parameter stiffness, where x_i = [(1 if level i), (0 otherwise)], represents the four levels of stiffness tested (1, 2.5, 5, and 10 kPa), with summation implied over i=2-4, and ε is random error. This regression model assumed a linear relationship between force and area [30,187] and quantitatively assessed if the partial slopes representing the parameters area and stiffness were significant predictors of traction force. The p-values of the linear regression model parameters indicated that both cell area and substrate stiffness were significant predictors of EC traction force (Table 4.1). A comparison of p-values between parameters stiffness (p = 0.0187) and area ($p < 0.0001$) suggests that cell area may be more influential in driving traction forces in single ECs.

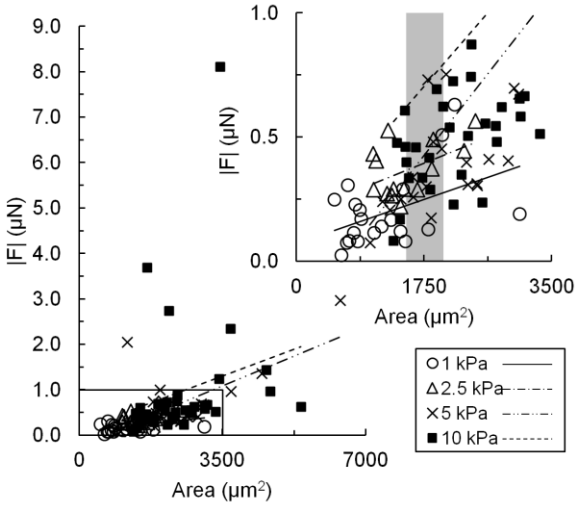

Figure 4.4. Plot of traction force magnitude vs. cell area fit with linear regression lines.
Plot of traction force $|F|$ versus cell area fit with linear regression lines for each stiffness level E = 1-10 kPa at constant collagen concentration (100 μg/mL). Inset represents magnification of the boxed region to clarify regression trends. Shaded region of inset highlights variable force output for cells of similar spread area.

Table 4.1. List of *p*-values for significance of predictors *E* and Area on |*F*|

Regression Model	Predictor of |*F*|	*p*-Value
Single cells/Eq. (1)	*E*	0.0187
	Area	<0.0001
Cell pairs/Eq. (2)	*E*	<0.0001
	Area	0.0010

Endothelial Traction Force and Area Increase with Increasing Matrix Ligand Concentration

Since increases in force correlate with both increases in substrate stiffness (Figure 4.3A) and spread cell area (Figure 4.3B), we asked whether force could be modulated by cell area when substrate stiffness was held constant and area was modulated using substrate ligand density. To test this, ECs were seeded on PA gels of constant stiffness (E = 5 kPa) with variable applied collagen concentration (0.01–100 μg/mL). EC traction force (Figure 4.5A) and cell area (Figure 4.5B) increased significantly (*) with increasing collagen concentration when substrate stiffness was held constant. To determine how cell area and ligand concentration contributed to force generation at constant stiffness, traction force vs. cell area was plotted for each collagen concentration and fit with linear regression lines (Figure 4.5C). The data suggested that for a given collagen concentration, force increased with area. To formally test whether area and ligand concentration were predictors of force, we applied the model presented in Eq. (1) where $\beta_i x_i$ was summed over i = 2-5 to represent the five levels of collagen concentrations tested (0.01, 0.1, 1, 10, and 100 μg/mL), and all other parameters were as described above. The analysis indicated that cell area was a significant predictor of traction force (p = 0.0002), but that ligand density was not (p =

0.9404). Importantly, these data show that traction forces are driven by cell area, not ligand density. Together with the results presented in Figure 4.3, these data indicate that traction force increased when cell area was increased through changes in either substrate stiffness (Figure 4.3A) or ligand density (Figure 4.5A).

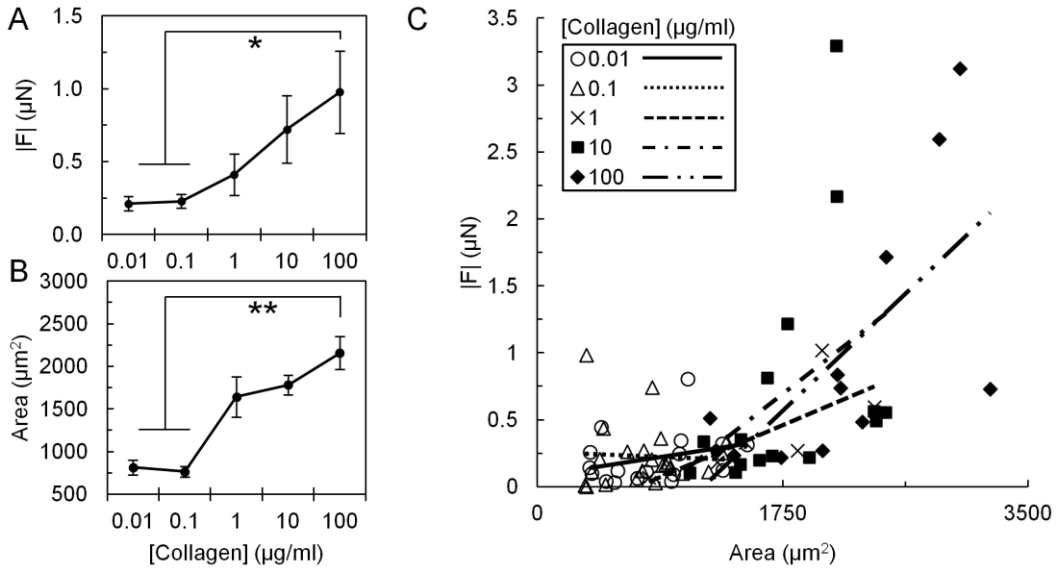

Figure 4.5. Traction force magnitude, cell area, and regression modeling for substrates of variable collagen concentration.
Traction force $|F|$ (**A**) and cell area (**B**) versus applied collagen concentration of 0.01-100 μg/mL at fixed substrate stiffness (E = 5 kPa). Mean ± SEM; * indicates $p < 0.001$; ** indicates $p < 0.0001$. (**C**) Plot of $|F|$ versus area for each collagen concentration on E = 5 kPa gels and fit with linear regression lines.

Similar to substrates derivatized with collagen, we determined that EC area increased with increasing concentrations of fibronectin (Figure 4.6). These data indicate that cell area is sensitive to collagen or FN matrix density.

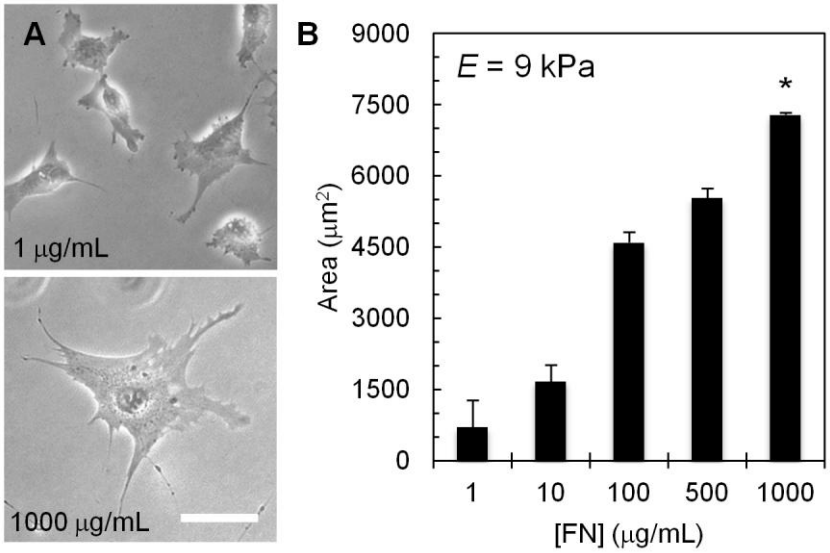

Figure 4.6. EC area increases with increasing fibronectin concentration.
ECs were plated on 9 kPa substrates derivatized with variable concentrations (1-1000 μg/mL) of fibronectin (FN). (**A**) Cells appeared spread on substrates derivatized with 1 μg/mL FN and increased in size up to 1000 μg/mL FN. Scale bar is 50 μm. (**B**) Quantification of cell area (n=50 for each condition) indicated a significant increase in cell area with increasing FN concentration (*$p<0.05$; ANOVA).

Endothelial Two-Cell Aggregates Exert Increased Traction Forces

Cells do not typically reside in isolation *in vivo*. While our data indicate that substrate stiffness and cell area both play a role in cell force generation in single cells, it is not clear if these relationships are maintained while cells are in contact with other cells. Two ECs in contact on E = 1 and 10 kPa gels were analyzed with TFM and modeled as a single force-generating unit (Figure 4.7). Note that cell–cell connections on compliant 1 kPa gels tend to be oriented end-to-end compared to cell–cell connections between cells on stiffer 10 kPa gels that exhibit increased spreading. Similarly to single cells (Figure 4.2), traction forces of cells in contact are contractile and greatest

at cell edges and in lamellipodia. As expected, $|F|$ of two cells in contact was significantly greater (*) than the force generated by single cells across the two substrate moduli tested (Figure 4.8). Notably the increase in traction force generation of two cells in contact compared to single cells is greater on stiff substrates (a 126% increase on 10 kPa gels compared to a 76% increase on 1 kPa gels).

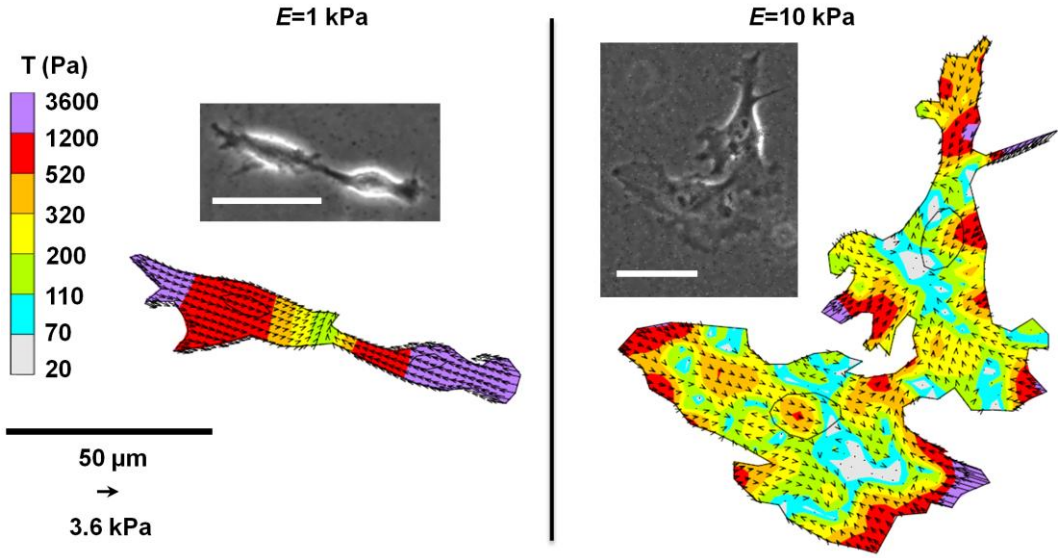

Figure 4.7. Representative images of cell morphology and traction stresses for two ECs in contact.
Representative images of two ECs with a portion of their membrane in contact on E = 1 and 10 kPa substrates were modeled as a single force generating unit with TFM. Inner circles depict localization of cell nuclei. Scale bars in phase images are 50 μm.

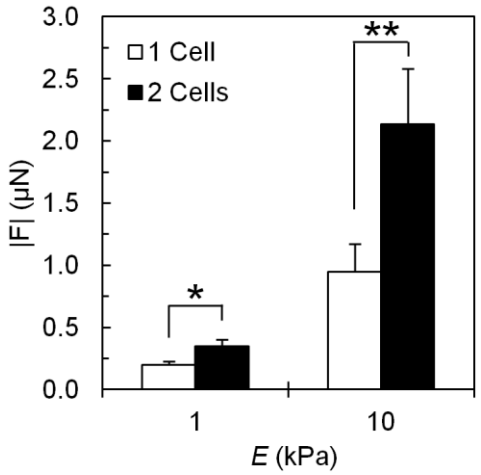

Figure 4.8. Traction force magnitude increases when ECs are in contact. Traction force $|F|$ of single and two ECs in contact on E = 1 and 10 kPa substrates at constant collagen concentration (100 μg/mL). Relative increases in force between single and two ECs in contact are 76% on 1 kPa gels and 126% on 10 kPa gels. Mean + SEM; * indicates $p<0.005$; ** indicates $p<0.001$.

To determine if cell area and substrate stiffness were significant predictors of traction force of cells in contact, as we found for single cells, we used an additive linear model of the form

$$Y = \beta_0 + \beta_1 x_1 + \beta_2 x_2 + \beta_3 x_3 + \varepsilon, \quad (2)$$

where Y, β_0, β_1, x_1, and ε are as defined above for Eq. (1), β_2 is the partial slope of qualitative variable x_2 representing the parameter stiffness (1 and 10 kPa), and β_3 is the partial slope of qualitative variable x_3 representing the parameter number of cells (one-cell and two-cell aggregates). Similarly to model Eq. (1), this model assumed a linear relationship between force and area and quantitatively accounted for the parameters substrate stiffness, cell area, and cell number in mediating traction force. Again, the linear regression model indicated that both cell area and substrate stiffness were significant predictors of traction force (Table 4.1). A comparison of p-values indicated that substrate stiffness was a more significant predictor of traction force than area for cells in contact ($p < 0.0001$ for stiffness compared to $p = 0.0010$ for area)

which was in contrast to our findings in single cells where area was more significant. Additionally, substrate stiffness was a more significant predictor of force for cells in contact compared to single cells ($p < 0.0001$ for cell pairs compared to $p = 0.0187$ for single cells). These data indicate that substrate stiffness plays a prominent role in directing traction forces of cells in contact.

4.5 Discussion

In this study, we show for the first time that both cell spread area and substrate stiffness are significant predictors of cellular traction force in endothelial cells, and that substrate ligand density does not directly drive traction generation. Our previous data indicate that EC area increases with increasing substrate stiffness [31,112], and EC traction force positively correlates with greater cell spread area [64]. Together, these findings support a model of interaction where traction force is driven by a coupling of cell area and substrate stiffness. Further, we demonstrate that traction force cannot be predicted by cell area alone—force also depends on underlying substrate stiffness (Figure 1). These results are important because they show for the first time that substrate stiffness can alter cellular force profiles independently of changes in cell area. Because matrix stiffening occurs in a number of disease states including atherosclerosis, wound healing, and cancer, these results have important ramifications for understanding the baseline force profiles of cells as a function of their extracellular mechanical environment.

To investigate the relationship between cell area and traction generation, cell area was manipulated experimentally by changing substrate stiffness and increasing the density of ligand on the surface of the substrate. In both cases, we found a positive correlation between cell area and traction force magnitude. When substrate stiffness was varied,

normalizing force by area showed an increase relative to stiffness, indicating that substrate stiffness (and not area alone) was driving an increase in force. When stiffness was held constant, cell area (and not ligand density) was driving an increase in force. Data from our lab and others indicates that increasing substrate stiffness or ligand density can lead to integrin clustering and increased focal adhesion number and size [29,31,71]. Since ligand density is not a predictor of traction force, it is unclear whether we can attribute changes in force to differential integrin clustering when stiffness is held constant. While integrin clustering may contribute to increases in force generation, our data suggest that substrate stiffness and cell area (whether modulated by stiffness or ligand density) are prominent and significant contributors to force.

While our study specifically focused on endothelial cells, the results may translate to other cell types as well. Substrate stiffness and cell area have been shown to influence traction force generation in other cell types, and should be the subject of future investigations. It has been demonstrated in 3T3 fibroblasts and mammary epithelial cells that increases in traction force generation with substrate stiffness are accompanied by an increase in cell area [16,86]. As was studied here, it would be interesting to investigate whether cell area, substrate stiffness, and traction stress generation are linked in other cellular systems and whether their interactions are universal.

In addition to studying single cell force generation, we also investigated the relationship between force, cell area, and substrate stiffness of cells in contact. Our goal in these studies was to determine whether the relationship we found for single cells, which indicated that both substrate stiffness and cell area were important

determinants of force generation, holds once cells are in contact. Very few studies have tackled the question of traction stress distribution of cells in contact. Because cell contact occurs in the healthy physiological state, these studies are critical to understanding cell contractility and response to the mechanical properties of the extracellular matrix *in vivo*.

Our results of traction forces of cells in contact indicate that both substrate stiffness and cell area predict force in two-cell aggregates. Importantly, these data show that once in contact, cells maintain sensitivity to substrate stiffness. We demonstrate for the first time that once in contact with an adjacent cell, ECs exert greater traction forces compared to single cells. The increase in traction force output by cell assemblies compared to single cells suggests an increase in cellular contractility with contact. It was shown previously that stress fiber organization follows cell–cell contact on compliant substrates [71]. An increase in actin fiber organization upon cell–cell contact likely facilitates increased cellular contractility thereby increasing traction force output compared to single ECs. An increase in traction force with cell contact has also been reported in epithelial cell monolayers that exert traction forces that are greater than stresses measured in single cells [188]. Taken together, these data suggest that the increase in traction force generation that is initiated upon cell–cell contact may be sustained during tissue formation and depend significantly on substrate stiffness.

Interestingly, the increase in traction force with cell–cell contact on compliant gels was less than two-fold greater (76%) while the increase on stiff gels was more than two-fold (126%). We have previously established that ECs are capable of sensing the traction forces exerted by adjacent cells that drive cell–cell interactions, and that cell–

cell connectivity changes with substrate stiffness; cells on compliant gels prefer cell–cell connections and cluster while those on stiffer substrates prefer cell–substrate interactions and migrate away from each other [36]. The difference in magnitude of increased traction force output with substrate stiffness may result from an optimization of cell–substrate and cell–cell interactions. It has been shown that integrins and cadherins, mediators of cell–substrate and cell–cell connections, respectively, are involved in crosstalk with intracellular mediators of contractility [171,189] that govern traction force. While our use of TFM to model two cells in contact did not account for changes in the temporal stability of cell–cell contacts with stiffness or potential effects of cadherin-mediated changes in cellular contractility, our measurements of traction forces during cell–cell contact further implicate substrate mechanics as an important modulator of cellular traction forces.

In summary, we have used TFM to quantify a relationship between cell spread area, substrate stiffness, and traction force generation. We have used a multilinear regression model to show for the first time that both cell area and substrate stiffness are significant predictors of traction force in endothelial cells. Our data underscore the importance of substrate stiffness and cell spreading as key contributors to the ability of cells to generate force.

CHAPTER 5

SUBSTRATE STIFFNESS ALTERS FIBRONECTIN SYNTHESIS AND DEPOSITION

Portions of this chapter are in preparation for submission.

5.1 Abstract

The mechanical microenvironment is an important mediator of cell function. In particular, the stiffness of the extracellular matrix (ECM) regulates cell responses including adhesion, migration, differentiation, and tissue morphogenesis. These responses are facilitated by cell-ECM interactions, and suggest that matrix stiffness fundamentally alters the interaction between cells and the ECM; however, this relationship is not well understood. Here, we investigate the role of substrate stiffness in mediating the synthesis and deposition of fibronectin (FN) by endothelial cells. We demonstrate that substrate stiffness alters the dynamics and density of FN deposition, and the expression of EDB-FN, an FN isoform specific to neovasculature. ECs on compliant substrates adopt a bipolar morphology and deposit unidirectional fibrils of FN in contrast to an omnidirectional web-like mesh deposited on stiff substrates. Unidirectional deposition of FN can be recapitulated on stiff substrates by enforcing a bipolar morphology. Differences in FN deposition with stiffness are due to changes in cell shape and the directionality of ROCK-mediated traction forces. These findings indicate that substrate stiffness is a crucial regulator of ECM synthesis and deposition, and suggest that the mechanical microenvironment fundamentally alters cell-ECM interactions.

5.2 Introduction

The mechanical microenvironment is an important regulator of cell function. The stiffness of the extracellular matrix (ECM) has emerged as a prominent mediator of cell adhesion, spreading, migration, and differentiation [71,86,112,149,190]. These responses all require cell-ECM interactions, and suggest that matrix stiffness fundamentally alters the interaction between cells and the ECM. Previously, we demonstrated that compliant matrices support the self-assembly of capillary networks that require the polymerization of fibronectin (FN) [98,112], a major ECM constituent that mediates cell adhesion, migration, and differentiation [191]. While these findings suggest that substrate stiffness mediates the differential expression and deposition of FN that enables capillary network assembly, this relationship is unknown.

FN is a dimeric glycoprotein required for embryonic development [99] and cardiovascular morphogenesis [100]. In tissues, FN may contain extra domain B (EDB), a type-III homology domain resulting from differential exon splicing [106]. While essentially undetectable in normal adult tissues [107], EDB-FN is a specific marker for angiogenic blood vessels [108] and may be an important clinical target for localizing tumor vasculature [109]. In cancer, solid tumors are associated with an increase in tissue stiffness [16], alterations in local vasculature [110], and growth requiring neovascularization [111]. These findings suggest that matrix stiffness plays a role in mediating angiogenic (EDB-containing) vessel formation; however, the sensitivity of EDB-FN expression to substrate stiffness is unknown.

During FN ECM assembly, compact FN dimers are converted into an insoluble fibrillar matrix [101]. Such fibril polymerization is associated with cell contractility that exposes cryptic self-assembly sites that may contribute to fibril assembly

[103,104]. Deposited FN fibrils are thus directed by cellular traction forces [173]. In addition, we have demonstrated that substrate stiffness and cell size are important contributors to endothelial cell contractility [149]. Taken together, these data suggest that FN is sensitive to substrate stiffness-mediated alterations in EC shape and endogenous traction forces, however, these relationships are poorly understood.

Here, we investigated the role of substrate stiffness in mediating FN deposition. We demonstrate that substrate stiffness regulates the dynamics of FN deposition through alterations in cell shape and the directionality of ROCK-mediated traction forces that guide fibril deposition. Furthermore, these data for the first time indicate that substrate stiffness is a mediator of EDB-FN synthesis and deposition. These findings suggest that the mechanical microenvironment fundamentally alters EC-FN interactions.

5.3 Materials & Methods

Cell Culture

Bovine aortic endothelial cells (BAEC; VEC Technologies, Rensselaer, NY) were maintained as described previously [149]. Primary human umbilical vein endothelial cells (HUVEC) were maintained at 37°C and 5% CO_2 in Medium 200 supplemented with 5% fetal bovine serum (Gibco, Life Technologies, Grand Island, NY), 2% low serum growth supplement, and used to passage 9. MCF10A human mammary epithelial cells (ATCC, Mannassas, VA) were maintained at 37°C and 5% CO_2 in Dulbecco's Modified Eagle Medium (Gibco) supplemented with 5% horse serum (Gibco), 1% penicillin-streptomycin (Gibco), 0.1% insulin, 0.05% hydrocortisone (Sigma-Aldrich, St. Louis, MO), 0.02% epidermal growth factor (Gibco), and 0.01% cholera toxin (Sigma).

Polyacrylamide Gel Synthesis and Stiffness Characterization

Variably compliant PA gels were prepared as described previously [28,30,112,149]. and derivatized with an applied type I collagen (BD, Franklin Lakes, NJ) concentration of 100 μg/mL [112]. Gels were synthesized with Young's Moduli (*E*) of 0.2-10 kPa to mimic physiologically relevant tissue stiffness [151]. Substrate stiffness was confirmed by measuring *E* at the gel surface as described previously [30,149].

Fibronectin Immunofluorescence Localization

Endothelial cells on PA gels were processed for fluorescence imaging as described previously [112]. Briefly, samples were fixed for 15 min in 3.7% (v/v) formaldehyde (JT Baker, Phillipsburg, NJ) in PBS (Gibco) and blocked with 3% (w/v) BSA (Sigma) in PBS for one hour. To localize fibronectin (FN), samples were incubated 1:50 in 1% (w/v) BSA in PBS with an anti-FN primary antibody (A17, or BC1 for EDB-FN only, Santa Cruz Biotechnology (SCBT), Santa Cruz, CA) overnight at 4°C and an Alexa Fluor-labeled secondary antibody (Molecular Probes, Life Technologies, Grand Island, NY) for one hour at room temperature. Actin was localized with Alexa Fluor-labeled phalloidin (Molecular Probes) and nuclei labeled with DAPI (Sigma). Fluorescent images were acquired with a Zeiss Axio Observer Z1m or a Zeiss 710 confocal microscope. Images were pseudo-colored and z-stacks were reconstructed with Zen software (v. 2009, Carl Zeiss, Germany). To determine FN solubility, samples were treated with 10% (w/v) sodium deoxycholate (DOC; EMD Chemicals, Gibbstown, NJ) in deionized water for 5-10 minutes before fixation.

Laminin Immunofluorescence Localization

MCF10A cells on PA gels were fixed as described above and stained for laminin-5

with an anti-laminin-γ2 primary antibody (GB3, SCBT). Confocal z-stacks were used for 3D reconstructions as described above.

Fibronectin Fluorescent Quantification

Images of fluorescently-labeled FN used for quantification were acquired under the same microscope exposure settings. To quantify the fluorescent signal, ImageJ [153] was used to measure the integrated density (the product of the image area and the mean gray-scale pixel value) of each input image (microscope fields of the FN channel) after subtraction of the mean gray-scale value to reduce background signal. Since the area of each image analyzed used for comparisons was of identical and constant area, the results were reported as simply the mean gray-scale pixel value.

Fibronectin Western blot

HUVECs were plated on 1 and 10 kPa PA gels, rinsed with ice-cold Tris-buffered saline (TBS), and lysed on ice with 2X Laemmli lysis buffer (62.5 mM Tris-HCl, 25% glycerol (JT Baker), 5% b-mercaptoethanol (BioRad, Hercules, CA), 2% sodium dodecyl sulfate (SDS; JT Baker), and 0.01% bromophenol blue (BioRad) in deionized water) after three days. The lysate was harvested, mixed, and spun at 14k x*g* at 4°C and the supernatant was removed for analysis. 1X Laemmli buffer was added to the supernatant and samples were heated for 5 min at 95°C. Equal volumes of sample were loaded into SDS-polyacrylamide gels and subjected to electrophoresis with a Mini-PROTEAN Tetra System (BioRad) in Tris-glycine running buffer (25mM Tris, 192 mM Glycine, 0.1% SDS). Proteins were transferred to nitrocellulose membranes (BioRad) with a Criterion Blotter system (BioRad) in cold transfer buffer (25 mM Tris and 192 mM Glycine). Membranes were blocked with 5% (w/v) milk (Nestlé, Wilkes-Barre, PA) in TBS-polyoxyethylene (20) sorbitan monolaurate (Tween; JT

Baker), incubated overnight 1:500 in TBS-Tween with an anti-fibronectin primary antibody (A17, or BC1 for EDB-FN, SCBT) at 4°C, and 1:2000 in TBS-Tween with 0.1% (v/v) milk with a horseradish peroxidase-conjugated secondary antibody for one hour at room temperature. Samples were images with a Las-4000 imaging system (Fujifilm Life Science, Japan) after addition of Immobilon Chemiluminescent Substrate (Millipore, Billerica, MA). Samples were stripped with Restore Stripping Buffer (Thermo Scientific, Logan, UT), re-blocked with milk, incubated 1:1000 in TBS-Tween with an anti-glyceraldehyde-3-phosphate dehydrogenase (GAPDH) primary antibody (6C5, Millipore) at room temperature for one hour, incubated 1:2000 in TBS-Tween with 0.1% (v/v) milk with a horseradish peroxidase-conjugated secondary antibody for forty-five minutes at room temperature, and reimaged. Densitometry was performed with imageJ and expressed as the fold change of the ratio of FN to GAPDH of samples from 10 kPa gels compared to 1 kPa gels. Data were the results of three independent experiments.

Laminin Western blot

MCF-10A human mammary epithelial cells were plated on 0.2 and 10 kPa PA substrates. Samples were lysed after three days, subjected to PAGE, transferred to nitrocellulose, and analyzed as described above, but treated with an anti-laminin-γ2 primary antibody (B2; SCBT). Data were the results of three independent experiments.

Fibronectin Quantitative Real-Time PCR

HUVECs were plated on 1 and 10 kPa PA gels, rinsed with PBS, and collected after the addition of 0.25% trypsin-EDTA (Gibco) for 10 min at 37°C after three days. Cells were pelleted, rinsed with PBS, and total RNA was purified with an RNeasy

Plus Mini Kit (Qiagen, Valencia, CA). To generate cDNA, 1 μg of total RNA per sample was mixed with 80 μM random primers (Invitrogen, Life Technologies, Grand Island, NY), 10 mM deoxynucleotide solution mix (New England Biolabs (NEBL), Ipswich, MA), nuclease-free water, and heated for 5 minutes at 75°C. After the addition of 40U/μL RNase inhibitor, and 200 U/μL M-MuLV Reverse Transcriptase in M-MuLV reaction buffer (NEBL), cDNA was synthesized in an iCycler thermal cycler (BioRad). cDNA was diluted 1:50 in deionized water, prepared for quantitative real-time PCR by the addition of 300 nM forward primer, 300 nM reverse primer (Integrated DNA Technologies (IDT), Coralville, IA), 1X iQ SYBR Green Supermix (BioRad), and analyzed with a My iQ Real-Time PCR Detection System (BioRad). The primers used for EDB-FN were 5'-CCTGGAGTACAATGTCAGTG-3' (Forward) and 5'-GGTGGAGCCCAGGTGACA-3' (Reverse) [192]. Primers for the reference gene GAPDH were 5'-CATGAGAAGTATGACAACAGCCT-3' (Forward) and 5'-AGTCCTTCCACGATACCAAAGT-3' (Reverse). The results were expressed as a fold change in gene expression of EDB-FN relative to GAPDH on 10kPa gels compared to 1 kPa gels using the Livak method. Data were the results of three independent experiments.

Fibronectin Transfection

To determine the quality of FN deposition in real time, BAECs were transfected with YFP-FN, a kind gift from Dr. Harold Erickson and Dr. Tomoo Ohashi. Plasmid DNA was amplified in DH5a cells (Invitrogen) and purified with a Quantum Prep Plasmid Midiprep Kit (BioRad). For transfection, BAEC were grown to 90% confluency in wells of six-well plates, washed twice with Optimem (Gibco), and incubated with 2 μg DNA plus 5 μL Lipofectamine 2000 (Invitrogen) in Optimem per well for five hours, and replenished with fresh complete Medium 199. Transfected ECs were plated on

PA substrates 24 hours after transfection and imaged with time-lapse microscopy beginning 48 hours after transfection.

ROCK Knockdown

To disrupt ROCK1-mediated cellular contractility, BAEC were plated on PA gels in the presence of 10 μM Y27632, a concentration we have shown previously to reduce cell-generated traction forces [170]. Samples were fixed at 4-48 hours after plating and stained to localize FN, actin, and nuclei as described above. ROCK1 was also disrupted with RNAi. BAEC were also treated with an siRNA against bovine ROCK1 (Invitrogen) or a control siRNA (SCBT). To knockdown ROCK1, BAEC were grown to 60-80% confluency in wells of six-well plates, washed twice with Optimem, and incubated with 20 pmol siRNA in 5 μL Lipofectamine 2000 in Optimem per well for 5 hours, and replenished with complete Medium 199. Transfected cells were plated on PA substrates 24 hours after transfection, and samples were fixed at 24-hour time points over the next three days and stained to localize FN, actin, and nuclei as described above. Separate experiments determined the expression of ROCK1 with Western blotting over the same three-day period as described above but using an anti-ROCK1 primary antibody (H-85; SCBT). Similarly, HUVEC were treated as described above for BAECs with siRNA against human ROCK1 (H-85; SCBT) or a control siRNA (SCBT), and stained to localize EDB-FN on the third day post-plating as described above. Western blotting was performed at this same time-point as described above but using an anti-ROCK1 primary antibody (H-85; SCBT).

Traction Force Microscopy

Traction force microscopy (TFM) was used to quantify cellular traction stresses as described previously [149]. Substrate strains generated by cells were converted to

traction stresses using the LIBTRC analysis library developed by Professor Micah Dembo of Boston University, who also invented the basic theory that underlies TFM [61,185]. LIBTRC was used to determine the cellular traction stresses, and their components projected along the long and short axis of the cell area by taking the integral of the absolute value of the traction magnitudes dotted with a unit vector directed along the long and short cell axis, respectively. Data were plotted as the relative percent each projection (long and short) contributed to the total of both projections. Traction vectors were omitted from every other node for pictorial clarity.

Fibronectin Polymerization Inhibitor

Fibronectin polymerization was inhibited by the addition of 500 nM pUR4B [193] to the cell suspension during plating [112]. Control samples were plated in the presence of control peptide III-11C [112] (kind gifts from Dr. Jane Sottile). Traction force microscopy was performed on n=60 and 72 cells for control and pUR4B treatment conditions, respectively, for cells on E=5 kPa PA gels 24 hours after plating. For area measurements over time, n=15 cells per condition on E=0.2 kPa PA gels were imaged with time-lapse microscopy and analyzed with imageJ to determine the projected cell area, and cell centroids at ten-minute intervals for a period of four hours starting 24 hours after plating. Migration speed was determined with MATLAB (The MathWorks, Inc., Natick, MA) code [175] that fit the mean-square cell displacement $\langle d^2 \rangle$, the time interval t, persistence time P, and cell speed S, to the random walk equation with nonlinear least-squares regression analysis: $\langle d^2 \rangle = 2S^2P(t-P[1-\exp(-t/P)])$ [194].

Micropatterning Polyacrylamide Substrates

Polyacrylamide substrates were micropatterned with methods adapted from Rape *et al*.

[195]. Silicon molds were fabricated with arrays of 15x300 μm^2 rectangular or 22x22 μm^2 square features as described previously [196], and used to cast PDMS stamps. Prior to gel polymerization, type I collagen (100 μg/mL) was mixed with 20 μmol/mL N-6-((acryloyl)amido)hexanoic acid (synthesized in our lab according to the method of Pless *et al*. (N6; [32])) in HEPES buffer (pH 8) (EMD Chemicals) for 2 hours on ice. This mixture was pipetted onto PDMS stamps (4 arrays of 4x7 mm^2 regions of features) and incubated for 30 minutes at room temperature to "ink" the stamps. Excess collagen-N6 mixture was removed, and inked stamps were placed in contact with clean glass 22x22 μm^2 coverslip for 5 minutes, and carefully removed. This stamped glass was used as the top coverslip in the traditional polyacrylamide gel-synthesis protocol [112]. Micropatterned 10 kPa PA substrates were fixed and stained as described above to localize collagen patterning with an anti-type I collagen primary antibody (Millipore) and an Alexa fluor-labeled secondary antibody (Molecular Probes).

Cell, Actin and FN Polarization Quantification

Cell elongation was determined for individual cells by measuring the aspect ratio (ratio of lengths of the major to minor axes of a fit ellipse) from cell outlines with ImageJ. Fluorescent images of actin and FN were acquired three days after plating cells, to allow fibril deposition, and processed with ImageJ to determine their respective angle of orientation. Cell outlines were traced and fit with an ellipse to determine the orientation angle of the long axis of the cell [80] and the overall orientation of the filamentous actin and FN associated with the cell with OrientationJ, a free ImageJ plug-in that characterizes the orientation and isotropy properties of a region of interest qualitatively with hue and quantitatively as an output angle with respect to the horizontal axis [197]. The output angles between cell and actin, and

actin and FN were compared. The overall angle range was converted to 0-90 degrees (acute supplementary angles were determined from obtuse output orientation angles) to determine the minimum difference in degrees between orientations.

Statistics

EDB-FN deposition (Figures 5.5B, 5.14C) resulted from n=10 and 40 fields of view per condition, respectively, and were analyzed with Student's *t* test. Actin and FN polarization data (Figure 5.7C-D) resulted from n=30 cells per condition and were analyzed with Student's *t* test. The aspect ratio of individual cells (not in contact with other cells) resulted from n=70 cells per condition (Figure 5.8C), and n=71 and 68 cells for E=0.2 and 10 kPa substrates, respectively (Figure 5.18E), and were analyzed with Student's *t* test. Traction polarization data (Figure 5.8D) resulted from n=24, 14, 25, and 38 cells on E=1, 2.5, 5, and 10 kPa substrates, respectively, for individual cells and were analyzed with ANOVA and Tukey's HSD test. For cell-cell contact, n=16 and 20 pairs of cells for E=1 and 10 kPa, respectively (Figures 5.8E-F) were analyzed with Student's *t* test. The sample size of cells on micropatterned substrates (Figure 5.9C) were n=58 and 29 for 1 cell pattern and 2 cell pattern, respectively. Patterned vs. non-patterned results for a given stiffness were compared with Student's *t* test. Quantification of FN deposition for Y27632 experiments (Figure 5.12B) and ROCK siRNA experiments (Figure 5.13C) resulted from n=8-12 and n=11-16 fields of view per condition, respectively, and were analyzed with 2-way ANOVA and Tukey's HSD test. Cell area measurements (Figures 5.12C, 5.13D) resulted from n=50 cells per condition and were also analyzed with 2-way ANOVA and Tukey's HSD test. Quantification of traction forces and area for cells treated with FN siRNA (Figures 5.16C-D) resulted from n=52 and n=57 cells for treatment and control conditions, respectively. Traction forces for cells treated with FN inhibitor pUR4B (Figure

5.16E) resulted from n=60 and 72 cells for control and pUR4B treatment, respectively, and n=15 cells per condition for area (Figure 5.16F) and migration data (Figure 5.16G), respectively, and were analyzed with Student's *t* test. All bar graphs were reported as mean +/- SEM. Analyses were performed with JMP after natural log transform (v.8-9, SAS, Cary, NC).

5.4 Results

Substrate Stiffness Alters the Quality and Dynamics of Fibronectin Deposition

Previously we investigated the role of substrate stiffness in mediating capillary network assembly, and demonstrated that network assembly requires FN polymerization [112]. Herein, we investigated the role of substrate stiffness in mediating EC-FN interactions.

ECs plated on compliant (E=0.2 kPa) substrates assembled a network-like morphology characterized by clusters of cells connected by cords of aligned cells and circular lacunae (Figure 5.1A "Actin/Nuclei). Immunostaining for FN revealed colocalization between the morphology of cell assemblies and FN staining (Figure 5.1A "FN"). When substrate stiffness was increased (E=10 kPa), network assembly did not occur, and both cells and FN staining were uniformly distributed across the substrate (Figure 5.1B).

Further investigation into the dynamics of FN deposition utilized ECs transfected with a plasmid encoding YFP-FN (a kind gift from Dr. Harold Erickson and Dr. Tomoo Ohashi) that were plated on compliant and stiff substrates and imaged with time-lapse fluorescence microscopy. On compliant substrates, ECs deposited thin and directed fibrils of FN during migration over the substrate surface (Figure 5.1C white arrow

head; yellow arrow head identifies a cell of interest; white arrow identifies migration path). In contrast ECs on stiff substrates deposited a web-like mesh of FN during migration (Figure 5.1D white arrow head).

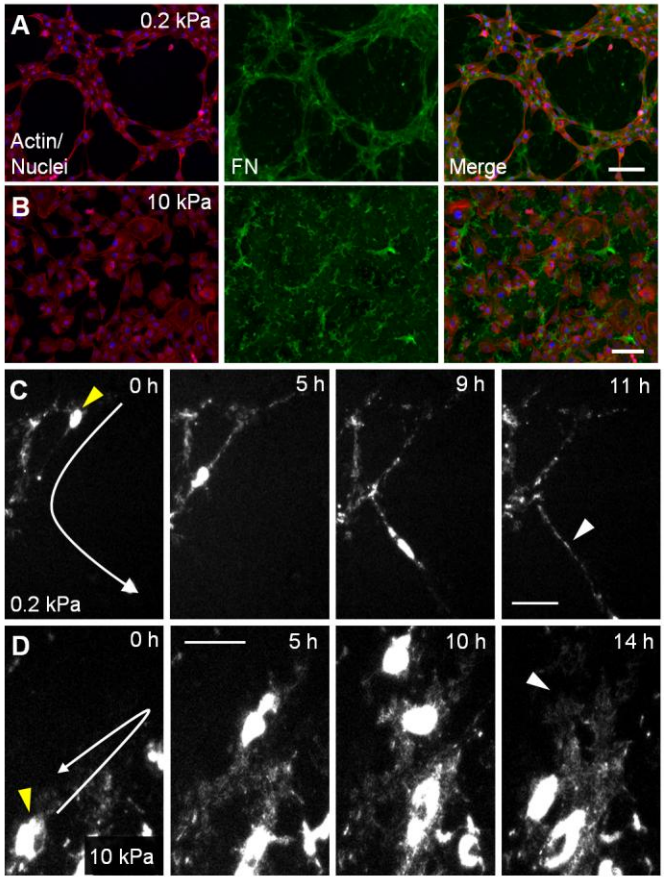

Figure 5.1. Substrate stiffness alters fibronectin deposition.
(**A**) ECs on compliant (*E*=0.2 kPa) substrates assembled a network morphology associated with fibronectin (FN). (**B**) Stiff (*E*=10 kPa) substrates did not support network formation but cells and FN were instead uniformly distributed. (**C**) ECs deposited thin and directed YFP-FN fibrils (white arrow head) on compliant substrates over time (white arrow identifies migration path; yellow arrow head identifies a cell of interest). (**D**) ECs on stiff substrates deposited a web-like mesh of YFP-FN over time (bars are 50 μm). YFP-FN was a gift from Dr. Harold Erickson and Dr. Tomoo Ohashi.

Assembled or polymerized FN fibrils are identified by their insolubility in deoxycholate (DOC) [101,198]. To determine whether EC in networks were

associated with assembled FN, networks on compliant substrates were treated with deoxycholate [198] and stained for FN. Our results indicated that cell networks on compliant substrates were associated with insoluble (assembled) FN (Figure 5.2A). Since DOC lyses cells, these data also indicated that the network morphology of FN was retained despite cell removal (confirmed by staining for actin and nuclei, not shown). On stiff substrates treated with DOC, insoluble FN appeared uniformly distributed across the substrate (Figure 5.2B).

To determine the spatial localization of FN in 3D, ECs on compliant and stiff substrates were fixed, stained for FN, and imaged with confocal microscopy. Image stacks were reconstructed and oriented to display the apical and basolateral surface. When plated on compliant substrates, ECs assembled into networks where FN was localized to the basolateral side (Figure 5.2C, "Basolateral"). Notably, extended cell processes ran atop tracks of fibrils of FN that appeared oriented in the direction of the long axis of the cell (Figure 5.2C, arrow heads). On stiff substrates, ECs were still enmeshed in FN primarily from the basolateral side (Figure 5.2D, "Basolateral"), but FN appeared as a web-like mesh beneath cells. Taken together, these data indicate that compliant substrates foster the development of EC networks associated with assembled FN that enmeshes cells from the basolateral side, and suggest that there are differences in the quality of FN deposition on compliant (oriented fibrils) vs. stiff (web-like mesh) substrates.

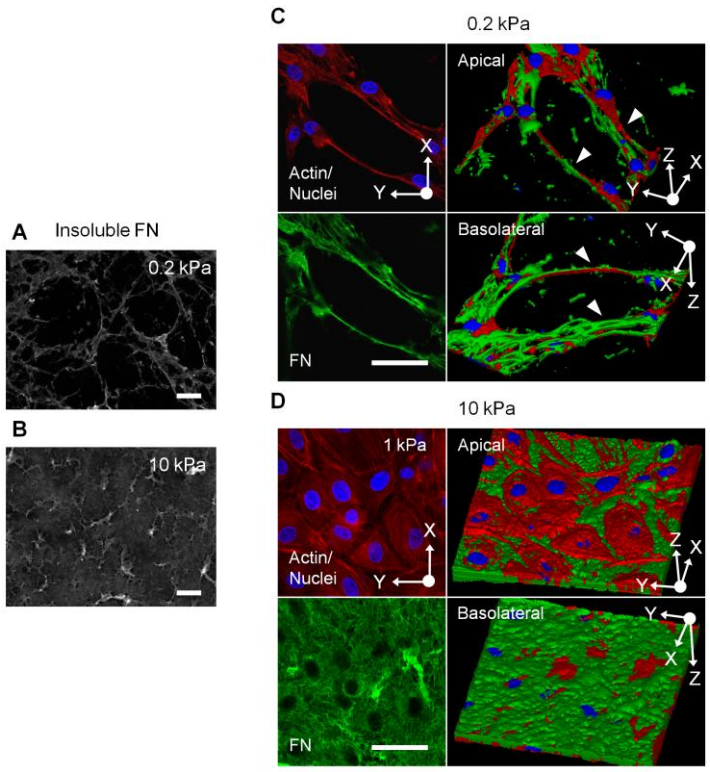

Figure 5.2. Substrate stiffness alters FN localization.
(**A**) On compliant (*E*=0.2 kPa) substrates, ECs assembled into networks associated with assembled (insoluble) fibronectin (FN). (**B**) Stiff (*E*=10 kPa) substrates did not support network formation and assembled FN was instead uniformly distributed. (**C**) 3D reconstruction of confocal z-stacks of ECs on compliant substrates oriented to display the apical and basolateral surface. Arrow heads indicate ECs assembled atop tracks of FN fibrils. (**D**) On stiff substrates, FN appeared as a web-like mesh beneath cells. Bars are 100 μm.

In addition to collagen, we investigated the solubility and localization of FN on substrates derivatized with an RGD sequence-containing peptide. Similar to collagen, we determined that networks on compliant (*E*=0.2 kPa) substrates were associated with insoluble FN (Figure 5.3A). On stiff (*E*=10 kPa) substrates, ECs and FN were uniformly distributed (Figure 5.3B), however insoluble FN formed a less extensive network compared to that observed on collagen-derivatized gels (*cf.* Figure 5.2B). This may be due to less robust FN-RGD interactions, as collagen contains an FN binding site [137] that may help retain fibrillar FN during processing for

immunostaining. 3D reconstructions of confocal slices indicated that EC assemblies occurred atop FN fibrils on compliant substrates (Figure 5.3C, arrow head). On stiff substrates, cells did not assemble networks and FN was again localized to the basolateral surface (Figure 5.3D). These data indicate that networks assemble atop FN fibrils on substrates derivatized with collagen or an RGD-containing peptide.

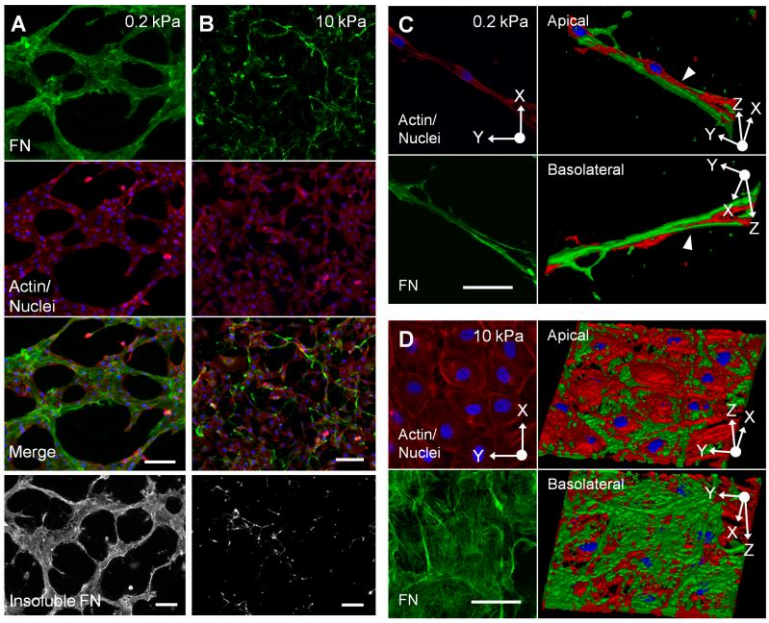

Figure 5.3. ECs on RGD-derivatized substrates assemble networks atop fibrillar assembled FN.
ECs were plated on compliant (*E*=0.2 kPa) and stiff (*E*=10 kPa) substrates derivatized with 100 μg/mL of an RGD sequence-containing peptide (NH_2-YAVTGRGDS-OH), and fixed and stained for FN. (**A**) On compliant substrates, ECs assembled into networks that were colocalized with FN. To determine FN insolubility, samples were treated with deoxycholate, and fixed and stained for FN. EC networks were associated with assembled FN ("Insoluble FN"). (**B**) In contrast, ECs and FN were uniformly distributed across stiff substrates. Treatment with deoxycholate indicated that assembled FN was distributed across the substrate. Scale bars are 100 μm. To determine the 3D localization of FN, samples were analyzed with confocal microscopy, and z-stacks were reconstructed to orient the apical and basolateral surface. (**C**) On compliant substrates, ECs formed network cords atop fibrils of oriented FN (arrow head). Image for "actin/nuclei" and "FN" are representative images from a slice in the z-stack. (**D**) On stiff substrates, ECs did not assemble networks, but were uniformly distributed atop omnidirectional FN. Scale bars are 50 μm.

Our findings suggest that substrate stiffness alters the dynamics of FN deposition. To investigate whether substrate stiffness mediates the dynamics of FN deposition, ECs were plated on compliant and stiff substrates, fixed at 4-48 hours after plating, and stained for FN. On compliant substrates, FN signal appeared colocalized with cells as background staining (Figure 5.4A "FN" and "Actin/Nuclei"). Staining for FN after treatment with DOC revealed that assembled FN deposition at 4 hours after plating was punctate (Figure 5.4A "Insoluble FN") suggesting that cell spreading precedes significant FN deposition. Small fibrils of FN were deposited by 24 hours after plating and appeared oriented and aligned with cells by 48 hours (Figure 5.4A). In contrast, ECs on stiff substrates were associated with short omnidirectional fibrils of FN as early as 4 hours after plating (Figure 5.4B). Over 4-48 hours assembled FN deposition on stiff substrates proceeded to cover the substrate surface and appeared as a web-like mesh (Figure 5.4B "Insoluble FN").

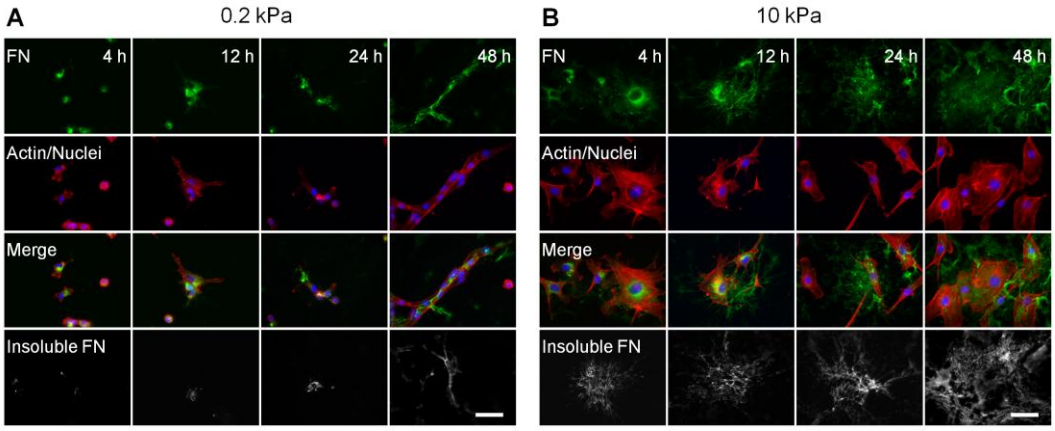

Figure 5.4. Substrate stiffness alters the dynamics and quality of FN deposition. (**A**) On compliant (*E*=0.2 kPa) substrates, FN deposition was punctate over 4-12 hours, with short fibrils deposited and elongated over 24-48 hours. (**B**) On stiff (*E*=10 kPa) substrates, FN deposition was omnidirectional as early as 4 hours after plating. Bars are 50 μm.

These data indicate that substrate stiffness mediates differences in the quality of FN deposition by ECs over time, *i.e.* compliant substrates foster the deposition of thin directed fibrils while stiff substrates promote a "painting" of web-like FN across the substrate.

Substrate Stiffness Mediates the Expression and Deposition of EDB-Fibronectin

EDB-FN is an isoform of FN that specifically localizes to angiogenic blood vessels [108] that may be an important clinical target for localizing tumor vasculature [109]. Our data suggest that there are differences in the density of FN deposition with stiffness. To determine whether the EDB isoform of FN was sensitive to substrate stiffness, ECs were plated on compliant (E=1 kPa) and stiff (E=10 kPa) substrates and grown to confluency. Fluorescent staining and quantification indicated that there was a significant increase in EDB-FN density with increasing substrate stiffness (Figure 5.5A-B). To quantify FN deposition, Western blots for EDB-FN and total FN were performed. As expected, there was a significant increase in EDB-FN with increasing substrate stiffness (Figure 5.5C). There was a slight but significant increase in the amount of total FN detected (Figure 5.5D), however normalizing the ratio of EDB-FN to total FN as determined by Western blotting indicated that there was a 30% increase in EDB-FN with increasing substrate stiffness (Figure 5.5E). Furthermore, quantitative real-time PCR was used to quantify the gene expression of EDB-FN. Our results indicated that EDB-FN gene expression increased approximately 2.5 fold on stiff substrates (Figure 5.5F). These data indicate that substrate stiffness alters the density of total FN deposition, and indicate that substrate stiffness mediates the expression and deposition of the EDB-isoform of FN.

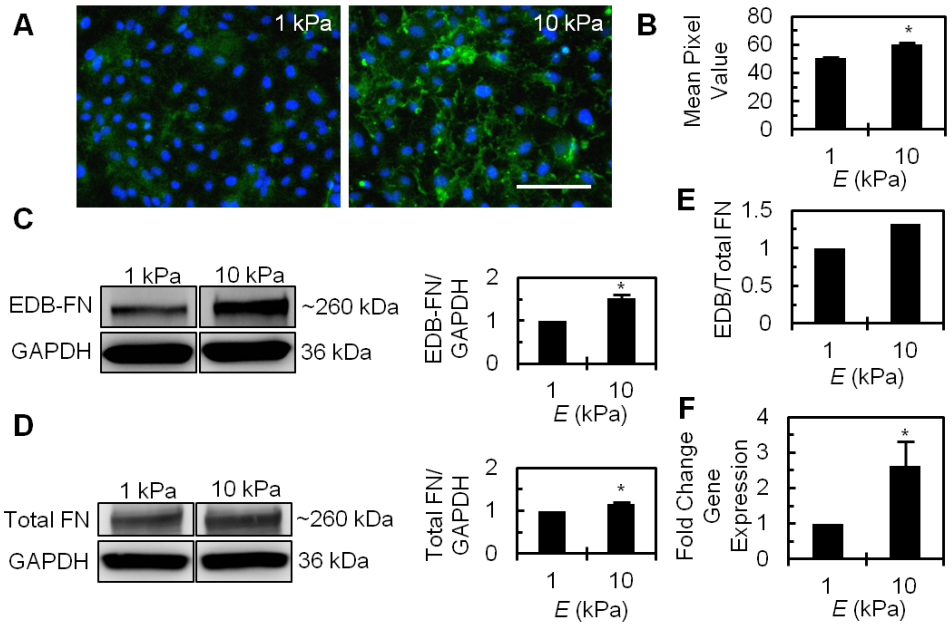

Figure 5.5. Substrate stiffness mediates the expression and deposition of EDB-fibronectin.
(**A**) Confluent ECs on compliant (*E*=1 kPa) and stiff (*E*=10 kPa) substrates were stained for EDB-FN (bar is 100 μm). (**B**) EDB-FN density increased significantly with increasing substrate stiffness (n=10 fields per condition). (**C**) Western blot for EDB-FN expression by ECs on compliant and stiff substrates indicated a significant increase with increasing substrate stiffness (3 independent experiments). (**D**) Western blot for total FN expression by ECs on compliant and stiff substrates indicated a slight but significant increase in total FN with increasing stiffness (3 independent experiments). Panels represent lanes from the same gel where empty lanes were removed for data consolidation. (**E**) The ratio of EDB-FN to total FN based on Western blot data indicated a 30% increase in EDB-FN expression with increasing stiffness. (**F**) EDB-FN gene expression as determined by quantitative real-time PCR indicated a significant increase in gene expression with increasing stiffness (3 independent experiments). Plots are mean + SEM, *p<0.05. PCR was performed with Dr. Libin Yuan.

When using PA substrates we have assumed that substrate-FN interactions were independent of substrate stiffness. To determine whether this was a valid assumption, we investigated FN binding to substrates derivatized with collagen. We incubated substrates directly with exogenous FN, or with complete media (serum in media contains FN), and examined FN-substrate interactions. While this method was

indirect, fluorescent localization and Western blot were a first approximation indicator that substrate-FN interactions were stiffness independent (Figure 5.6A-B). Moreover, to confirm the source of EDB-FN to cells (since serum used in the media contains FN) we utilized Western blotting to show that EDB-FN was undetectable in serum (Figure 5.6C). These data suggest that FN-substrate interactions are independent of substrate stiffness and that ECs are the source of EDB-FN.

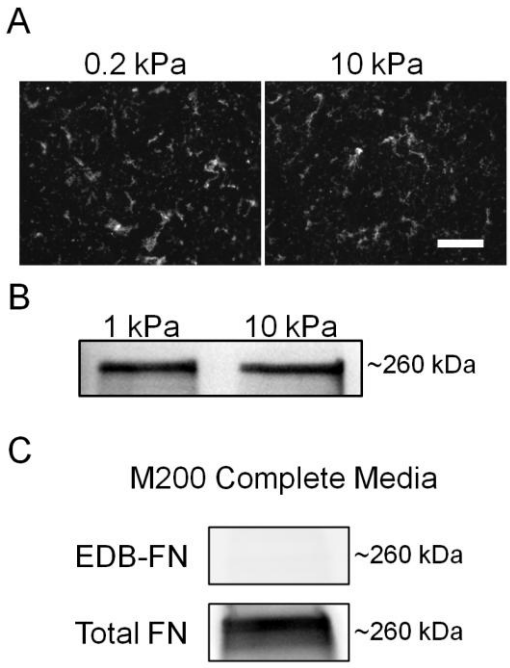

Figure 5.6. FN controls.
(**A**) Compliant (*E*=0.2 kPa) and stiff (*E*=10 kPa) substrates were synthesized and derivatized with collagen, and incubated with 50 μg/mL FN, and fixed and stained for FN. FN signal was uniformly distributed across the surface on compliant and stiff substrates. Scale bar is 100 μm. (**B**) 1 and 10 kPa substrates were incubated with complete Media 199 for 24 hours, incubated with Laemmli buffer, and analyzed with SDS-PAGE and Western blot. A Western blot for FN indicated a similar amount of FN across stiffness levels. (**C**) Complete Media 200 was subjected to analysis with SDS-PAGE and Western blot. A Western blot for EDB-FN indicated that no EDB-FN was detectable in the media. In contrast, and as expected, total FN was detectable.

Fibronectin Orientation Correlates with Actin Cytoskeletal Polarity

Our data suggest that substrate stiffness mediates differences in the orientation of FN deposition. To determine and quantify the spatial orientation of FN deposition with regard to substrate stiffness, ECs were plated on compliant (E=0.2 kPa) and stiff (E=10 kPa) substrates, and stained to localize actin and FN. The overall orientation of cells, their actin cytoskeleton, and associated FN was determined using OrientationJ. On compliant substrates, actin and FN staining appeared fibrillar and oriented in the direction of the long axis of cells (Figure 5.7A; close-up view of an individual cell). The prevalence of blue-purple pseudo-coloring in both actin and FN images on compliant substrates indicated a similar actin cytoskeletal and FN fibril orientation with respect to the horizontal axis (inset in "actin" image is a legend for hue with orientation angle). In contrast, the actin and FN staining exhibited a more uniform distribution of orientations in cells on stiff substrates (Figure 5.7B; close up view of an individual cell). The rainbow hue of both actin and FN pseudo-colored images on stiff substrates indicated a multidirectional distribution of orientations with respect to the horizontal axis.

To quantify these observations, the overall orientation angle of actin was compared to the orientation angle of the cell with OrientationJ to determine the minimum difference between orientation angles in degrees. This analysis indicated that there was a significant increase in the *difference* in orientation angles (*i.e.* less correlation) between cells and their actin cytoskeleton with increasing substrate stiffness (Figure 5.7C). Similarly, the difference in orientation angles between the actin cytoskeleton and FN also increased with increasing substrate stiffness (Figure 5.7D). These results indicate that there is a significant correlation between the orientation of cells and their actin cytoskeleton, and between the actin cytoskeleton and the local FN matrix in cells

on compliant substrates, and that this correlation is diminished with increasing substrate stiffness.

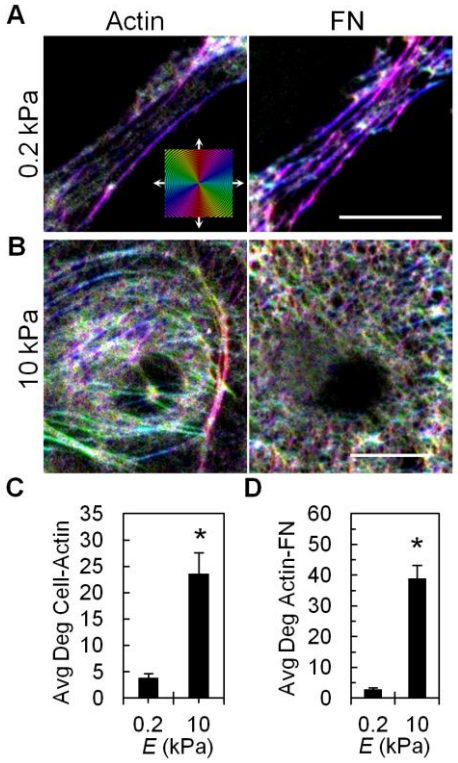

Figure 5.7. FN orientation correlates with actin cytoskeletal polarity.
(**A**) Close-up of fibrillar and oriented actin and FN associated with an EC on a compliant (*E*=0.2 kPa) substrate analyzed with OrientationJ. Inset is a legend for hue with orientation angle. (**B**) Close-up of actin and FN associated with an EC on a stiff (*E*=10 kPa) substrate indicated a more uniform distribution of actin and FN (bars are 50 μm). (**C-D**) Quantification of the difference in orientation angle (in degrees) between cells and their actin cytoskeleton (**C**) and between the actin cytoskeleton and FN (**D**) indicated an increase (less correlation) with increasing substrate stiffness (n=30 per stiffness, mean + SEM, *p<0.05).

Substrate Stiffness Alters Traction Force Polarization

Substrate stiffness mediates differences in the quality and orientation of FN deposition, and suggests that these differences are due in part to alterations in the orientation of the EC actin cytoskeleton (Figures 5.4, 5.7). FN assembly into fibrils requires cell-generated forces [103,104] suggesting that differences in FN deposition

may be due to alterations in actomyosin interactions that generate contractility [54,56,199]. However, the role of substrate stiffness in mediating force directionality that may be responsible for FN deposition is not well characterized.

To investigate the role of substrate stiffness in mediating traction force polarity, ECs on compliant (E=1 kPa) and stiff (E=10 kPa) substrates were analyzed with Traction Force Microscopy (TFM), a technique used to measure endogenous cellular traction forces [30,149]. On compliant substrates, cells adopted an elongated and bipolar morphology with force vectors oriented toward the cell area centroid (Figure 5.8A; single cell), but appeared more multipolar on stiffer substrates (Figure 5.8B; single cell). Quantification of the aspect ratio of individual cells indicated a significant decrease in aspect ratio (*i.e.* more circular) with increasing substrate stiffness (Figure 5.8C). The directionality of traction forces exerted by the cells was determined by projecting the total magnitude of the traction force along the long and short axis of the cell. Traction force projections along the long axis of the cell decreased significantly with increasing substrate stiffness (E=1-10 kPa) in isolated cells (Figure 5.8D, gray bars).

These results arise from single isolated cells, however cell-cell interactions occur during FN deposition over time. To determine whether cell-cell interactions alter traction force polarity, ECs making a cell-cell contact were analyzed with TFM. When two ECs on a compliant substrate made a cell-cell connection, their elongated morphologies were maintained. Analysis with TFM, where the cells in contact were modeled as a single force-generating unit, indicated that traction forces maintained polarization toward the center of the aggregate cell area centroid (Figure 5.8A, two cells). Quantification indicated that traction forces remained polarized when two cells

came into contact (Figure 5.8E). When cell-cell contact was made with an adjoining cell on stiff substrates, individual cell morphology remained spread and traction forces were oriented toward the center within each cell region (Figure 5.8B, two cells). Cells in contact on stiff substrates exhibited a significant decrease in force polarization along the long axis of the cell aggregate area (Figure 5.8F), *i.e.* cells exert omnidirectional forces.

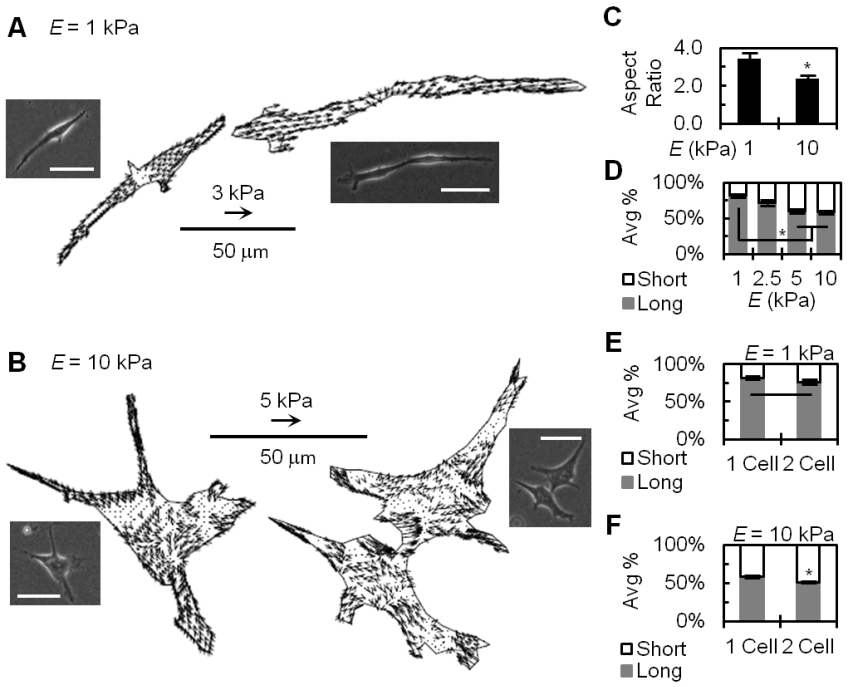

Figure 5.8. Substrate stiffness alters traction force polarization.
(**A**) ECs on compliant (*E*=1 kPa) substrates adopted an elongated and bipolar morphology with traction forces directed toward the area centroid. An elongated morphology and polarized forces were maintained with cell-cell contact. (**B**) ECs on stiff (*E*=10 kPa) substrates appeared more multipolar. Cells in contact retained a spread morphology with traction forces oriented toward the aggregate cell area centroid (bars are 50 μm). (**C**) The aspect ratio of individual cells decreased (became more circular) with increasing substrate stiffness (n=70 per stiffness). (**D**) Quantification of traction force projections along the long and short axis of cells. Force projections along the long axis decreased significantly with increasing substrate stiffness in isolated cells (n=24, 14, 25, 38 per stiffness, respectively). (**E-F**) Force projections between single cells and two cells in contact exhibited no significant difference between force polarization along the long axis (n=16 pairs) on compliant substrates (**E**) but significantly decreased (n=20 pairs) on stiff substrates (**F**). Plots are mean +/- SEM, *p<0.05.

These data indicate that in addition to mediating the magnitude of EC-generated traction forces [149], substrate stiffness alters cell shape and the orientation forces. Furthermore, they suggest that the maintenance of polarized traction forces despite cell-cell interaction may contribute to FN polarization on compliant substrates.

FN Deposition is Directed by Enforcing Cell Polarity

Our results indicate that stiff substrates facilitate the multipolar spreading of ECs that are accompanied by traction forces that exhibit a near-uniform distribution and an omnidirectional web-like mesh of deposited FN (Figures 5.1-5.4), and suggest that polarized traction forces on compliant substrates guide the deposition of directional FN. To determine whether enforcing an elongated cell morphology on stiff (E=10 kPa) substrates was correlated with an alteration in the directionality of traction forces and FN deposition, ECs were plated on stiff substrates micropatterned with adhesive rectangular island of collagen (Figure 5.9A) and analyzed with TFM. Instead of exhibiting a multipolar morphology, single cells and two-cells in contact on stiff patterned substrates exhibited an elongated bipolar morphology and distribution of traction forces that appeared oriented along the long axis of the cell (Figure 5.9B), a phenotype similar to cells on compliant substrates (*cf*. Figure 5.8A). Quantification of traction forces in elongated cells on patterned substrates ("1 Cell Patt"; "2 Cell Patt") revealed a significant increase in force polarization along the long axis of the cell area compared to non-patterned cells in single cells and two cells in contact ("1 Cell; 2 Cell), respectively (Figure 5.9C; gray bars). Fluorescent localization of FN indicated that elongated cells on micropatterned substrates were accompanied by directed fibrils of FN (Figure 5.9D arrow heads; inset is a magnification of the boxed region pseudocolored with OrientationJ). Note the prevalence of green pseudocoloring indicating a preferred (left-right) orientation of FN similar to oriented FN observed in

cells on compliant substrates (*cf*. Figure 5.7A). In contrast, cells on non-patterned substrates exhibited a uniform distribution of orientations of FN (Figure 5.9E, inset is a magnification of the boxed region; note the rainbow hue of FN signal). These data indicate that the quality of FN normally observed on compliant substrates (unidirectional fibrils) can be recapitulated on stiff substrates by enforcing an elongated cell morphology with concomitant polarization of traction forces.

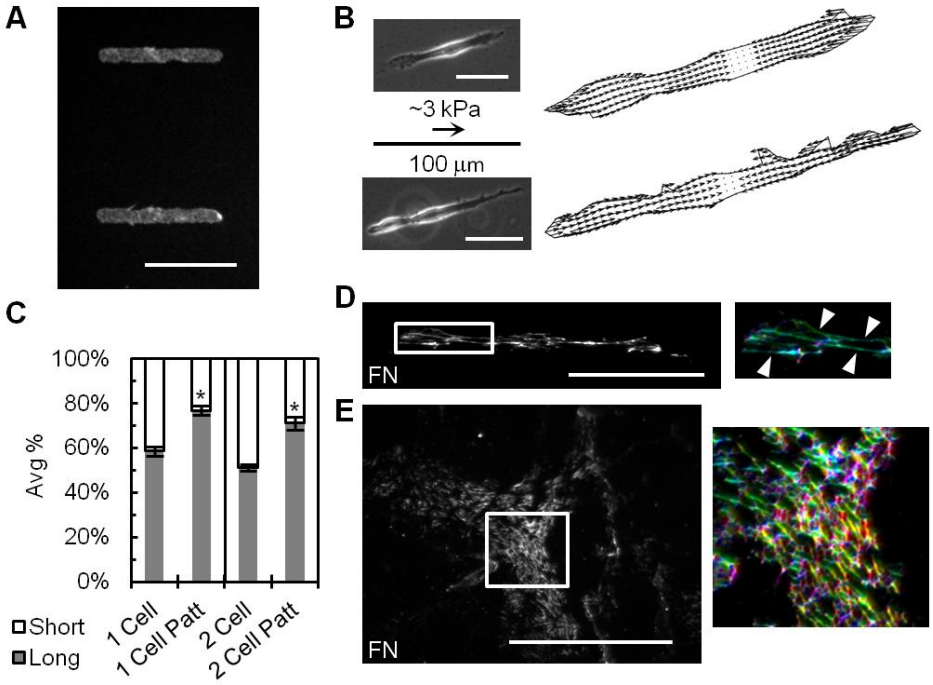

Figure 5.9. FN deposition is directed by enforcing cell polarity.
(**A**) Stiff (*E*=10 kPa) substrates were micropatterned with adhesive islands of collagen (bar is 200 μm). (**B**) Single ECs and two ECs in contact plated on micropatterned substrates exhibited an elongated bipolar morphology and traction forces oriented along the long axis of the cell (bars are 100 μm). (**C**) Cells on patterned ("Patt") substrates exhibited a significant increase in force polarization vs. non-patterned substrates when forced into an elongated morphology (n=58, 29 for 1 Cell Patt and 2 Cell Patt, respectively). (**D-E**) Fluorescent localization of FN associated with elongated ECs on micropatterned (**D**) vs. non-patterned substrates (**E**). Arrow heads point to oriented FN. Insets are magnifications of the boxed regions pseudocolored with OrientationJ (bars are 100 μm). Plots are mean ± SEM, *p<0.05. Silicon masters used to patterned gels were prepared by Jonathan Charest.

In addition to the orientation of traction forces, we determined that enforcing an elongated cell morphology on stiff substrates reduced the total magnitude of traction force exerted by individual cells or cells in contact compared to cells on non-patterned substrates (Figure 5.10). These data indicate that restricted cell spreading alters the magnitude of traction force generation in isolated ECs and ECs in contact.

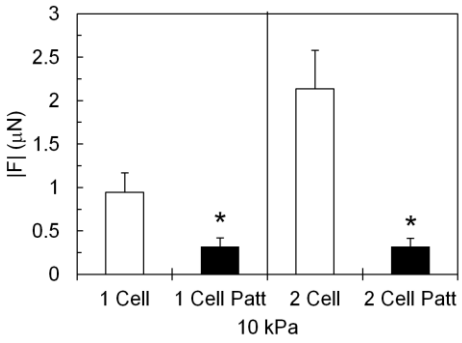

Figure 5.10. Enforcing an elongated cell morphology reduces traction force magnitude on stiff substrates.
ECs were plated on stiff (*E*=1-10 kPa) micropatterned substrates that enforced a bipolar elongated morphology and analyzed with traction force microscopy. On patterned substrates, single cells ("1 Cell Patt") exhibited a significant reduction in traction force magnitude compared to individual cells allowed to spread unrestricted ("1 Cell"). Similarly, traction force magnitude was significantly reduced for two cells in contact on micropatterned substrates ("2 Cell Patt") compared to two cells allowed to spread unrestricted ("2 Cell") (*$p<0.05$, Student's *t* test).

ROCK-Mediated Contractility and Cell Area Regulate FN Deposition

It is established in fibroblasts that endogenous contractility mediates FN assembly [104,173]. Our data suggest that substrate stiffness alters FN deposition by modulating contractility-mediated traction force polarity. Cellular contractility is mediated in part by the Rho signaling pathway, where ROCK is a downstream effector of Rho [200,201]. We have shown previously that ROCK is a critical mediator of EC contractility and that Y27632 treatment decreases the magnitude of traction forces in ECs (Figure 5.11, [170]). To determine whether ROCK-mediated contractility

mediates FN deposition in ECs, cells were plated on stiff (*E*=10 kPa) substrates in the presence of the ROCK inhibitor Y27632, fixed at 4-48 hours after plating, and stained for FN. Samples treated with Y27632 exhibited a decrease in assembled FN deposition compared to control samples at each time point over 48 hours (Figure 5.12A; insoluble FN images were acquired by staining FN after DOC treatment and were taken at the same exposure settings as control samples for each time point). Quantification of the fluorescent signal from DOC-treated samples indicated that there was a significant decrease in the density of insoluble FN fluorescent signal at each time point over 48 hours (Figure 5.12B). FN deposition of Y27632-treated samples appeared to lag behind the deposition observed in control samples, and appeared to correlate with the 12-16 hour half-life of Y27632 [202]. However, there was recovery of deposition in Y27632-treated samples over time (Figure 5.12B; compare control bar at 12 hours with Y27 bar at 48 hours). Quantification of cell area indicated that the decrease in FN deposition was not accompanied by alterations in cell area (Figure 5.12C). Separate analogous experiments that used RNAi to disrupt ROCK found similar results (Figure 5.13).

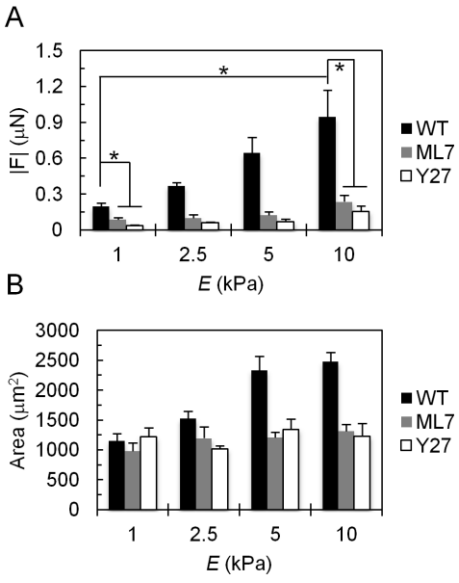

Figure 5.11. Inhibiting ROCK or myosin light chain kinase reduces traction force magnitude.
ECs were plated on variably compliant (*E*=1-10 kPa) substrates, allowed to adhere overnight, treated with 50 μM myosin light chain kinase inhibitor (ML7) or 10 μM ROCK inhibitor (Y27632) for 30 minutes, and analyzed with traction force microscopy. (**A**) Treatment with ML7 or Y27632 significantly reduced traction force magnitude exerted by ECs on all substrates. (**B**) Cell area was reduced with ML7 or Y27632 treatment on 2.5-10 kPa substrates, but was not changed significantly on 1 kPa substrates (*$p<0.05$; ANOVA). Portions of this data appeared in Huynh *et al*. [170].

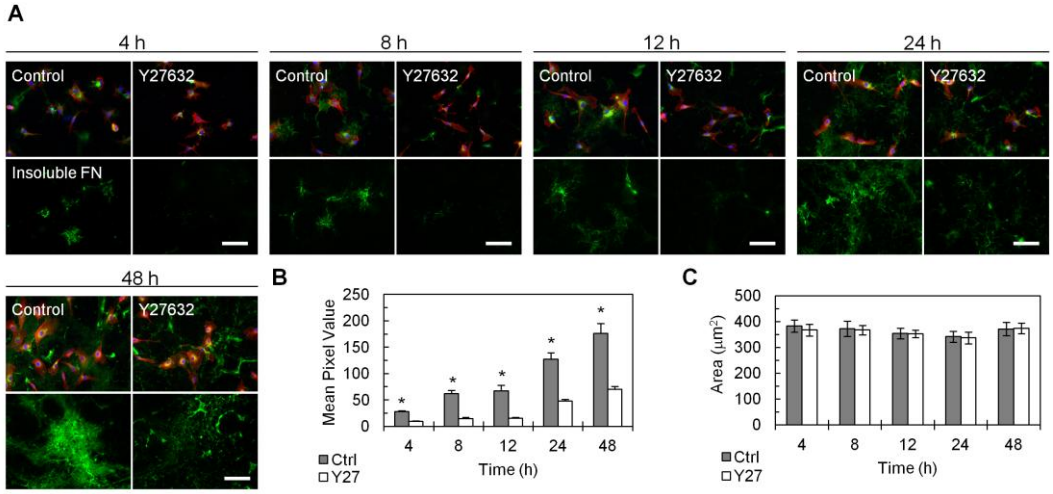

Figure 5.12. ROCK-mediated contractility mediates FN deposition (Y27).
(**A**) ECs plated on stiff (*E*=10 kPa) substrates with 10 μM Y27632 exhibited a decrease in assembled FN deposition compared to control samples at each time point over 4-48 hours (bars are 100 μm). (**B**) Quantification of insoluble FN signal (acquired at the same exposure settings) indicated a significant decrease in FN density at each time point over 48 hours between Y27632 treatment (Y27) and control (Ctrl) (n=8-12 fields per condition per time point). (**C**) There was no change in cell area between Y27632 treatment and control samples (n=50 per condition per time point). Plots are mean +/- SEM, *p<0.05.

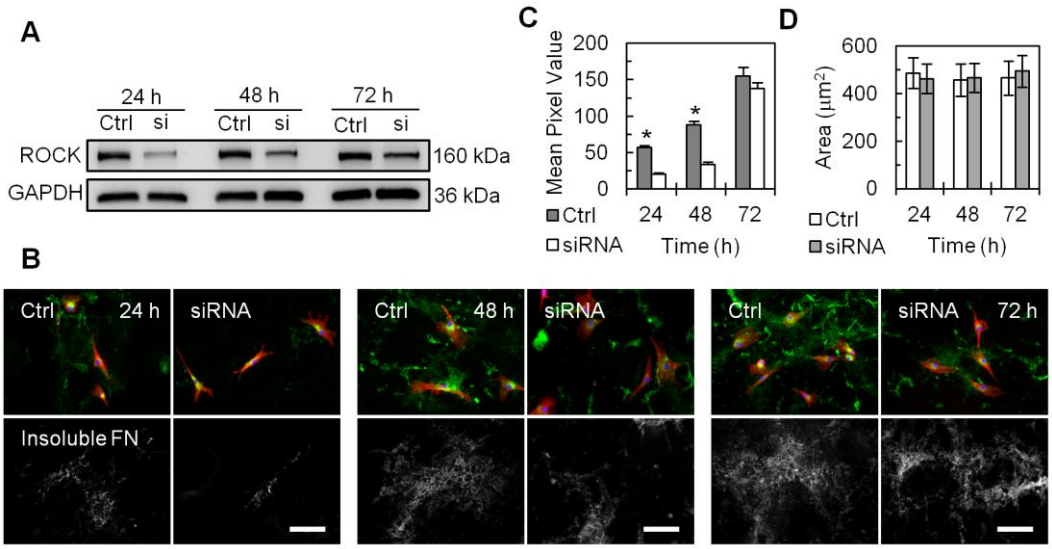

Figure 5.13. ROCK-mediated contractility mediates FN deposition (siRNA). (**A**) Western blot of ROCK after treatment with siRNA against ROCK (si) compared to control (Ctrl) over 72 hours. (**B**) ECs treated with siRNA against ROCK were plated on stiff substrates and stained for FN over 72 hours (bars are 100 μm). (**C**) Quantification of FN density indicated a significant decrease in insoluble FN with siRNA treatment against ROCK over 48 hours compared to controls, but similar levels of FN density by 72 hours (n=11-16 fields per condition per time point). (**D**) Knockdown of ROCK with siRNA was not accompanied by alterations in cell area compared to controls (n=50 per condition per time point). Plots are mean +/- SEM, * indicates $p<0.05$).

To determine if EDB-FN was sensitive to ROCK-mediated contractility, ECs treated with siRNA for ROCK were plated on stiff (E=10 kPa) substrates and stained for EDB-FN. Western blotting for ROCK indicated a knockdown with siRNA treatment compared to controls (Figure 5.14A). Fluorescent staining and quantification of EDB-FN indicated a decrease in EDB-FN with siRNA treatment compared to controls (Figure 5.14B-C). Taken together, these results indicate that the deposition of FN and the EDB-FN isoform by ECs depends on ROCK-mediated contractility.

In addition to ROCK-mediated contractility, cell shape directs FN deposition (Figure 5.9). To determine the role of cell area in mediating FN deposition, ECs were plated

on stiff (E=10 kPa) micropatterned substrates that restricted cell spreading. EDB-FN and total FN deposition was disrupted on micropatterned substrates that restricted spreading (Figure 5.14D). In contrast, fibrillar EDB-FN and total FN deposition was observed in control ECs that were allowed to spread fully (Figure 5.14E). These results indicate that cell area regulates FN and EDB-FN deposition, and suggest that in addition to the polarity of traction forces, substrate stiffness alters FN expression through changes in cell area.

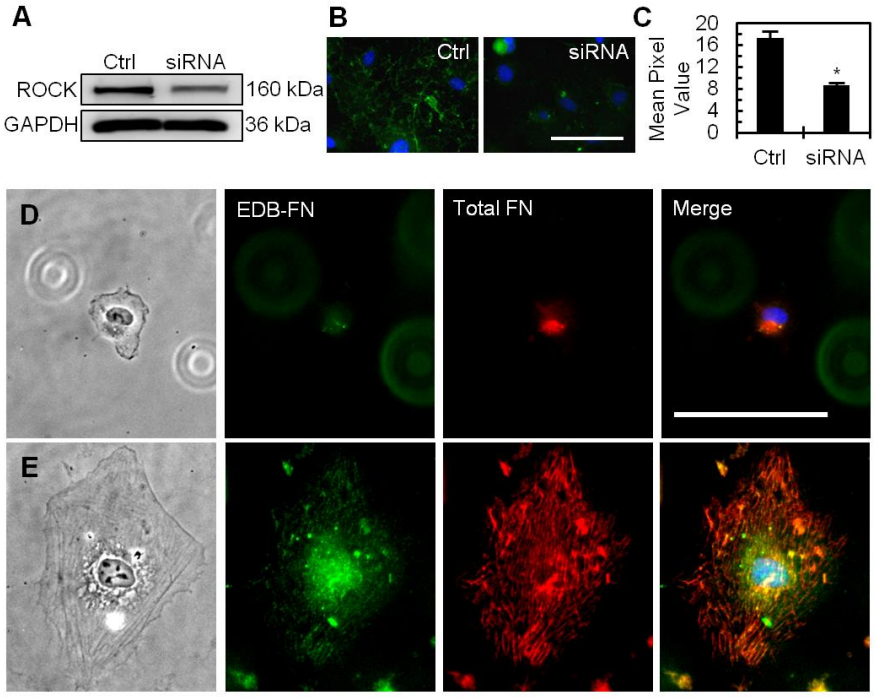

Figure 5.14. ROCK-mediated contractility and cell area mediate EDB-FN deposition.
(**A**) Western blot for ROCK expression after treatment with siRNA against ROCK compared to control. (**B**) Fluorescent staining for EDB-FN after treatment with siRNA against ROCK on stiff (E=10 kPa) substrates. (**C**) Quantification of EDN-FN density after ROCK siRNA treatment indicated a significant decrease in EDB-FN compared to controls (n=40 fields per condition). (**D**) Fluorescent staining of EDB-FN and total FN in an EC on a stiff (E=10 kPa) micropatterned substrate that restricted cell spreading. (**E**) Fluorescent staining of EDB-FN and total FN in an EC on a stiff control substrate where spreading was not restricted (bars are 100 μm). Plots are mean + SEM, *$p<0.05$.

Based on our findings that a disruption in ROCK-mediated contractility reduced FN deposition, we hypothesized that increasing cellular contractility on compliant substrates would in turn increase FN deposition. To test this hypothesis, cells were transfected with a plasmid encoding constitutively active Rho (RhoV14, an upstream activator of ROCK and cellular contractility) and plated on compliant (E=0.2 kPa) and stiff (E=10 kPa) substrates. Our data indicated that there was not a significant increase in FN deposition on either substrate (Figure 5.15). Moreover, there appeared to be a reduction in FN deposition on stiff substrates (Figure 5.15). A lack or reduction of increased FN deposition was likely due to a disruption in contractile dynamics. Recent data suggests that dynamic traction forces are requisite for FN [173], *i.e.* tonic contraction, via inhibition or stimulation of contractility, prevents FN assembly. Our results, while preliminary, suggest that FN deposition by ECs requires dynamic cellular traction forces.

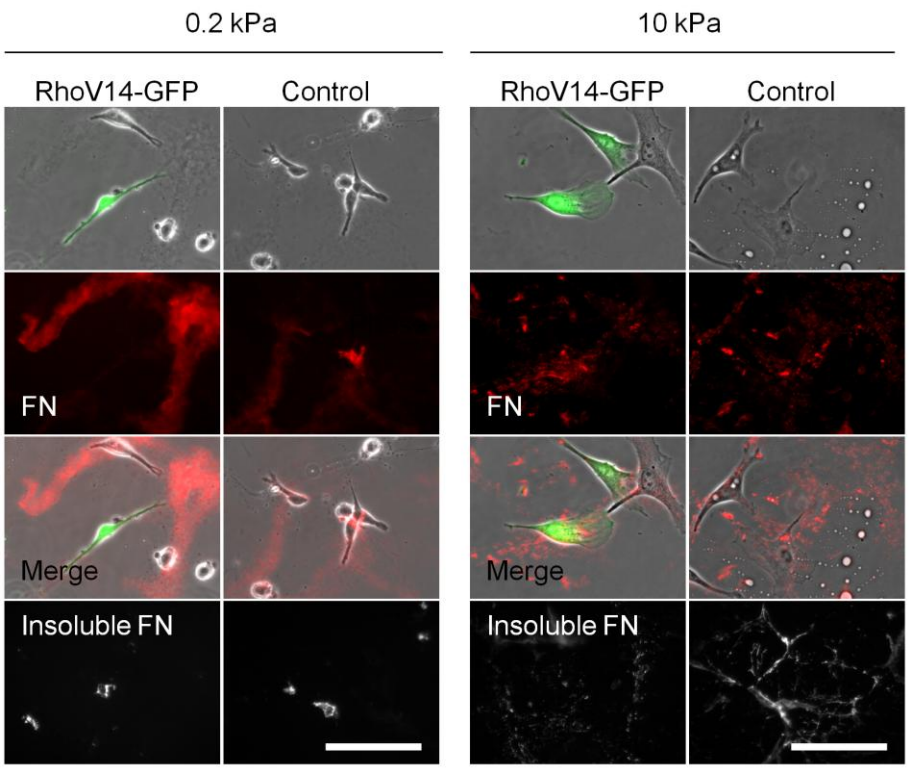

Figure 5.15. Constitutively active Rho reduces assembled FN deposition on stiff substrates.
ECs were transfected with a plasmid encoding GFP-tagged constitutively active Rho (RhoV14-GFP), plated on compliant (E=0.2 kPa) and stiff (E=10 kPa) substrates for 24 hours, and fixed and stained for FN. On compliant substrates, significant FN was not detectible near transfected cells (phase image and "FN"). To localize assembled FN, samples were treatment with deoxycholate and stained for FN. Detected FN was punctate or in small fibers in both RhoV14-GFP samples and controls. On stiff substrates, short fibrils of FN were detected in both RhoV14-GFP samples and controls. However, treated with deoxycholate indicated a reduction in assembled FN ("Insoluble FN") with RhoV14-GFP treatment. Scale bars are 100 μm.

Disrupted Fibronectin Deposition or Polymerization Does Not Alter Traction Force Magnitude

Our results demonstrate that cellular contractility alters FN deposition. To determine whether FN deposition in turn alters cell contractility, cells were treated with siRNA against FN, plated on stiff (E=5 kPa), substrates, and analyzed with TFM. Our results indicated that there was no significant difference in the magnitude of traction forces exerted by siRNA-treated cells, or cell spread area, compared to controls (Figure 5.16A-D). Alternatively to FN knockdown, FN assembly was be inhibited with the small peptide pUR4B [193] (a kind gift from Dr. Jane Sottile, University of Rochester). Our results indicated that the magnitude of traction forces, cell spread area, and migration speed exhibited no significant difference between ECs treated with pUR4B compared to controls (Figure 5.16E-G). Taken together, these data suggest that FN synthesis or assembly did not alter cellular shape, migration, or contractility.

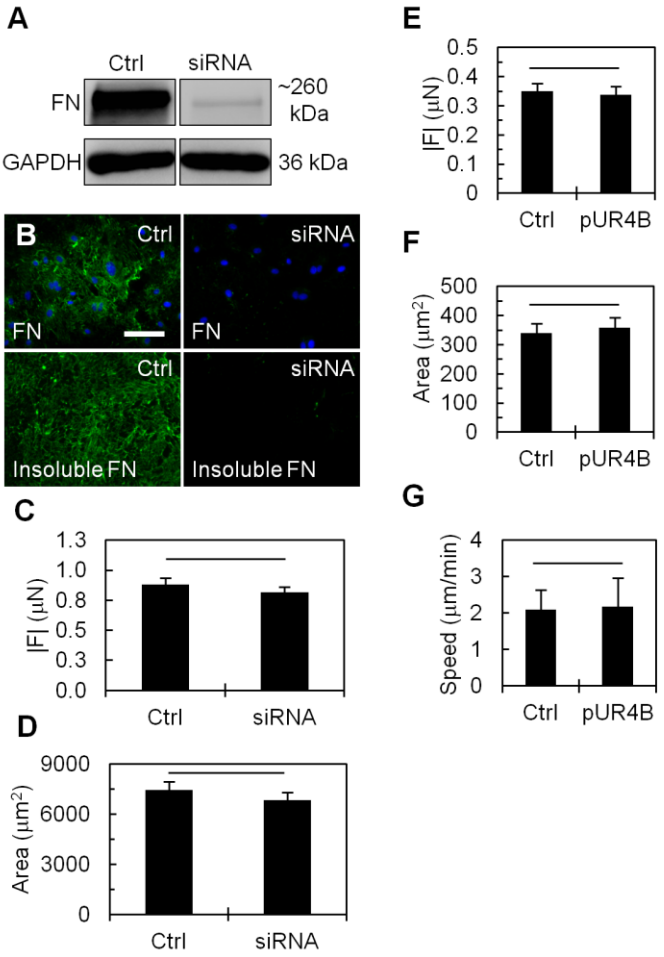

Figure 5.16. Disrupted fibronectin deposition or polymerization does not alter traction force magnitude.
(**A**) Western blot for FN after treatment with siRNA against FN or control (Ctrl). Panels represent lanes from the same gel where empty lanes were removed for data consolidation. (**B**) Fluorescent staining for FN after treatment with siRNA against FN confirmed a decrease in insoluble FN fluorescent signal in treated samples compared to controls (bar is 100 μm). (**C**) Quantification of traction force magnitude (|*F*|) generated by ECs treated with siRNA against FN compared to controls on stiff (*E*=5 kPa) substrates. (**D**) Plot of cell area of ECs treated with siRNA against FN compared to controls on stiff (*E*=5 kPa) substrates (n=57, 52 for control and siRNA, respectively). (**E**) Quantification of traction forces generated by ECs treated with FN polymerization inhibitor pUR4B (500 nM) compared to controls (500 nM III-11C control peptide) (Ctrl) on stiff (*E*=5 kPa) substrates (n=60, 72 for control and pUR4B, respectively). (**F**) Plot of cell area after treatment with pUR4B compared to controls on stiff (*E*=5 kPa) substrates. (**G**) Quantification of EC migration speed on compliant (*E*=0.2 kPa) substrates after treatment with pUR4B compared to controls (n=15 per condition). Plots are mean + SEM.

In addition to utilizing mean square-displacement to track cell migration, we measured cell displacement with three other metrics. These data indicate that pUR4B treatment did not alter cell displacement (Figure 5.17A-C)

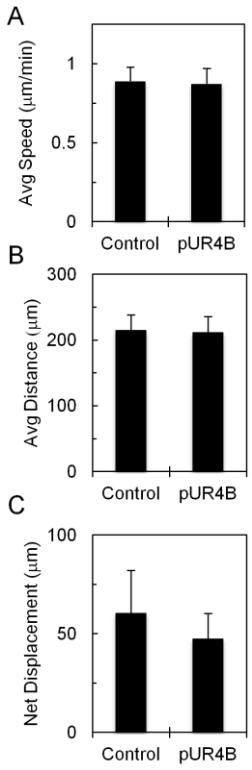

Figure 5.17. Inhibiting FN polymerization does not alter cell displacement. ECs were plated on compliant (E=0.2 kPa) substrates, treated with 500 nM pUR4B FN polymerization inhibitor or 500 nM III-11C control peptide (gifts from Dr. Jane Sottile), and analyzed with time lapse microscopy every 10 minutes for 4 hours. The cell centroid was used to calculated three measures of cell displacement that exhibited no significant difference between treatment and control samples. (**A**) Average speed determined with the distance formula calculated between successive time points. (**B**) Average total distance traveled calculated by summation of distance between successive time points. (**C**) Net cell displacement calculated from the initial and final time point centroid locations (no significant difference, Student's t test).

Substrate Stiffness Mediates Laminin Deposition in Epithelial Cells

Our data investigated the role of substrate stiffness in mediating cell-ECM interactions by determining the interactions between ECs and FN. To determine if these interactions were unique to ECs, we investigated the role of substrate stiffness in mediating laminin deposition in mammary epithelial cells (MEC). Since this cell type, analogous to ECs with FN, requires laminin for network assembly [160], we hypothesized that MECs may exhibit similar responses to alterations in substrate stiffness. Analogously to ECs with FN, MECs plated on compliant (E=0.2 kPa), but not stiff (E=0.2 kPa) substrates formed network assemblies associated with laminin (Figure 5.18A-B). 3D reconstructions of confocal z-stacks indicated that network cords of MECs occurred atop tracks of laminin on compliant substrates and on the basolateral surface of cells on stiff substrates (Figure 5.18C-D). Individual MECs exhibited a decrease in aspect ratio with increasing substrate stiffness, and an increase in laminin expression (Figure 5.18E-F). These data indicate that substrate stiffness regulates laminin matrix deposition in MECs, and suggest that the alteration of ECM deposition by substrate stiffness is not unique to ECs.

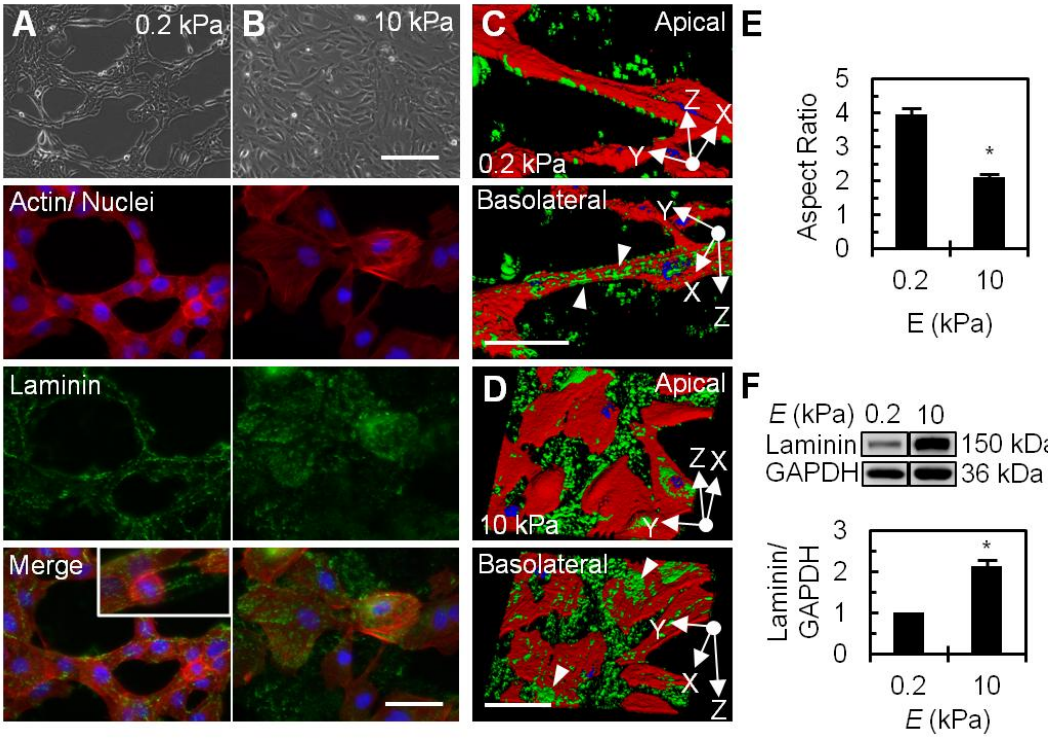

Figure 5.18. Substrate stiffness mediates laminin deposition in epithelial cells. (**A**) MCF-10A mammary epithelial cells (MEC) were plated on compliant (*E*=0.2 kPa) substrates formed network assemblies associated with laminin (inset in merge image depicts laminin signal that traversed a retracted cell within a network cord). (**B**) Stiff (*E*=10 kPa) substrates did not support network assembly, but instead cells and laminin were uniformly distributed. (**C**) 3D reconstructions of confocal z-stacks of laminin indicated that cords of MECs occurred atop tracks of laminin on compliant substrates. (**D**) Laminin was found on the basolateral surface of MECs on stiff substrates (bars are 50 μm). (**E**) Quantification of MEC aspect ratio indicated a significant decrease (more circular) with increasing substrate stiffness (n=71, 68 per stiffness, respectively). (**F**) Western blot of laminin expression by MEC on compliant and stiff substrates. Quantification indicated a significant increase in laminin expression with increasing substrate stiffness (3 independent experiments). Panels represent lanes from the same gel where empty lanes were removed for data consolidation. Plots are mean + SEM, * indicates $p<0.05$.

5.5 Discussion

The interactions between cells and the ECM enable cell responses. Herein we investigated the role of substrate stiffness in mediating cell-ECM interactions. We determined that substrate stiffness mediates the synthesis and deposition of FN by altering EC shape and traction force directionality. In addition, we demonstrated that the synthesis and deposition of EDB-FN, an FN isoform specific to angiogenic blood vessels, is sensitive to substrate stiffness.

Cell-ECM interactions have been studied extensively in fibroblast models, where it is thought that cell contractility facilitates FN fibril assembly by inducing conformational changes in FN that expose self-assembly sites. While the exact mechanisms governing conformational changes in FN are still under debate [203-205], fibril assembly is directed by traction forces [173]. Lemmon *et al*. demonstrated that the orientation of a traction force vector applied to an FN fibril directs the growth orientation of that fibril, and that FN assembly is regulated by the contractile machinery of the cell [173]. Similarly, our data indicate that FN assembly by ECs is directed by the orientation of endogenous traction forces, and that the dynamics of FN assembly are altered by perturbations to ROCK-mediated contractility that are sensitive to substrate stiffness. These findings suggest that FN assembly by ECs is sensitive to perturbations in the mechanical microenvironment that impinge on traction forces generated by the cell. Furthermore, we have shown that FN deposition can be directed by constraining the directionality of both cell spreading and traction forces. This has ramifications for tissue engineering, where EC-controlled FN deposition may aid the development of vascularized constructs.

As FN matrix matures, growing fibrils are converted to a DOC-insoluble form [101].

While the exact mechanisms are still under investigation, FN insolubility is thought to result from strong protein-protein interactions [206,207]. Our findings indicate that FN assembly is sensitive to ROCK-mediated contractility, and suggest that the conversion of FN to an insoluble form requires cell-generated force. More work is needed to understand the specific role that traction forces have in mediating the soluble-insoluble transition in FN.

The EDB-containing isoform of FN is preferentially localized at sites of angiogenic blood vessel formation. While not required for angiogenesis or survival [208,209], EDB-FN expression in ECs may contribute to changes in cell spreading, motility, FN assembly, and capillary morphogenesis *in vitro* [192,209]. Inclusion of the EDB domain is thought to unmask cryptic sequences in FN that can affect cell adhesion and spreading [210,211]. This may facilitate adhesive interactions and cellular contractility associated with integrin $\alpha_5\beta_1$ [192], a receptor pairing for FN [212,213] whose interaction is crucial for vertebrate survival [99,214,215]. Recent experiments indicate that $\alpha_5\beta_1$ functions as a catch-bond that alternates between tensional states in responses to cellular contractility, and is sensitive to substrate stiffness [216]. Our data indicate that increased substrate stiffness increases the synthesis and deposition of EDB-FN, and that EDB-FN deposition is regulated by ROCK-mediated contractility. Taken together, these findings suggest that substrate stiffness may affect EDB-FN interactions through feedback mechanisms relating contractility to $\alpha_5\beta_1$-FN interactions and FN conformation, however, more work is needed to fully characterize these interactions.

Our findings may have important ramifications for the understanding of tumor angiogenesis, where EDB-FN is a specific marker for angiogenic vasculature [109]

found localized in brain [108], breast [217], and liver [218] tumor environments. The tumor microenvironment is often accompanied by an increase in tissue stiffness [16], a feature exploited by physicians in the clinical detection of tumors. Our data indicate that increasing substrate stiffness is sufficient for increasing both the synthesis and the deposition of EDB-FN. This suggests that changes in the micromechanical environment of tumors may contribute to EDB-FN expression in angiogenic blood vessels. Interestingly, EDB-FN was also detected at the mRNA level early after injury in a model of hepatic fibrosis [219]. While these changes preceded fibrosis and tissue stiffening that accompanies chronic liver disease [220], they suggest that EDB-FN expression is an early biomarker of disease.

CHAPTER 6

CONCLUSIONS AND FUTURE DIRECTIONS

6.1 Conclusions

We investigated the role of substrate stiffness in regulating capillary network assembly and determined that network assembly results from a balance between cell-cell and cell-matrix adhesion that gives rise to the propensity for cell-cell connectivity.

In Chapter 2, we hypothesized that the mechanical microenvironment plays a role in mediating endothelial cell (EC) network assembly. This hypothesis resulted from the observation that experiments in the literature investigating EC network assembly all shared a common thread—the use of compliant substrates. Moreover, in addition to collagen and fibrin gels used to study angiogenesis *in vitro* [19,22-25], the *Matrigel Assay* had emerged as a gold-standard for determining cellular angiogenic potential [20,21]. While matrigel provided cells with a complex semi-native ECM, it was also a compliant substrate, with an elastic modulus on the order of hundreds of pascals [16,221]. Thus, we sought to determine whether substrate stiffness was a contributor to EC network assembly.

We determined that network assembly was controllable by altering substrate stiffness. Compliant (E<1 kPa) substrates enabled network self-assembly while stiff (E>1 kPa) substrates did not. Moreover, we could induce network assembly on stiff substrates by reducing the substrate ligand concentration suggesting that network assembly resulted from a balance between substrate stiffness and matrix density, and ultimately changes in cell-cell vs. cell-matrix adhesion. We used collagen-derivatized substrates, but

were able to recapitulate these findings with fibronectin, and RGD-derivatized substrates suggesting that the stiffness of the substrate was modulating network assembly independent of ligand type. This work was the first demonstration that the stiffness of the local microenvironment was an important factor regulating capillary network assembly.

Inspired by the work of Zhou *et al*., who determined that network formation in 3D fibrin gels required fibronectin (FN) polymerization [98], we determined that network assembly on compliant 2D substrates was also associated with FN. We demonstrated that ECs secrete and polymerize FN that is requisite for network assembly and stabilizes cell-cell interactions. These findings were the impetus for our additional work that focused on investigating the mechanisms of how substrate stiffness regulates capillary network assembly.

Initially we asked whether the sensitivity of network assembly to substrate stiffness was unique to ECs, or whether it was a more universal phenomenon. In Chapter 3 we determined that substrate stiffness also mediated mammary and mesenchymal cell network assembly. Our initial hypothesis regarding network assembly came from the work of Guo *et al*. who postulated that substrate stiffness mediates tissue formation by altering cell preferences for cell-cell vs. cell-matrix adhesion [87]. In Chapter 3, we presented data that confirmed this hypothesis. In ECs, substrate stiffness altered the spatial localization of vascular endothelial (VE)-cadherin, a protein important for endothelial cell-cell connectivity. At the same time, cells on compliant substrates were less adherent to the substrate than those on stiff substrates that did not exhibit significant VE-cadherin mediated cell-cell interactions. Differences in substrate adhesion were likely due to changes in focal adhesion size and density that increased

with increasing substrate stiffness.

In vascular, mammary, and mesenchymal tissue-derived cells, we determined that compliant substrates fostered network assembly that was associated with i) ECM colocalization and ii) a reduction in cell-matrix adhesion. Moreover, analogous to ECs with FN, mammary epithelial cell network assembly required laminin, a mammary basement membrane protein [222,223]. In contrast, we determined that some cell types did not assemble networks, and that these cells i) did not colocalize with ECM and ii) did not exhibit a reduction in cell-matrix adhesion on compliant substrates. However, in laminin-deficient mammary cells that did not assemble networks, network formation was induced by providing these cells with exogenous laminin. These findings indicate that in addition to cell-cell and cell-matrix adhesion, cell-matrix interactions govern network formation. These data suggest that substrate stiffness promotes network assembly by regulating preferences for cell-cell and cell-matrix adhesion, and were the first demonstration that matrix stiffness regulates network assembly in a variety of cell types.

Capillary network assembly is a complex biological process, and we determined that substrate stiffness altered cell-cell and cell-matrix interactions that enabled network assembly. To sense substrates stiffness, cells use contractility and tractions forces in part to probe the mechanical microenvironment [35]. Reinhart-King *et al*. had shown previously that traction forces create strains in compliant substrates that other cells can sense and respond to [36]. In Chapter 4, we examined the role of substrate stiffness in mediating EC traction forces in individual cells and during cell-cell contact, an early event of network assembly. We first determined that cell area and the magnitude of traction forces increased with increasing substrate stiffness. However, normalizing the

traction force magnitude by cell area still led to an increase in force magnitude with stiffness suggesting that stiffness was contributing to force development in ECs. Using regression modeling, we demonstrated that substrate stiffness and cell area were significant predictors of traction force in single ECs and ECs in contact. These findings suggest that ECs sense and respond to the stiffness of the microenvironment by altering cellular contractility, a critical mediator of cellular responses like spreading, migration, and cell-cell interactions. These findings were the first demonstration that substrate stiffness was a significant contributor to ECs in contact.

In Chapter 5, we revisited FN. In addition to being requisite for network assembly, FN polymerization requires cell-generated traction forces that enable matrix assembly and deposition [103,104]. Based on our observations in Chapters 2-3, we hypothesized that substrate stiffness mediated the regulation of FN deposition by ECs. We determined that substrate stiffness mediated the deposition of FN by altering cell shape and the directionality of ROCK-mediated traction forces. We also demonstrated that substrate stiffness altered the expression and deposition of EDB-FN, an FN isoform preferentially localized to neovasculature. This was the first demonstration that substrate stiffness mediated FN synthesis and deposition by ECs.

Ultimately, the findings presented in this dissertation have implications for controlling angiogenesis for therapeutic use. For example, a current limitation in tissue engineering is the creation of vascularized tissue constructs. Our data suggest that the stiffness of the biomaterial scaffold as well as the relationship between ECs and the matrix protein FN within the scaffold are important design considerations. Additionally, our findings suggest that angiogenesis is particularly sensitive to the stiffness of the ECM. This may be an important consideration during cancer, where

tumor growth is associated with changes in ECM stiffness [16] that may enable angiogenesis.

6.2 Future Directions

Despite the progress we have made, much work remains to fully understand the role of the mechanical microenvironment in mediating a complex response like angiogenesis. There are several avenues of approach necessary to proceed in this field.

1) Does matrix stiffness regulate capillary network assembly *in vivo*?

The work we have presented was completed solely on a 2D construct *in vitro*. Future studies should test whether our findings may be recapitulated in a 3D microenvironment *in vivo*. To do this, it is crucial to develop constructs that vary stiffness independently of protein concentration. Current work utilizing glycated collagen gels may enable this work [224,225]. Other challenges in 3D are measuring cellular contractility via traction forces. While traction force measurements in 3D are a recent accomplishment [226], the development of robust methods to measure contractility in 3D will greatly elucidate the understanding of how traction forces enable cell behaviors in 3D.

Our findings should be validated by *in vivo* models that better recapitulate the true physiological conditions of angiogenesis. This may be possible with animal models of angiogenesis coupled with techniques that introduce variable stiffness 3D constructs either embedded with cells, or that allow cell ingrowth during angiogenesis.

2) What is the role of cell-cell interactions?

We have started to investigate how cell-cell interactions mediate angiogenesis by

investigating traction forces during cell-cell contact. During angiogenesis, ECs work *en masse* to form a new capillary. In this work, we have begun to understand the relationship between VE-cadherin-mediated cell-cell interaction and FN regulation, and undoubtedly cell-cell interactions play a role in mediating all EC responses during angiogenesis. Future work should further investigate these relationships.

3) What is the role of supporting cell types?

Cell behaviors *in vivo* occur in a complex microenvironment that is nearly always made up of cells from several lineages. In addition to ECs, the vasculature is comprised of smooth muscle cells, pericytes, blood cells, and fibroblasts. Future work should consider the role of these other cells types as generators of mechanical and chemical signaling events. For example, we have determined that substrate stiffness alters EC monolayer permeability, a response that facilitates changes in leukocyte transmigration [170]. However, more work is needed to understand the role of supporting cell types in mediating angiogenesis.

4) What are the molecular signaling pathways?

Our approach in understanding the role of the mechanical microenvironment in mediating angiogenesis was primarily a biophysical endeavor. Future work should focus on understanding how matrix stiffness alters EC proteomics and signaling that enable the behaviors required for angiogenesis.

CHAPTER 7

BRINGING POLYMER SCIENCE TO THE CLASSROOM

7.1 Abstract

In 2010, I served as a National Science Foundation STEM Fellow in GK-12 Education. During this time, I developed novel curricula based on my research for local middle school science students. This chapter overviews my GK-12 experience, and culminates with an article based on our work in the classroom submitted to *Science Scope*.

7.2 Introduction

In the spring of 2010, I was awarded a fellowship from the National Science Foundation Science, Technology, Engineering, and Mathematics (STEM) GK-12 program. The goal of the STEM program is to bridge the gap between basic science concepts and current research. As a STEM fellow, I was paired with a teacher from a local school, and we worked together both in my lab, on an original research project, and in the classroom, implementing new science activities based on my work.

In the summer of 2010, I was paired with Jackie Henkel and Mike McNall, 7th grade science teachers from Eagle Hill Middle School, in Fayetteville, NY. Over the course of the summer and the subsequent school year, I worked to develop projects that would introduce students to polymers, and the utility of polymers for studying biological phenomena. This was an invaluable experience that helped me learn about and practice teaching, and ways to communicate science effectively.

7.3 The Role of Substrate Stiffness in Mediating Cell Proliferation

During the summer of 2010, I worked with Jackie supervising a research project that she conducted in our lab. Her project was to determine the role of substrate stiffness in mediating cell proliferation, a project I had started working on with Tracy Cheung while she was an undergraduate in our lab. I taught Jackie how to make polyacrylamide substrates, to culture, plate, and fix cells, and to stain and image samples with fluorescence microscopy. We quantified and analyzed Jackie's data and prepared a poster that she presented at the end of the summer research program. Jackie determined that endothelial cell proliferation rate increased with increasing substrates stiffness (Figure 7.1). The raw data from Jackie's experiments were used to develop a laboratory activity where students were asked to determine the role of substrate stiffness in mediating cell proliferation. This was a rewarding experience for me because I was able to teach Jackie about current research in biomedical engineering, and to brainstorm ideas with her about possible projects to implement in her classroom. Jackie's poster was hung in her classroom at Eagle Hill for her students to see.

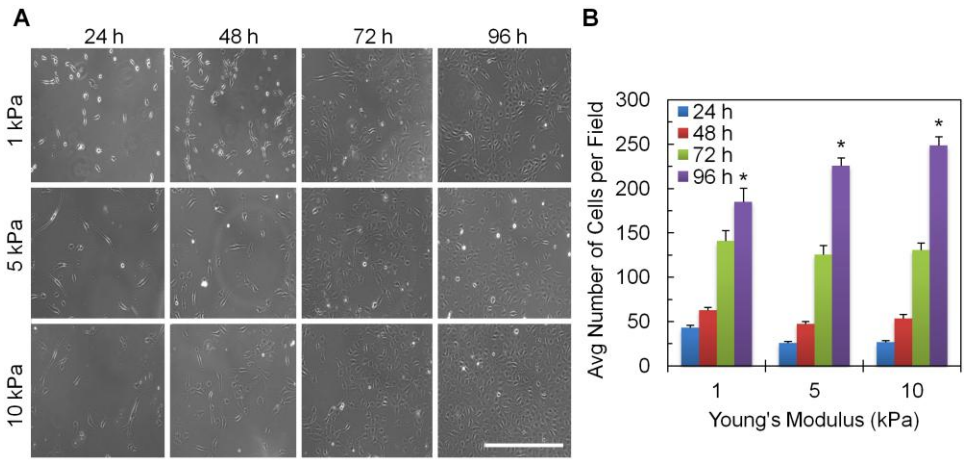

Figure 7.1. EC proliferation increases with increasing substrate stiffness. Endothelial cells were plated on variable compliant (*E*=1-10 kPa) substrates and imaged every 24 hours over four days. (**A**) Representative phase contrast images for each time point and stiffness (scale bar is 500 μm). (**B**) To measure proliferation, phase images were used to determine the average number of cells per microscope field for each stiffness and time point. Mean + SEM, *p<0.05, ANOVA.

7.4 The Approach

During the academic year (September 2010-June 2011), I worked with students at Eagle Hill a few times a month. In the beginning my role was to observe and assist lab activities that Jackie and Mike had developed previously. In the winter of 2011 I was able to present my own curriculum to the class.

I developed three lesson plans that focused on polymer stiffness. These lessons were shaped as modules rooted in New York State education requirements for middle school science to accompany units in chemistry, physics, and biology. Jackie and Mike were instrumental in helping facilitate the development and implementation of the activities. They both were a wealth of knowledge about pedagogical methods and were a helpful sounding board when I approached them with ideas for activities.

The lessons were all structured the same way, and took place over three consecutive days. On the first day, I presented the students with a lecture that gave the conceptual foundation to the lesson. The students followed along with a "notes" worksheet that I created to accompany the lecture. This was done so that the students would not get bored during the lecture, and also so that they would have a copy of the main content of the lesson. The worksheets contained examples and problems that I designed to test their understanding. These examples were placed throughout the lecture and were used to break the lecture format into interactive periods, a tool that helped keep students interested. After giving the students time to work independently, we discussed the answers as a class to check understanding. On the second and third day, the students worked on a lab activity that I designed to accompany the lecture. The activities were focused on polymers, their characterization, and their role in biology. Several days to weeks after the lesson, Mike administered a quiz to the students. This same quiz was given to students several days before my initial lecture, and served as a tool to assess student learning.

7.5 The Lessons

7.5a Introduction to Polymers

The first lesson plan I designed and implemented was called “Introduction to Polymers” and accompanied the chemistry unit. I wanted to build on the chemistry unit that was focused on the elements in the periodic table and types of matter by presenting polymers as a type of material that is ubiquitous and relevant for biomedical research.

My presentation overviewed the classes of polymers, methods to name polymers, the role of crosslinkers in polymers, the chemical and physical properties of polymers, and

examples of polymers used in medical devices. During my lecture, students worked through an accompanying notes handout (Appendix J.1a).

The accompanying laboratory activity allowed students to synthesize their own polymers—"silly putty" made from mixing ratios of borax and glue. It also asked them to hypothesize, design, and execute an experiment to determine the role of chemical crosslinkers in mediating polymer stiffness. This activity went over very well with students—they really enjoyed making and playing with the putty.

The students came up with several methods to characterize polymer stiffness including i) recording the time it took for a polymer ball to change a given diameter (the putty is viscoelastic), ii) recording the length the polymer stretched while hanging off the desk edge over a given time period, and iii) recording the bounce height of a polymer ball dropped from a given height. These methods reinforced the concept of measurement that was a central theme throughout the school year. The students were asked to determine what ratios of monomer to crosslinker made the stiffest polymer, to characterize and make a plot of their results, and to communicate their findings to the class. Not all ratios of monomer and crosslinker can be used to make a polymer; this led to a class discussion about how this could happen (usually students added too much monomer). Notably, while discussing results as a class, one group claimed that a specific ratio of monomer to crosslinker was the stiffest, while another group said that this same ratio did not polymerize. This led to a class discussion about the need to repeat research findings in science to confirm hypotheses.

As determined by the pre-and post-quiz (Appendix J.1b) results, there was a significant increase in quiz scores given after the lesson was complete (Figure 7.2

"3/11/11"). To determine if there was knowledge retention from the lesson, we administered the quiz again four months later. Again, there was a significant increase in scores (Figure 7.2 "6/23/11"). It is not clear whether students remembered the actual content or simply the correct quiz answers, however, these findings suggested that the students were able to retain some information from the lesson. I was extremely happy with these results, but would have been happy if they came away with nothing other than an understanding that polymers are an important material found in items all around them.

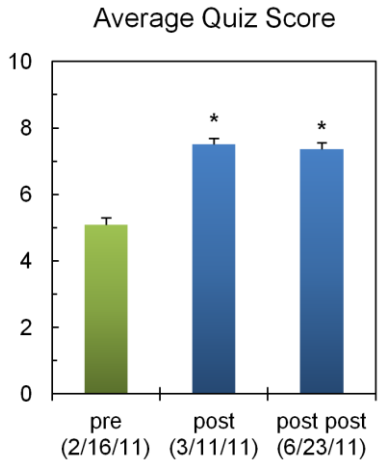

Figure 7.2: "Introduction to Polymers" quiz scores.
Pre-and post-lesson testing was used to assess curriculum efficacy. The mean quiz score increased significantly (*$p<0.0001$) for the quiz administered after lesson implementation (post). Three months later, students retained a significant increase in quiz score (post post) compared to pre-quiz scores. Quiz score out of 10 points.

7.5b Mechanical Testing of Polymers

As the students progressed chemistry to a unit in physics, I wanted to implement a lesson about more detailed methods to characterize polymer stiffness. This lesson was admittedly more ambitious than the previous lesson, but I wanted to challenge the students. Mike agreed that it would be challenging but that the students would get a

taste for how to apply physics.

Like my first lesson plan, the activity started with a presentation about the concepts of force, Newton's Second Law, stress and strain, and Young's Modulus. The accompanying worksheet (Appendix J.2a) contained example problems where students could calculate and convert between their mass and weight, find the stress and strain in a cylinder or block under application of a force, and calculate Young's Modulus from a plot of stress vs. strain with SI units.

The laboratory was framed as a biomedical problem (Appendix J.2b). The goal of the lab was to determine the Young's Modulus of rubber, and to determine whether rubber is a mechanically suitable material for making replacement teeth. The students were supplied with a set of hooked weights, rubber bands, ring stands, rulers, and calculators. To determine the Young's Modulus, the students needed to make a plot of stress vs. strain. This was done by hanging three different weights from one end of a rubber band looped over a ring stand laid parallel to their desks (Figure 7.3). Making measurements of the rubber band before and after stretching, and knowing the mass of the attached weight, the students populated a table with values they obtained for mass, force, area, stress, and strain. The values of stress and strain were plotted, and an approximate best-fit line was used to determine the Young's Modulus.

Figure 7.3. Mechanical testing apparatus.
The mechanical testing apparatus consists of a laboratory ring stand laid over the side of the desk. The rubber band is looped over the end of the stand and a hooked weight is hung from the bottom of the band.

This was a challenging activity, and I wasn't sure how far the students would be able to get through the lab. However, I was surprised that most students were able to measure and calculate stress and strain for three different weights applied to a rubber band. Some students were even able to make a plot of stress vs. strain, but they had trouble calculating the Young's Modulus (slope of the line) and understanding how changes in the slope related to changes in polymer stiffness. This was due to the fact that the students at this grade level had not yet formally learned how to plot lines and calculate line slope in math class. I was surprised and pleased that the students were able to work with the concepts of stress and strain despite not fully making the connection to Young's Modulus. There was a significant increase in quiz (Appendix J.2c) scores suggesting that the students did retain some of the information I presented after the completion of the lesson (Figure 7.4).

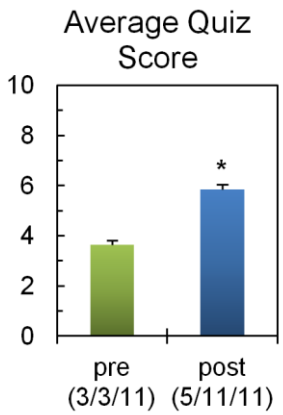

Figure 7.4. "Mechanical Testing of Polymers" quiz scores.
Pre-and post-lesson testing was used to assess the efficacy of the Mechanical Testing of Polymers unit. The mean post-quiz score (post) increased significantly (*$p<0.0001$) compared to the pre-quiz (pre). Quiz score out of 10 points.

7.5c Polymer Stiffness and Cell Proliferation

This activity was the culmination of my GK-12 experience. I designed a lesson stemming from biology where students investigated the role of substrate stiffness in mediating cell proliferation. This research problem came directly from my research and from work that Jackie completed in lab with me before the start of the school year.

The presentation and notes (Appendix J.3a) were an overview of cell biology, where I introduced students to the hierarchy of structure and function in the body, described cells and extracellular matrix, discussed scientific research in practice, and presented some of my own work showing that substrate stiffness alters cell spread area in 2D.

The lab activity was framed as a discovery experiment where students were asked to determine whether substrate stiffness influences cell proliferation. The tie-in to biomedical research is considering the role of the mechanical microenvironment of tumors that are often stiffer than the local surrounding tissue they reside in. This

activity was a paper lab where students were taught about fluorescence staining and microscopy as a method to identify cells, and asked to ascertain whether stiffness affected cell growth. We did this by supplying pictures representing data that Jackie had acquired over the summer. Students were asked to count the number of cells per microscope field, to make plots of their findings, and to communicate their results to the class. This was a relatively easy activity, and most students determined that proliferation increased with increased substrate stiffness, results determined in our lab. At the end of the lecture, we discussed what this could mean in the context of cancer (could we influence tumor growth by treating ECM stiffness?). While we did not have sufficient time for pre- and post-quiz assessment, the students were interested in current research in biomedical science.

7.6 Conclusion

I had a great time working with Jackie, Mike, and the students at Eagle Hill. I learned a lot about teaching methods and ways to communicate science. More than learning a set of facts about polymers, I hope that the students gained an appreciation for scientific research, and that science, while challenging, can also be fun.

7.7 Science Scope Article

The following article, entitled *Biomedical Application of Polymers: Inquiry based Exercises for the Classroom*, was submitted to *Science Scope*.

Abstract

Polymers are a class of materials that are found in everyday objects like plastic water bottles and polyester fabrics. In biomedical sciences, polymers help treat disease through applications like sutures or replacement joints. Polymers are also used in

research laboratories to study biological phenomena. Here, we present two classroom activities that introduce middle school science students to polymers, polymer stiffness, and the role of polymers in biomedical research. These activities allow students to synthesize polymers and to determine how crosslinkers affect polymer stiffness. In addition, they allow students to discover the role of polymer stiffness in mediating cell proliferation by analyzing original research data collected at Cornell University. The activities are grounded in New York State education requirements and can be used to enrich fundamental science concepts with current research.

Introduction

Take a minute to look at the items sitting around you right now (go ahead, we'll wait). Maybe you see a plastic water bottle, or sheets of paper, or even a polyester raincoat. These items might look very different, and help us perform different tasks, but they are all made from a class of materials called polymers. In biomedical sciences, polymeric materials play an important role in treating disease and are found in applications ranging from sutures used for wound closure to joint-replacement implants.

Depending on their intended biomedical use, polymers are designed with specific chemical and mechanical properties. One important property is polymer stiffness. For example, we want polymers that touch our eyes (contact lenses) to be much softer (less stiff) than those used in replacement hips designed to withstand our bodyweight with every step.

What exactly are polymers and how can we tailor their stiffness? What role does polymer stiffness play in biomedical sciences? Here, we present two classroom

activities that introduce middle school science students to polymers, and allow them to conduct experiments synthesizing polymers and understanding their application in biomedical research. These activities were designed in collaboration with New York State middle school seventh-grade science teachers and a Cornell University Biomedical Engineering graduate student, and are grounded in state education requirements. The overall goal of these activities was to introduce students to the role of polymers in biomedical sciences to enrich fundamental science concepts with current research.

I. What are polymers?

Polymers are large molecules made up of repeating parts, where the repeating parts, or monomers, are chemical compounds. As a material, most polymers can be classified as either *synthetic* ("plastics" used for food and beverage containers, sports equipment, and medical devices like contact lenses) or *natural* (polymers synthesized by cells in plants and animals, like cellulose and DNA).

If we could look at the chemical structure of a polymer, we would see long chains of repeating monomers tied together like beads on a string. Crosslinkers are other compounds that tie monomer strings together. The physical properties of polymers are determined by the chemistry of both the monomer and crosslinker. Examples of physical properties that are altered by changes in polymer chemistry include density, melting temperature, and stiffness.

Activity I: Polymer Synthesis

Overview

This activity was designed to introduce students to polymers and built upon a

chemistry unit focused on the scientific method, the periodic table, and types of matter. Students synthesized their own polymers and were asked to hypothesize, design, and execute an experiment to determine the role of chemical crosslinkers in mediating polymer stiffness. A presentation and accompanying worksheet (available at http://climb.bme.cornell.edu/polymer.php) overviewed the classes of polymers, methods to name polymers, the role of crosslinkers in polymers, the physical properties of polymers, and examples of polymers used in medical devices. Pre- and post-lesson quizzes were used to assess student performance.

Materials and Teacher Preparation

The teacher should prepare a 50% (v/v) mixture of glue (Elmer's Glue-All, $3/L) in water ("Solution A", monomer) by combining 1.9 L water and 1.9 L glue in a 3.8 L plastic (1 gal) jug. To prepare a 7.4% (w/v) mixture of sodium tetraborate decahydrate (borax; VWR cat# AA40114-36, $29/500 g) in water ("Solution B", crosslinker), combine 272 g of borax and 3.7 L water in a 3.8 L jug and shake to mix thoroughly. 3.8 L each of solutions A and B were used for 30 groups of 4 students. Extra reagents can be stored for several years at room temperature.

The teacher should review the MSDS information for sodium tetraborate decahydrate and glue (available from vendor). Students should be supplied with splash safety goggles, aprons, gloves, and should wash their hands after the activity. Gloves are recommended as the polymer may dry skin after prolonged handling.

Performing the Activity

Groups of 3-4 students should be supplied with one plastic cup of "Solution A" (125 mL), one plastic cup of "Solution B" (125 mL), an empty 237 mL (8 oz) plastic cup, spoons, a ruler, and a timer. Food coloring may be added to Solution A and stirred to incorporate. Students are directed to add three-parts Solution A to one-part solution B in the empty cup, and to stir until the solution polymerizes (3-5 minutes). Once solidified, students can remove the polymer from the cup and knead it with their hands (Figure 7S.1). The polymer displays time-dependent properties (viscoelastic) and will flow over time. The polymer can be stored in zip-lock bags for many days.

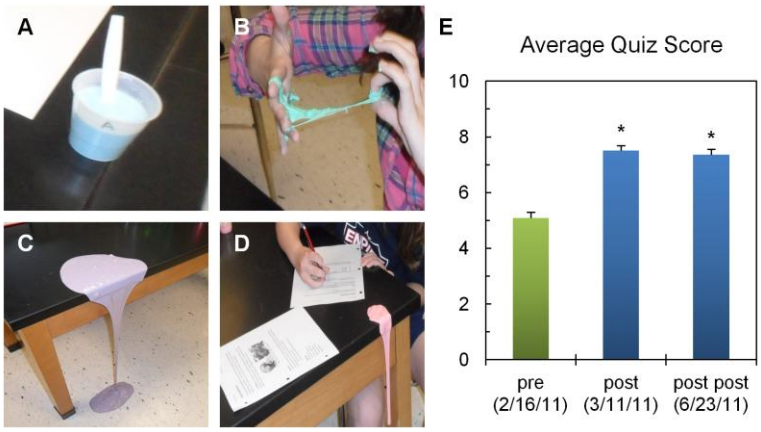

Figure 7S.1. Polymer synthesis in the classroom.
(**A**) Solution A colored with blue food coloring in a plastic cup with a plastic spoon used for mixing. (**B**) A student kneads the polymer in her hands during synthesis. (**C**) The polymer displays viscoelastic (time-dependent) properties and flows over the desk edge with time. (**D**) A student completes the lab activity worksheet while her polymer spills over the desk. (**E**) A comparison of quiz scores from pre- and post-lesson testing indicated a significant increase (*$p<0.0001$) in score for both post-lesson time points compared to the pre-lesson score. Score out of 10.

To determine the role of crosslinkers in polymer stiffness based on their hypothesis, students will mix ratios of Solutions A and B of their choosing, and will measure polymer stiffness (see example worksheet). Note that not all ratios of monomer and

crosslinker will make polymers—instead the mixture will remain watery.

Students may need help brainstorming ways to measure the stiffness of their polymer. Common examples devised by students included recording the change in length of a hanging polymer strip over a given time period and recording the bounce height of a polymer ball dropped from a given height.

Once each group has synthesized and characterized several polymers, students should report their findings to the class. In general, students found that increasing ratios of crosslinker increased polymer stiffness. This facilitated a discussion about the chemistry of the polymer and why this might be happening (additional crosslinker decreases monomer chain mobility and rigidifies the polymer). Groups in our classroom identified discrepancies in the reported data. This stimulated a class-wide discussion about sources of scientific error ("Are you *certain* that you used a ratio of 3:1?") and the need for reproducibility and documentation in scientific experimentation.

II. Does tissue stiffness affect cell behavior?

Over half a million deaths were attributed to cancer in 2011, and 1.6 million new cases of cancer are projected for 2012 [227]. Cancer is a disease characterized by the abnormal and uncontrolled growth of cells that may result in tumor formation and metastasis (relocation of tumor cells throughout the body). Many cancers are first detected as a hard lump in a soft tissue, a feature exploited by physicians in tumor detection. An interesting theory that is being studied by cancer scientists is, once a tumor develops, does the increase in tissue stiffness affect cell function?

Cell proliferation is the cycle of cell growth and division where one cell becomes two, a process that is exploited in cancer. In the body, most cells are in constant contact with protein scaffolds outside the cell that support cell attachment and give tissues structure. This *extracellular matrix* is the site of increased stiffness during tumor growth [16]. One hypothesis is that increased matrix stiffness increases cell size, and subsequently nuclear volume and DNA synthesis that enable proliferation. In fact, it has been shown that cell size can be altered by changing matrix stiffness [112,176].

Researchers at Cornell University are investigating whether the stiffness of the tumor extracellular matrix plays a role in affecting cell growth to understand the relationship between stiffness and cancer. This is done by growing cells on polymer substrates of tunable stiffness, and measuring cell behaviors like migration or growth. By altering the ratios of monomer and crosslinker, researchers synthesize polymers with a stiffness that mimics the stiffness of body tissues, like blood vessels, bones, or tumors. In contrast to traditional glass or plastic substrates, polymer substrates provide a more "physiologically relevant" platform to study cell behavior. This research will aid in the understanding of the role of tissue stiffness as a regulator of cell behavior, and may one day help researchers design new cancer treatments.

Activity II: Polymer Stiffness and Cell Growth

Overview

This activity was designed to allow students to determine the role of stiffness in mediating cell proliferation and built upon a biology unit focused on body systems. Students were asked to analyze data resulting from an experiment conducted by their teacher at Cornell University (Figure 7S.2). In this experiment, cells were grown on

polymers with a range of stiffness (1-10 kPa) over three days. The purpose of the experiment was to determine if polymer stiffness had an effect on the rate of cell proliferation. A presentation and accompanying worksheet (available at http://climb.bme.cornell.edu/matrix.php) overviewed the hierarchy of tissue organization in the body, presented pictures of cells and their extracellular matrix in tissues like bone and blood vessels, detailed functions that cells can perform (adhere, change shape, migrate, communicate), and presented data from research publications indicating that cell size increases when cells are grown on polymers of increasing stiffness [112,176]. Due to time constraints, quizzes were not administered for this lesson.

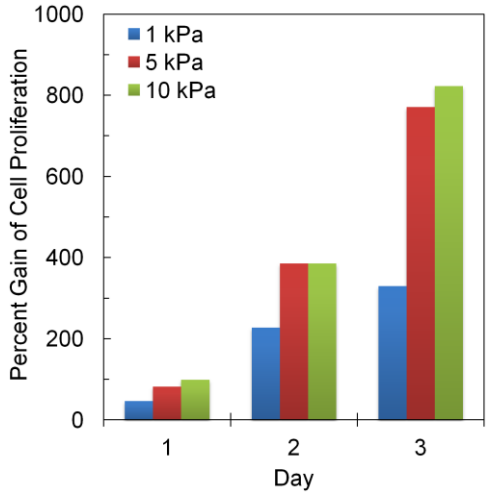

Figure 7S.2. Cell growth increases with increasing polymer substrate stiffness. Plot of the percent gain in cell proliferation over three days with respect to substrate stiffness. Cells were grown on polymer substrates with Young's Moduli of 1, 5, and 10 kPa and were imaged over 3 days after plating. The results indicated that there was an increase in proliferation with time and with increasing polymer stiffness.

Materials and Teacher Preparation

The teacher should remind or teach students about the principles of microscopy to understand how the experimental data was collected.

Performing the Activity

Students are given copies of the laboratory activity (see example worksheet) and asked to hypothesize whether polymer stiffness influences cell proliferation. Students are presented with images representing microscope fields-of-view containing cells stained to localize their nucleus with fluorescence microscopy (Figure 7S.3). Students count cells from images representing polymers of different stiffness at two time points. They are asked to make a plot of their data, to identify potential sources of experimental error (what if a cell has more than one nucleus?), and to report their findings to the class. The experimental data suggests that cell proliferation increases with increasing polymer stiffness, a finding that led to a discussion in our class hypothesizing new cancer treatments (can we influence tumor growth by targeting matrix stiffness?). Students seemed genuinely excited about working with data from current research.

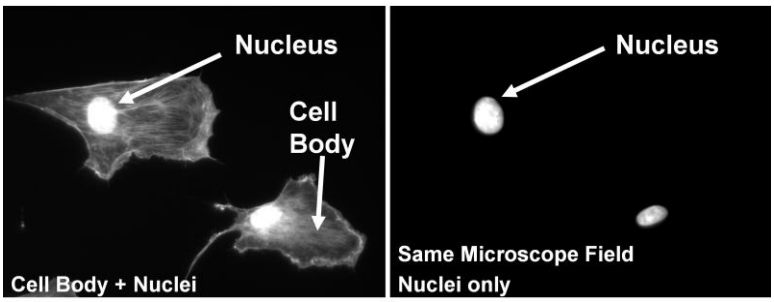

Figure 7S.3. Cells stained and imaged with fluorescence microscopy.
Cells from a cow aorta (bovine aortic endothelial cells) were fixed with formaldehyde and stained to localize nuclei and actin, a structural protein used to identify the cell body. The nuclei images were segregated and used to determine the number of cells per field of view.

Conclusion

We have designed two activities centered on polymer stiffness and rooted in units of chemistry and biology. The activities allow students to synthesize polymers, and to

learn about the use of polymers in biomedical research. The activities can be completed individually or as a series to enrich existing middle school science curricula with concepts from current research in biomedical science.

Worksheet: Polymer Synthesis

Materials

- Plastic cups, teaspoons
- A cup of "Solution A" (50% v/v glue in water)
- A cup of "Solution B" (7.4% w/v borax in water)
- Food coloring
- Ruler, timer

Safety

Splash safety goggles, aprons, and gloves are recommended.

Procedure

1) Label a cup with "3:1."
2) Add 3 teaspoons of solution A to the cup.
3) Add 1 teaspoon of solution B to the cup.
4) Stir the mixture until all of the liquid is gone.
5) Once you have a polymer gel, take it out of the cup and knead it with your hands.

Questions

1) Write down your observations of the polymer (color, shape, stiffness, etc.).
2) What happens when you pull the polymer apart quickly? Why do you think this happens?
3) What happens when you pull the polymer apart slowly? Why do you think this happens?
4) Roll the polymer into a ball and let it sit on the table for a few minutes. How does the polymer change? Why do you think this happens?
5) Would you characterize the polymer as a solid or a liquid? Why?

Design an experiment to determine how the amount of polymer crosslinker alters the stiffness of the polymer.

1) State your hypothesis:
2) Record the ratios of solution A to solution B you used here:
    i) ___:___
    ii) ___:___
    iii) ___:___
3) Based on your observations, what happens to the stiffness of the polymer when you change the amount of crosslinker?
4) Describe the methods you used to measure polymer stiffness.
5) How will you communicate your findings to the rest of the class? Explain/show below.

Worksheet: Substrate Stiffness and Cell Proliferation

Dr. L. wants to know whether substrate stiffness affects cell proliferation. In the laboratory, she put cells on polymers with a stiffness of 1 or 10 kPa. Dr. L. then stained the cell nuclei so that she could see the cells when she looked at them with a microscope.

Research Question and Hypothesis
Does substrate stiffness influence cell division? Yes or No and why—write your hypothesis here.

Procedure
To determine whether substrate stiffness influences cell proliferation, Dr. L. took images 24 hours and 48 hours after she put cells on the 1 and 10 kPa substrates. She took 2 images from each condition at each time point (see images below).

1. Dr. L. asks you to analyze her data by counting the number of cells present in each condition to determine whether matrix stiffness influences cell proliferation.

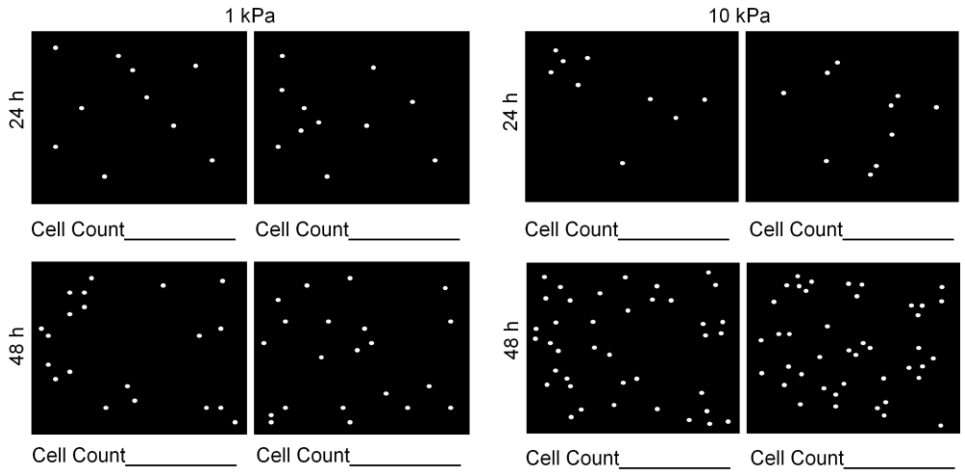

2. Using the count data from above, calculate the <u>average number of cells</u> per condition and make a bar graph of the data.

Questions

1. Is your hypothesis correct or incorrect? Does matrix stiffness influence cell proliferation? How do you know?
2. Identify one problem with this experiment. How can you fix it?
3. During cancer, uncontrolled cell division contributes to tumor growth. These tumors are often detected by physicians as a hard lump in soft tissue. Cancer treatments use drugs that target and prevent cell division. In light of the <u>data from this experiment</u>, what target may be an alternative avenue for cancer treatment? Why?

APPENDIX A

Protocol for Coverslip Activation

Modified from the methods of Wang and Pelham [28] and Reinhart-King [228].

1. Line up coverslips on top of 100 mm diameter Petri dishes (non-tissue culture treated). Any glass substrate is amenable to activation: for six-well dishes, use 22 mm square coverslips (No. 1); for traction force microscopy, use 45x50 mm rectangular coverslips (No. 1).
    a. Tip: For washing steps below, five 22 mm square coverslips will fit into one Petri dish; use one Petri dish per 45x50 mm coverslip.
2. Using forceps briefly pass the glass coverslip through flame of a Bunsen burner 3x. Be careful, if the glass gets too hot, it will break. If the glass is not hot enough, the NaOH will not spread well.
3. Using a clean cotton swab, immediately apply 0.1 N NaOH to flamed side.
4. Repeat steps 1 and 2 until the required number of slides have been coated.
5. Allow coverslips to dry inside chemical fume hood (approximately 10-20 minutes).
6. When slips are dry, re-coat with NaOH and allow to dry.
7. Remove 70% glutaraldehyde from -20 °C freezer and place inside fume hood approximately 10 minutes prior to use.
8. In fume hood: Add 30 µL/22 mm square, or 80 µL/45x50 mm rectangle, of 3-aminopropyl-trimethyoxysilane (APTMS) to each coverslip and spread quickly using a glass Pasteur pipette. The amount scales with the size of the coverslip, and should be just enough to cover the coverslip surface.
    a. Tips: Work in groups of two or more slips. Spread the drop until the glass looks evenly coated and glossy. Use one pipette per group. To spread the drop, it is easiest to pick up the coverslip with a gloved hand and spread. Discard gloves after this step.
    b. Note: once the drop is deposited on the glass, it should be spread quickly before the APTMS starts to dry.
    c. Note: APTMS is corrosive. Be sure not to get APTMS on the lid of the bottle. Otherwise, you will need a wrench to loosen the lid.
9. Allow coverslips to dry for 5 minutes inside chemical fume hood. Do not allow to dry for more than 10 minutes.
10. Place each coverslip in a Petri dish filled with MilliQ water. Wait until APTMS layer starts to crack, or an oily residue is visible in the dish.
    a. Tip: Make sure coverslips are not overlapping in dish—use a pipette to move them being careful to not touch the activated surface.
11. Shake dishes to dislodge APTMS from each slip and discard water.
12. Rinse 3x with MilliQ water. Incubate for 5 minutes between each rinse.
    a. Be sure coverslips are rinsed thoroughly—if not, the APTMS will react with the glutaraldehyde in the next step to form a yellow/orange-red precipitate making the coverslip unusable.

13. In fume hood: Dilute 70% glutaraldehyde stock solution 1:140 in 1X PBS (without calcium and magnesium, pH 7.1). Each 22 mm square coverslip requires 200 µL, each 45x50 mm rectangle requires 500 µL.
    a. Tip: To calculate amount of glutaraldehyde necessary, divide total number of mL of solution needed by 140.
        i. Note: Glutaraldehyde is very viscous. Wait for it to come to room temperature and pipette up very slowly, waiting for a few seconds before moving the pipette tip out of the glutaraldehyde, giving the glutaraldehyde time to enter the pipette tip.
        ii. Vortex the solution to mix thoroughly.
14. Pipette the required volume of glutaraldehyde solution per slip onto parafilm.
15. Invert slips on the droplet of glutaraldehyde solution ("activated" side down).
16. Incubate for 30 minutes.
17. Remove slips from parafilm, invert ("activated" side up), and return to Petri dish. Dispose of glutaraldehyde solution in waste a hazardous waste. Wash each coverslip 3x with MilliQ water. Incubate for 5 minutes between each rinse.
18. Remove coverslips from dishes and place on a clean paper towel.
19. Allow slides to dry inside fume hood. This step can be performed overnight if necessary.
20. Store slips in coverslip boxes in a dessicator at room temperature. Slips can be stored and remain "active" for many months.

APPENDIX B

Protocol for Polyacrylamide Gel Synthesis

Modified from the methods of Wang and Pelham [28] and Reinhart-King [228].

1. Activate glass coverslips as described in Appendix A. These coverslips are the "bottom" substrate that the gel becomes covalently bound to during polymerization. Polymerization proceeds between this bottom slip and a "top" coverslip that will determine the size of the gel.
2. Coat clean "top" coverslips with RainX. The size of the coverslip used is based on the desired size of the gel. Usually 18 mm diameter circles, or 22 mm squares, are used with 22 mm square and 45x50 mm rectangular coverslips. Apply RainX using a clean cotton swab and allow to dry for at least 5 minutes. Buff off excess with a kimwipe. Use canned air to dust the coverslip.
    a. Tip: Make sure to buff the edges well.
3. If making gels for traction force microscopy, place 20 µL fluorescent beads per 5 mL tube (see Step 7) into an eppendorf tube and sonicate for 10 minutes.
4. Remove N6 and from the refrigerator and allow to come to room temperature before opening. Do not open if cold.
5. Combine the following components in a 50 mL centrifuge tube to prepare the gel mixture needed. Compliance is based on the ratio of stock acrylamide (40%) to bis-acrylamide (2%).

Young's Modulus (kPa)	**Volume acrylamide (mL)**	**Volume bis-acrylamide (mL)**	**HEPES pH6 (mL)**	**Temed (µL)**	**MilliQ water (mL)**
0.2	1.50	0.40	2.6	10	13.99
0.5	1.50	0.50	2.6	10	13.89
1.0	1.50	1.00	2.6	10	13.39
2.5	2.50	1.00	2.6	10	12.39
5.0	3.75	1.75	2.6	10	10.39
9.0	3.78	2.75	2.6	10	9.31
10	3.75	3.50	2.6	10	8.64
15	6.00	1.30	2.6	10	8.59
20	6.00	1.90	2.6	10	7.99
30	6.00	2.80	2.6	10	7.09

6. pH the solution to 6.0 by adding 45-50 µL of 2M HCl.
7. Remove 845 µL of acrylamide mixture and place in a 5 mL plastic culture tube. Add 20 µL of fluorescent beads and 60 µL of water (80 µL total, variable ratio). Place the tube(s) into a vacuum flask and degas for 30 minutes. The vacuum flask is sealed with a large stopper.
    a. Tip: Mix the gel solution by rocking the tube and pipetting up and down gently before the removal of 845 µL.

    b. The vacuum flasks can hold up to four 5 mL tubes.
8. Weigh out 5.6 mg of N6 linker in an eppendorf tube—be precise.
9. Add 70 µL of 200 proof ethyl alcohol (molecular biology grade) to N6. Pipette solution until well mixed and add it to the 845 µL of acrylamide mixture.
    a. Tip: Mechanically mix the N6 with a pipette tip until it is a saturated solution.

10. To initiate polymerization:
    a. Add 5 µL freshly prepared 10% ammonium persulfate (APS) (0.1 grams in 1 mL of MilliQ water).
    b. Mix gently by pipetting up and down being careful not to introduce bubbles.
        i. Tip: Once APS is added, work quickly. Lay out all materials and micropipettes ahead of time.
        ii. Tip: Initiate polymerization in increasing stiffness, *i.e.* 0.2 kPa gels are first to polymerize and last to remove top coverslips.

11. Add 20-30 µL (for 18 mm diameter "top" slips on 22 mm square "bottom" slips) of gel solution to activated coverslips from step 1. This volume is scaled based on the desired size/thickness of the gel.
12. Gently press the drop of gel solution with RainX-coated glass circle by carefully touching the round coverslip to the edge of the drop and then lowering it slowly using forceps.
    a. For traction gels: invert the coverslip sandwich onto a 60 mm dish so that the beads can sink to the *top* of the gel.
13. Allow polymerization to occur for 30 minutes. The edges of the gel should recede beneath the top coverslip. Lower stiffness gels may need to polymerize up to 35 min.
14. While gels are polymerizing, remove protein from fridge/freezer and place/thaw on ice.
15. Dilute the protein in ice-cold 50 mM HEPES (pH8) to the desired concentration (usually 1-100 µg/mL).
    a. Tip: Need 200 µL of protein/gel minimum.
16. Peel off cover slip from each gel using a clean razor blade.
17. Add 200 µL of the dissolved protein to the gels: deposit 200 µL of protein solution onto parafilm. Invert the gel onto the drop.
    a. Tip: Introduce no bubbles. The gel can be lifted slightly on its edge with a razor blade to remove bubbles.
18. Incubate at 4°C for 2 hours.
19. Remove gels from parafilm and place in labeled 6-well plates.
20. In a tube, mix a 1:1000 volume of ethanolamine with 50 mM HEPES (pH8). (1 µL of ethanolamine for each 1 mL of HEPES buffer). Each gel requires 200 µL of solution.
21. Dispense 200 µL of the ethanolamine/HEPES solution directly onto the gels. There is no need to rinse off the protein first.
    a. Tip: Make sure the dispensed volume covers the gel.
22. Incubate gels at room temperature for 30 minutes.

23. Rinse gels with MilliQ water—add liquid to side of well, not directly on gel.
24. Place gels in MilliQ water and store at 4C for up to 2 weeks (total experimental time including cell-seeding; best to use gels ASAP).

APPENDIX C

Advanced Methods for Polyacrylamide Gel Synthesis: Double Gels and Micropatterned Gels

Double Gels

This is a polyacrylamide gel ("base gel") cast with a thin gel at the top surface ("top gel") incorporated with fluorescent beads. This will ensure that fluorescent beads are in a single plane at the surface of the gel for traction force microscopy or mechanical testing

1. Activate glass coverslips (Appendix A).
2. Synthesize polyacrylamide gels (Appendix B) with the following amendments to the steps indicated:
    a. Step 7: For each stiffness wanted, degas a 5 mL tube of gel mix with no beads, and a vial with 0.5-2 uL of beads (be sure to sonicate the beads as described in step 3).
    b. Step 11: Prepare base gel with the no-bead gel mix. Use 40 uL of gel mix sandwiched between two 22 mm square coverslips (one activated and one RainX-treated). Proceed with steps 12-16.
    c. Step 16: After polymerization, remove the top coverslip and add the "top" gel: Add 20 uL of initiated gel mix (step 10) with beads under another RainX-coated 22 mm square top coverslip (could also use a patterned glass square from below).
    d. Proceed with Steps 13-24.

Micropatterned Gels

This is a gel micropatterned with adhesive islands transferred from PDMS stamps. Modified from the methods of Rape *et al*. [195].

1. Combine N6 linker and collagen in HEPES pH8 at the desired concentration on ice for 2 hours.
2. Cut out PDMS stamps to the desired size and shape (a 2x2 array works well for 22x22 mm glass coverslips).
3. Clean coverslips to be patterned with ethanol and remove dust with canned air.
4. After 2 hours, apply collagen to stamp surface (“inking”) in a bubble on top—let sit for 30 min at RT.
5. After inking, gently remove excess collagen by dabbing the *side* of the stamp on a paper towel. Hold stamps with forceps but make sure the features do not touch the paper towel.
6. Air dry the stamps until no excess collagen is visible.
7. Place inked stamps on clean coverslips and press gently. Incubate for 5 min.

8. Remove stamp vertically and carefully with forceps—do not let stamp move around or retouch glass during removal.
9. Use the patterned glass as the top coverslip in the conventional gel-making protocol (Appendix B)

Notes:
-Patterns on the glass coverslip may not be visible—but they exist!
-Do not use RainX on the patterned coverslip
-This procedure can also be used with the Double Gel protocol—see above.

APPENDIX D

Protocol for N6 Linker Synthesis

Modified from the methods of Swift [229] and Reinhart-King [228].

Structure of N6 [N-6-((acryloyl)amino)hexanoic acid, succinimidyl ester]

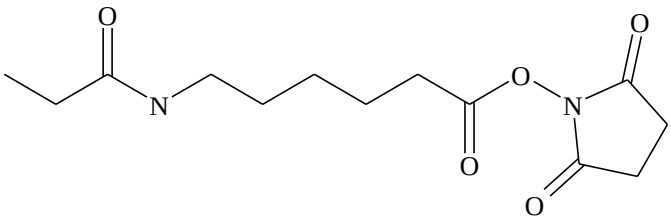

Molecular Weight: 283 g/mol
Formula: $C_{13}H_{18}N_2O_5$

It should be noted that this linker is now available from Invitrogen (Cat # A-20770).

1. Assemble the following in a fume hood:

   250 mL Erlenmeyer flask
   Ice bath with beaker containing 150 mL DI water
   Stir plate
   9 cm filter (ceramic with long neck) with fine glass filter paper
   Vacuum flask with tubing and filter
   250 mL beaker
   100 µL pipetter with tips
   pH meter
   spatula
   crystallization dish
   Plastic transfer pipettes
   10 g 6-amino hexanoic acid (do not use "caproic" acid)
   10 g $Ca(OH)_2$
   7.0 mL acryloyl chloride in 10 mL graduated cylinder
   2 mL 12 N HCl in 10 mL beaker
   100 mL beaker of 50 mL dry (100 proof) ethanol; for cleaning the pH probe
2. To the 150 mL DI water in the ice bath, add 10 g 6-amino hexanoic acid and a stir bar
3. Stir at 0°C in the ice bath until dissolved
4. Add 10 g $Ca(OH)_2$ to the solution on the stir plate. Note--it will not fully dissolve
5. Add acryloyl chloride in 1 mL aliquots every 2 minutes, continuing to stir at 0°C

6. 2 minutes after the final addition of acryloyl chloride, filter with 9 cm filter (with glass filter paper) on vacuum flask

    *All filter steps take place with filter paper and upon a vacuum flask
7. Put liquid filtrate in a 250 mL beaker with a stir bar and place in the ice bath
8. Use 100 uL aliquots of 12 N HCl to pH to 2.6, continuing to stir with a stir bar. Note--pH will start above 12; it should take about 8.4 mL to get down to 2.6
9. Filter with 9 cm filter
10. Keep ice cold and wait for precipitate to form; should be thick and white
11. Remove precipitate using a spatula and put in the crystallization dish on ice
12. Clean the pH probe with pH 2 ethanol
13. Take samples for TLC in small vials: 1. 40 uL of filtrate. 2. a small sample of precipitate

Drying of 6-acrylamidohexanoic acid

OVEN DRY ALL GLASSWARE PRIOR TO USE

1. Assemble the following in the fume hood:

    2 ice baths
    2x 250 mL beakers
    4x 250 mL Erlenmeyer flasks
    1x 500 mL Erlenmeyer flask
    4.7 cm filter
    Stir plate with stir bar and thermometer
    100 mL 1:1 mix of chloroform and dry ethanol in wide-mouth 500 mL Erlenmeyer
    130 g Na_2SO_4
    6 g activated carbon (charcoal)
    Diatomaceous earth
2. Place Erlenmeyer flask with 1:1 chloroform and ethanol in ice bath for 10 minutes
3. Add precipitate (thin white paste) and stir at 0°C until dissolved
4. Add 130 g Na_2SO_4 and 6 g activated carbon. Mix by swirling to dehydrate
5. Make a 250 mL suspension of diatomaceous earth in dry ethanol. No need to measure, just combine to make a slurry. Pour over the 4.7 cm filter to form a 1 inch plug. Rinse the plug with ethanol and change the receiver flask
6. Vacuum filter the suspension and repeat---create a fresh plug
7. Place the clear solution in a dry 250 mL beaker
8. Heat the bath to 40-50°C and evaporate the solution to 10-30 mL while stirring. Note--place a vacuum hose with filter *above* the solution surface to significantly reduce evaporation time (lower vapor pressure)

    *Pull vacuum *above* evaporating mixture for all Evaporation steps
9. Place the syrup in the ice bath
10. Clean up except the ice baths

Synthesis of N6

1. Assemble the following in a chemical fume hood:

   Ice bath on stir plate
   200 mL ice-cold ethanol in a dry 250 mL flask
   8.7 g NHS
   17 g EDAC
2. Add 200 mL ice-cold ethanol to product syrup and place flask in ice bath
3. Add 8.7 g NHS and 17 g EDAC
4. Stir 3-4 hours at 0°C
5. Take TLC sample: Label 3
6. Evaporate and reduce syrup by half at 45°C while stirring
7. Clean up

Extraction of N6

1. Assemble the following in a chemical fume hood:

   500 mL separatory funnel
   Ice bath
   Stir plate
   4x 250 mL flasks
   2x 500 mL flasks
   4.7 cm filter with filter paper
   200 mL methylene chloride
   0.2 mL glacial acetic acid
   Sodium bicarbonate
   65 g anhydrous sodium sulfate
2. Pre-chill the methylene chloride in an ice bath
3. Add 200 mL methylene chloride and 0.2 mL glacial acetic acid to product syrup
4. Stir on ice 10 minutes
5. Prepare a 500 mL flask of saturated sodium bicarbonate solution in water at 0°C. No need to mix, just add enough sodium bicarbonate so that an over-saturated suspension is made
6. Mix 200 mL of suspension from step 5 with product syrup in a 500 mL flask. Separate in a separatory funnel and retain lower phase
7. Repeat, always retain lower phase, filter into fresh flasks
8. Repeat twice more with cold water
9. Add 65 g anhydrous sodium sulfate to product
10. Filter using 4.7 cm filter
11. Transfer to a 250 mL flask and evaporate at ~40°C (solution will boil)
12. Clean up

Assemble the following in a chemical fume hood:

Stir plate

Dry 100 mL crystallization dish

1. Add 200 mL dry ethyl acetate to product syrup
2. Evaporate to 100 mL at 60°C
3. Pour into crystallization dish and add seed crystals of N6
4. Leave at room temperature for 10 minutes, then cover with parafilm and place in refrigerator 1-2 hours
5. Move to -20°C freezer and leave overnight
6. Recover crystals (will look like wet N6) —break up crystals with a spatula and place in a 9 cm filter atop a vacuum flask for 30 min to dry out crystals. When done the crystals should look like dry fine powder
7. Reduce the volume of the supernatant by 50% and re-do crystallization

Note--the first crystallization will reduce the 100 mL solution to about 50 mL and yield approximately 3-4 g of N6

Run Mass Spectrometry on final sample. N6 is the peak at 283:

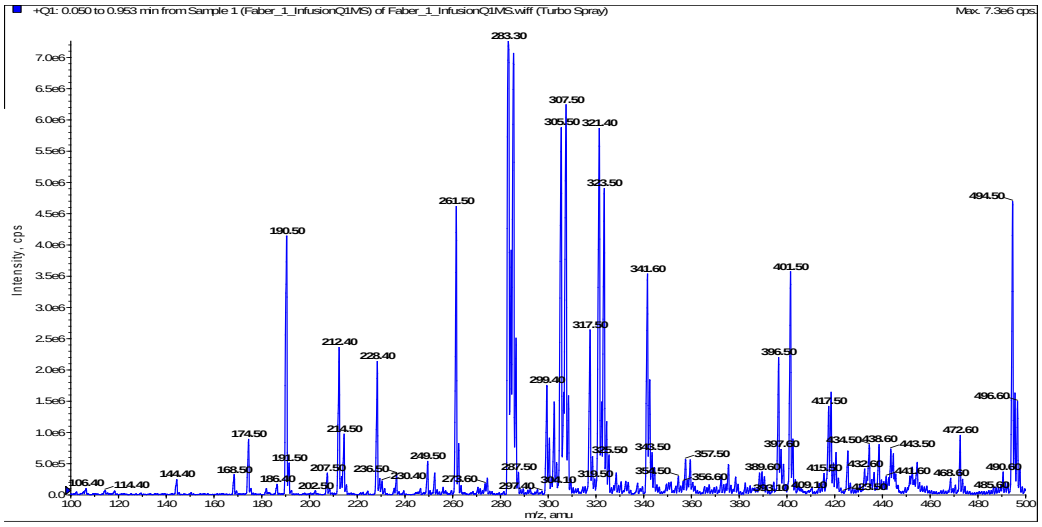

APPENDIX E

Protocol for Mechanical Testing of Polyacrylamide Gels

Assemble to following materials:

- Thick polyacrylamide gels (polymerize 80-100 μL of gel mix) cast on 45x50 mm coverslips
- Traction chambers
- Steel (440C) ball bearings (0.64 mm diameter), Abbott Ball Company
- Magnetic stir bars
- Forceps
- Media

Steps:

1. Cast thick gels embedded with fluorescent beads (10-20 μL) onto large coverslips and assemble gels in traction chambers. Gels may be cast with a thin layer of beads at the surface if desired (Appendix C).
2. Equilibrate gels in media in an incubator.
3. Load gel into stage insert for traction chambers on scope—run stage incubator.
4. Attach a single steel ball to forceps (magnetic) and hold over chamber.
5. Use fingers to carefully remove ball from forceps and drop onto the gel.
6. Use a magnet beneath the sample to move the ball around to a desired position on top of the gel.
7. Find the ball in a field of view (20X objective works well) and focus on the depressed bead field beneath the ball.
8. Record the z-location of this focal plane with the "mark and find" menu in Axiovision (Z1).
9. Use the magnetic stir bar to remove the steel ball from its initial position.
10. Refocus the scope on the bead field at the top surface of the gel.
11. Record the z-location (Z2).

12. The absolute value of the difference between Z1 and Z2 is the indentation depth, δ, used in the following equation to determine the Young's Modulus at the surface of the gel, based on Hertz theory [86]:

$$E = (3(1-\nu^2) f) / (4\delta^{3/2} r^{1/2})$$

Where
E = Young's Modulus
v = Poisson's ratio
f = W – F_b (ball weight - buoyant force of the ball)
[see diagram and calculation below]
r = ball radius
δ = indentation depth [see diagram below]

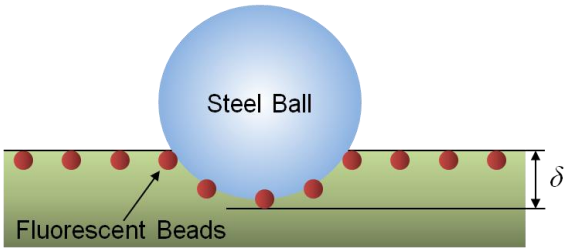

Notes:
-We assume v = Poisson's ratio = 0.3 [183]
-Density = ρ = 7200 kg/m^3
-To calculate f:

$$f = W\text{-}F_b$$

where
W = weight of ball = [(mass of ball * g)]: W_{ball}=mg
F_b = buoyant force of ball =
[density of ball * *volume of ball submerged into gel* * g]: $F_b = \rho Vg$

Since mass (m) =ρV, we can write:

$W_{ball}=\rho_{ball}*V_{ball}*g$

$F_b = \rho_{ball}*V_{submerge}*g$

where $V_{submerge} = (1/3)\pi\delta^2(3r-\delta)$

This is the formula of a sphere cap with sphere radius r *and height* δ *(which is the indentation depth in this analysis)*

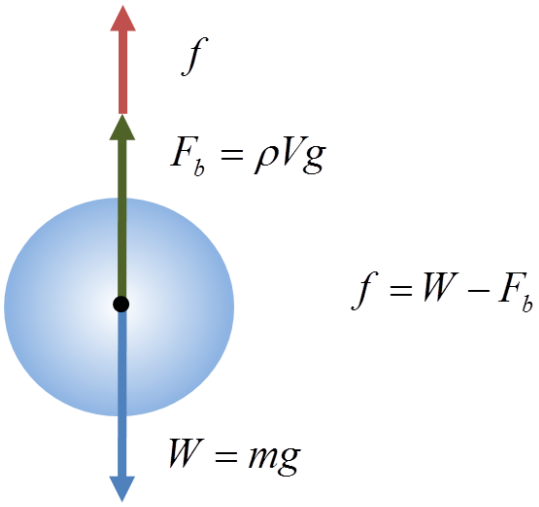

APPENDIX F

Protocol for Immunofluorescence Staining of Cells on Polyacrylamide Gels

Volumes are for gels in wells of a six-well dish

1. Aspirate media and rinse the samples 3x with PBS. Dispense against the well wall, not onto the gel.
2. To fix samples, add 2 mL of 3.7% (v/v) formaldehyde in PBS for 15 min at RT.
3. Wash 3x with PBS for 5 min each.

Notes: -During **wash**ing periods, place samples on a rocker
-Samples can be stored in PBS at 4°C at this point for a couple of days if necessary

4. To permeabilize cells, add 2 mL 1% (v/v) Triton (octyl phenol ethoxylate) in PBS for 5 min at RT
5. Wash 3x with 0.02% (v/v) Tween 20 (polyoxyethylene 20 sorbitan monolaurate) in PBS for 5 min each
6. To block samples, wash 1x with 3% (w/v) BSA in 0.02% (v/v) Tween 20 in PBS for 1 hour

7. Prepare 1' antibody in 1% (w/v) BSA in PBS. Dilute antibodies according to the manufacturer's recommendation on the product data sheet. 1:50 is often a good dilution (1 μL of antibody in 50 μL BSA/PBS)

8. Add drops (100 μL/gel) of 1' antibody mix in 1% (w/v) BSA in PBS onto parafilm. Place gel upside down on the drop, trying to avoid bubbles
9. If also staining for actin, incubate samples in a humidified chamber overnight at 4°C (phalloidin will attenuate the immunofluorescent signal). If not staining for actin, incubate for 1 hour at RT. To create a humidified chamber, place samples in a large Petri dish that contains wet kimwipes.
10. Wash 3x with 1% (w/v) BSA in 0.02% (v/v) Tween in PBS for 5 min each
11. Prepare 2' antibodies in 1% (w/v) BSA in PBS (dilute according to the manufacturer's specification—usually 1:200-1:1000. Spin 2' antibody at 14k x*g* for 2 min at 4ºC before use
12. Add drops (100 μL/gel) of 2' antibody mix in 1% (w/v) BSA in PBS onto parafilm. Place gel upside down on the drop, trying to avoid bubbles
13. Incubate in a humidified chamber for 1 hour at RT

Note: If using more that 2 antibodies, repeat antibody and wash steps as often as needed

14. Wash 3x with 0.02% (v/v) Tween 20 in PBS for 5 min each
15. Wash 3x with PBS for 5 minutes each
16. To mount, place a drop of Vectashield mounting media on a coverslip (larger than the one the gel was cast on). Use a kimwipe to dry the glass on back of the gel sample, and invert the gel onto the drop

17. Image through the larger coverslip to obtain the best image, *i.e.* the coverslip without the bound gel should be the one closest to the objective lens

Additional Notes and Tips:

Staining for F-actin

- To colocalize F-actin, incubate inverted samples on a drop (100 μL/gel) of phalloidin (1:40 in PBS) on parafilm for 1-2 hours after Step 15. Wash 3x with PBS and mount.
- To stain for F-actin alone, incubate samples on a drop of phalloidin after blocking (Step 6) for 1-2 hours and proceed to Step 14.

Staining for nuclei

- Incubate inverted samples on a drop (100 μL/gel) of DAPI (0.1 mg/mL in MilliQ water) on parafilm for 10 min. Wash 3x with PBS and mount.

Staining for paxillin/vinculin

- Fix samples in 3.7% (v/v) formaldehyde in PBS for 5 min (Step 2). Block samples with 40% (v/v) heat-denatured FBS in PBS (Step 6).

Staining for mitochondria

- Incubate live cells with 200 nM MitoTracker in 2 mL media for 30 min in incubator. Image immediately. If staining fixed samples, proceed to Step 1.

Staining for trans-Golgi

- Complete Steps 1-3. Before permeabilization (Step 4), add 5 μg/mL wheat germ agglutinin in 2 mL PBS for 10 min. Proceed to Step 4.

If background signal is significant, try

- Fixing with 70% (v/v) ethanol in water, or 100% methanol for 5-30 min
- Blocking with 5-10% (w/v) BSA in PBS, or 10% (v/v) goat serum in PBS, or 10-40% (v/v) heat-denatured FBS in PBS for 1-2 hours
- Washing with 0.05-0.10% (v/v) Tween 20 in PBS during washing steps
- Increasing duration of washing steps

APPENDIX G

Protocol for BrdU Incorporation for Cells on Polyacrylamide Gels
Developed with Kelly McBride

Plate and BrdU Incorporation

1. Grow cells to 90% confluence in T25 culture flask
2. Add serum free media and incubate overnight
3. Passage cells onto the gels in a six-well dish
    a. 50k cells/well for 0.2 kPa gels
    b. 30k cells/well for other stiffnesses
4. 4 hours later, add BrdU 1:100 in 2 mL of fresh media per well
5. Incubate at 37ºC for 2 hours-overnight

Fix and Stain

1. Aspirate media and wash 3x with PBS
2. Fix with 3.7% (v/v) formaldehyde in PBS for 5 min at RT
3. Wash 3x with PBS for 5 min each
    a. Samples can be stored at 4ºC for a few days if necessary
4. To permeabilize, add 1% (v/v) Triton (octyl phenol ethoxylate) in PBS for 5 min at RT
5. To denature DNA (and allow BrdU to bind), add 2N HCl for 1 hour at 37ºC
    a. Remove acid to waste container
6. Wash 3x with PBS for 5 minutes each
7. Wash 3x with 0.02% (v/v) Tween 20 (polyoxyethylene 20 sorbitan monolaurate) in PBS for 5 min each
8. To block, wash 1x with 0.1% (v/v) in 0.02% (v/v) Tween 20 in PBS for 1 hour
9. Incubate with 1’ antibody (anti-BrdU) 1:100 in 1% (w/v) BSA in PBS for 1 hour at room temperature
    a. Invert samples onto 100 µL drop per gel on parafilm
10. Wash 3x with 0.1% (v/v) in 0.02% (v/v) Tween 20 in PBS for 5 minutes each
11. Incubate with 2’ antibody (anti-BrdU) 1:200 in 0.1% (v/v) FBS in PBS for 1 hour at RT
    a. Spin 2’ antibody at 14k x*g* for 2 min at 4ºC before use
    b. Invert samples onto 100 µL drop per gel on parafilm
12. Wash 3x with 0.02% (v/v) Tween 20 in PBS for 5 minutes
13. Image immediately
    a. Dry the back of the gel glass, and invert the sample onto a drop of Vectashield on a large coverslip

APPENDIX H

Protocol for Harvesting Cells from Polyacrylamide Gels for SDS-PAGE/Western Blot or qPCR Analysis

For SDS-PAGE/Western Blot

Materials

- Cells grown on 45x50 mm gels (2x per condition)
- 1X TBS
- Ice bucket
- 100 mm Petri dishes
- Lysis buffer
- Cotton-tipped applicators
- Razor blade
- Cell scrapers

Procedure

1. Prepare a lysis chamber, one per gel
    a. Add a 100 μL drop of lysis buffer to a 100 mm diameter Petri dish on ice
2. Remove samples from incubator and rinse cells 4-5x with ice-cold TBS
3. Carefully remove cells from any exposed glass with a cotton-tipped applicator, and remove the sample with a razor blade
4. Carefully dry the back of the sample to remove excess TBS
5. Invert the sample onto the drop of lysis buffer and incubate 5-10 min
6. Carefully agitate the sample with a cell scraper. Lift the sample from the dish and carefully scrape the contents of the gel surface into the dish
7. Collect the sample with the cell scraper, and collect in sterile 1.7 mL centrifuge tubes. Combine lysate from 2x gels per condition.
8. Spin 5 min at 14k x*g* at 4 °C
9. Save supernatant in a new tube
10. Proceed with conventional SDS-PAGE/Western blot, or snap freeze in liquid nitrogen and store at -80 °C

For qPCR

Materials

- Cells grown on 45x50 mm gels (1x per sample is usually sufficient)
- 500 mL 0.25% TE/gel
- 1X PBS
- Media
- 100 mm Petri dishes
- 15 mL tubes
- Cotton-tipped applicators
- Razor blade
- Cell scrapers

Procedure

1. Prepare a lysis chamber, one per gel
    a. Add a 100 μL drop of TE to a 100 mm diameter Petri dish on ice
2. Remove samples from incubator, and rinse carefully 4-5x with PBS
3. Carefully remove cells from any exposed glass with a cotton-tipped applicator, and remove the sample with a razor blade
4. Invert the sample onto the drop of TE and return to the incubator for 10 min
    a. Check cells under scope until balled up/detached from substrate
5. Flip sample back over with razor blade and rinse the gel gently with 1 mL complete media
    a. Gently squirt media over the surface of the cell to detach any balled up cells
6. Use cell scraper to pool media and collect in 15 mL centrifuge tube
7. Repeat steps 1-6 for all samples
8. Pellet cells (spin 5 min @ 400 x*g*; pellet may not be visible!)
    a. Wash very gently with PBS to remove all traces of media/trypsin
    b. Carefully pipette out excess PBS
9. Proceed with conventional RNA harvest and purification immediately
    a. Less ideal but still works: cell pellets (remove all PBS) may be snap frozen in liquid nitrogen and stored at -80 °C

APPENDIX I

Protocol for Transfection of Endothelial Cells

This procedure can be used for plasmid DNA and siRNA transfection of endothelial cells (bovine aortic or human umbilical vein)

Timeline

Day -1: Plate cells in a vessel
Day 0: Transfect cells
Day 1: Transfer cells to gels
Day 2: Begin imaging

Materials

- Cells
    - For plasmids: cells in a 6-well dish 90% confluent
    - For siRNA: cells in a 6-well dish 60-80% confluent
- Lipofectamine 2000
- Optimem
- plasmid DNA
- Sterile 1.7 mL centrifuge tubes

Procedure

1. The day before transfection, seed
    - For plasmids: 300k cells/well in a 6-well dish
    - For siRNA: 200k cells/well in a 6-well dish

The day of transfection (Day 0)

1. Add 500 μL Optimem to a 1.7 mL centrifuge tube (6x, one for each well)
2. Add
    - For plasmids: 2 μg DNA—mix and sit 5 min RT
    - For siRNA: 2 μL stock siRNA solution—mix and sit 5 min RT
3. Add
    - For plasmids: 5 μL Lipofectamine—mix and sit 20 min RT
    - For siRNA: 6 μL Lipofectamine and sit 20 min RT
4. Was cells gently 2x with Optimem
5. Add 1.5 mL Optimem to well
6. Add the ~500 μL DNA/siRNA/Lipofectamine/Optimem mix to each well (2 mL final volume per well)
    -swirl/rock to mix, avoid bubbles
7. Put in incubator 4-6 h. Check cells every few hours for significant debris or vacuole formation

8. Remove mix, wash 2x with sterile PBS
9. Replenish fresh media
10. Plate the next day (Day 1)
11. Assay the next day (Day 2)

APPENDIX J

GK12 Module Teaching Materials

J.1a "Introduction to Polymers" Notes Handout

Polymer Notes

Polymers are all around us! Materials like plastic and wood are made up of polymers.

Kinds of Polymers

Many polymers are found in nature (natural), and others are made by people (synthetic). Fill in the blanks with 3 items that contain natural or synthetic polymers:

Natural:
1) **DNA**
2) **Wood**
3) **Rubber**

Synthetic:
1) **Plastic**
2) **Toys**
3) **Contact lenses**

What is a Polymer?

A polymer is a large **molecule** made up of repeating parts.

An Example: Polyester

Let's take a closer look at what a polymer is. Maybe you have heard of a polymer called polyester. Polyester is a fabric used to make clothing like raincoats, pants, and shirts. This fabric is made of long chains of a compound called an ester. These ester compounds are made of **elements** on the **periodic table**, mostly carbon, oxygen, and hydrogen.

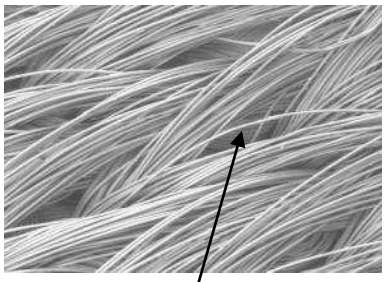

Polyester fibers are used to make fabrics for clothing

If we look closely at the polyester fibers, we would see chains of ester compounds tied together:

…—ester—ester—ester—ester—ester—ester—ester—…

These repeating units are held together by **covalent** bonds.
A covalent bond is formed when atoms in a compound **share** electrons.

Each chain is made of *thousands* of esters tied together like beads on a string:

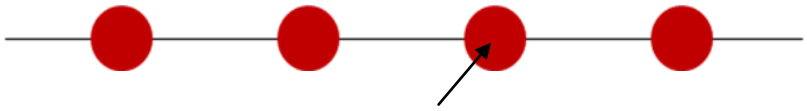

Naming Polymers

Polymer names come from the repeating unit found in the polymer.
For example, raincoats are made from the polymer called polyester. This polymer is made from thousands of *repeating* ester compounds.

As you can see, the name of the polymer is taken by combining "poly" with the name of the repeating unit, "ester", to form "polyester".

Exercise: Fill in the blanks by completing the polymer name *or* repeat unit.
I've done the first one for you:

Repeating unit	**Polymer name**
ester	Polyester
ether	Poly**ether**
ethylene	Poly**ethylene**
styrene	Polystyrene (Styrofoam)
amine	Polyamine

Polymer crosslinkers

A *crosslinker* is a compound that is used to chemically bond polymer chains together. This gives the polymer stability and helps to determine the physical properties of the polymer.

The diagram below is a close-up of some polymer chains in a polymer fiber.
Draw *crosslinkers* between the polymer chains:

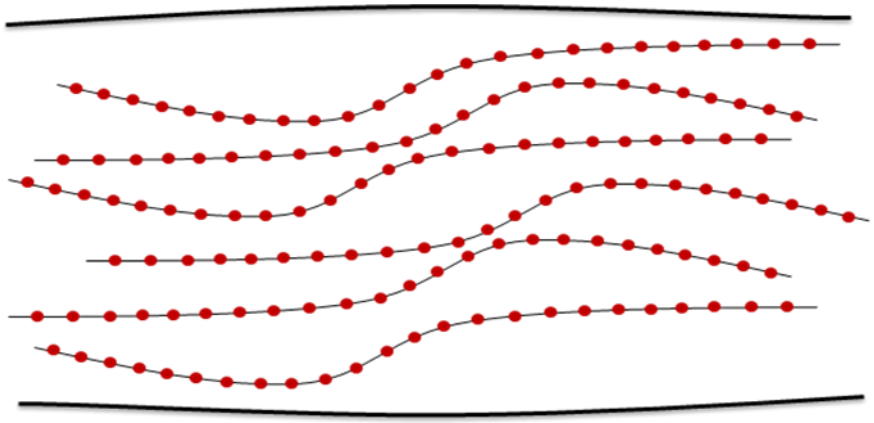

Circle one:
The (**chemical** | physical) make-up of polymers and their crosslinkers determine the (chemical | **physical**) properties of polymers.

List 2 physical properties of polymers:
1) **Density**
2) **Stiffness**

J.1b "Introduction to Polymers" Quiz

1) What is a polymer?
   A. A collection of negatively charged ions
   B. A small compound made of hydrogen and oxygen
   C. A large molecule made of repeating units
   D. An element in the periodic table

2) Which is an example of a synthetic polymer?
   A. Metal
   B. Plastic
   C. Protein
   D. Glass

3) Which is an example of a natural polymer?
   A. Plastic
   B. Sand
   C. Rock
   D. Wood

4) Which of the following may be made of polymers?
   A. Food and beverage containers
   B. Sports Equipment
   C. Medical devices
   D. All of the above

5) What is the repeating unit in the polymer called *polyurethane*
   A. propylene
   B. saccharide
   C. amine
   D. urethane

6) What is the name of the polymer shown below:
   —ethylene—ethylene—ethylene—ethylene—ethylene—
   A. Polyether
   B. Polyester
   C. Polyethylene
   D. Polyethyleneimine

7) What kind of chemical bond holds polymer repeat units together?
   A. Ionic
   B. Covalent
   C. Metallic
   D. Hydrogen

8) What is a crosslinker?
   A. A compound that bonds polymer chains together
   B. An element in the Lanthanide series
   C. An atom that spins in a magnetic field
   D. The repeating mer unit in a polymer

9) What properties of polymers are altered by crosslinkers?
   A. Density
   B. Stiffness
   C. Transparency
   D. All of the above

10) Rank the following types of matter from ***smallest*** to ***largest***
   A. element, atom, compound, polymer
   B. atom, element, compound, polymer
   C. atom, element, polymer, compound
   D. compound, atom, element, polymer

Mechanical Testing Notes

Forces

-A force is a **push** or a **pull**

-The SI unit of force is the **Newton**. It has units of N = **kgm/s^2**

-Draw 2 forces acting on the block below:

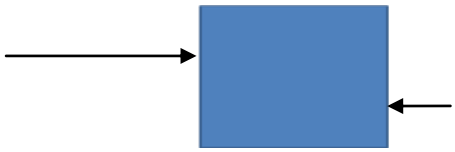

Newton 2

-Newton's 2nd Law states that force equals mass times acceleration, or, **F=ma**

-The SI unit of force is **Newton**

-The SI unit of mass is **kilogram (kg)**

-The SI unit of acceleration is **m/s^2**

On Earth, the value of acceleration due to gravity is **9.81** m/s^2

A natural form of Newton 2 is the formula for weight: Weight = (mass)(acc. due to gravity), or, **W=mg**

Example -Use Newton 2 to calculate your mass

F=ma 1 lb = 4.45 N
W=mg

1) Convert your weight in lb to N

$$150\ \mathbf{lb}\left(\frac{4.45\ \mathbf{N}}{1\ \mathbf{lb}}\right) = 668\ \mathbf{N}$$

2) Solve W=mg for m

m=W/g

$$m = 668\ \mathbf{N} / 9.81\ \mathbf{m/s^2}$$

3) Plug in the values and solve

$$m = 68\ \mathbf{kg}$$

My mass is 68 kg. This value is the same regardless of what planet you're on!

Example -Use Newton 2 to calculate your weight on Mars

F=ma $a_{Mars}=g_{Mars}=3.71\ m/s^2$ 1lb = 4.45 N

W=mg m=_____kg (from above)

1) Solve W=mg for W

$$W = (68\ \mathbf{kg})(3.71\ \mathbf{m/s^2})$$
$$W = 252\ \mathbf{N}$$

My weight is 252 N. This value would change if you traveled to the moon!

2) Convert your weight in N to lb

$$252\mathbf{N}\left(\frac{1\ \mathbf{lb}}{4.45\ \mathbf{N}}\right) = 57\ \mathbf{lb}$$

Stress

-Stress is a measure of force divided by the cross-sectional area that the force acts on.
-Stress = Force/Area
-The Greek letter sigma (σ) is used to represent stress

-The SI unit of force is **Newton**

-The SI unit of Area is **m^2**

-The SI unit of stress is **N/m^2** = Pascals (Pa)

Example -Find the stress acting in the cylinder

stress = Force / Area
$\sigma = F/A$

F=**3.14 N**

$A=\pi(1m)^2 =$ **$3.14m^2$**

$\sigma = F/A=3.14N/3.14m^2 =$ **1Pa**

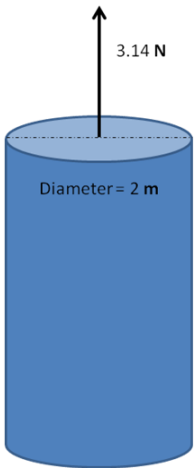

Strain

-Strain is a measure how much a material elongates under an applied force.
-Strain = $(L_f-L_i)/L_i$
-The Greek letter epsilon (ε) is used to represent strain

-The SI unit of length is meter **(m)**

-The SI unit of strain is **unitless** or **(length/length)**

Example -Find the strain in the block

strain = $(L_f-L_i)/L_i$
$\varepsilon = (L_f-L_i)/L_i$

$L_i =$ **1mm**

$L_f =$ **5mm**

ε = (5mm-1mm)/1mm
=**4 mm/mm**

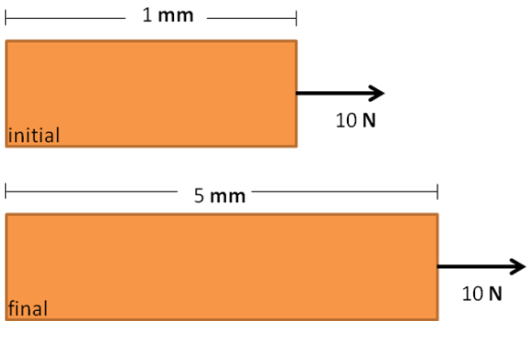

Stress vs. Strain Curves and Young's Modulus

-For nearly all materials, we can measure stress and strain in the same sample and plot the results.

-If we calculate the slope of the line of the plot of stress vs. strain, we can find an important material parameter called **Young's Modulus**

-Young's Modulus is a measure of material **stiffness**

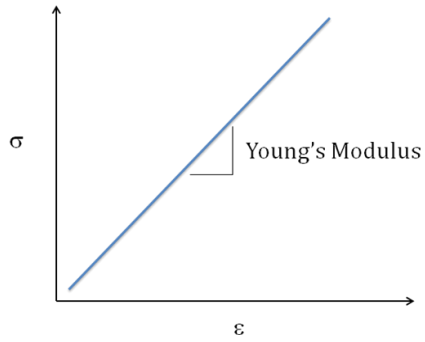

Example -Identify the stiffest material.

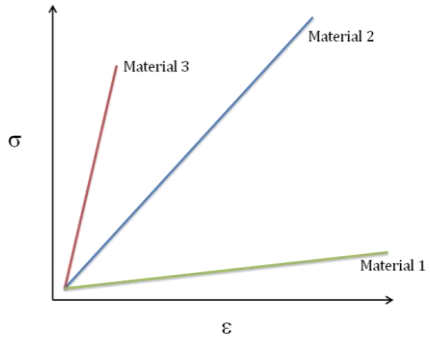

How do you know this material is the stiffest?

Material 3--it has the greatest slope

J.2b "Mechanical Testing of Polymers " Activity

Introduction

You are an engineer working at HappyTooth Inc., the newest biomedical company that specializes in making replacement teeth. Your job is to determine if new materials are mechanically suitable for use as replacement teeth. One day, your supervisor tells you that HappyTooth Inc. recently purchased the RubberTree Corporation, a small company that specializes in rubber production. Since you now have access to large amounts of free rubber, your supervisor asks you if rubber is a suitable material for making replacement teeth.

In this lab, you will investigate the mechanical properties of rubber, a common natural polymer. The goal of this lab is to determine the Young's Modulus of rubber, and to determine whether rubber is a mechanically suitable material for making replacement teeth.

Background

Rubber is a natural polymer made by *Hevea brasiliensis***,** or rubber tree. These trees contain special sap called *latex* that is used to make rubber.

Hevea brasiliensis plant

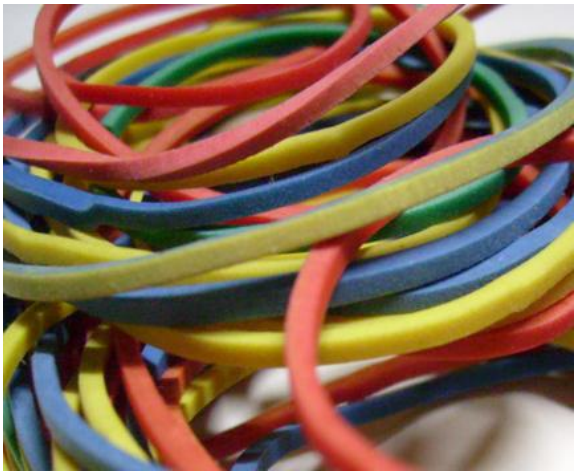

rubber bands

The special latex sap is a natural polymer of **isoprene**. In a process known as vulcanization, **isoprene monomers** are heated with **sulfer (the crosslinker)** to form rubber.

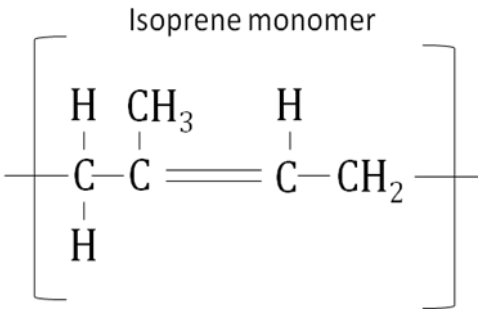

Rubber Polymer Chemistry
Note the **sulfur atoms** that crosslink the monomers:

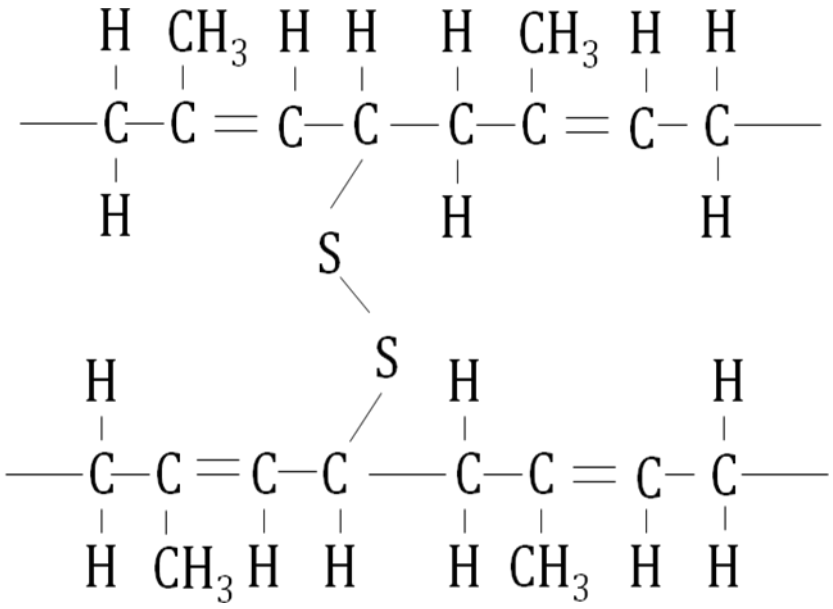

Materials
Rubber bands
Weights
Metric ruler
Marker
Calculator
Ring stand

Procedure and Questions

1) Choose three weights from the set and place them in ascending order. Start with the smallest mass.

2) Record the mass used **in kilograms** in the column labeled "m (*kg*)" in the Experimental Data Table.

3) For the mass chosen, calculate the amount of force the mass exerts due to gravity. Record the force **in Newtons** in the column labeled "F (*N*)"

   a. Write the equation you will use: **F=ma**

   b. This famous equation is also known as Newton's **Second** Law of Motion

4) Measure the dimensions of the cross-sectional area of the rubber band you're using. Record the area **in square meters** the column labeled "A (m^2)"

5) Calculate the stress that the mass chosen in (2) will exert on the cross sectional area determined in (4). Record the stress **in Pascals** in the column labeled "σ (*Pa*)"

   a. Write the equation you will use: **σ=F/A**

6) Make 2 marks on the rubber band with a marker. Measure the distance between the marks and record this *initial length* **in meters** in the column labeled "L_i (*m*)"

7) Hang the mass from the rubber band. While suspended, carefully measure the distance between the 2 marks. Record this *final length* **in meters** in the column labeled "L_f (*m*)"

8) Calculate the amount of strain produced in the rubber band by the mass. Record the strain in the column labeled "ε"

   a. Write the equation you will use:

   b. What are the units of strain? Why? **unitless or length/length**
   Strain may be reported as a percent for comparison among materials

9) Copy the values for stress and strain into the smaller table on p. 4

10) Use the values from (9) to make a plot of stress vs. strain

11) Calculate the Young's Modulus of the rubber band

   a. Write the equation you will use:

   b. What is the Young's Modulus of the rubber band?

12) The Young's Modulus of a typical human tooth is approximately 100 GPa. Is rubber a suitable material for making replacement teeth?

Experiment Data Table

#	m (*kg*)	F (*N*)	A (m^2)	σ (*Pa*)	L_i (*m*)	L_f (*m*)	ε
1							
2							
3							

Copy the values of **σ** and **ε** to the table below:

ε	σ (*Pa*)
ε_1=_____	σ_1=_____
ε_2=_____	σ_2=_____
ε_3=_____	σ_3=_____

Scratch work:

Plot of stress (σ) vs. strain (ε)

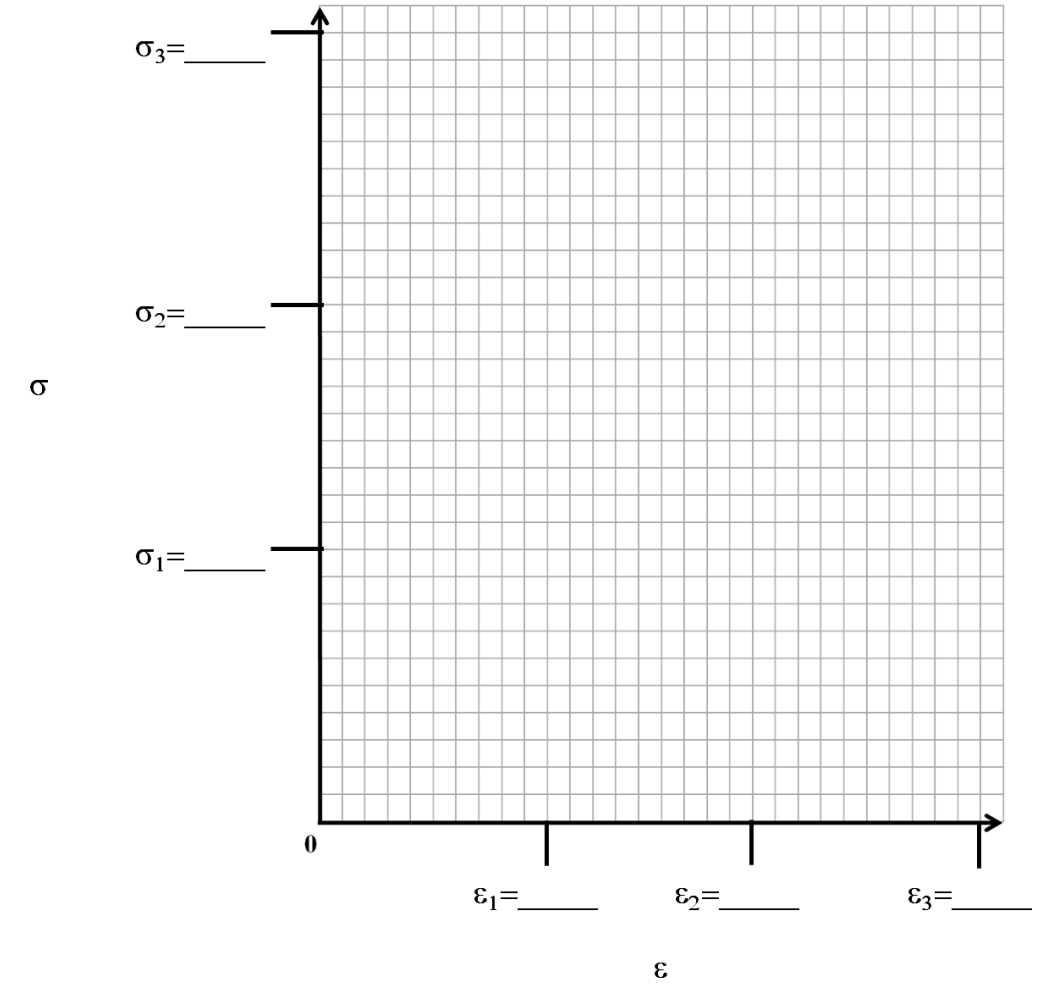

Reference Table

Variables	**Units**	**Pronunciation of Units**
m = mass	*kg*	kilogram
F = Force	$N = kg\frac{m}{s^2}$	Newton = kilogram meter per second squared
a = acceleration due to gravity	$\frac{m}{s^2}$	=_____ meters per second squared
A = Area	m^2	square meter
L_i = initial length	*m*	meter
L_f = final length	*m*	meter
σ = stress [Greek sigma]	$Pa = \frac{N}{m^2}$	Pascal = Newton per meter squared
ε = strain [Greek epsilon]	unitless	
Δ = change [Greek Delta]	unitless	
E = Young's Modulus	$Pa = \frac{N}{m^2}$	Pascal = Newton per meter squared

Note: Do not confuse mass (m, a **variable** representing the amount of matter in an object) with meter (*m*, a **unit** of length)

Formulas	**Pronunciation of Formulas**
F = ma	Force equals mass times acceleration -or informally: Force *is* mass times acceleration
$\sigma = \frac{F}{A}$	Stress equals Force divided by Area -or informally: Stress *is* Force *over* Area
$\varepsilon = \frac{L_f - L_i}{L_i}$	Strain equals final length minus initial length divided by initial length
$E = \frac{\Delta\sigma}{\Delta\varepsilon}$	Young's Modulus equals change in stress divided by change in strain -or informally: Delta stress *over* Delta strain

J.2c "Mechanical Testing of Polymers " Quiz

1) What is the value of acceleration due to gravity?
   a) 101.3 Nm^2
   b) 9.81 m/s^2
   c) 8.34 N/m^2
   d) 32.1 m/s

2) Weight is defined as a measure of:
   a) Force times acceleration due to gravity
   b) Mass times acceleration due to gravity
   c) Stress per unit area
   d) Stress per unit length

3) Stress is defined as a measure of:
   a) Force times area
   b) Force divided by area
   c) Elongation divided by time
   d) Elongation times force

4) Strain is defined as a measure of:
   a) Force times area squared
   b) Force divided by area squared
   c) Elongation per unit length
   d) Elongation divided by force

5) Which of the following physical parameters would change if you were on the surface of the moon?
   a) Weight
   b) Acceleration due to gravity
   c) Mass
   d) Density
   e) a & b
   f) All of the Above

6) "Young's Modulus" is a measure of which material property?
   a) Temperature
   b) Density
   c) Stiffness
   d) Porosity

7) Shown below is a plot of stress vs. strain. Which material has the greatest Young's Modulus?

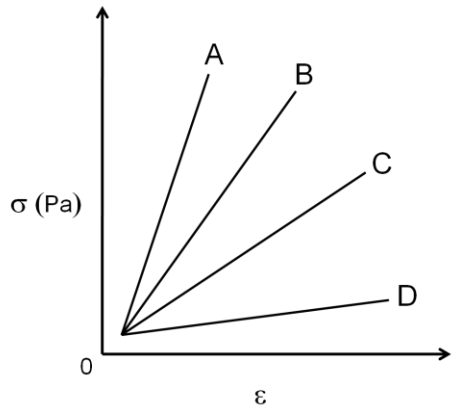

a) A
b) B
c) C
d) D

8) Given the plot of stress vs. strain, what is the Young's Modulus of the material?

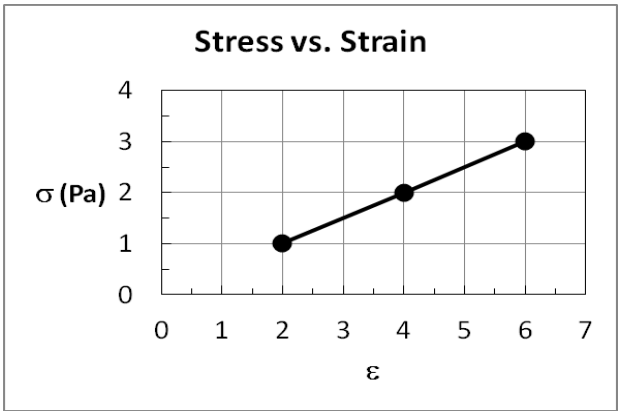

a) 3 Pa
b) 0.5 Pa
c) 6 Pa
d) 2 Pa

9) What monomer is contained in natural rubber?
   a) Styrene
   b) Butadiene
   c) Neoprene
   d) Isoprene

10) Which element is commonly used as a crosslinker in natural rubber production?
   a) Sulfur
   b) Phosphorous
   c) Boron
   d) Nitrogen

Cell Biology Notes

Body System Hierarchy

-The major systems in the body are organized in a hierarchy of structure and function. From the largest to smallest, they are **system > organ > tissue > cell**

-The functional part of organs are **cells** AND **matrix**

-The **matrix** are proteins (biological polymers) that give cells mechanical integrity

Cells

-There are many types of cells in the body.
-Cells are capable of a variety of behaviors including:

1. **AdhesionSpreading**
2. **Migration**
3. **Communication**

The Study of Biology

Biological research is usually performed in one of two ways:

1) **in vitro** (in glass)

2) **in vivo** (in the living)

We study biology to understand cell function. This knowledge helps us to **understand and treat disease**.

Case Study: Matrix stiffness and cell responses

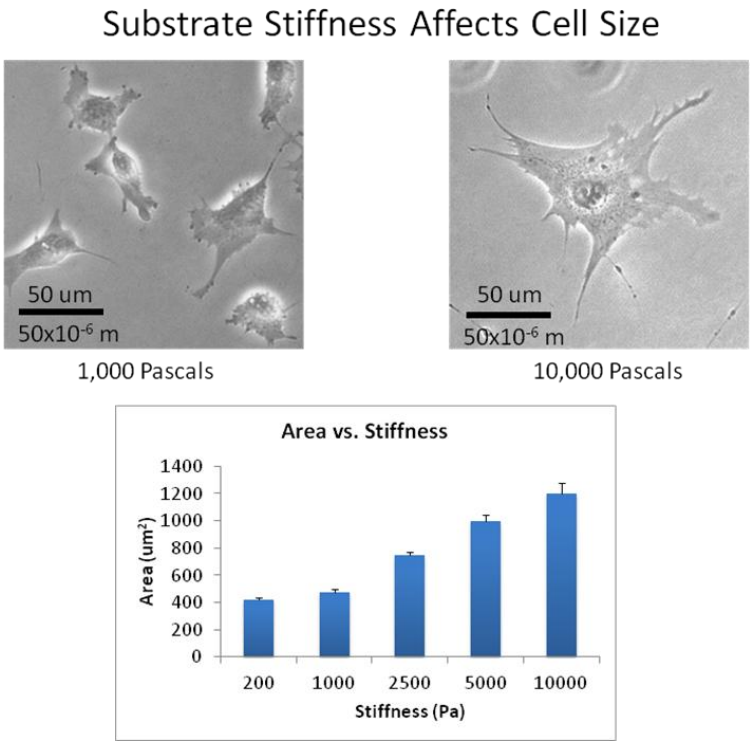

-Cell spreading (cell size) is altered by the stiffness of the matrix the cells are grown on.
-Cells were grown on matrices of increasing stiffness (200 - 10,000 Pa). The bar plot of cell area vs. stiffness indicates that area increases with increasing matrix stiffness.

What other cell behaviors are sensitive to matrix stiffness?

REFERENCES

1. Foty, R.A. and M.S. Steinberg, The differential adhesion hypothesis: a direct evaluation. *Dev Biol*. 278(1):255-63, 2005.
2. Krieg, M., Y. Arboleda-Estudillo, P.H. Puech, J. Kafer, F. Graner, D.J. Muller, and C.P. Heisenberg, Tensile forces govern germ-layer organization in zebrafish. *Nat Cell Biol*. 10(4):429-36, 2008.
3. Fam, N.P., S. Verma, M. Kutryk, and D.J. Stewart, Clinician guide to angiogenesis. *Circulation*. 108(21):2613-8, 2003.
4. Ide, A.G., N.H. Baker, and S.L. Warren, Vascularization of the Brown-Pearce rabbit epithelioma transplant as seen in the transparent ear chamber. *Am J Roentgenol*. 42:891-899, 1939.
5. Goldmann, E., The Growth of Malignant Disease in Man and the Lower Animals, with special reference to the Vascular System. *Proc R Soc Med*. 1(Surg Sect):1-13, 1908.
6. Algire, G.H. and H.W. Chalkley, Vascular reactions of normal and malignant tissues in vivo. I. Vascular reactions of mice to wounds and to normal and neoplastic implants. *J Nat Cancer Inst*. 6:73, 1945.
7. Greene, H.S., Heterologous Transplantation of Mammalian Tumors : I. The Transfer of Rabbit Tumors to Alien Species. *J Exp Med*. 73(4):461-74, 1941.
8. Folkman, J., P. Cole, and S. Zimmerman, Tumor behavior in isolated perfused organs: in vitro growth and metastases of biopsy material in rabbit thyroid and canine intestinal segment. *Ann Surg*. 164(3):491-502, 1966.
9. Gimbrone, M.A., Jr., R.H. Aster, R.S. Cotran, J. Corkery, J.H. Jandl, and J. Folkman, Preservation of vascular integrity in organs perfused in vitro with a platelet-rich medium. *Nature*. 222(5188):33-6, 1969.
10. Folkman, J., Tumor angiogenesis: therapeutic implications. *N Engl J Med*. 285(21):1182-6, 1971.
11. Folkman, J. and C. Haudenschild, Angiogenesis in vitro. *Nature*. 288(5791):551-6, 1980.
12. Leung, D.W., G. Cachianes, W.J. Kuang, D.V. Goeddel, and N. Ferrara, Vascular endothelial growth factor is a secreted angiogenic mitogen. *Science*. 246(4935):1306-9, 1989.
13. Nicosia, R.F., What is the role of vascular endothelial growth factor-related molecules in tumor angiogenesis? *Am J Pathol*. 153(1):11-6, 1998.
14. Reddy, G.K., AGE-related cross-linking of collagen is associated with aortic wall matrix stiffness in the pathogenesis of drug-induced diabetes in rats. *Microvasc Res*. 68(2):132-42, 2004.
15. Martin, A., M.R. Komada, and D.C. Sane, Abnormal angiogenesis in diabetes mellitus. *Med Res Rev*. 23(2):117-45, 2003.
16. Paszek, M.J., N. Zahir, K.R. Johnson, J.N. Lakins, G.I. Rozenberg, A. Gefen, C.A. Reinhart-King, S.S. Margulies, M. Dembo, D. Boettiger, D.A. Hammer, and V.M. Weaver, Tensional homeostasis and the malignant phenotype. *Cancer Cell*. 8(3):241-54, 2005.
17. Jain, R.K., Normalization of tumor vasculature: an emerging concept in antiangiogenic therapy. *Science*. 307(5706):58-62, 2005.

18. Staton, C.A., S.M. Stribbling, S. Tazzyman, R. Hughes, N.J. Brown, and C.E. Lewis, Current methods for assaying angiogenesis in vitro and in vivo. *Int J Exp Pathol*. 85(5):233-48, 2004.
19. Vailhe, B., X. Ronot, P. Tracqui, Y. Usson, and L. Tranqui, In vitro angiogenesis is modulated by the mechanical properties of fibrin gels and is related to alpha(v)beta3 integrin localization. *In Vitro Cellular & Developmental Biology. Animal*. 33(10):763-73, 1997.
20. Deroanne, C.F., C.M. Lapiere, and B.V. Nusgens, In vitro tubulogenesis of endothelial cells by relaxation of the coupling extracellular matrix-cytoskeleton. *Cardiovascular Research*. 49(3):647-58, 2001.
21. Kuzuya, M., S. Satake, H. Miura, T. Hayashi, and A. Iguchi, Inhibition of endothelial cell differentiation on a glycosylated reconstituted basement membrane complex. *Experimental Cell Research*. 226(2):336-45, 1996.
22. Vernon, R.B., S.L. Lara, C.J. Drake, M.L. Iruela-Arispe, J.C. Angello, C.D. Little, T.N. Wight, and E.H. Sage, Organized type I collagen influences endothelial patterns during "spontaneous angiogenesis in vitro": planar cultures as models of vascular development. *In Vitro Cellular & Developmental Biology. Animal*. 31(2):120-31, 1995.
23. Kuzuya, M., S. Satake, S. Ai, T. Asai, S. Kanda, M.A. Ramos, H. Miura, M. Ueda, and A. Iguchi, Inhibition of angiogenesis on glycated collagen lattices. *Diabetologia*. 41(5):491-9, 1998.
24. Nehls, V. and R. Herrmann, The configuration of fibrin clots determines capillary morphogenesis and endothelial cell migration. *Microvascular Research*. 51(3):347-64, 1996.
25. Sieminski, A.L., R.P. Hebbel, and K.J. Gooch, The relative magnitudes of endothelial force generation and matrix stiffness modulate capillary morphogenesis in vitro. *Experimental Cell Research*. 297(2):574-84, 2004.
26. Georges, P.C. and P.A. Janmey, Cell type-specific response to growth on soft materials. *Journal of Applied Physiology*. 98(4):1547-53, 2005.
27. Chen, C.S., J.L. Alonso, E. Ostuni, G.M. Whitesides, and D.E. Ingber, Cell shape provides global control of focal adhesion assembly. *Biochem Biophys Res Commun*. 307(2):355-61, 2003.
28. Wang, Y.L. and R.J. Pelham, Jr., Preparation of a flexible, porous polyacrylamide substrate for mechanical studies of cultured cells. *Methods in Enzymology*. 298:489-96, 1998.
29. Engler, A., L. Bacakova, C. Newman, A. Hategan, M. Griffin, and D. Discher, Substrate compliance versus ligand density in cell on gel responses. *Biophysical Journal*. 86(1 Pt 1):617-28, 2004.
30. Reinhart-King, C.A., M. Dembo, and D.A. Hammer, Endothelial cell traction forces on RGD-derivatized polyacrylamide substrata. *Langmuir*. 19(5):1573-1579, 2003.
31. Reinhart-King, C.A., M. Dembo, and D.A. Hammer, The dynamics and mechanics of endothelial cell spreading. *Biophysical Journal*. 89(1):676-89, 2005.
32. Pless, D.D., Y.C. Lee, S. Roseman, and R.L. Schnaar, Specific cell adhesion to immobilized glycoproteins demonstrated using new reagents for protein and glycoprotein immobilization. *The Journal of Biological Chemistry*.

258(4):2340-9, 1983.
33. Flanagan, L.A., Y.E. Ju, B. Marg, M. Osterfield, and P.A. Janmey, Neurite branching on deformable substrates. *Neuroreport*. 13(18):2411-5, 2002.
34. Sims, T.J., L.M. Rasmussen, H. Oxlund, and A.J. Bailey, The role of glycation cross-links in diabetic vascular stiffening. *Diabetologia*. 39(8):946-51, 1996.
35. Discher, D.E., P. Janmey, and Y.L. Wang, Tissue cells feel and respond to the stiffness of their substrate. *Science*. 310(5751):1139-43, 2005.
36. Reinhart-King, C.A., M. Dembo, and D.A. Hammer, Cell-Cell Mechanical Communication through Compliant Substrates. *Biophysical Journal*. 95(12):6044-6051, 2008.
37. Isenberg, B.C., P.A. Dimilla, M. Walker, S. Kim, and J.Y. Wong, Vascular smooth muscle cell durotaxis depends on substrate stiffness gradient strength. *Biophys J*. 97(5):1313-22, 2009.
38. Wang, H.B., M. Dembo, and Y.L. Wang, Substrate flexibility regulates growth and apoptosis of normal but not transformed cells. *Am J Physiol Cell Physiol*. 279(5):C1345-50, 2000.
39. Levental, K.R., H. Yu, L. Kass, J.N. Lakins, M. Egeblad, J.T. Erler, S.F. Fong, K. Csiszar, A. Giaccia, W. Weninger, M. Yamauchi, D.L. Gasser, and V.M. Weaver, Matrix crosslinking forces tumor progression by enhancing integrin signaling. *Cell*. 139(5):891-906, 2009.
40. Delon, I. and N.H. Brown, Integrins and the actin cytoskeleton. *Curr Opin Cell Biol*. 19(1):43-50, 2007.
41. Hynes, R.O., Integrins: bidirectional, allosteric signaling machines. *Cell*. 110(6):673-87, 2002.
42. Legate, K.R. and R. Fassler, Mechanisms that regulate adaptor binding to beta-integrin cytoplasmic tails. *J Cell Sci*. 122(Pt 2):187-98, 2009.
43. Geiger, B., J.P. Spatz, and A.D. Bershadsky, Environmental sensing through focal adhesions. *Nat Rev Mol Cell Biol*. 10(1):21-33, 2009.
44. Maniotis, A.J., C.S. Chen, and D.E. Ingber, Demonstration of mechanical connections between integrins, cytoskeletal filaments, and nucleoplasm that stabilize nuclear structure. *Proc Natl Acad Sci U S A*. 94(3):849-54, 1997.
45. Chicurel, M.E., C.S. Chen, and D.E. Ingber, Cellular control lies in the balance of forces. *Curr Opin Cell Biol*. 10(2):232-9, 1998.
46. Katsumi, A., A.W. Orr, E. Tzima, and M.A. Schwartz, Integrins in mechanotransduction. *J Biol Chem*. 279(13):12001-4, 2004.
47. Riveline, D., E. Zamir, N.Q. Balaban, U.S. Schwarz, T. Ishizaki, S. Narumiya, Z. Kam, B. Geiger, and A.D. Bershadsky, Focal contacts as mechanosensors: externally applied local mechanical force induces growth of focal contacts by an mDia1-dependent and ROCK-independent mechanism. *J Cell Biol*. 153(6):1175-86, 2001.
48. Galbraith, C.G., K.M. Yamada, and M.P. Sheetz, The relationship between force and focal complex development. *J Cell Biol*. 159(4):695-705, 2002.
49. Kaibuchi, K., S. Kuroda, and M. Amano, Regulation of the cytoskeleton and cell adhesion by the Rho family GTPases in mammalian cells. *Annu Rev Biochem*. 68:459-86, 1999.
50. Rodriguez, O.C., A.W. Schaefer, C.A. Mandato, P. Forscher, W.M. Bement, and C.M. Waterman-Storer, Conserved microtubule-actin interactions in cell

movement and morphogenesis. *Nat Cell Biol*. 5(7):599-609, 2003.
51. Kumar, S., I.Z. Maxwell, A. Heisterkamp, T.R. Polte, T.P. Lele, M. Salanga, E. Mazur, and D.E. Ingber, Viscoelastic retraction of single living stress fibers and its impact on cell shape, cytoskeletal organization, and extracellular matrix mechanics. *Biophys J*. 90(10):3762-73, 2006.
52. Lu, L., Y. Feng, W.J. Hucker, S.J. Oswald, G.D. Longmore, and F.C. Yin, Actin stress fiber pre-extension in human aortic endothelial cells. *Cell Motil Cytoskeleton*. 65(4):281-94, 2008.
53. Ingber, D., Integrins as mechanochemical transducers. *Curr Opin Cell Biol*. 3(5):841-8, 1991.
54. Lee, J., M. Leonard, T. Oliver, A. Ishihara, and K. Jacobson, Traction forces generated by locomoting keratocytes. *J Cell Biol*. 127(6 Pt 2):1957-64, 1994.
55. Ghosh, K., C.K. Thodeti, A.C. Dudley, A. Mammoto, M. Klagsbrun, and D.E. Ingber, Tumor-derived endothelial cells exhibit aberrant Rho-mediated mechanosensing and abnormal angiogenesis in vitro. *PNAS*. 105(32):11305-10, 2008.
56. Harris, A.K., P. Wild, and D. Stopak, Silicone rubber substrata: a new wrinkle in the study of cell locomotion. *Science*. 208(4440):177-9, 1980.
57. Tan, J.L., J. Tien, D.M. Pirone, D.S. Gray, K. Bhadriraju, and C.S. Chen, Cells lying on a bed of microneedles: an approach to isolate mechanical force. *Proc Natl Acad Sci U S A*. 100(4):1484-9, 2003.
58. Sniadecki, N.J. and C.S. Chen, Microfabricated silicone elastomeric post arrays for measuring traction forces of adherent cells. *Methods Cell Biol*. 83:313-28, 2007.
59. Galbraith, C.G. and M.P. Sheetz, A micromachined device provides a new bend on fibroblast traction forces. *Proc Natl Acad Sci U S A*. 94(17):9114-8, 1997.
60. Balaban, N.Q., U.S. Schwarz, D. Riveline, P. Goichberg, G. Tzur, I. Sabanay, D. Mahalu, S. Safran, A. Bershadsky, L. Addadi, and B. Geiger, Force and focal adhesion assembly: a close relationship studied using elastic micropatterned substrates. *Nat Cell Biol*. 3(5):466-72, 2001.
61. Dembo, M., T. Oliver, A. Ishihara, and K. Jacobson, Imaging the traction stresses exerted by locomoting cells with the elastic substratum method. *Biophys J*. 70(4):2008-22, 1996.
62. Marganski, W.A., M. Dembo, and Y.L. Wang, Measurements of cell-generated deformations on flexible substrata using correlation-based optical flow. *Methods in Enzymology*. 361:197-211, 2003.
63. Dembo, M. and Y.L. Wang, Stresses at the cell-to-substrate interface during locomotion of fibroblasts. *Biophys J*. 76(4):2307-16, 1999.
64. Lemmon, C.A., N.J. Sniadecki, S.A. Ruiz, J.L. Tan, L.H. Romer, and C.S. Chen, Shear force at the cell-matrix interface: enhanced analysis for microfabricated post array detectors. *Mech Chem Biosyst*. 2(1):1-16, 2005.
65. Bhadriraju, K., M. Yang, S. Alom Ruiz, D. Pirone, J. Tan, and C.S. Chen, Activation of ROCK by RhoA is regulated by cell adhesion, shape, and cytoskeletal tension. *Exp Cell Res*. 313(16):3616-23, 2007.
66. Beningo, K.A., M. Dembo, I. Kaverina, J.V. Small, and Y.L. Wang, Nascent focal adhesions are responsible for the generation of strong propulsive forces

in migrating fibroblasts. *J Cell Biol*. 153(4):881-8, 2001.
67. Ingber, D.E. and J. Folkman, Mechanochemical switching between growth and differentiation during fibroblast growth factor-stimulated angiogenesis in vitro: role of extracellular matrix. *The Journal of Cell Biology*. 109(1):317-30, 1989.
68. Davis, G.E. and D.R. Senger, Endothelial extracellular matrix: biosynthesis, remodeling, and functions during vascular morphogenesis and neovessel stabilization. *Circulation Research*. 97(11):1093-107, 2005.
69. Genes, N.G., J.A. Rowley, D.J. Mooney, and L.J. Bonassar, Effect of substrate mechanics on chondrocyte adhesion to modified alginate surfaces. *Arch Biochem Biophys*. 422(2):161-7, 2004.
70. Ghibaudo, M., A. Saez, L. Trichet, A. Xayaphoummine, J. Browaeys, P. Silberzan, A. Buguin, and A. Ladoux, Traction forces and rigidity sensing regulate cell functions. *Soft Matter*. 4:1836-1843, 2008.
71. Yeung, T., P.C. Georges, L.A. Flanagan, B. Marg, M. Ortiz, M. Funaki, N. Zahir, W. Ming, V. Weaver, and P.A. Janmey, Effects of substrate stiffness on cell morphology, cytoskeletal structure, and adhesion. *Cell Motility and the Cytoskeleton*. 60(1):24-34, 2005.
72. Pelham, R.J., Jr. and Y. Wang, Cell locomotion and focal adhesions are regulated by substrate flexibility. *Proc Natl Acad Sci U S A*. 94(25):13661-5, 1997.
73. Ingber, D.E., D. Prusty, Z. Sun, H. Betensky, and N. Wang, Cell shape, cytoskeletal mechanics, and cell cycle control in angiogenesis. *J Biomech*. 28(12):1471-84, 1995.
74. Roca-Cusachs, P., J. Alcaraz, R. Sunyer, J. Samitier, R. Farre, and D. Navajas, Micropatterning of single endothelial cell shape reveals a tight coupling between nuclear volume in G1 and proliferation. *Biophys J*. 94(12):4984-95, 2008.
75. Huang, S., C.S. Chen, and D.E. Ingber, Control of cyclin D1, p27(Kip1), and cell cycle progression in human capillary endothelial cells by cell shape and cytoskeletal tension. *Mol Biol Cell*. 9(11):3179-93, 1998.
76. Mammoto, A., S. Huang, K. Moore, P. Oh, and D.E. Ingber, Role of RhoA, mDia, and ROCK in cell shape-dependent control of the Skp2-p27kip1 pathway and the G1/S transition. *J Biol Chem*. 279(25):26323-30, 2004.
77. Huang, S. and D.E. Ingber, A discrete cell cycle checkpoint in late G(1) that is cytoskeleton-dependent and MAP kinase (Erk)-independent. *Exp Cell Res*. 275(2):255-64, 2002.
78. Chen, C.S., M. Mrksich, S. Huang, G.M. Whitesides, and D.E. Ingber, Geometric control of cell life and death. *Science*. 276(5317):1425-8, 1997.
79. Chen, C.S., M. Mrksich, S. Huang, G.M. Whitesides, and D.E. Ingber, Micropatterned surfaces for control of cell shape, position, and function. *Biotechnol Prog*. 14(3):356-63, 1998.
80. Zemel, A., H. Rehfeld, A.E.X. Brown, D.E. Discher, and S.A. Safran, Optimal Matrix Rigidity for Stress-Fibre Polarization in Stem Cells. *Nature Physics*.1-15, 2010.
81. Zemel, A. and S.A. Safran, Active self-polarization of contractile cells in asymmetrically shaped domains. *Phys Rev E Stat Nonlin Soft Matter Phys*. 76(2 Pt 1):021905, 2007.

82. Mammoto, A., S. Huang, and D.E. Ingber, Filamin links cell shape and cytoskeletal structure to Rho regulation by controlling accumulation of p190RhoGAP in lipid rafts. *J Cell Sci*. 120(Pt 3):456-67, 2007.
83. Mammoto, A., K.M. Connor, T. Mammoto, C.W. Yung, D. Huh, C.M. Aderman, G. Mostoslavsky, L.E. Smith, and D.E. Ingber, A mechanosensitive transcriptional mechanism that controls angiogenesis. *Nature*. 457(7233):1103-8, 2009.
84. Peyton, S.R. and A.J. Putnam, Extracellular matrix rigidity governs smooth muscle cell motility in a biphasic fashion. *J Cell Physiol*. 204(1):198-209, 2005.
85. Jannat, R.A., M. Dembo, and D.A. Hammer, Neutrophil adhesion and chemotaxis depend on substrate mechanics. *J Phys Condens Matter*. 22(19):194117, 2010.
86. Lo, C.M., H.B. Wang, M. Dembo, and Y.L. Wang, Cell movement is guided by the rigidity of the substrate. *Biophys J*. 79(1):144-52, 2000.
87. Guo, W.H., M.T. Frey, N.A. Burnham, and Y.L. Wang, Substrate rigidity regulates the formation and maintenance of tissues. *Biophysical Journal*. 90(6):2213-20, 2006.
88. Nishimura, T. and M. Takeichi, Remodeling of the adherens junctions during morphogenesis. *Curr Top Dev Biol*. 89:33-54, 2009.
89. Ko, K.S., P.D. Arora, and C.A. McCulloch, Cadherins mediate intercellular mechanical signaling in fibroblasts by activation of stretch-sensitive calcium-permeable channels. *J Biol Chem*. 276(38):35967-77, 2001.
90. Ganz, A., M. Lambert, A. Saez, P. Silberzan, A. Buguin, R.M. Mege, and B. Ladoux, Traction forces exerted through N-cadherin contacts. *Biol Cell*. 98(12):721-30, 2006.
91. Ladoux, B., E. Anon, M. Lambert, A. Rabodzey, P. Hersen, A. Buguin, P. Silberzan, and R.M. Mege, Strength dependence of cadherin-mediated adhesions. *Biophys J*. 98(4):534-42, 2010.
92. Ogita, H. and Y. Takai, Cross-talk among integrin, cadherin, and growth factor receptor: roles of nectin and nectin-like molecule. *Int Rev Cytol*. 265:1-54, 2008.
93. Schwartz, M.A. and D.W. DeSimone, Cell adhesion receptors in mechanotransduction. *Current Opinion in Cell Biology*. 20(5):551-556, 2008.
94. Dejana, E., M. Corada, and M.G. Lampugnani, Endothelial cell-to-cell junctions. *The FASEB Journal*. 9(10):910-8, 1995.
95. Kris, A.S., R.D. Kamm, and A.L. Sieminski, VASP involvement in force-mediated adherens junction strengthening. *Biochem Biophys Res Commun*. 375(1):134-8, 2008.
96. Nelson, C.M., D.M. Pirone, J.L. Tan, and C.S. Chen, Vascular endothelial-cadherin regulates cytoskeletal tension, cell spreading, and focal adhesions by stimulating RhoA. *Mol Biol Cell*. 15(6):2943-53, 2004.
97. Liu, Z., J.L. Tan, D.M. Cohen, M.T. Yang, N.J. Sniadecki, S.A. Ruiz, C.M. Nelson, and C.S. Chen, Mechanical tugging force regulates the size of cell-cell junctions. *Proc Natl Acad Sci U S A*. 107(22):9944-9, 2009.
98. Zhou, X., R.G. Rowe, N. Hiraoka, J.P. George, D. Wirtz, D.F. Mosher, I. Virtanen, M.A. Chernousov, and S.J. Weiss, Fibronectin fibrillogenesis

regulates three-dimensional neovessel formation. *Genes & Development*. 22(9):1231-43, 2008.
99. George, E.L., E.N. Georges-Labouesse, R.S. Patel-King, H. Rayburn, and R.O. Hynes, Defects in mesoderm, neural tube and vascular development in mouse embryos lacking fibronectin. *Development*. 119(4):1079-91, 1993.
100. George, E.L., H.S. Baldwin, and R.O. Hynes, Fibronectins are essential for heart and blood vessel morphogenesis but are dispensable for initial specification of precursor cells. *Blood*. 90(8):3073-81, 1997.
101. McKeown-Longo, P.J. and D.F. Mosher, Binding of plasma fibronectin to cell layers of human skin fibroblasts. *J Cell Biol*. 97(2):466-72, 1983.
102. Magnusson, M.K. and D.F. Mosher, Fibronectin: structure, assembly, and cardiovascular implications. *Arterioscler Thromb Vasc Biol*. 18(9):1363-70, 1998.
103. Baneyx, G., L. Baugh, and V. Vogel, Fibronectin extension and unfolding within cell matrix fibrils controlled by cytoskeletal tension. *Proc Natl Acad Sci U S A*. 99(8):5139-43, 2002.
104. Zhong, C., M. Chrzanowska-Wodnicka, J. Brown, A. Shaub, A.M. Belkin, and K. Burridge, Rho-mediated contractility exposes a cryptic site in fibronectin and induces fibronectin matrix assembly. *J Cell Biol*. 141(2):539-51, 1998.
105. Gao, M., D. Craig, O. Lequin, I.D. Campbell, V. Vogel, and K. Schulten, Structure and functional significance of mechanically unfolded fibronectin type III1 intermediates. *Proc Natl Acad Sci U S A*. 100(25):14784-9, 2003.
106. Zardi, L., B. Carnemolla, A. Siri, T.E. Petersen, G. Paolella, G. Sebastio, and F.E. Baralle, Transformed human cells produce a new fibronectin isoform by preferential alternative splicing of a previously unobserved exon. *EMBO J*. 6(8):2337-42, 1987.
107. Carnemolla, B., E. Balza, A. Siri, L. Zardi, M.R. Nicotra, A. Bigotti, and P.G. Natali, A tumor-associated fibronectin isoform generated by alternative splicing of messenger RNA precursors. *J Cell Biol*. 108(3):1139-48, 1989.
108. Castellani, P., L. Borsi, B. Carnemolla, A. Biro, A. Dorcaratto, G.L. Viale, D. Neri, and L. Zardi, Differentiation between high- and low-grade astrocytoma using a human recombinant antibody to the extra domain-B of fibronectin. *Am J Pathol*. 161(5):1695-700, 2002.
109. Neri, D. and R. Bicknell, Tumour vascular targeting. *Nat Rev Cancer*. 5(6):436-46, 2005.
110. Padera, T.P., B.R. Stoll, J.B. Tooredman, D. Capen, E. di Tomaso, and R.K. Jain, Pathology: cancer cells compress intratumour vessels. *Nature*. 427(6976):695, 2004.
111. Gimbrone, M.A., Jr., S.B. Leapman, R.S. Cotran, and J. Folkman, Tumor dormancy in vivo by prevention of neovascularization. *J Exp Med*. 136(2):261-76, 1972.
112. Califano, J.P. and C.A. Reinhart-King, A Balance of Substrate Mechanics and Matrix Chemistry Regulates Endothelial Cell Network Assembly. *Cellular and Molecular Bioengineering*. 1(2-3):122-132, 2008.
113. Odde, D.J. and X.E. Guo, Editorial: Outstanding Papers from the 2008 Biomedical Engineering Society (BMES) Annual Meeting. *Cellular and Molecular Bioengineering*. 1(2-3):109, 2008.

114. Intengan, H.D. and E.L. Schiffrin, Vascular remodeling in hypertension: roles of apoptosis, inflammation, and fibrosis. *Hypertension*. 38(3 Pt 2):581-7, 2001.
115. Schwarzbauer, J.E. and J.L. Sechler, Fibronectin fibrillogenesis: a paradigm for extracellular matrix assembly. *Curr Opin Cell Biol*. 11(5):622-7, 1999.
116. Davis, G.E. and D.R. Senger, Endothelial extracellular matrix: biosynthesis, remodeling, and functions during vascular morphogenesis and neovessel stabilization. *Circ Res*. 97(11):1093-107, 2005.
117. Kubota, Y., H.K. Kleinman, G.R. Martin, and T.J. Lawley, Role of laminin and basement membrane in the morphological differentiation of human endothelial cells into capillary-like structures. *J Cell Biol*. 107(4):1589-98, 1988.
118. Vernon, R.B., J.C. Angello, M.L. Iruela-Arispe, T.F. Lane, and E.H. Sage, Reorganization of basement membrane matrices by cellular traction promotes the formation of cellular networks in vitro. *Lab Invest*. 66(5):536-47, 1992.
119. Vernon, R.B., S.L. Lara, C.J. Drake, M.L. Iruela-Arispe, J.C. Angello, C.D. Little, T.N. Wight, and E.H. Sage, Organized type I collagen influences endothelial patterns during "spontaneous angiogenesis in vitro": planar cultures as models of vascular development. *In Vitro Cell Dev Biol Anim*. 31(2):120-31, 1995.
120. Ingber, D.E. and J. Folkman, Mechanochemical switching between growth and differentiation during fibroblast growth factor-stimulated angiogenesis in vitro: role of extracellular matrix. *J Cell Biol*. 109(1):317-30, 1989.
121. Vailhe, B., X. Ronot, P. Tracqui, Y. Usson, and L. Tranqui, In vitro angiogenesis is modulated by the mechanical properties of fibrin gels and is related to alpha(v)beta3 integrin localization. *In Vitro Cell Dev Biol Anim*. 33(10):763-73, 1997.
122. Deroanne, C.F., C.M. Lapiere, and B.V. Nusgens, In vitro tubulogenesis of endothelial cells by relaxation of the coupling extracellular matrix-cytoskeleton. *Cardiovasc Res*. 49(3):647-58, 2001.
123. Sieminski, A.L., R.P. Hebbel, and K.J. Gooch, The relative magnitudes of endothelial force generation and matrix stiffness modulate capillary morphogenesis in vitro. *Exp Cell Res*. 297(2):574-84, 2004.
124. Ingber, D.E. and J. Folkman, How does extracellular matrix control capillary morphogenesis? *Cell*. 58(5):803-5, 1989.
125. Jiang, G., A.H. Huang, Y. Cai, M. Tanase, and M.P. Sheetz, Rigidity sensing at the leading edge through alphavbeta3 integrins and RPTPalpha. *Biophys J*. 90(5):1804-9, 2006.
126. Guo, W.H., M.T. Frey, N.A. Burnham, and Y.L. Wang, Substrate rigidity regulates the formation and maintenance of tissues. *Biophys J*. 90(6):2213-20, 2006.
127. Ryan, P.L., R.A. Foty, J. Kohn, and M.S. Steinberg, Tissue spreading on implantable substrates is a competitive outcome of cell-cell vs. cell-substratum adhesivity. *Proc Natl Acad Sci U S A*. 98(8):4323-7, 2001.
128. Engler, A., L. Bacakova, C. Newman, A. Hategan, M. Griffin, and D. Discher, Substrate compliance versus ligand density in cell on gel responses. *Biophys J*. 86(1 Pt 1):617-28, 2004.
129. Yeung, T., P.C. Georges, L.A. Flanagan, B. Marg, M. Ortiz, M. Funaki, N.

Zahir, W. Ming, V. Weaver, and P.A. Janmey, Effects of substrate stiffness on cell morphology, cytoskeletal structure, and adhesion. *Cell Motil Cytoskeleton*. 60(1):24-34, 2005.
130. Ingber, D.E., Fibronectin controls capillary endothelial cell growth by modulating cell shape. *Proc Natl Acad Sci U S A*. 87(9):3579-83, 1990.
131. Wang, Y.L. and R.J. Pelham, Jr., Preparation of a flexible, porous polyacrylamide substrate for mechanical studies of cultured cells. *Methods Enzymol*. 298:489-96, 1998.
132. Reinhart-King, C.A., M. Dembo, and D.A. Hammer, The dynamics and mechanics of endothelial cell spreading. *Biophys J*. 89(1):676-89, 2005.
133. Pless, D.D., Y.C. Lee, S. Roseman, and R.L. Schnaar, Specific cell adhesion to immobilized glycoproteins demonstrated using new reagents for protein and glycoprotein immobilization. *J Biol Chem*. 258(4):2340-9, 1983.
134. Sottile, J. and J. Chandler, Fibronectin matrix turnover occurs through a caveolin-1-dependent process. *Mol Biol Cell*. 16(2):757-68, 2005.
135. Morla, A., Z. Zhang, and E. Ruoslahti, Superfibronectin is a functionally distinct form of fibronectin. *Nature*. 367(6459):193-6, 1994.
136. Klein, E.A., Y. Yung, P. Castagnino, D. Kothapalli, and R.K. Assoian, Cell adhesion, cellular tension, and cell cycle control. *Methods Enzymol*. 426:155-75, 2007.
137. Mao, Y. and J.E. Schwarzbauer, Fibronectin fibrillogenesis, a cell-mediated matrix assembly process. *Matrix Biol*. 24(6):389-99, 2005.
138. Connolly, J.O., N. Simpson, L. Hewlett, and A. Hall, Rac regulates endothelial morphogenesis and capillary assembly. *Mol Biol Cell*. 13(7):2474-85, 2002.
139. Zhou, X., R.G. Rowe, N. Hiraoka, J.P. George, D. Wirtz, D.F. Mosher, I. Virtanen, M.A. Chernousov, and S.J. Weiss, Fibronectin fibrillogenesis regulates three-dimensional neovessel formation. *Genes Dev*. 22(9):1231-43, 2008.
140. Hocking, D.C., J. Sottile, and K.J. Langenbach, Stimulation of integrin-mediated cell contractility by fibronectin polymerization. *J Biol Chem*. 275(14):10673-82, 2000.
141. Liu, Y. and D.R. Senger, Matrix-specific activation of Src and Rho initiates capillary morphogenesis of endothelial cells. *Faseb J*. 18(3):457-68, 2004.
142. Gamble, J.R., L.J. Matthias, G. Meyer, P. Kaur, G. Russ, R. Faull, M.C. Berndt, and M.A. Vadas, Regulation of in vitro capillary tube formation by anti-integrin antibodies. *J Cell Biol*. 121(4):931-43, 1993.
143. Feder, J., J.C. Marasa, and J.V. Olander, The formation of capillary-like tubes by calf aortic endothelial cells grown in vitro. *J Cell Physiol*. 116(1):1-6, 1983.
144. Olander, J.V., M.E. Bremer, J.C. Marasa, and J. Feder, Fibrin-enhanced endothelial cell organization. *J Cell Physiol*. 125(1):1-9, 1985.
145. Tomasini-Johansson, B.R., N.R. Kaufman, M.G. Ensenberger, V. Ozeri, E. Hanski, and D.F. Mosher, A 49-residue peptide from adhesin F1 of Streptococcus pyogenes inhibits fibronectin matrix assembly. *J Biol Chem*. 276(26):23430-9, 2001.
146. Sottile, J. and D.C. Hocking, Fibronectin polymerization regulates the composition and stability of extracellular matrix fibrils and cell-matrix adhesions. *Mol Biol Cell*. 13(10):3546-59, 2002.

147. Ryan, P.L., R.A. Foty, J. Kohn, and M.S. Steinberg, Tissue spreading on implantable substrates is a competitive outcome of cell-cell vs. cell-substratum adhesivity. *Proceedings of the National Academy of the Sciences of the United States of America*. 98(8):4323-7, 2001.
148. Vestweber, D., VE-cadherin: the major endothelial adhesion molecule controlling cellular junctions and blood vessel formation. *Arterioscler Thromb Vasc Biol*. 28(2):223-32, 2008.
149. Califano, J.P. and C.A. Reinhart-King, Substrate stiffness and cell area drive cellular traction stresses in single cells and cells in contact. *Cellular and Molecular Bioengineering*. 3(1):68-75, 2010.
150. Debnath, J., S.K. Muthuswamy, and J.S. Brugge, Morphogenesis and oncogenesis of MCF-10A mammary epithelial acini grown in three-dimensional basement membrane cultures. *Methods*. 30(3):256-68, 2003.
151. Engler, A., Richert, L., Wong, J., Picart, C., Discher D., Surface probe measurements of the elasticity of sectioned tissue, thin gels and polyelectrolyte multilayer films: correlations between substrate stiffness and cell adhesion. *Surface Science*. 570:142-154, 2004.
152. Lampugnani, M.G., M. Corada, L. Caveda, F. Breviario, O. Ayalon, B. Geiger, and E. Dejana, The molecular organization of endothelial cell to cell junctions: differential association of plakoglobin, beta-catenin, and alpha-catenin with vascular endothelial cadherin (VE-cadherin). *J Cell Biol*. 129(1):203-17, 1995.
153. Rasband, W.S., ImageJ. *U.S. National Institutes of Health, Bethesda, Maryland, USA, http://rsb.info.nih.gov/ij/*. 1997-2009.
154. Garcia, A.J., P. Ducheyne, and D. Boettiger, Quantification of cell adhesion using a spinning disc device and application to surface-reactive materials. *Biomaterials*. 18(16):1091-8, 1997.
155. Corada, M., F. Liao, M. Lindgren, M.G. Lampugnani, F. Breviario, R. Frank, W.A. Muller, D.J. Hicklin, P. Bohlen, and E. Dejana, Monoclonal antibodies directed to different regions of vascular endothelial cadherin extracellular domain affect adhesion and clustering of the protein and modulate endothelial permeability. *Blood*. 97(6):1679-84, 2001.
156. Dejana, E., F. Orsenigo, C. Molendini, P. Baluk, and D.M. McDonald, Organization and signaling of endothelial cell-to-cell junctions in various regions of the blood and lymphatic vascular trees. *Cell and Tissue Research*. 335(1):17-25, 2009.
157. Bonaccurso, E., B. Cappella, and K. Graf, Local mechanical properties of plasma treated polystyrene surfaces. *The Journal of Physical Chemistry B*. 110(36):17918-24, 2006.
158. Volberg, T., B. Geiger, J. Kartenbeck, and W.W. Franke, Changes in membrane-microfilament interaction in intercellular adherens junctions upon removal of extracellular Ca2+ ions. *J Cell Biol*. 102(5):1832-42, 1986.
159. Streuli, C.H., C. Schmidhauser, N. Bailey, P. Yurchenco, A.P. Skubitz, C. Roskelley, and M.J. Bissell, Laminin mediates tissue-specific gene expression in mammary epithelia. *J Cell Biol*. 129(3):591-603, 1995.
160. Stahl, S., S. Weitzman, and J.C. Jones, The role of laminin-5 and its receptors in mammary epithelial cell branching morphogenesis. *J Cell Sci*. 110 (Pt 1):55-63, 1997.

161. Hens, J.R., P. Dann, J.P. Zhang, S. Harris, G.W. Robinson, and J. Wysolmerski, BMP4 and PTHrP interact to stimulate ductal outgrowth during embryonic mammary development and to inhibit hair follicle induction. *Development*. 134(6):1221-30, 2007.
162. Evensen, L., D.R. Micklem, A. Blois, S.V. Berge, N. Aarsaether, A. Littlewood-Evans, J. Wood, and J.B. Lorens, Mural cell associated VEGF is required for organotypic vessel formation. *PLoS One*. 4(6):e5798, 2009.
163. Martin, K.J., C.P. Kwan, K. Nagasaki, X. Zhang, M.J. O'Hare, C.M. Kaelin, R.E. Burgeson, A.B. Pardee, and R. Sager, Down-regulation of laminin-5 in breast carcinoma cells. *Mol Med*. 4(9):602-13, 1998.
164. Royce, S.G., L. Tan, A.A. Koek, and M.L. Tang, Effect of extracellular matrix composition on airway epithelial cell and fibroblast structure: implications for airway remodeling in asthma. *Ann Allergy Asthma Immunol*. 102(3):238-46, 2009.
165. Moore, K.A., S. Huang, Y. Kong, M.E. Sunday, and D.E. Ingber, Control of embryonic lung branching morphogenesis by the Rho activator, cytotoxic necrotizing factor 1. *J Surg Res*. 104(2):95-100, 2002.
166. Gumbiner, B.M., Cell adhesion: the molecular basis of tissue architecture and morphogenesis. *Cell*. 84(3):345-57, 1996.
167. Kleinman, H.K. and G.R. Martin, Matrigel: basement membrane matrix with biological activity. *Semin Cancer Biol*. 15(5):378-86, 2005.
168. LeBleu, V.S., B. Macdonald, and R. Kalluri, Structure and function of basement membranes. *Exp Biol Med (Maywood)*. 232(9):1121-9, 2007.
169. Benton, G., E. Crooke, and J. George, Laminin-1 induces E-cadherin expression in 3-dimensional cultured breast cancer cells by inhibiting DNA methyltransferase 1 and reversing promoter methylation status. *FASEB J*. 23(11):3884-95, 2009.
170. Huynh, J., N. Nishimura, K. Rana, J.M. Peloquin, J.P. Califano, C.R. Montague, M.R. King, C.B. Schaffer, and C.A. Reinhart-King, Age-Related Intimal Stiffening Enhances Endothelial Permeability and Leukocyte Transmigration. *Sci Transl Med*. 3(112):112ra122, 2011.
171. Wang, Y., G. Jin, H. Miao, J.Y. Li, S. Usami, and S. Chien, Integrins regulate VE-cadherin and catenins: dependence of this regulation on Src, but not on Ras. *Proc Natl Acad Sci U S A*. 103(6):1774-9, 2006.
172. van Nieuw Amerongen, G.P., C.M. Beckers, I.D. Achekar, S. Zeeman, R.J. Musters, and V.W. van Hinsbergh, Involvement of Rho kinase in endothelial barrier maintenance. *Arterioscler Thromb Vasc Biol*. 27(11):2332-9, 2007.
173. Lemmon, C.A., C.S. Chen, and L.H. Romer, Cell traction forces direct fibronectin matrix assembly. *Biophys J*. 96(2):729-38, 2009.
174. Friedl, P. and K. Wolf, Tumour-cell invasion and migration: diversity and escape mechanisms. *Nat Rev Cancer*. 3(5):362-74, 2003.
175. Reinhart-King, C.A., Endothelial cell adhesion and migration. *Methods Enzymol*. 443:45-64, 2008.
176. Califano, J.P. and C.A. Reinhart-King, Exogenous and endogenous force regulation of endothelial cell behavior. *Journal of Biomechanics*. 43 (1):79-86, 2010.
177. Chen, C.S., Mechanotransduction - a field pulling together? *J Cell Sci*. 121(Pt

20):3285-92, 2008.
178. An, S.S., B. Fabry, X. Trepat, N. Wang, and J.J. Fredberg, Do biophysical properties of the airway smooth muscle in culture predict airway hyperresponsiveness? *Am J Respir Cell Mol Biol*. 35(1):55-64, 2006.
179. Munevar, S., Y. Wang, and M. Dembo, Traction force microscopy of migrating normal and H-ras transformed 3T3 fibroblasts. *Biophys J*. 80(4):1744-57, 2001.
180. Paszek, M.J. and V.M. Weaver, The tension mounts: mechanics meets morphogenesis and malignancy. *J Mammary Gland Biol Neoplasia*. 9(4):325-42, 2004.
181. Li, B., F. Li, K.M. Puskar, and J.H. Wang, Spatial patterning of cell proliferation and differentiation depends on mechanical stress magnitude. *J Biomech*. 42(11):1622-7, 2009.
182. Nelson, C.M., R.P. Jean, J.L. Tan, W.F. Liu, N.J. Sniadecki, A.A. Spector, and C.S. Chen, Emergent patterns of growth controlled by multicellular form and mechanics. *Proc Natl Acad Sci U S A*. 102(33):11594-9, 2005.
183. Li, Y., Z.B. Hu, and C.F. Li, New Method for Measuring Poisson Ratio in Polymer Gels. *Journal of Applied Polymer Science*. 50(6):1107-1111, 1993.
184. Marganski, W.A., M. Dembo, and Y.L. Wang, Measurements of cell-generated deformations on flexible substrata using correlation-based optical flow. *Methods Enzymol*. 361:197-211, 2003.
185. Dembo, M. and Y.L. Wang, Stresses at the cell-to-substrate interface during locomotion of fibroblasts. *Biophysical Journal*. 76(4):2307-16, 1999.
186. Ott, R.L. and M. Longnecker. An Introduction to Statistical Methods and Data Analysis. Duxbury Press, 2001, 1184 pp.
187. Wang, N., E. Ostuni, G.M. Whitesides, and D.E. Ingber, Micropatterning tractional forces in living cells. *Cell Motil Cytoskeleton*. 52(2):97-106, 2002.
188. du Roure, O., A. Saez, A. Buguin, R.H. Austin, P. Chavrier, P. Silberzan, and B. Ladoux, Force mapping in epithelial cell migration. *Proc Natl Acad Sci U S A*. 102(7):2390-5, 2005.
189. Tsai, J. and L. Kam, Rigidity-dependent cross talk between integrin and cadherin signaling. *Biophys J*. 96(6):L39-41, 2009.
190. Engler, A.J., S. Sen, H.L. Sweeney, and D.E. Discher, Matrix elasticity directs stem cell lineage specification. *Cell*. 126(4):677-89, 2006.
191. Berrier, A.L. and K.M. Yamada, Cell-matrix adhesion. *J Cell Physiol*. 213(3):565-73, 2007.
192. Cseh, B., S. Fernandez-Sauze, D. Grall, S. Schaub, E. Doma, and E. Van Obberghen-Schilling, Autocrine fibronectin directs matrix assembly and crosstalk between cell-matrix and cell-cell adhesion in vascular endothelial cells. *J Cell Sci*. 123(Pt 22):3989-99, 2010.
193. Tomasini-Johansson, B.R., N.R. Kaufman, M.G. Ensenberger, V. Ozeri, E. Hanski, and D.F. Mosher, A 49-residue peptide from adhesin F1 of Streptococcus pyogenes inhibits fibronectin matrix assembly. *The Journal of Biological Chemistry*. 276(26):23430-9, 2001.
194. Lauffenburger, D.A. and J.J. Linderman. Receptors: Models for Binding, Trafficking, and Signaling. Oxford University Press, 1993, pp.
195. Rape, A.D., W.H. Guo, and Y.L. Wang, The regulation of traction force in

relation to cell shape and focal adhesions. *Biomaterials*. 32(8):2043-51, 2010.
196. Charest, J.M., J.P. Califano, S.P. Carey, and C.A. Reinhart-King, Fabrication of Substrates with Defined Mechanical Properties and Topographical Features for the Study of Cell Migration. *Macromolecular Bioscience*. 12(1):12-20, 2012.
197. Fonck, E., G.G. Feigl, J. Fasel, D. Sage, M. Unser, D.A. Rufenacht, and N. Stergiopulos, Effect of aging on elastin functionality in human cerebral arteries. *Stroke*. 40(7):2552-6, 2009.
198. Choi, M.G. and R.O. Hynes, Biosynthesis and processing of fibronectin in NIL.8 hamster cells. *J Biol Chem*. 254(23):12050-5, 1979.
199. Pollard, T.D. and R.R. Weihing, Actin and myosin and cell movement. *CRC Crit Rev Biochem*. 2(1):1-65, 1974.
200. Mehta, D. and A.B. Malik, Signaling mechanisms regulating endothelial permeability. *Physiol Rev*. 86(1):279-367, 2006.
201. Shyy, J.Y. and S. Chien, Role of integrins in endothelial mechanosensing of shear stress. *Circ Res*. 91(9):769-75, 2002.
202. Ishizaki, T., M. Uehata, I. Tamechika, J. Keel, K. Nonomura, M. Maekawa, and S. Narumiya, Pharmacological properties of Y-27632, a specific inhibitor of rho-associated kinases. *Mol Pharmacol*. 57(5):976-83, 2000.
203. Erickson, H.P., Stretching fibronectin. *J Muscle Res Cell Motil*. 23(5-6):575-80, 2002.
204. Ohashi, T., A.M. Augustus, and H.P. Erickson, Transient opening of fibronectin type III (FNIII) domains: the interaction of the third FNIII domain of FN with anastellin. *Biochemistry*. 48(19):4189-97, 2009.
205. Smith, M.L., D. Gourdon, W.C. Little, K.E. Kubow, R.A. Eguiluz, S. Luna-Morris, and V. Vogel, Force-induced unfolding of fibronectin in the extracellular matrix of living cells. *PLoS Biol*. 5(10):e268, 2007.
206. Chen, H. and D.F. Mosher, Formation of sodium dodecyl sulfate-stable fibronectin multimers. Failure to detect products of thiol-disulfide exchange in cyanogen bromide or limited acid digests of stabilized matrix fibronectin. *J Biol Chem*. 271(15):9084-9, 1996.
207. Ohashi, T. and H.P. Erickson, Revisiting the mystery of fibronectin multimers: the fibronectin matrix is composed of fibronectin dimers cross-linked by non-covalent bonds. *Matrix Biol*. 28(3):170-5, 2009.
208. Astrof, S., D. Crowley, E.L. George, T. Fukuda, K. Sekiguchi, D. Hanahan, and R.O. Hynes, Direct test of potential roles of EIIIA and EIIIB alternatively spliced segments of fibronectin in physiological and tumor angiogenesis. *Mol Cell Biol*. 24(19):8662-70, 2004.
209. Fukuda, T., N. Yoshida, Y. Kataoka, R. Manabe, Y. Mizuno-Horikawa, M. Sato, K. Kuriyama, N. Yasui, and K. Sekiguchi, Mice lacking the EDB segment of fibronectin develop normally but exhibit reduced cell growth and fibronectin matrix assembly in vitro. *Cancer Res*. 62(19):5603-10, 2002.
210. Balza, E., F. Sassi, E. Ventura, A. Parodi, S. Fossati, W. Blalock, B. Carnemolla, P. Castellani, L. Zardi, and L. Borsi, A novel human fibronectin cryptic sequence unmasked by the insertion of the angiogenesis-associated extra type III domain B. *Int J Cancer*. 125(4):751-8, 2009.
211. Hashimoto-Uoshima, M., Y.Z. Yan, G. Schneider, and I. Aukhil, The

alternatively spliced domains EIIIB and EIIIA of human fibronectin affect cell adhesion and spreading. *J Cell Sci*. 110 (Pt 18):2271-80, 1997.
212. Hynes, R.O. and K.M. Yamada, Fibronectins: multifunctional modular glycoproteins. *J Cell Biol*. 95(2 Pt 1):369-77, 1982.
213. Pierschbacher, M.D. and E. Ruoslahti, Variants of the cell recognition site of fibronectin that retain attachment-promoting activity. *Proc Natl Acad Sci U S A*. 81(19):5985-8, 1984.
214. Yang, J.T., H. Rayburn, and R.O. Hynes, Embryonic mesodermal defects in alpha 5 integrin-deficient mice. *Development*. 119(4):1093-105, 1993.
215. Goh, K.L., J.T. Yang, and R.O. Hynes, Mesodermal defects and cranial neural crest apoptosis in alpha5 integrin-null embryos. *Development*. 124(21):4309-19, 1997.
216. Friedland, J.C., M.H. Lee, and D. Boettiger, Mechanically activated integrin switch controls alpha5beta1 function. *Science*. 323(5914):642-4, 2009.
217. Koukoulis, G.K., A.A. Howeedy, M. Korhonen, I. Virtanen, and V.E. Gould, Distribution of tenascin, cellular fibronectins and integrins in the normal, hyperplastic and neoplastic breast. *J Submicrosc Cytol Pathol*. 25(2):285-95, 1993.
218. Koukoulis, G.K., J. Shen, I. Virtanen, and V.E. Gould, Immunolocalization of cellular fibronectins in the normal liver, cirrhosis, and hepatocellular carcinoma. *Ultrastruct Pathol*. 19(1):37-43, 1995.
219. Jarnagin, W.R., D.C. Rockey, V.E. Koteliansky, S.S. Wang, and D.M. Bissell, Expression of variant fibronectins in wound healing: cellular source and biological activity of the EIIIA segment in rat hepatic fibrogenesis. *J Cell Biol*. 127(6 Pt 2):2037-48, 1994.
220. Georges, P.C., J.J. Hui, Z. Gombos, M.E. McCormick, A.Y. Wang, M. Uemura, R. Mick, P.A. Janmey, E.E. Furth, and R.G. Wells, Increased stiffness of the rat liver precedes matrix deposition: implications for fibrosis. *Am J Physiol Gastrointest Liver Physiol*. 293(6):G1147-54, 2007.
221. Soofi, S.S., J.A. Last, S.J. Liliensiek, P.F. Nealey, and C.J. Murphy, The elastic modulus of Matrigel as determined by atomic force microscopy. *J Struct Biol*. 167(3):216-9, 2009.
222. Warburton, M.J., D. Mitchell, E.J. Ormerod, and P. Rudland, Distribution of myoepithelial cells and basement membrane proteins in the resting, pregnant, lactating, and involuting rat mammary gland. *J Histochem Cytochem*. 30(7):667-76, 1982.
223. Monaghan, P., M.J. Warburton, N. Perusinghe, and P.S. Rudland, Topographical arrangement of basement membrane proteins in lactating rat mammary gland: comparison of the distribution of type IV collagen, laminin, fibronectin, and Thy-1 at the ultrastructural level. *Proc Natl Acad Sci U S A*. 80(11):3344-8, 1983.
224. Roy, R., A.L. Boskey, and L.J. Bonassar, Non-enzymatic glycation of chondrocyte-seeded collagen gels for cartilage tissue engineering. *J Orthop Res*. 26(11):1434-9, 2008.
225. Roy, R., A. Boskey, and L.J. Bonassar, Processing of type I collagen gels using nonenzymatic glycation. *J Biomed Mater Res A*. 93(3):843-51, 2009.
226. Legant, W.R., J.S. Miller, B.L. Blakely, D.M. Cohen, G.M. Genin, and C.S.

Chen, Measurement of mechanical tractions exerted by cells in three-dimensional matrices. *Nat Methods*. 7(12):969-71, 2010.
227. ACS, Cancer Facts & Figures. *American Cancer Society, Atlanta*. Available at http://www.cancer.org/Research/CancerFactsFigures/CancerFactsFigures/index, 2011-12.
228. Reinhart-King, C.A., *Traction forces exerted by endothelial cells on deformable substrates*. 2006, Doctoral Thesis: University of Pennsylvania.
229. Swift, D.G., *The extent and rate of antigen-antibody-mediated adhesion of rat basophilic leukemia cell to surfaces in a linear shear field*. 1998, Doctoral Thesis: University of Pennsylvania.